

Metabolic Status Modulates Tumour Cell Sensitivity to Apoptotic Stimuli

Thesis submitted for the degree of
Doctor of Philosophy
at the
University of Leicester

By
Gareth James Miles (MSc Leicester)
MRC Toxicology Unit

September 2015

Metabolic Status Modulates Tumour Cell Sensitivity to Apoptotic Stimuli

By Gareth Miles¹

¹MRC Toxicology Unit, University of Leicester, Hodgkin Building, PO BOX 138, Lancaster Rd, Leicester, LE1 9HN

Chronic lymphocytic leukaemia and mantle cell lymphoma (MCL) are resistant to TNF Related Apoptosis Inducing Ligand (TRAIL), which induces apoptosis via DISC-mediated activation of caspase-8, cleavage of Bid and activation of the mitochondrial cell death pathway. Cancer cells preferentially utilise aerobic glycolysis ('Warburg effect') for proliferative growth, and this is a potential therapeutic target.

Using MCL-derived cell lines (UPN1 and Z138) the interplay between cancer cell metabolism and cell death was investigated. From this study it was found that active glycolysis appears to be critically required for the full execution of programmed necroptosis. Furthermore, it was observed that 2-deoxyglucose (2DG), a non-metabolisable glucose analogue and hexokinase inhibitor rapidly (0-1h) enhances the sensitivity and potentiates the effects of TRAIL and ABT-737 by inhibiting glycolysis. Extra-cellular flux analysis shows that 2DG rapidly inhibits glycolysis, inducing metabolic reprogramming to transiently increase oxidative-phosphorylation. Despite this increase in oxidative phosphorylation, ATP levels are reduced to 50%, an effect which is maintained for up to 20 h. We now show that the effects of 2DG are not restricted, solely to inhibition of glycolysis, and involve a rapid activation of signalling cascades. Early activation of the AMPK pathway produces a rapid inhibition of protein translation and decrease in the levels of the anti-apoptotic protein Mcl-1, an effect which appears to be independent of canonical AMPK kinases LKB1 and CaMKK- β . Additionally, it was observed that cells maintained in galactose media are extremely sensitive to drugs that induce mitochondrial liabilities, however less sensitive to canonical inducers of apoptosis. As such, mass spectrometry analysis of immunopurified mitochondria were analysed to assess changes in the mitochondrial proteome following metabolic reprogramming. This showed that expression of the proteins which make up the mitochondrial oxidative phosphorylation system was up-regulated. Bioinformatics pathway mapping demonstrated that galactose grown cells switched towards a pro-survival phenotype.

Acknowledgments

I would like to thank my two supervisors Prof. Kelvin Cain and Prof. Marion MacFarlane, firstly, for giving me the opportunity carry out a PhD, and for the huge amount of support, guidance and training they have both given me over the last 4 years (professionally and emotionally). It has been an absolute pleasure working for you both, and I am excited to be staying on a little longer to publish some of the beautiful work that we have achieved together. I hope one day to be as understanding and patient with students of my own. Thank you.

I would also like to thank all of my colleagues in lab 416, for all the time spent training me and discussing data with me, imparting all of your wisdoms. The members of 416 made my time at the MRC an enjoyable, relaxed and friendly experience, and I am proud to call you all friends. I would like to thank Dr Claudia Langlais for all the collaborative work we carried out, there was more than one very late night isolating mitochondria from a few billion cells, and I could not have done it without you. I would like to thank Rebekah Jukes-Jones for her semi-grounded sanity, and her ability to always put a smile on my face, and all her hard work on the mass spectrometry experiments. I would also like to thank Carolyn Jones for all her work on the polysome profiling experiments and helpful technical discussions.

I want to thank Dr Ian Powley and John Nellis for their incredible friendship and for the many, many days we have spent in the pub, my liver is looking forward to a rest. I want to thank everyone else in the Hodgkin Building for just being an upbeat fun crowd, it means work is never dull.

Finally, my Mum and Dad, who bought my wife and I a house to live in (apparently we have to give it back now – not impressed), sent us groceries (occasionally), always came to visit with wine and gave us both a huge amount of support over the last four years. My cat Gizmo, an unusual acknowledgment, but he sat by me (literally) for almost every minute while I was writing up. My wife, Kylie, for just being amazing, cooking all the dinners and looking after me in that last few months, you're my best friend and I love you xx.

Thank you.

Table of Contents

Abstract	i
Acknowledgments	ii
Table of Contents	iii
List of Figures	2
List of Tables	5
Abbreviations	6

Chapter 1

1 Introduction	10
1.1 Cancer	11
1.2 Apoptosis and necrosis	12
1.3 Caspases	13
1.3.1 Initiator caspases	13
1.3.2 Executioner caspases	15
1.4 Apoptotic pathways	16
1.4.1 Intrinsic apoptotic cell death	16
1.4.2 Extrinsic apoptotic cell death	19
1.4.3 Necroptosis	21
1.5 Cancer metabolism	22
1.5.1 Inhibitors of GLUT's	26
1.5.2 2-deoxy-D-glucose-mediated inhibition of glycolysis	27
1.6 Galactose metabolism	28
1.7 Mitochondrial oxidative phosphorylation	29
1.8 Signal transduction	32
1.8.1 AMP-activated protein kinase (AMPK)	32
1.8.2 Protein kinase B (Akt)	35
1.8.3 Cross talk into apoptotic and survival signalling	36
1.9 mTOR signalling and protein translation	37
1.1 Aims	40

Chapter 2

2 Materials and Methods	42
2.1 Materials	43
2.2 Methods	44
2.2.1 Tissue culture	44
2.2.2 Induction of apoptosis	45
2.2.3 Measuring apoptosis	46
2.2.4 Whole cell protein expression	46
2.2.5 Preparing cell lysates	47
2.2.6 Determining protein concentration	47
2.2.7 Immunoblotting	47
2.2.8 Detection of mitochondrial superoxide	49
2.2.9 siRNA transient nucleofection	49
2.2.10 Polysome profiling	50
2.2.11 Assessment of global protein synthesis: [³⁵S] methionine cysteine incorporation and trichloroacetic acid (TCA) protein precipitation	51
2.2.12 Extracellular flux analysis	52
2.2.13 ATP levels	53
2.3 Immunopurification of mitochondria for mass spectrometry	53
2.3.1 Subcellular fractionation	53
2.3.2 Immobilising antibodies	54
2.3.3 Cross-linking	54
2.3.4 Immunoprecipitation	54
2.4 Mass spectrometry	55
2.4.1 Sample preparation	55
2.4.2 Mass spectrometry analysis	56
2.4.3 Database search and protein identification	56
2.4.4 Label free quantitation using TransOmics	56
2.4.5 Ingenuity pathway analysis	57

Chapter 3 - Glucose deprivation prevents UPN1 cells from switching to TRAIL-induced necroptosis	
3 Results chapter 1	58
3.1 Introduction	59
3.2 Results	61
3.2.1 Glucose deprivation alters the cell death phenotype in response to TRAIL treatment in a dose-dependent manner	61
3.2.2 Glucose deprivation alters the cell death phenotype in response to TRAIL within 3 h	63
3.2.3 The pan-caspase inhibitor zVAD.fmk does not completely block TRAIL-induced cell death in glucose^{+ve} cells	65
3.2.4 Glucose^{-ve} cells are unable to switch to TRAIL-induced necroptosis	67
3.2.5 Glucose deprivation induces minimal changes in whole cell protein expression of key anti- and pro-apoptotic proteins	69
3.2.6 Glucose^{-ve} UPN1 cells undergo mitochondrial metabolic reprogramming	70
3.2.7 Glucose deprived UPN1 cells generate an extracellular acidification rate independently of glycolysis	75
3.3 Discussion	77
Chapter 4 - 2DG rapidly and transiently activates a non-canonical AMPK signalling pathway potentiating intrinsic and extrinsic-induced cell death	
4 Results chapter 2	81
4.1 Introduction	82
4.2 Results	84
4.2.1 2DG rapidly sensitises Z138 cells to ABT-737	84
4.2.2 2DG rapidly sensitises Z138 cells to TRAIL	86
4.2.3 2DG results in metabolic reprogramming – transiently increasing oxidative phosphorylation while ablating	88

glycolysis	
4.2.4 2DG induces a rapid reduction in expression of Mcl-1	92
4.2.5 2DG results in AMPK- α T172 de-phosphorylation and Akt S473 phosphorylation	95
4.2.6 2DG treatment induces a rapid AMPK activation event	97
4.2.7 2DG results in Akt de-phosphorylation before hyper-phosphorylation	99
4.2.8 2DG rapidly inhibits global protein synthesis	102
4.2.9 Canonical AMPK activators do not induce phosphorylation of AMPK- α T172	104
4.2.10 Inhibition of AMPK kinase CaMKK- β with STO-609 and transient knockdown of LKB1 does not prevent 2DG-mediated phosphorylation of AMPK- α T172	108
4.3 Discussion	110
4.3.1 2DG rapidly reprograms metabolism and sensitises Z138 cells to apoptosis	110
4.3.2 2DG activates both AMPK and Akt	112
Chapter 5 - Galactose grown cells as an <i>in vitro</i> model for investigating drug-induced mitochondrial toxicity	
5 Results chapter 3	116
5.1 Introduction	117
5.2 Results	119
5.2.1 Galactose ^{+ve} Z138 cells undergo metabolic reprogramming	119
5.2.2 Oligomycin may induce non-canonical programmed cell death in galactose ^{+ve} cells	124
5.2.3 Rotenone induces necrosis in galactose ^{+ve} cells	124
5.2.4 Antimycin induces necrosis in galactose ^{+ve} cells	126
5.2.5 Galactose ^{+ve} cells are less sensitive to respiratory chain inhibition	128

5.2.6 Phenformin induces necrosis in galactose ^{+ve} cells	131
5.2.7 Galactose ^{+ve} cells are less sensitive to TRAIL-induced cell killing, and have a limited capacity to switch to TRAIL-induced necroptosis	132
5.2.8 Galactose ^{+ve} cells are less sensitive to the Bcl-2/Bcl-x _L inhibitor ABT-737.	137
5.2.9 Etoposide induces necrosis at low concentrations in galactose ^{+ve} cells	139
5.2.10 Characterisation of the mitochondrial proteome by label-free quantitative mass spectrometry	141
5.2.11 Ingenuity analysis predicts Akt survival signalling is switched on in galactose ^{+ve} cells	145
5.2.12 Galactose ^{+ve} cells have elevated basal superoxide levels and are less able to convert glucose to lactic acid.	148
5.3 Discussion	152
5.3.1 The mode of cell death, not the degree, appears to be critical for identifying drug-induced mitochondrial toxicity	152
5.3.2 The mitochondrial proteome can accurately be evaluated by mass spectrometry	156
Chapter 6 - Final Discussion	
6 Final Discussion	159
6.1 Overview	160
6.2 Metabolism and (programmed) necrosis	160
6.3 Targeting cancer cell metabolism as a therapeutic strategy	163
6.4 Future work	165
7 Appendix	167
8 References	179

List of Figures

Chapter 1 - Introduction

Figure 1-1 Initiator caspases.....	13
Figure 1-2 Executioner caspases.....	14
Figure 1-3 Bcl-2 family members and their respective binding partners.....	16
Figure 1-4 Models of intrinsic apoptosis.....	17
Figure 1-5. Extrinsic death receptor mediated cell death and intrinsic mitochondrial mediated cell death.....	19
Figure 1-6 TRAIL-induced necroptosis.....	21
Figure 1-7 Sugar metabolism.....	23
Figure 1-8 Mitochondrial oxidative phosphorylation.....	29
Figure 1-9 AMPK subunit structures.....	32
Figure 1-10 The functions of AMPK.....	33
Figure 1-11 AMPK and Akt regulation of protein translation.....	37

Chapter 3 - Glucose deprivation prevents UPN1 cells from switching to TRAIL-induced necroptosis

Figure 3-1 Glucose deprivation alters the cell death phenotype in response to TRAIL treatment in a dose-dependent manner.....	61
Figure 3-2 Glucose deprivation alters the cell death phenotype in response to TRAIL within 3 h.....	63
Figure 3-3 Caspase inhibition does not completely block TRAIL-induced cell death in glucose ^{+ve} UPN1 cells.....	65
Figure 3-4 Metabolic reprogramming prevents UPN1 cells from switching to TRAIL-induced necroptosis.....	67
Figure 3-5 Metabolic reprogramming induces minimal changes in key pro- and anti-apoptotic proteins.....	69
Figure 3-6 Representative examples of bioenergetics data obtained from a Seahorse XF24 analyser.....	71

Figure 3-7 Glucose deprivation results in metabolic reprogramming of UPN1 cells.	72
Figure 3-8 Schematic representation of changes that occur as a result of glucose deprivation.....	79

Chapter 4 - 2DG rapidly and transiently activates a non-canonical AMPK signalling pathway potentiating intrinsic and extrinsic-induced cell death

Figure 4-1 2DG rapidly sensitises Z138 cells to ABT-737.....	84
Figure 4-2 2DG rapidly sensitises Z138 cells to TRAIL.....	86
Figure 4-3 2DG treatment induces metabolic reprogramming in Z138 cells	88
Figure 4-4 2DG rapidly reduces expression of Mcl-1 but not other Bcl-2 family members	92
Figure 4-5 2DG results in AMPK de-phosphorylation and Akt phosphorylation	95
Figure 4-6 2DG induces a rapid and transient AMPK event.....	97
Figure 4-7 2DG induces Akt de-phosphorylation before hyper-phosphorylation	99
Figure 4-8 2DG treatment rapidly reduces global protein synthesis.....	102
Figure 4-9 Traditional AMPK activators do not induce AMPK- α T172 phosphorylation.....	104
Figure 4-10 Inhibition of AMPK kinase CaMKK- β and knockdown of LKB1 does not prevent 2DG-mediated phosphorylation of AMPK- α T172	108
Figure 4-11 Model of the identified results following 2DG treatment.....	114

Chapter 5 - Galactose grown cells as an *in vitro* model for investigating drug-induced mitochondrial toxicity

Figure 5-1 Culturing Z138 cells in galactose induces metabolic reprogramming	119
Figure 5-2 Galactose ^{+ve} cells are sensitive to oligomycin-induced cell death.	123
Figure 5-3 Rotenone induces necrosis in galactose ^{+ve} cells.....	125

Figure 5-4 Antimycin induces necrosis in galactose ^{+ve} cells.....	127
Figure 5-5 Galactose ^{+ve} cells are less sensitive to respiratory chain inhibition.	128
Figure 5-6 Galactose ^{+ve} cells are sensitive to phenformin-induced cell death	131
Figure 5-7 Galactose ^{+ve} cells are less able to switch to TRAIL-induced necroptosis	133
Figure 5-8 ABT-737 induces apoptosis.	135
Figure 5-9 Etoposide induces necrosis at low concentrations in galactose ^{+ve} cells	137
Figure 5-10 Principal component analysis from the mitochondrial proteome data	139
Figure 5-11 Mass spectrometry analysis of immunopurified mitochondria can identify 76% of the proteins involved in oxidative phosphorylation.....	140
Figure 5-12 Proteins in the mitochondrial respiratory chain are up-regulated in galactose ^{+ve} Z138 cells.....	141
Figure 5-13 Quantitative label-free mass spectrometry can accurately predict changes in the protein expression from the mitochondrial proteome	143
Figure 5-14 Ingenuity can accurately predict signal transduction events from mitochondrial proteome data.....	144
Figure 5-15 Z138 cells cultured in galactose have elevated mitochondrial superoxide.....	145
Figure 5-16 Galactose ^{+ve} cells cannot divert as much glucose into lactic acid compared to glucose ^{+ve} cells.....	147
Figure 5-17. Schematic representation of a selection of changes in galactose ^{+ve} cells that were predicted by TransOmics coupled to Ingenuity™	148
Figure 5-18 Galactose ^{+ve} cells undergo necrosis when the mitochondria are compromised.....	155

Chapter 6 - Final Discussion

Figure 6-1 Glucose deprivation and galactose supplemented media inhibits TRAIL- induced necroptosis, and 2DG activates AMPK independently of LKB1 and CaMKK-β	158
---	-----

Chapter 7 - Appendix

Figure 7-1 Noxa has a half-life of ~30 min	165
Figure 7-2 AMPK activators do not activate AMPK in Z138 cells	166
Figure 7-3 AMPK activators do not sensitise Z138 cells to TRAIL or ABT-737167	
Figure 7-4 AMPK inhibition with compound C is toxic to Z138 cells.....	168
Figure 7-5 Insulin receptor tyrosine kinase inhibition does not prevent Akt activation following 2DG treatment.....	169
Figure 7-6 Z138 cells cultured in both glucose and galactose are resistant to metformin.	170
Figure 7-7 ABT-737 inhibits the mitochondrial respiratory chain	171
Figure 7-8 Ingenuity™ can successfully predict the activation status of signal transduction pathways	172
Figure 7-9 Proteins involved in protein synthesis are down-regulated	175

List of Tables

Chapter 2 – Materials and Methods

Table 2.1 Table detailing all primary antibodies used for immunoblotting	47
Table 2.2 Table detailing all secondary antibodies used for immunoblotting ...	48

Chapter 7 - Appendix

Table 7-1 An example of the data Ingenuity uses to predict activation or inhibition of 1 protein.	174
--	-----

Abbreviations

ACC	Acetyl Coenzyme A Carboxylase
ADP	Adenosine diphosphate
ADP	Adenosine diphosphate
AIF	Apoptosis inducing factor
Akt	Protein kinase B
AMP	Adenosine monophosphate
AMPK	AMP-activated protein kinase
ANT	Adenine nucleotide translocator
Apaf-1	Apoptotic protease activating factor 1
ATP	Adenosine triphosphate
Bad	Bcl2-associated agonist of cell death
Bak	Bcl-2 homologous antagonist/killer
Bax	Apoptosis regulator Bax
Bcl-2	B-cell lymphoma 2
Bcl-b	Bcl-2-like protein 10
Bcl-w	Bcl-2-like protein 2
Bcl-xL	B-cell lymphoma extra large
Bid	BH3-interacting domain death agonist
Bik	Bcl-2-interacting killer
Bim	Bcl2-interacting mediator of cell death
Bmf	Bcl-2-modifying factor
Bok	Bcl-2-related ovarian killer protein
BSA	Bovine serum albumin
CARD	caspase recruitment domain
Caspase	Cysteine-dependant aspartyl specific proteases
CCND1	Cyclin D1
CHX	Cycloheximide
Complex I	NADH dehydrogenase
Complex II	Succinate dehydrogenase
Complex III	Cytochrome c oxidoreductase

Complex IV	Cytochrome c oxidase
CR	Complete remission
DD	Death domain
DED	Death effector domain
Deptor	DEP domain containing mTOR-interacting protein
DISC	Death inducing signalling complex
DMEM	Dulbecco's Modified Essential Medium
DMSO	Dimethyl Sulphoxide
DNA	Deoxyribonucleic acid
ECAR	Extracellular acidification rate
ECL	Enhanced chemiluminescence
EDTA	Ethylenediaminetetraacetic Acid
eIF4	Eukaryotic initiation factor 4
ER	Endoplasmic reticulum
ETC	Electron transport chain
FACS	Fluorescence activated cell sorting
FADD	Fas-associated protein with death domain
FCCP	Carbonyl cyanide-4-(trifluoromethoxy)phenylhydrazone
FDG-PET	(¹⁸ F)fluoro-D-glucose positron emission tomography
FITC	Fluorescein isothiocyanate
FSC	Forward Scatter Channel
G6P	Glucose-6-phosphate
GK	Glucokinase
GLUT	Glucose transporters
GSK-3 β	Glycogen synthase kinase-3 β
HEPES	(4-(2-hydroxyethyl)-1-piperazineethanesulfonic acid)
HIF	Hypoxia inducible factor
Hrk	Activator of apoptosis harakiri
IGHV	Immunoglobulin heavy chain variable region
IKK	I kappa B kinase
IMS	Inter membrane space
LKB1	Liver kinase B1 homolog
MCL	Mantle cell lymphoma

Mcl-1	Myeloid cell leukaemia 1
MDM2	E3 ubiquitin-binding ligase Mdm2
MLKL	Mixed lineage kinase domain like protein
MOMP	Mitochondrial outer membrane permeabilisation
mSin1	Mitogen-activated protein kinase 2-associated protein 1
mTOR	Mammalian target of rapamycin
NAD	Nicotinamide adenine dinucleotide
NADP	Nicotinamide adenine dinucleotide phosphate
Nec-1	Necrostatin 1
Noxa	Phorbol-12-myristate-13-acetate-induced protein 1
OCR	Oxygen consumption rate
Omi	Serine protease HTRA2, mitochondrial
OPG	Osteoprotegerin
PAGE	Polyacrylamide Gel Electrophoresis
PBS	Phosphate Buffered Saline
PDE3B	Phosphodiesterase 3B
PFK1	Phosphofructokinase 1
PFK2	Phosphofructokinase 2
PI	Propidium iodide
Pi	Phosphate
PI3K	phosphatidylinositol 3-kinase
PIP	Phosphatidylinositol phosphate
PPP	Pentose phosphate pathway
PRAS40	Proline rich Akt substrate of 40 kDa
Protor	Protein observed with Rictor
PS	Phosphatidyl serine
Puma	p53 up-regulated modulator of apoptosis
Raptor	Regulatory-associated protein of mTOR
R-hyper- CVAD	hyperfractionated cyclophosphamide, vincristine, Adriamycin and dexamethasone
Rictor	Rapamycin-insensitive companion of mTOR
RIPK	Receptor interacting kinase
RNA	Ribonucleic acid

ROS	Reactive oxygen species
RPM1	Roswell Park Memorial Institute
SAPK	Stress-activated protein kinase
Smac	Diablo homolog, mitochondrial
SNP	Single nucleotide polymorphism
SOX11	Transcription factor SOX-11
tBid	Truncated Bid
TCA	Tricarboxylic acid cycle
TNF	Tumour necrosis factor
TRAF2	TNF receptor-associated factor 2
TRAIL	TNF-related apoptosis-inducing ligand
TSC1	Tuberous Sclerosis 1
TSC2	Tuberous Sclerosis 2
UBF1	upstream binding factor 1
UCP	uncoupler protein
UDP	Uridine diphosphate
UPR	Unfolded protein response
UTP	Uridine triphosphate
zVAD.fmk	Carbobenzoxy-Val-Ala-Asp-(O-methyl)-fluoromethylketone
µg	microgram
µl	microlitre
µM	micromolar
2DG	2-Deoxy-D-glucose
2DG-6-P	2-Deoxy-D-glucose-6-phosphate
4EBP	Eukaryotic translation initiation factor 4E binding protein

1 Introduction

1.1 Cancer

Cancer is a blanket term for a plethora of highly invasive and aggressive related diseases, in 2012 there was 14.1 million new reported cases of cancer globally, and 8.2 million deaths (Ferlay *et al.*, 2015). All cancers undergo uncontrollable rapid growth and proliferation (hyperplasia and hypertrophy), that does not stop and spreads into surrounding tissues and frequently metastasise to other areas of the body; with increasing time the tumour cells become more abnormal, and do not die when they should (reviewed in Evan & Vousden, 2001). They can originate from genetic mutations as result of exposure to external agents/stimuli or from inherited genetic lesions (reviewed in Stratton *et al.*, 2009). Most cancers form solid tumours, generating a large mass of poorly differentiated unspecialised tissues that are highly resistant to chemotherapeutic approaches (reviewed in Minchinton & Tannock, 2006). However, some cancers are 'liquid', for example leukaemia's and lymphomas of the blood, and do not form solid tumours. One such cancer type is a non-Hodgkin's lymphoma, mantle cell lymphomas (MCL), a heterogeneous disease, which recently has been shown to develop from two distinct molecular pathways, resulting in two different subtypes (Navarro *et al.*, 2012; Jares *et al.*, 2012). The first and most common is characterised by the acquisition of a genetic translocation $t(11;14)(q13;q32)$ in pre-B-cells in the bone marrow. Upon maturation and entering the periphery lymphoid organs these cells do not enter the follicular germinal centre; they have limited or no *IGHV* somatic mutations and express SOX11, they are genetically unstable and result in an aggressive cancer (Jares *et al.*, 2012; Navarro *et al.*, 2012). The second, rare subtype, also harbour the $t(11;14)$, however they overexpress *CCND1* and harbour many *IGHV* somatic hyper-mutations. This subtype is stable and can present as asymptomatic for long periods of time. However, acquisition of additional mutations (e.g. P53) results in the disease becoming extremely aggressive (Navarro *et al.*, 2012; Jares *et al.*, 2012).

Regardless of subtype, MCL tends to be a disease of elderly individuals, and presents one of the worst clinical outcomes for all lymphoma types – and remains largely incurable (Ghielmini & Zucca, 2009). Following relapse there is no standard of care in place and managing the disease is challenging; the current treatment

decision is based on patient age and fitness (reviewed in Campo & Rule, 2015). In the last decade cytarabine based therapies for younger patients have been used and the front line therapy is R-HyperCVAD alternating with high-dose methotrexate/cytarabine alternating with rituximab high-dose methotrexate/cytarabine, these highly aggressive treatment regimens are often not completed due to the age and frailty of the individuals (Campo & Rule, 2015). There are currently 4 new drugs licensed for MCL across Europe and America, namely, ibrutinib, bortezomib, lenalidomide and temsirolimus. Despite these new drugs passing clinical trials and acquiring a licence for use, the percentage of complete remission (CR) is still low; the highest is 21% for ibrutinib, while the CR for temsirolimus is only 2% (Campo & Rule, 2015). Therefore, it is apparent that a greater understanding of the pathways that regulate MCL and why they are so resistant to chemo-therapeutics is required to overcome the drug-resistance in order to develop more successful therapeutic strategies.

1.2 Apoptosis and necrosis

Apoptosis is an evolutionary conserved system for controlled cellular suicide and was first described in a seminal paper in 1972 (Kerr *et al.*, 1972). Apoptosis is a non-inflammatory mode of cell death, which is distinct from necrosis which is inflammatory (Rock & Kono, 2008). Cells undergoing apoptosis go through an ordered sequence of events resulting in an altered morphology (Saraste & Pulkki, 2000). The cells shrink alongside pyknosis (irreversible condensation of chromatin); from there they undergo membrane blebbing and karyorrhexis (the fragmentation of the nucleus) (Saraste & Pulkki, 2000). These events result in the 'budding' of apoptotic bodies which contain cytoplasm and organelles; with and without nuclear fragments, which are subsequently phagocytosed by macrophages, parenchymal cells or neoplastic cells and degraded in phagolysosomes (reviewed in Elmore, 2007). Apoptosis and mitosis function together in equilibrium to tightly regulate the number of cells in multi-cellular organisms (Topham & Taylor, 2013). Deregulation of this equilibrium results in a number of adverse pathological conditions, for example, too much apoptosis results in neurodegeneration or autoimmune diseases, while not enough leads to the development of cancer (Topham & Taylor, 2013).

Conversely, necrosis is an unstructured, un-programmed form of cell death that results in an inflammatory response (Rock & Kono, 2008). Unlike apoptotic cells, necrotic cells initially swell, a process referred to as oncosis (cell death by swelling), which occurs concomitantly with the clumping of nuclear chromatin and plasma membrane blebbing. Necrosis is the endpoint phenotype, whereby the cells plasma membrane loses integrity and ruptures resulting in cytosolic spill-out into the interstitial tissues resulting in inflammation (Majno & Joris, 1995).

1.3 Caspases

During apoptosis a vast array of morphological alterations occur and these cellular changes are primarily mediated by proteins called caspases (Cysteine-dependent aspartyl specific proteases) (reviewed in Parrish *et al.*, 2013). The active site, GACXG is a pentapeptide sequence common between all caspases where X is R, Q or G (Wilson *et al.*, 1994; Fuentes-Prior & Salvesen, 2004). They function by cleaving a plethora of cellular substrates by recognising a tetrapeptide site P₄, P₃, P₂ and P₁ (Talanian *et al.*, 1997; Thornberry *et al.*, 1997; Stennicke *et al.*, 2000). Processing of caspase substrates can either inhibit or activate the target molecule. Caspases involved in apoptosis have been classified into two distinct groups, these being the initiator caspases and the effector caspases (McIlwain *et al.*, 2013).

1.3.1 Initiator caspases

Initiator caspases comprise caspases-8, -9 and -10, and they normally exist in the cell as monomeric zymogens that contain a long N-terminal pro-domain (Donepudi & Grutter, 2002). In the case of caspase-8 and caspase-10 the pro-domain contains two death effector domains (DED's), while caspase-9 contains a caspase recruitment domain (CARD) (reviewed in Park, 2012). Initiator caspases additionally contain a large subunit and small subunit (Figure 1-1). Following an activation signal, they undergo proximity-driven dimerization and recruitment to adaptor molecules at multi-protein activating complexes (Parrish *et al.*, 2013; Boatright & Salvesen, 2003). In the case of caspase-8, this alone results in catalytically active caspase-8 molecules with a restricted substrate repertoire (Hughes *et al.*, 2009). Full activation of caspase-8 is achieved by autocatalytic cleavage at both D374 and D384, resulting in an increased substrate repertoire (Hughes *et al.*, 2009).

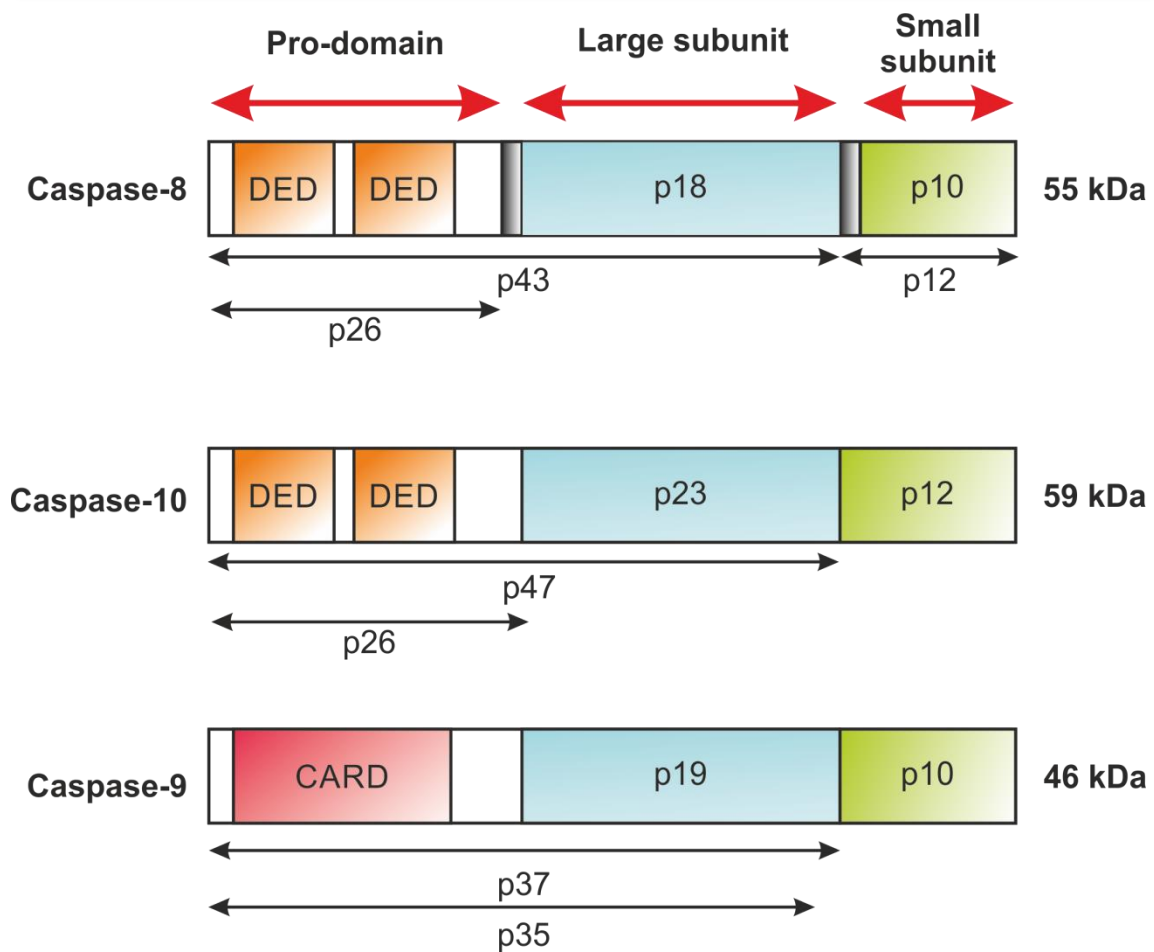


Figure 1-1 Initiator caspases. Caspase-8, -10 and -9 are present as monomeric zymogens in the cell. They each contain a long pro-domain at the N terminus, which for caspase-8 and -10 has two DEDs and for caspase-9 has a CARD domain. They all contain a large subunit (blue) and a small subunit (green). In the case of caspase-8 these are separated by linker regions (black). These proteins absolutely require dimerization and cleavage at their respective activating complexes for full activation.

There are at least 8 isoforms of caspase-8 that have been identified and the most abundant are caspase-8a (55 kDa) and caspase-8b (53 kDa) (Scaffidi *et al.*, 1997). Following activation of the extrinsic pathway by binding of death ligands to the cognate transmembrane death receptor, caspase-8 is recruited to the death inducing signalling complex (DISC) and activated, thus allowing the processing and activation the executioner caspases (Hughes *et al.*, 2009; Dickens *et al.*, 2012a; Parrish *et al.*, 2013).

In addition to caspase-8, caspase-10 can also bind into the native TRAIL and CD95 DISC via its N-terminal DEDs in a FADD dependent manner and process executioner caspases (Kischkel *et al.*, 2001). Caspase-10 has a similar structure to

that of caspase-8 (Figure 1-1), and although it can bind into the DISC, it may not be able to functionally substitute for caspase-8 (Sprick *et al.*, 2002).

Caspase-9 is the initiator caspase of the intrinsic (mitochondrial) apoptotic pathway (Wurstle *et al.*, 2012). It is similar in structure to caspase-8 and caspase-10, although instead of DEDs it has a CARD domain that allows it to bind into a multiprotein complex called the apoptosome (Cain *et al.*, 2002; Acehan *et al.*, 2002)

1.3.2 Executioner caspases

Executioner caspases includes caspases-3, -6 and -7 and exist as dimeric zymogens under physiological conditions (Donepudi & Grutter, 2002). The dimerization step is completed upon their synthesis; therefore activation requires only minimal proteolytic cleavage in the linker region (Figure 1-2). The proteolytic activity of executioner caspases is restrained by the short linker region that connects the small and large subunits in the catalytic domain (Parrish *et al.*, 2013). Processing of the linker region by initiator caspases, results in a conformation change favouring exposure of the executioner caspases active site (Boatright &

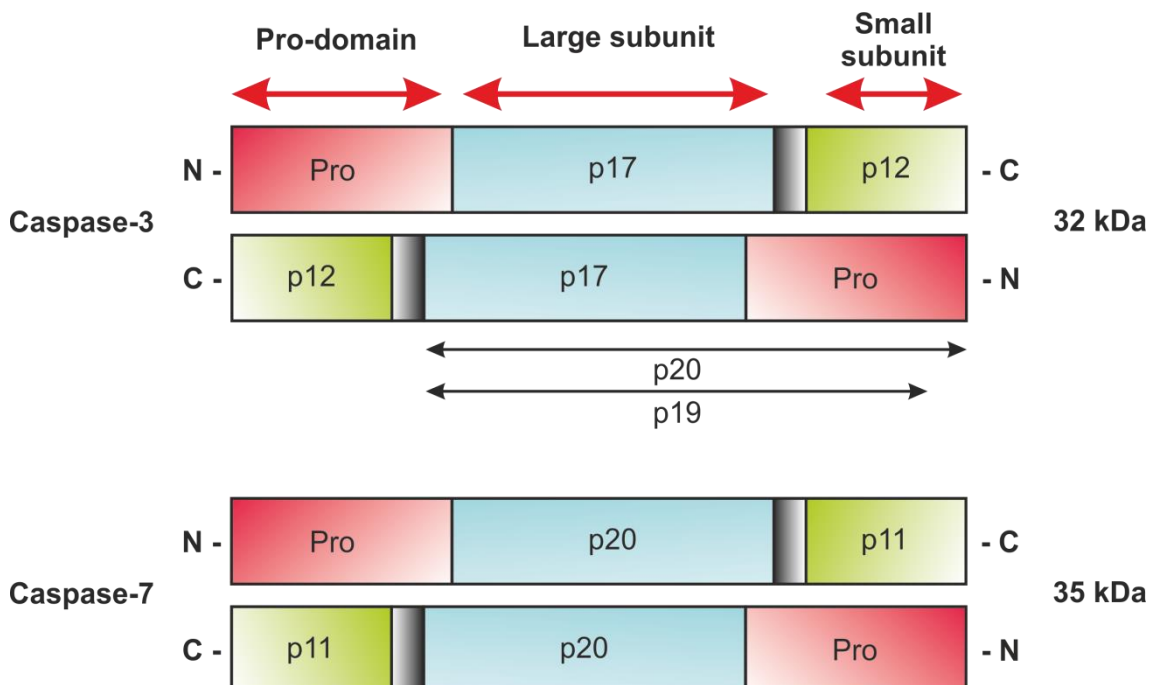


Figure 1-2 Executioner caspases. The executioner caspase-3 and -7 are formed as inactive dimers. Proteolysis by the initiator caspases in the linker region (black) results in full activation and subsequent initiation of apoptosis. They contain a short pro-domain (red), a large subunit (blue) and a small subunit (green).

Salvesen, 2003). Caspase-3 is a 32 kDa protein which has a short pro-domain and two subunits, the large p17 and small p12 (Figure 1-2). It was first identified by sequence homology to the Ced-3 (caspase in the nematode worm) (Fernandes-Alnemri *et al.*, 1994) and subsequently recognised as being a critical caspase in the disassembling of the cell in 1995 (Nicholson *et al.*, 1995). Caspase-7 is a 35 kDa protein that is also synthesised as a dimeric zymogen (Riedl *et al.*, 2001). It contains a short pro-domain with the large p20 and small p11 subunits (Figure 1-2) and is processed in the same way as caspase-3 (Riedl *et al.*, 2001).

1.4 Apoptotic pathways

1.4.1 Intrinsic apoptotic cell death

The intrinsic or mitochondrial cell death pathway leads to apoptosis by activation from a plethora of stimuli, which include: DNA Damage; genotoxic stress; viral infection; cytokines, survival and growth factor withdrawal (Tait & Green, 2010). In addition to this, chemotherapeutic drugs have been specifically designed to activate the intrinsic cell death pathway, for example, the clinically relevant ABT-263 (Davids & Letai, 2012). These stimuli result in cellular stress that disrupts the balance of mitochondrial associated pro- and anti-apoptotic proteins (reviewed in Billard, 2013). A super-family known as the Bcl-2 family of proteins, comprise a range of proteins that can be classified into three main categories, these being the anti-apoptotic; pro-apoptotic and BH3 only proteins (reviewed in Shamas-Din *et al.*, 2013). Anti-apoptotic proteins comprise: Bcl-2; Bcl-x_L; Mcl-1; Bcl-w; Bcl-b and Bcl-2A1 (Youle & Strasser, 2008). Pro-apoptotic Bcl-2 family proteins consist of: Bax; Bak and Bok; it is Bax and Bak that appear to be critical for initiating mitochondrial outer membrane permeabilisation (MOMP) (Youle & Strasser, 2008). The third class; BH3 only proteins, is the largest class, which are also pro-apoptotic in function, this class consists of: Bid; Bad; Bik; Hrk; Bim; Bmf; Noxa and Puma (see Figure 1-3) (reviewed in Happonen *et al.*, 2012). These proteins possess a conserved BH3 domain and they function to regulate the activity of anti-apoptotic Bcl-2 family members (reviewed in Happonen *et al.*, 2012). Under normal cellular conditions, anti-apoptotic Bcl-2 proteins bind to Bax and Bak and repress their pro-apoptotic activity. In the presence of cellular stress however, BH3 only proteins de-repress Bax and Bak by sequestering/inhibiting anti-apoptotic Bcl-2 family proteins (Youle & Strasser, 2008)

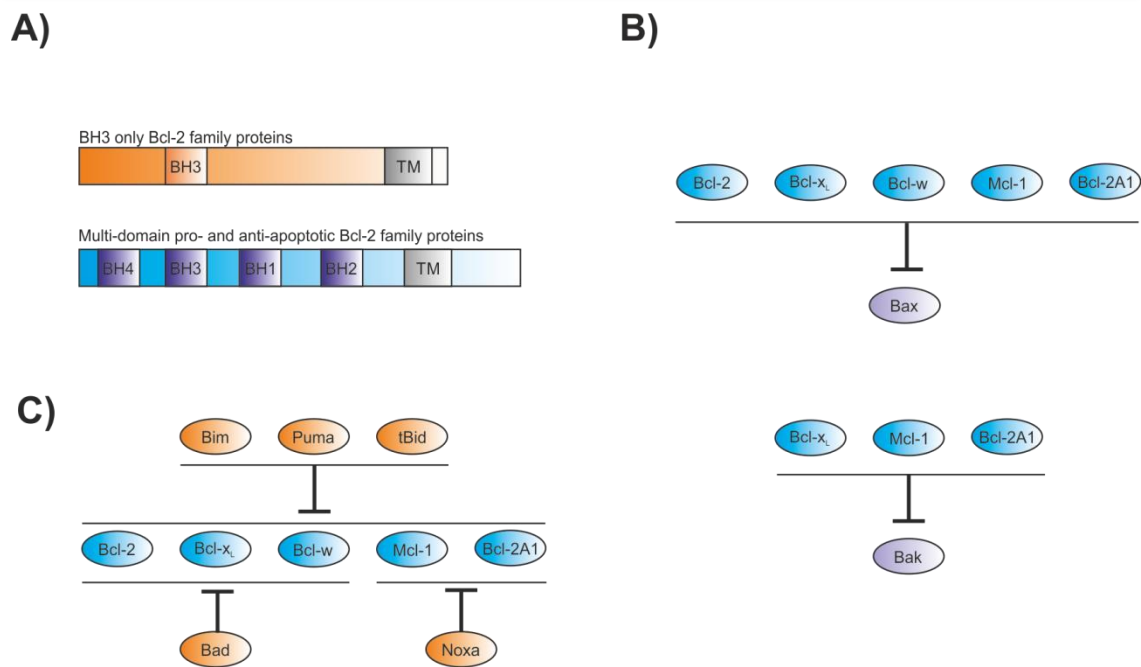


Figure 1-3 Bcl-2 family members and their respective binding partners. A) BH3 only Bcl-2 family members only contain the BH3 and transmembrane (TM) domains, while all other Bcl-2 family members contain BH1-4. **B)** All anti-apoptotic Bcl-2 family proteins can bind to Bax, while only Bcl-x_L, Mcl-1 and Bcl-2A1 can bind to Bak. **C)** Bim, Puma and tBid can engage all anti-apoptotic Bcl-2 proteins, while Bad and Noxa appear to have specific binding affinities. Schematic modified from Czabotar *et al.*, 2014

There are currently two models of intrinsic apoptosis induction; the direct activation model, which proposes that certain BH3 only proteins, namely, tBid, Bim and Puma directly engage and activate Bax and Bak resulting in Bak/Bax oligomerisation (Letai *et al.*, 2002; Kuwana *et al.*, 2005; Certo *et al.*, 2006). Other BH3 only proteins that do not possess this direct action binding affinity are called sensitisers (such as Bad), and in the direct model of activation function to dissociate anti-apoptotic Bcl-2 members from direct BH3 activators, thus liberating them for engaging Bak/Bax and subsequent engagement of MOMP (Figure 1-4) (reviewed in Czabotar *et al.*, 2014).

In the second indirect model of activation, anti-apoptotic Bcl-2 proteins sequester Bak and Bax (Chen *et al.*, 2005; Willis *et al.*, 2005; Willis *et al.*, 2007). This model proposes that BH3 only proteins bind to the anti-apoptotic proteins, thus liberating Bak to 'spontaneously' permeabilise the outer mitochondrial membrane; also freeing Bax to subsequently translocate to outer mitochondrial membrane and also induce MOMP (Figure 1-3) (reviewed in Czabotar *et al.*, 2014).

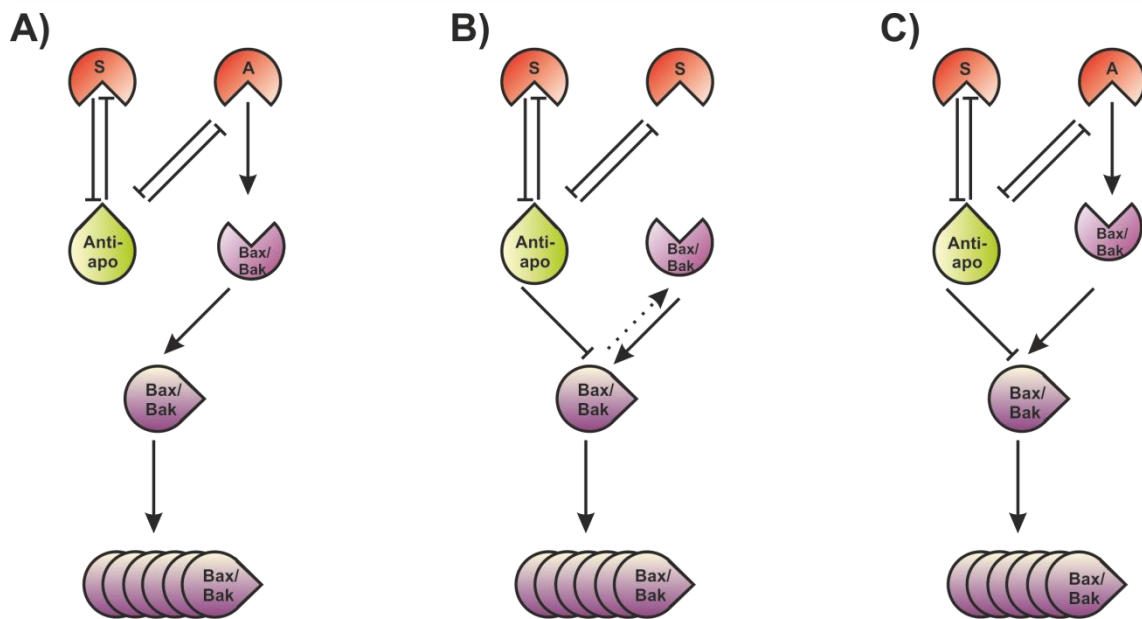


Figure 1-4 Models of intrinsic apoptosis. In this scheme, modified from Czabotar *et al.*, 2014, there are three models. **A)** The direct activation model states that BH3 activator proteins (denoted as A in red) directly activate Bak and Bax. Activator BH3 only proteins are sequestered by anti-apoptotic Bcl-2 family members, and can be liberated from this association by the sensitiser BH3 only proteins (denoted as S in red) by sequestering the anti-apoptotic proteins thus freeing the activators to initiate apoptosis. **B)** The indirect activation model stipulates that Bak and Bax are already primed for apoptosis induction, and thus the anti-apoptotic proteins must bind to them inhibiting MOMP. In addition, anti-apoptotic proteins also bind to the BH3 only proteins. In this model it is the ratio of anti-apoptotic versus BH3 proteins that determines if apoptosis is engaged. The more BH3 only proteins to sequester the anti-apoptotic proteins the more likely Bax and Bak will be free to oligomerise and initiate MOMP. **C)** The unified model hypothesises that both A and B occur together, the anti-apoptotic proteins sequester and inhibit the BH3 only proteins, Bak and Bax, but additionally, certain BH3 only proteins when freed will directly activate Bak and Bax.

However, there is currently a lot of discussion about the probability that the two models are not mutually exclusive, and in fact, in certain circumstances, both models may apply, this is referred to as the unified model (Llambi *et al.*, 2011), whereby anti-apoptotic Bcl-2 proteins have to sequester both BH3 only proteins, Bax and Bak.

In essence, apoptotic stimulus results in Bax/Bak oligomerisation at the OMM, initiating the permeabilization of the OMM (Figure 1-5). This subsequently results in the release of soluble apoptogenic molecules from the mitochondrial inter-membrane space (IMS) into the cytosol (Hüttemann *et al.*, 2011). One such molecule, Cytochrome c, when released, results in the energy dependent oligomerisation of apoptosis protease activating factor-1 (Apaf-1), producing a

heptameric protein ring called the apoptosome (Cain *et al.*, 2002). The apoptosome complex binds to monomeric caspase-9 resulting in cleavage and formation of a holoenzyme complex that facilitates caspase-9 dimerisation and activation (Renatus *et al.*, 2001). Active caspase-9 then cleaves and activates executioner caspase-3 and caspase-7 to promote apoptosis. At this stage, apoptosis can be inhibited by X chromosome-linked inhibitor of apoptosis (XIAP), a protein that can bind to processed caspases-3, -7 and -9 by a two-site binding mechanism (reviewed in Berthelet & Dubrez, 2013). Binding of XIAP to caspases not only inhibits their enzymatic activity but can induce K48 ubiquitination of caspase-3, thus targeting it for proteasome degradation (reviewed in Marivin *et al.*, 2012). To ensure caspases are not inhibited by XIAP, negative regulators of IAPs are released during MOMP from the IMS into the cytosol. SMAC and OMI bind to IAPs to positively regulate caspase activity (Martins *et al.*, 2002).

1.4.2 Extrinsic apoptotic cell death

An alternative apoptotic pathway is the extrinsic or death receptor pathway (Figure 1-5) (reviewed in Dickens *et al.*, 2012b). This pathway is mediated by the Tumour Necrosis Factor (TNF) Superfamily, which currently consists of 27 ligands and 29 receptors in humans (reviewed in Bremer, 2013). Initiation of the extrinsic pathway results from extra-cellular binding of a ligand such as TNF-related apoptosis inducing ligand (TRAIL) to its cognate pre-associated homotrimeric extra-cellular transmembrane death-receptor (Holoch & Griffith, 2009). TRAIL is a type II transmembrane protein, which is cleaved from the cell membrane by metalloproteases (Walczak & Haas, 2008). Upon processing, the solubilized TRAIL forms homotrimers by interactions through their extracellular domain. TRAIL can bind to one of five receptors, known as: TRAIL-R1, -R2, -R3, -R4 and Osteoprotegerin (OPG) (MacFarlane *et al.*, 1997; MacFarlane, 2003).

It is only through binding to TRAIL-R1 and TRAIL-R2 that apoptosis is initiated (Holoch & Griffith, 2009). TRAIL-R3, -R4 and OPG are considered decoy receptors. Binding of TRAIL to the cognate homotrimeric receptors results in a conformational change on the intracellular face of the receptor, revealing the receptors' intracellular death domain (DD) (Holoch & Griffith, 2009). The exposed DD facilitates homotypic binding of adaptor molecule Fas-associated death domain (FADD) to the receptor.

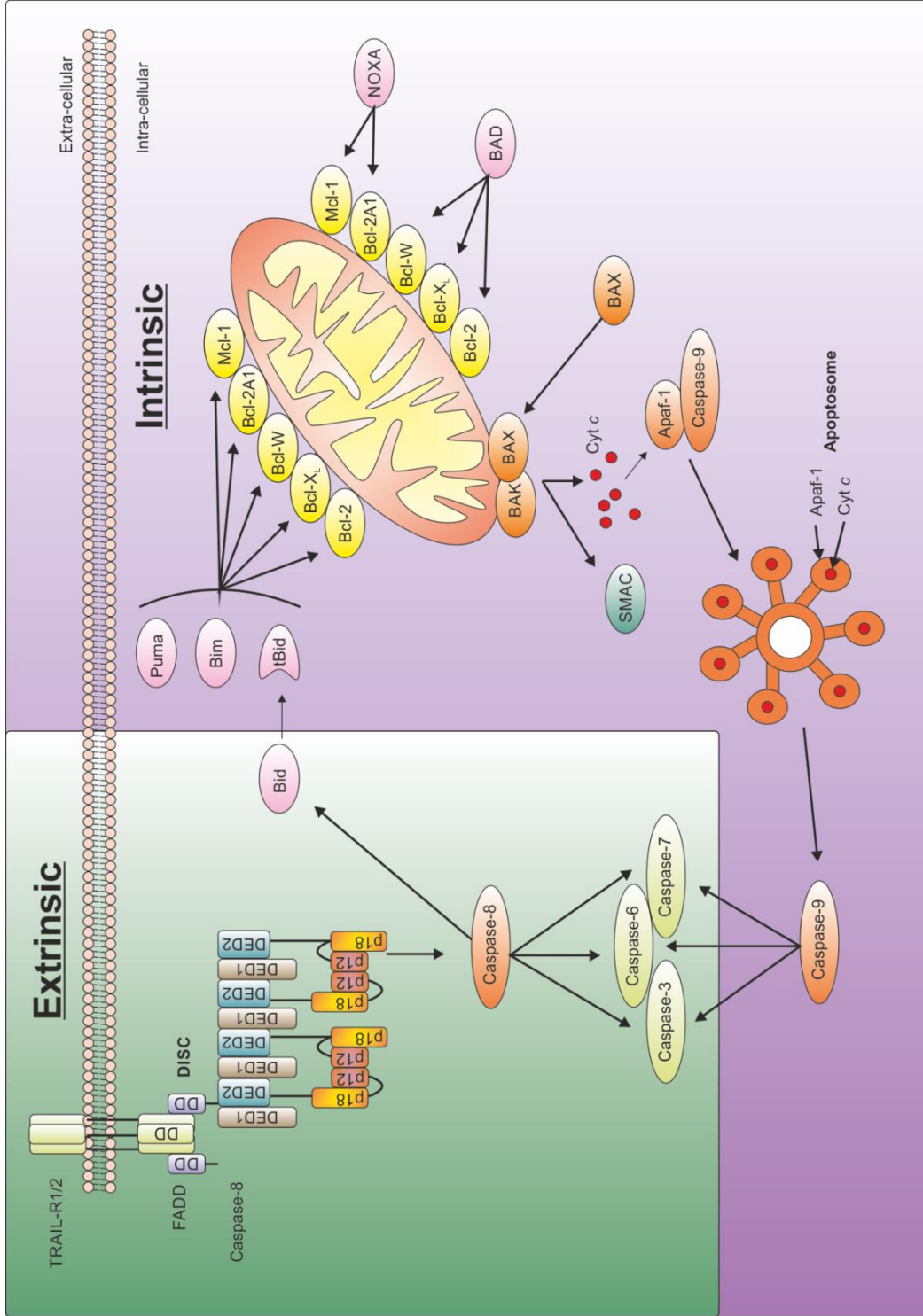


Figure 1-5. Extrinsic death receptor mediated cell death and intrinsic mitochondrial mediated cell death. The left panel (green) depicts TRAIL binding to its cognate death receptor, leading to the chaining of caspase-8 and subsequent activation. The right panel (purple) shows the Bcl-2 family proteins and their respective binding partners. Following a variety of stresses a subset of these proteins is activated to engage MOMP, releasing apoptogenic factors into the cytosol, leading to the apoptosome formation and activation of caspase-9

Caspase-8 can then be recruited to this scaffold by binding to FADDs' N-terminal death effector domain (DED) with its own, where chains of caspase-8 form (Dickens *et al.*, 2012a). This protein complex is referred to as the Death Inducing Signalling Complex (DISC) (Kischkel *et al.*, 1995). As mentioned previously, this death complex orchestrates caspase-8 dimerisation and pro-domain processing to release active caspase-8 dimers which cleave and activate effector caspases-3 and -7. In addition to this, the extrinsic cell death pathway can cross-talk with the mitochondrial pathway by caspase-8 mediated cleavage of Bid to tBid (Li *et al.*, 1998; Luo *et al.*, 1998). Bid is a BH3 only protein that is post-translationally activated by cleavage, and promotes apoptosis by avidly binding to Bcl-x_L, Bcl-w, Bcl-2A1 and Mcl-1; which subsequently leads to activation of Bax and Bak, thus resulting in permeabilization of the OMM, this process is referred to as the mitochondrial amplification loop (Youle & Strasser, 2008)

1.4.3 Necroptosis

Apoptosis was once considered the sole form of programmed cell death, however recent evidence suggests that certain types of necrosis are also tightly regulated processes, an example being 'necroptosis' (Han *et al.*, 2011). Necroptosis is thought to be an evolutionary conserved back-up mechanism, used to clear viral infections that can inhibit caspase-dependent apoptosis (Cho *et al.*, 2011; Kaiser *et al.*, 2013). Necroptosis is signalled through the necrosome, a multi-protein complex which contains receptor interacting protein-1 and -3 kinase (RIPK1 and RIPK3) (Li *et al.*, 2012) and the RIPK3 downstream target, mixed lineage domain-like (MLKL) protein (Sun *et al.*, 2012; Zhao *et al.*, 2012). RIPK-3 and MLKL are critically required for the engagement of necroptosis, although the mechanisms by which MLKL engages cell death is still unknown (reviewed in Linkermann & Green, 2014) (Figure 1-6). The necrosome is formed if caspase-8 is inhibited and cannot cleave and inactivate RIPK1 and RIPK3, thus allowing necroptosis to proceed in certain cell lines instead of apoptosis (Han *et al.*, 2011). Activation of necroptosis results in oncosis, and this leads to the rupture of the plasma membrane (necrosis); which appears to be mediated by the oligomerisation of activated MLKL proteins targeted to phosphatidyl inositol phosphates (PIP's) at the lipid rafts at the inner leaflet of the plasma membrane resulting in its permeabilisation and leakage of PIP containing liposomes (Dondelinger *et al.*, 2014). It is clear that necroptotic

signalling induces ionic fluxes across the plasma membrane, but whether this process is additionally dependent on plasma membrane channels is controversial. However, recent reports have shown that necroptosis induces an influx of Ca^{2+} ions (Cai *et al.*, 2014) and Na^+ ions and efflux of K^+ (Chen *et al.*, 2014), and that these events precede the incorporation of propidium iodide into the cell's DNA, which requires the loss of plasma membrane integrity (reviewed in Galluzzi *et al.*, 2014).

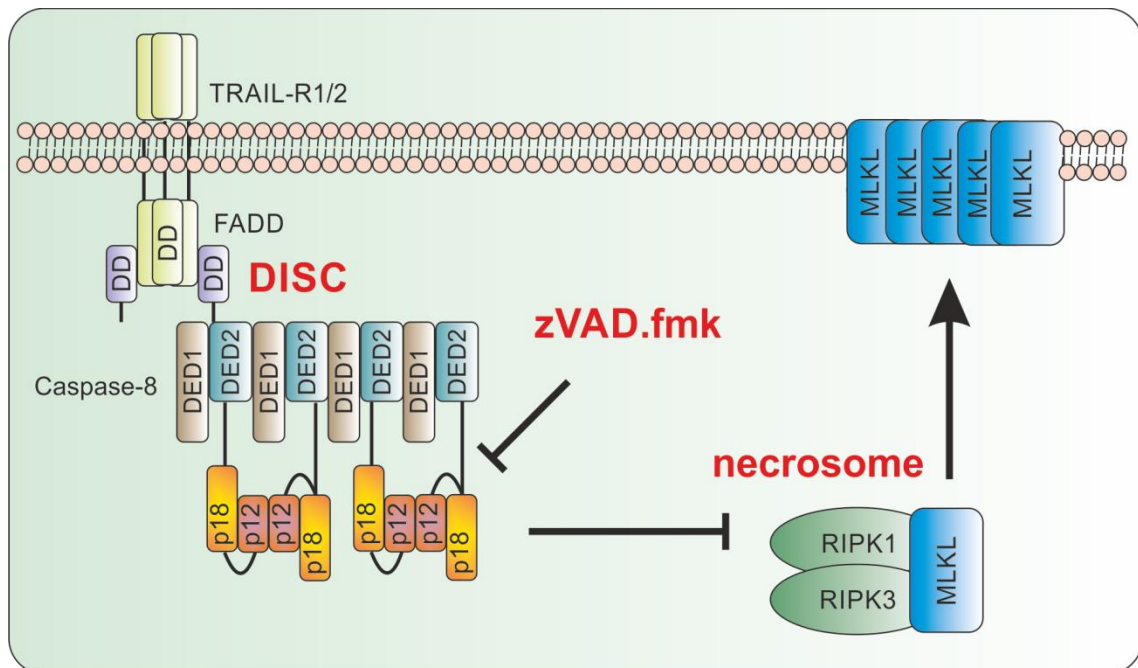


Figure 1-6 TRAIL-induced necroptosis. Inhibition of caspase-8 (by zVAD.fmk) results in the formation of the necrosome. This allows MLKL to oligomerise at the plasma membrane and induce cell-death through unknown mechanisms

1.5 Cancer metabolism

Otto Warburg first described a phenomenon whereby tumour cells forgo energetically favourable oxidative phosphorylation and instead utilise aerobic glycolysis, this process was subsequently termed the 'Warburg effect' (Warburg *et al.*, 1927; Warburg, 1956). There are many hypothesised reasons for the occurrence of the Warburg effect in tumourigenesis, and it is likely that many, if not all these suppositions are in fact correct. For example this phenomenon benefits the tumour microenvironment and may be a functional consequence of spatial heterogeneity in oxygen and nutrient availability within a solid tumour (reviewed in

Cantor & Sabatini, 2012). Cells residing on the outer portions of a tumour mass are spatially nearby existing vasculature and therefore have high accessibility to supplies of oxygen and nutrients, thus may undergo oxidative phosphorylation (Kianercy *et al.*, 2014). In contrast, tumour cells in the centre of the tumour proper are likely to be further away from vasculature if the process of angiogenesis and vasculogenesis has not occurred, and are therefore likely to display a glycolytic phenotype (reviewed in Boroughs & DeBerardinis, 2015). However, an alternate model proposes that there may be a symbiotic metabolic relationship between neighbouring tumour cells (Kianercy *et al.*, 2014). For example, hypoxic cells in the interior of the tumour proper may produce lactate through glycolysis, which is excreted and delivered in *trans* to adjacent tumour cells growing under normoxic conditions, and this lactate can be utilised for increased oxidative phosphorylation (Bensinger & Christofk, 2012; Boroughs & DeBerardinis, 2015).

The Warburg effect is considered a hallmark of cancer (reviewed in Hanahan & Weinberg, 2011; Hsu & Sabatini, 2008), and is vitally important for rapid tumour cell growth and proliferation. During rapid proliferation, cells produce increased amounts of reactive oxygen species (ROS) that can damage macromolecules, induce senescence and cause apoptosis (reviewed in Cairns *et al.*, 2011). Increased glucose metabolism has a two-fold benefit under these conditions, conversion of glucose to glucose-6-phosphate (G6P) is directed into the pentose phosphate shunt pathway (PPP) producing an increase in the production of: ribose sugars; glycerol and non-essential amino acids (Patra & Hay, 2014). Secondly, for every three G6P that enters the PPP, five: ATP, NADH and pyruvate are produced and importantly six nicotinamide adenine dinucleotide phosphate's (NADPH) are produced (reviewed in Tennant *et al.*, 2010) (Figure 1-7). NADPH is not only crucial for macromolecular biosynthesis, but serves as an antioxidant to protect against the aforementioned increased ROS levels (Gorrini *et al.*, 2013). Therefore high glycolytic flux functions to support tumour cell proliferation and protect from increased ROS, by the shunting of carbons to key subsidiary biosynthetic pathways (reviewed in Cairns *et al.*, 2011)

This enhanced demand for glucose is used diagnostically, where 2-deoxy-2-¹⁸F-fluoro-D-glucose (FDG), a non-metabolisable glucose analogue is used in FDG-PET scanning to visualise tumours (Gambhir, 2002). This increased

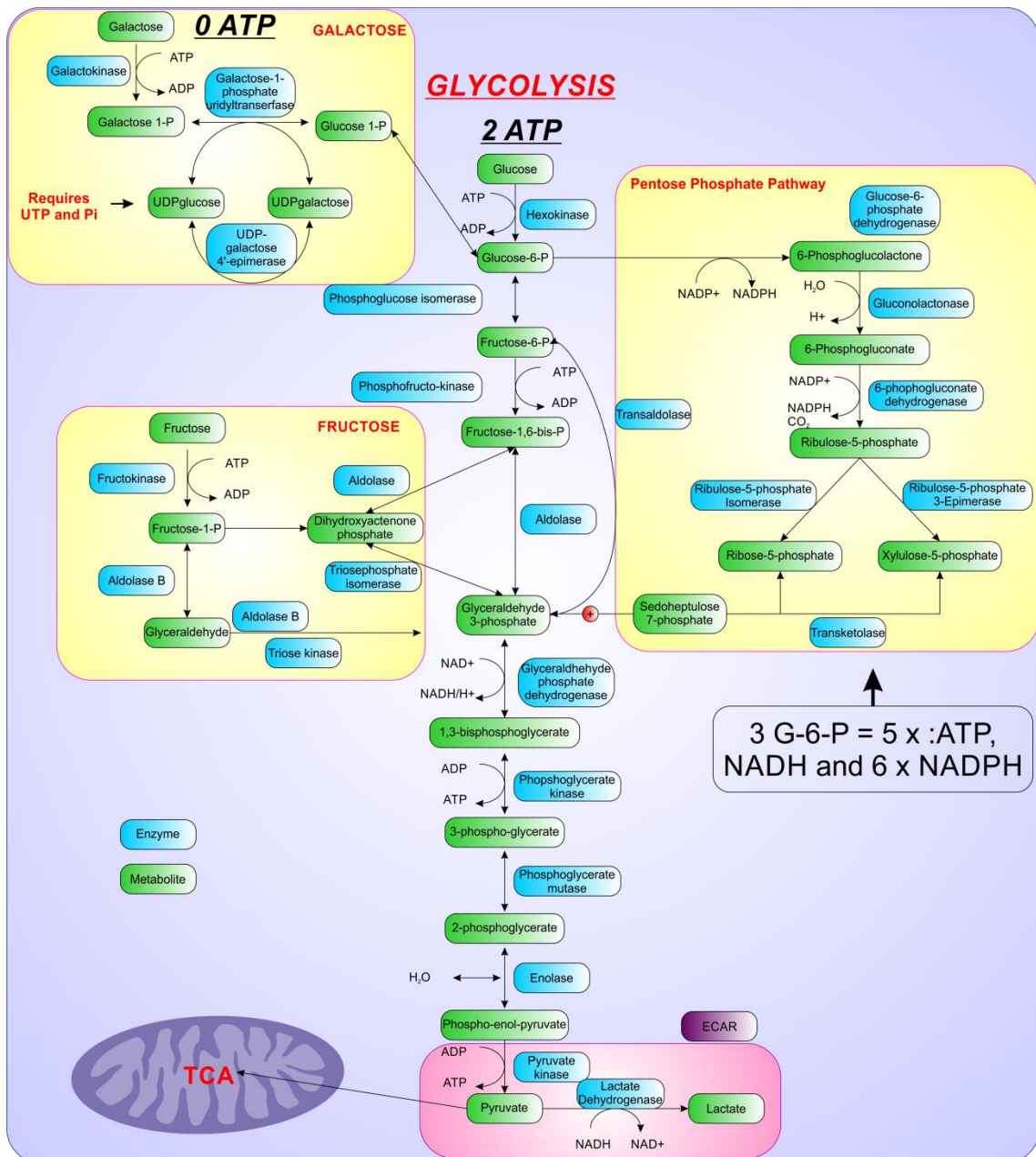


Figure 1-7 Sugar metabolism. Cancer cells preferentially utilise aerobic glycolysis, although this generates less ATP than mitochondrial oxidative phosphorylation, it allows the cells to generate macromolecular precursors and reducing equivalents through the oxidative arm of the PPP (right panel, yellow) in the form of NADPH to help protect against excessive levels of ROS. Additionally, high glycolytic flux results in increased lactate excretion from the cell (bottom pink panel), thus generating an acid tumour microenvironment generating numerous survival advantages. Galactose can be metabolised in the absence of glucose (top left yellow panel), however this does not generate any ATP and so the carbon flux through glycolysis is instead diverted in to the mitochondrial TCA cycle (bottom left) instead of to lactate production.

glucose uptake is normally correlated with a more aggressive cancer phenotype and a poor prognosis (reviewed in Gillies *et al.*, 2008). As many malignancies require increased levels of glucose, there has been a huge effort to therapeutically target the pathways that alter tumour cell metabolism (Vander Heiden, 2011; Zhao *et al.*, 2013; Tennant *et al.*, 2010). The types of therapeutic approaches have been divided into two categories, direct and indirect inhibition of tumour cell metabolism (reviewed in Tennant *et al.*, 2010). Briefly, indirect inhibition of tumour metabolism denotes an approach whereby cell signalling pathways that regulate metabolism are targeted therapeutically. Increased glycolytic flux is regulated by the following proteins/pathways: Hypoxia inducible factor (HIF); p53, Myc, PI3K/Akt pathway and the AMPK/LKB1 pathway. The roles of the latter two pathways in cancer cell metabolism are discussed in section 1.8. Direct inhibition of tumour metabolism, refers to directly targeting metabolic enzymes themselves, for example by blocking hexokinase with either: 2-deoxyglucose (2DG), Lonidamine or 3-bromopyruvate. The aim of these therapeutic strategies is to induce caspase-dependent apoptosis (reviewed in Tennant *et al.*, 2010; Vander Heiden, 2011).

There are many studies which have shown that glucose deprivation alone can induce cell death. For example, glucose deprivation can strikingly result in a caspase-8-dependent form of cell death that is not dependent on death receptor interactions in Bak/Bax double knockout MEFs and Hela cells (Caro-Maldonado *et al.*, 2010). However most studies have shown that glucose deprivation induces caspase-dependent apoptosis. Dividing lymphocytes are critically sensitive to glucose deprivation, and this is the result of upregulated Noxa expression, which inhibits Mcl-1 anti-apoptotic activity (Alves *et al.*, 2006). Additionally, the immortalised murine bone marrow-derived cell line, BAF-3 undergoes caspase-dependent apoptosis following glucose deprivation (Gonin-Giraud *et al.*, 2002) as do the murine pro B cell line, FL5.12 (Vander Heiden *et al.*, 2001). It has also been shown that the multidrug-resistant breast carcinoma cell line MCF-7/ADR undergoes apoptosis following glucose deprivation (Lee *et al.*, 1997). Glucose deprivation induces Puma-dependent apoptosis in activated primary T lymphocytes (Zhao *et al.*, 2008), and apoptosis inducing factor (AIF) and caspase-3-dependent apoptosis in acute T cell leukaemia cells as the result of increased reactive oxygen species (Mendivil-Perez *et al.*, 2013).

It should also be noted that normal human cells also appear to be sensitive to glucose deprivation-induced cell death *in vitro*, for example, the normal human diploid lung fibroblasts and human foreskin fibroblasts undergo apoptosis following glucose deprivation (Yuneva *et al.*, 2007)

As discussed, tumour cells display increased rates of glycolysis which is critical for their rapid proliferation and resistance to traditional therapies, and provides many therapeutic windows for killing or sensitising tumour cells, some of which are discussed below.

1.5.1 Inhibitors of GLUT's

Glucose deprivation *in vitro* as well as caloric restriction *in vivo* has shown potential promise as a means of targeting cancer (reviewed in Zhao *et al.*, 2013). The caveat to this approach is that glucose deprivation studies *in vitro* cannot be exactly replicated in a physiological environment within an individual. Instead, it may be possible to therapeutically target glucose metabolism by either inhibiting glucose uptake or inhibiting glucose metabolism. Malignant transformation frequently results in the upregulation of plasma membrane glucose transporters 1-4 (reviewed in Medina & Owen, 2002). The glucose transporter family consists of 25 members, 11 are sodium-dependent transporters and the remaining 14 are sodium-independent (Joost & Thorens, 2001; Joost *et al.*, 2002). This up-regulation and increased surface expression is a result of altered oncogenic signalling such as hyper-activated Akt signalling (Barthel *et al.*, 1999; Samih *et al.*, 2000; Kim *et al.*, 2007) or HIF-1 α activation (Hu *et al.*, 2003; Yasuda *et al.*, 2008). The resultant effect being that cancerous cells have a much higher capacity to uptake glucose for hyperplasia, and this appears to confer resistance to chemotherapeutics. Increased GLUT expression levels can be targeted *in vitro* with GLUT inhibitors, the hypothesis is that it should mimic the effects of glucose deprivation, and therefore result in the same apoptotic/sensitisation effects to traditional therapies as previously described. Phloretin, a naturally occurring compound found in apples and pears which competitively inhibits glucose transporters and has been shown to reverse hypoxia-induced daunorubicin resistance in colon adenocarcinoma SW620 cells and myelogenous leukaemia K562 cells (Cao *et al.*, 2007). Additionally, phloretin has been shown to induce apoptosis as a single agent in HepG2 cells (Wu *et al.*, 2009), however this was reversed by pre-treatment with high

concentrations of glucose (100 mM). Importantly, HepG2 SCID mice showed reduced tumour volume following phloretin treatment alone (Wu *et al.*, 2009). The high levels of glucose required to out compete phloretin are not physiological and therefore may be a potentially viable therapeutic strategy. An additional small molecule inhibitor of glucose transporters, WZB117 has also been shown to induce cell death *in vitro* and *in vivo* in lung cancer models, however the mode of cell death appeared to be necrosis, likely due to depletion of cellular ATP (Liu *et al.*, 2012).

1.5.2 2-deoxy-D-glucose-mediated inhibition of glycolysis

Following entry of glucose into the cell through GLUTs, glucose is metabolised by glycolysis. The first step in glycolysis is the irreversible phosphorylation of glucose to glucose-6-phosphate by hexokinase, trapping G6P in the cell. G6P has three potential fates: (i) conversion to glucose 1-phosphate, (ii) conversion to fructose 6 phosphate following the glycolytic pathway or (iii) conversion to 6-phosphogluconolactone via shunting into the oxidative arm of the pentose phosphate pathway (Jiang *et al.*, 2014). Following either ii or iii generates survival advantages for cancer cells in the forms of increased ATP or production of NADPH and macromolecular precursors, respectively (Jiang *et al.*, 2014). If hexokinase can be inhibited, then flux through both glycolysis and the PPP can be inhibited. This will result in the reduction of ATP regeneration, a lack of reducing equivalents; ribose sugars for nucleic acid synthesis and a diminished antioxidant capacity. There are currently three well described inhibitors of Hexokinase, these being 2-deoxy-D-glucose (2DG), 3-bromopyruvate and lonidamine, the latter specifically targeting hexokinase bound to mitochondria (Oudard *et al.*, 1995).

2DG is a glucose analogue that can be phosphorylated by hexokinase into 2-deoxyglucose-6-phosphate (2DG-6-P) which cannot be further metabolised, as such the build-up of 2DG-6-P results in allosteric inhibition of hexokinase (Sols & Crane, 1954; Newsholme *et al.*, 1968). For many years 2DG was used as a glucose deprivation mimetic, however recent studies from our laboratory have shown that they can produce opposing effects on sensitisation to apoptotic inducers (Robinson *et al.*, 2012; MacFarlane *et al.*, 2012). Nevertheless, the effects of 2DG on tumour cell killing have been studied in detail. Certain cell lines cultured in normoxia are sensitive to 2DG-induced cell killing as a single agent through

inhibition of N-linked glycosylation (Kurtoglu *et al.*, 2007). Active glycolysis and subsidiary catabolic carbon pathways emerging from glycolysis are required for N-linked glycosylation of proteins. Metabolism of glucose results in the generation of mannose-6-phosphate by phosphomannose isomerase, which is subsequently converted to mannose-GDP which is required for the formation of N-linked oligosaccharides; conversion of 2DG to 2DG-GDP competes with mannose-GDP, and results in generation of aberrant oligosaccharides and the disrupted synthesis of glycoproteins (Zhang *et al.*, 2014). This results in the activation of the unfolded protein response and subsequently leads to ER stress and cell death (Ramirez-Peinado *et al.*, 2011), other studies have also shown that 2DG inhibits N-glycosylation of proteins, disrupting ER/protein integrity, thus leading to endoplasmic reticulum stress and the unfolded protein response (Xi *et al.*, 2011; Xi *et al.*, 2013; Yu & Kim,).

Certain cell lines cultured in normoxia are sensitive to 2DG-induced cell killing as a single agent through regulation of Bcl-2 family members (Zagorodna *et al.*, 2012). However, 2DG largely appears to have little efficacy as a single agent, but many studies have looked at combining it with other agents, and it appears to synergise with a plethora of therapeutics. Metastatic melanoma lines show increased sensitivity to cisplatin and staurosporine when treated in combination with 2DG (Giammarioli *et al.*, 2012). Prostate cancer lines become sensitive to metformin when treated in combination with 2DG (Ben Sahra *et al.*, 2010). TRAIL-induced apoptosis is enhanced by 2DG in leukaemic cells (Robinson *et al.*, 2012) and melanoma cells (Liu *et al.*, 2009; Qin *et al.*, 2010).

Another published mechanism by which 2DG can exert a pro-apoptotic sensitising effect on multiple tumour lineages is that 2DG directly inhibits glycolysis thus increasing in the AMP:ATP ratio and activating AMPK. Phosphorylation and activation of AMPK results in inhibition of protein translation, and ultimately leads to a rapid decrease in the expression of proteins with short half-lives; chiefly Mcl-1 (Pradelli *et al.*, 2010; MacFarlane *et al.*, 2012).

1.6 Galactose metabolism

Two ways to analyse the function of glycolysis in cancer cell metabolism and its related features, such as chemotherapeutic resistance and survival advantages are

to study cells deprived of glucose or to treat them with the anti-glycolytic and hexokinase inhibitor 2DG as previously discussed. An alternative way to study the effect is to culture cells in the absence of glucose, but in the presence of galactose. Many drugs induce mitochondrial toxicity, and this is often missed in the drug development process and leads to drug withdrawal from the market (Will & Dykens, 2014). The realisation that cells cultured in galactose have a fully functional glycolytic pathway but are completely dependent on mitochondrial oxidative phosphorylation for ATP generation allows the simultaneous study of the importance of ATP derived from glycolytic metabolism while also identifying drugs that induce mitochondrial toxicity.

Galactose is imported into the cell through the same GLUTs as glucose, however, GLUTs have a much lower affinity for galactose and so the sole sugar available for glycolysis is imported in at a much slower rate (Wagner *et al.*, 1991). In addition to this, once in the cytoplasm galactose is metabolised about 8 times slower than glucose (Kase *et al.*, 2013), which means most of the ATP is generated from mitochondrial oxidative phosphorylation and from exogenously supplemented glutamine. It is often stated that galactose metabolism generates a net yield of 0 ATP, this is because for the metabolism of galactose to proceed, UDP-glucose must first be generated from glucose-1-phosphate and UTP, thus utilising a UTP (Grun *et al.*, 1990; Lee *et al.*, 2009), thus the net energy gain is 0 (Figure 1-7).

1.7 Mitochondrial oxidative phosphorylation

The mitochondrial respiratory chain produces most of the cells' energy (ATP) and is colloquially termed the 'powerhouse of the cell'. This is achieved by transfer of electrons through four complexes embedded in the mitochondrial inner membrane (see Figure 1-8) (Nicholls & Ferguson, 2013a). The NADH dehydrogenase complex (complex I), oxidises the electron carrier NADH and H^+ to form NAD, and obtains 2 electrons (Nicholls & Ferguson, 2013a). These electrons are passed through flavin mononucleotide and then a series of iron centres, and finally on to the iron sulphur centre. These 2 electrons create a proton gradient which pulls in 2 H^+ from the matrix that bind to ubiquinone, reducing it to ubiquinol (Nicholls & Ferguson, 2013a). Complex I then pumps 4 H^+ from the matrix into the inter membrane space (IMS).

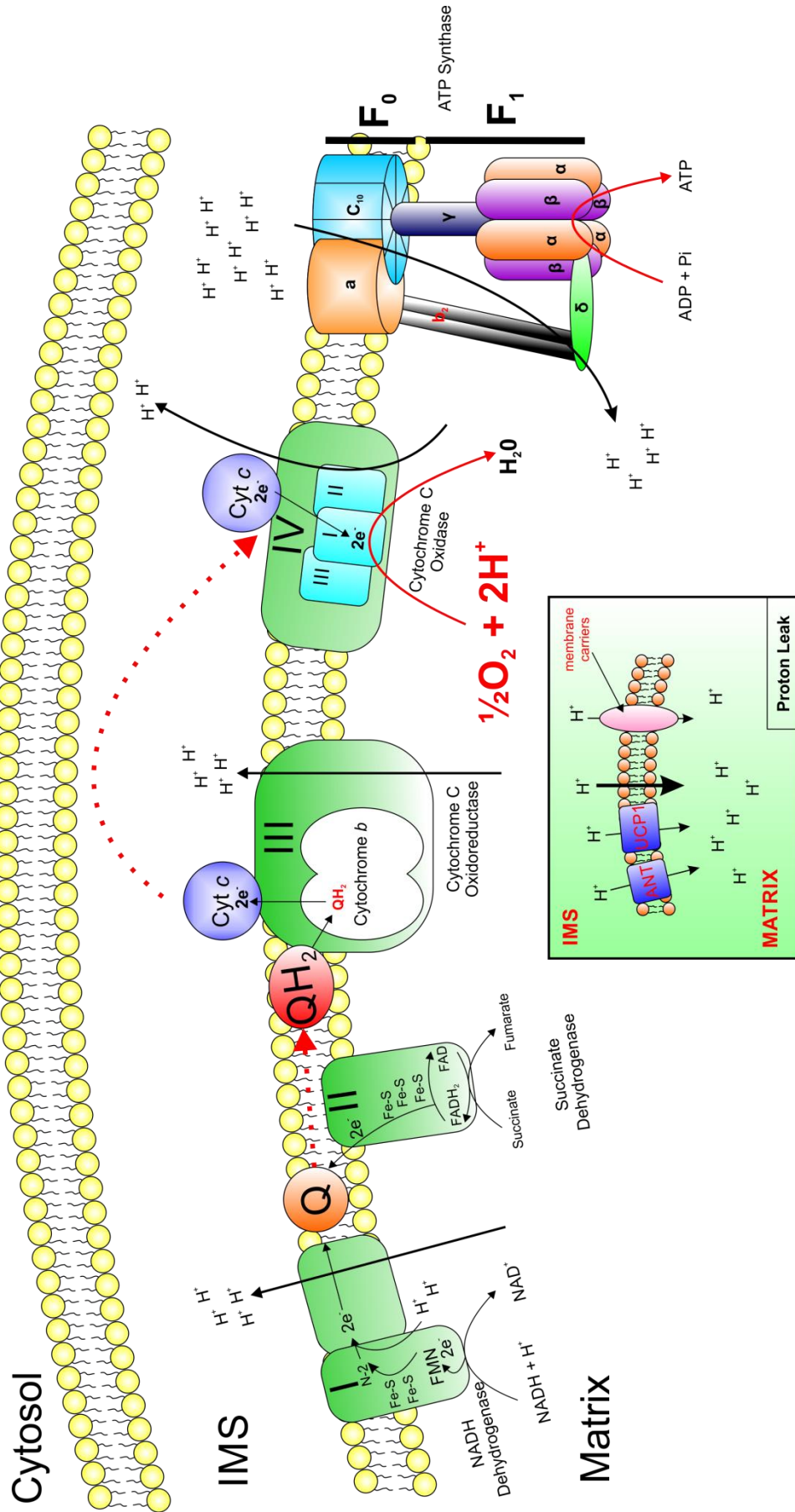


Figure 1-8 Mitochondrial oxidative phosphorylation. Schematic overview of mitochondrial oxidative phosphorylation system. The protons are represented as the exact amount that are moved from the matrix to the IMS at each complex and back following the oxidation of one NADH + H⁺. A total of 10 protons generate 2.5 ATP. Conversion of succinate to fumarate results in a total of 6 H⁺ and thus 1.5 ATP. The mitochondrial proton leak (bottom box) functions by largely unknown mechanisms, but they likely involve uncoupler proteins (UCP), adenine nucleotide translocator (ANT), ubiquinol. FMN is flavin mononucleotide. Fe-S are iron centres. N-2 is the iron sulphur centre.

Ubiquinol moves through the inner membrane and associates with cytochrome *c* oxidoreductase (complex III). Complex III, oxidises ubiquinol to ubiquinone, in this process, the 2 electrons are transferred to cytochrome *c* (Nicholls & Ferguson, 2013a). During this process, complex III also pumps 4 H⁺ from the matrix to the IMS. Cytochrome *c* is mobile and moves through the IMS where it associates with cytochrome oxidase (complex IV) (Nicholls & Ferguson, 2013a). Complex IV contains 3 main subunits, I, II and III. The two electrons on cytochrome *c* are transferred to complex IV with the subsequent reduction of $\frac{1}{2}\text{O}_2 + 2\text{H}^+$ to H₂O. During this process, complex IV pumps 2 H⁺ from the matrix to the IMS. Oxygen is the final electron acceptor, and the redox reactions occurring in the electron transport chain result in a net yield of 10 H⁺ transferred from the matrix to the IMS from the oxidation of one NADH + H⁺ (Nicholls & Ferguson, 2013a).

The 10 H⁺ in the IMS are pumped through the ATP synthase (complex V) from the IMS back to the matrix, converting ADP + Pi in the matrix to ATP. To produce one ATP, 4 H⁺ are required to be pumped through complex V, therefore the oxidation of one NADH results in 2.5 ATP (Nicholls & Ferguson, 2013b). Understanding this system is crucial for analysing bioenergetics data generated on a Seahorse extracellular flux analyser, which measures the consumption of oxygen in real time. Using a selection of mitochondrial inhibitors, various bioenergetics parameters can be determined (see Figure 3-6). Firstly, inhibition of complex V by the inhibitor oligomycin stops the pumping of protons from the IMS back to the matrix, thus inhibiting mitochondrial ATP generation and the flow of electrons down the mitochondrial electron transport chain (Brand & Nicholls, 2011). If the ETC is tightly coupled to the ATP synthase then there should be no remaining mitochondrial oxygen consumption. In most cells the ETC is not completely coupled to the ATP synthase, meaning that leakage of protons occurs from the IMS back to the matrix independently of complex V (Brand & Nicholls, 2011). The mechanisms that drive the proton leak are not completely understood, and likely involve a variety of mechanisms. Firstly, the water wires theory states that single file chains of water can span the mitochondrial inner membrane, and this facilitates the transport of protons back to the matrix (Tepper & Voth, 2005). The abundance of adenine nucleotide translocase (ANT) also appears to directly correlate with the extent of proton leakage (Brand *et al.*, 1999; Brand *et al.*, 2005), and the combination of all

mitochondrial inner membrane carrier proteins; the function of the proton leak is additionally not completely understood, however the mild uncoupling generated from it is believed to protect against excessive mitochondrial ROS (reviewed in Jastroch *et al.*, 2010). The best known example of the proton leak is through the uncoupler protein 1 (UCP1), which is found in brown adipose tissue, this protein results in a by-pass of the ATP synthase, allowing for non-shivering thermogenesis; this process typically occurs during mammalian hibernation to maintain the core body temperature (Fedorenko *et al.*, 2012).

Using the protonophore carbonyl cyanide-4-(trifluoromethoxy)phenylhydrazone (FCCP), the ETC can proceed in the absence of the ATP synthase, which is a measure of the maximal rate at which the ETC can function (Brand & Nicholls, 2011). FCCP is a lipid permeable chemical that is either protonated or unprotonated depending on the pH of the cellular compartment that it is localised to. Thus, FCCP is protonated in the IMS where it moves to the matrix down the pH gradient and gets deprotonated, liberating H⁺ into the matrix, which can subsequently be pumped back to the IMS through complexes I, III and IV. Inhibition of complex I is achieved by rotenone, which binds to the iron sulphur cluster in NDUFS2 (Fendel *et al.*, 2008), completely ablating electron flow at the most upstream complex of the ETC. Any remaining oxygen consumption after the addition of rotenone is generated either by succinate dehydrogenase and complex III or non-mitochondrial means.

1.8 Signal transduction

1.8.1 AMP-activated protein kinase (AMPK)

The AMP-activated protein kinase (AMPK) senses small changes in cellular energy status and is activated under conditions of energetic stress (Hardie, 2011). It is a heterotrimeric protein complex composed of a catalytic α subunit and two regulatory subunits (β and γ) (Figure 1-9), which are expressed in essentially all eukaryotic organisms. The catalytic subunit has two known isoforms, $\alpha 1$ and $\alpha 2$, encoded by PRKAA1 and PRKAA2 respectively (Hardie, 2007). The regulator β subunit also has two known isoforms, $\beta 1$ and $\beta 2$, encoded by PRKAB1 and PRKAB2 respectively (Hardie, 2007). The regulatory γ subunit contains three known isoforms, $\gamma 1$, $\gamma 2$ and $\gamma 3$, encoded by PRKAG1, -2 and -3, respectively

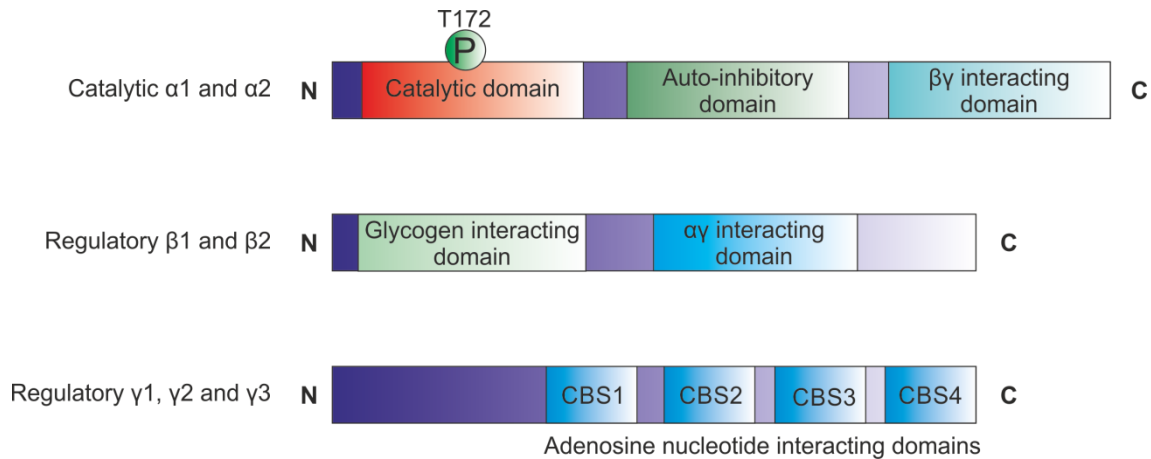


Figure 1-9 AMPK subunit structures. There are three subunits, the catalytic α isoforms, which are phosphorylated at T172 by LKB1 and CaMKK- β . The regulatory β isoforms, which interact with glycogen, and the regulatory γ isoforms which contain the adenosine nucleotide binding sites.

(Hardie, 2007). Any different combination of each isoform can combine to generate a functional heterotrimeric protein complex with varied expression profiles throughout different tissues (reviewed in Moffat & Harper, 2010)

Increased AMP:ATP ratios can result from energetic stress induced by the inhibition of ATP production, or a rapid increase in ATP consumption. This results in two AMP molecules binding to the Bateman domains in the AMPK- γ subunit of the heterotrimeric protein complex (Scott *et al.*, 2004) (Figure 1-9). This binding results in a conformational change in the AMPK- γ subunit exposing the active site on the AMPK- α subunit (Threonine-172), where it gets phosphorylated and activated by Liver kinase B1 homolog (LKB1). LKB1 is active in cells when associated in a heterotrimeric complex with Ste20-Related Adaptor (STRAD) and Mouse protein 25 (MO25) (Hawley *et al.*, 2003; Woods *et al.*, 2003). AMPK can additionally be activated by phosphorylation on AMPK- α T172 by Ca^{2+} /calmodulin-dependent protein kinase kinase- β (CaMKK- β) in response to increased cytoplasmic calcium loading (Woods *et al.*, 2005)

As a general rule, the AMPK pathway decreases anabolic processes and increases catabolic cellular processes (see Figure 1-10) to inhibit ATP requiring processes and simultaneously generate ATP respectively (Hardie, 2015). Following energetic stress, adenylate kinase attempts to maintain ATP levels by catalysing 2ADP to one each of ATP and AMP, thus exacerbating the rise in AMP

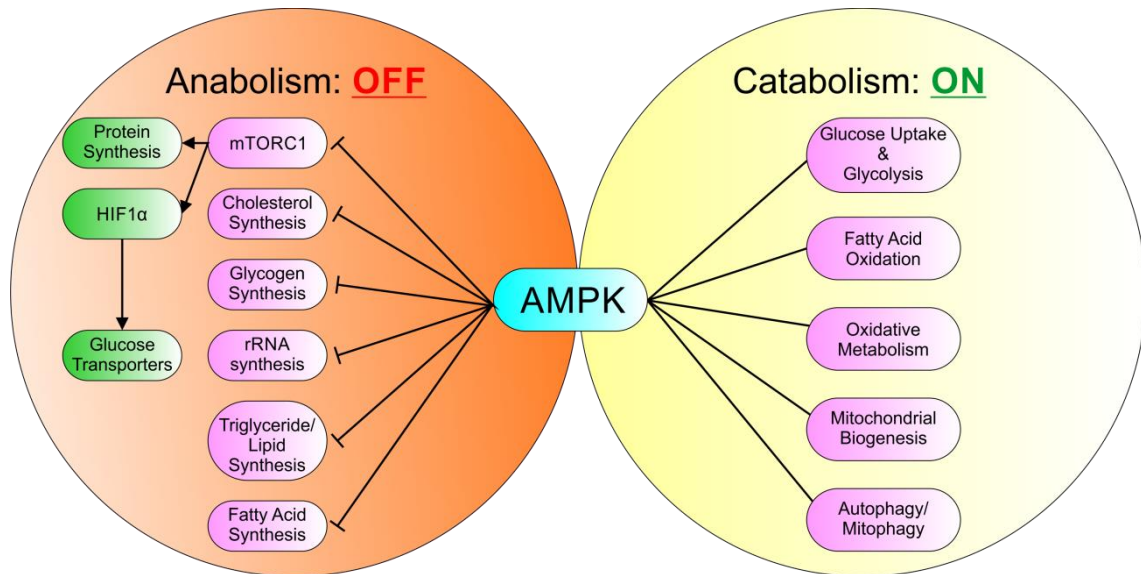


Figure 1-10 The functions of AMPK. Following energetic stress, AMPK is activated to switch off a variety of anabolic ATP consuming processes (left, orange circle), such as protein translation and glycogen synthesis. Simultaneously, AMPK switches on ATP generating catabolic pathways to try and increase intracellular ATP levels (right, yellow circle) such as increasing glycolytic flux and activating fatty acid oxidation.

levels, which are always much larger than the respective decrease in ATP levels (Gowans *et al.*, 2013). The focus of this thesis is on how metabolic status modulates tumour cell sensitivity to apoptotic stimuli, as such inhibitors of ATP production by inhibiting glycolysis or the oxidative phosphorylation system are routinely used, which implicates AMPK as an important regulator of the outcomes.

Upon activation, AMPK inhibits protein, glycogen, rRNA and sterol synthesis to reduce cellular anabolism (Lim *et al.*, 2010). AMPK inhibits protein synthesis through the inhibition of mTORC1 by direct phosphorylation of tuberous sclerosis 2 (TSC2) (Inoki *et al.*, 2003b) and the mTOR binding partner raptor (Gwinn *et al.*, 2008). Examples of catabolic processes mediated by AMPK include activation of the 58 kDa H-PFK2 isoform and the u-PFK2 and I-PFK2 isoforms (reviewed in Ros & Schulze, 2013), resulting in increased glycolysis; inhibition of Acetyl Co-enzyme A carboxylase to increase fatty acid oxidation and increased GLUT4 plasma membrane translocation to increase glucose transport (Lim *et al.*, 2010). AMPK is thus a positive regulator of glycolytic flux. In addition, following energetic stress,

AMPK is responsible for increased mitochondrial biogenesis, a critical adaptation to increase cellular ATP content (Zong *et al.*, 2002; Scarpulla, 2008; Jornayvaz & Shulman, 2010)

1.8.2 Protein kinase B (Akt)

The PI3K/Akt pathway is an important regulator of cellular metabolism, PI3K is a class 1A phosphatidylinositol 3-kinase that functions by phosphorylating phosphatidylinositol(4,5)P₂ (PIP₂) into phosphatidylinositol(3,4,5)P₃ (PIP₃) (reviewed in Martini *et al.*, 2014). PIP₃ functions a second messenger to recruit proteins containing a Pleckstrin Homology (PH) domain to the plasma membrane, such as protein kinase B (Akt) (Vivanco & Sawyers, 2002). Akt is expressed in three different isoforms, Akt1 and Akt2 which appear to be ubiquitously expressed, and Akt3 that appears to have a more confined tissue distribution (Agarwal *et al.*, 2013). Elevated expression of Akt is a major contributing factor in cancer cell survival (Martini *et al.*, 2014), and as such there are a plethora of described genetic aberrations that result in increased Akt signal transduction. Akt1 amplification has been found to occur in gastric cancers, and this confers resistance to platinum based therapies (Liu *et al.*, 2007), while somatic mutations have been found in breast, bladder, lung, ovarian and colorectal carcinomas (Knowles *et al.*, 2009). There are a variety of single nucleotide polymorphisms (SNP), most of which are correlated with poor prognosis and therapeutic resistance (reviewed in Martini *et al.*, 2014)

At the plasma membrane Akt is phosphorylated on T308 by PDK1 and on S473 by mTORC2, allowing it to exert its kinase activity on its cellular targets (Martini *et al.*, 2014). Both phosphorylation events appear to be critically required for full activation of Akt kinase activity (Hart & Vogt, 2011). Akt was originally identified as a key regulator of insulin receptor signalling (Burgering & Coffey, 1995). Akt is a positive regulator of protein translation, *via* direct phosphorylation of TSC2 and the proline-rich Akt substrate of 40 kDa (PRAS40).

Many targets for Akt are involved in cellular metabolism, for example Akt regulates cell surface glucose transporters (GLUTs) by inducing expression of GLUT1 and GLUT3 (Hajdich *et al.*, 1998; Barthel *et al.*, 1999) and facilitating GLUT4 translocation to the plasma membrane (Watson *et al.*, 2004). In addition, Akt

phosphorylates glycogen synthase kinase-3 β (GSK-3 β) resulting in its inactivation and subsequent activation of glycogen synthase and cyclin D1 (Vivanco & Sawyers, 2002). Other metabolic proteins regulated by Akt include: phosphorylation of PDE3B to regulate intracellular cyclic nucleotide levels (Kitamura *et al.*, 1999); phosphorylation of the 58 kDa isoform of H-PFK2 (reviewed in Ros & Schulze, 2013) and subsequent activation of PFK1 leading to conversion of fructose-6 phosphate to fructose-1,6 bisphosphate (Deprez *et al.*, 1997). Also, Akt is believed to up-regulate the levels of mitochondrial-associated hexokinase (Majewski *et al.*, 2004b; Majewski *et al.*, 2004a)

1.8.3 Cross talk into apoptotic and survival signalling

The Akt and AMPK pathways also serve to function as direct or indirect modulators of a variety of pro- and anti-apoptotic proteins. For example, Akt directly phosphorylates the BH3 only protein Bad at Serine-136, which results in Bad and 14-3-3 proteins forming a complex, thus inhibiting its pro-apoptotic function (Datta *et al.*, 1997). Also, Akt phosphorylates and inactivates GSK-3 β , preventing Mcl-1 phosphorylation and thus inhibiting targeted proteasome degradation, potentially extending the short 90 min half-life of the anti-apoptotic protein (Inuzuka *et al.*, 2011; Maurer *et al.*, 2006). I κ B kinase (IKK) can also transiently associate with Akt resulting in its activation, thus leading to enhanced gene transcription of both Bcl-2 and Bcl-x_L (Romashkova & Makarov, 1999). In addition, Akt antagonizes mitochondrial-hexokinase dissociation in the presence of tBid thus preventing Bax/Bak activation (Majewski *et al.*, 2004b). Over expression of Akt therefore functions to avoid apoptosis by regulating a variety of Bcl-2 family proteins.

In contrast the AMPK pathway has paradoxically been reported to have both pro-apoptotic and anti-apoptotic effects (Shaw *et al.*, 2004; Saitoh *et al.*, 2004; Li *et al.*, 2003a; Xiang *et al.*, 2004; Stefanelli *et al.*, 1998; Durante *et al.*, 1999; Kefas *et al.*, 2003b; Kefas *et al.*, 2003a; Dagon *et al.*, 2006; Dagon *et al.*, 2005). LKB1 is best known for its role in Peutz-Jeghers syndrome. Hereditary germ line mutations in LKB1 result in individuals presenting with benign tumours that are incapable of malignancy (Hemminki *et al.*, 1998; Jenne *et al.*, 1998). Additionally, there has been great interest in the LKB1-AMPK pathway as a therapeutic target; as a result, studies have demonstrated that AMPK is required for cell growth and survival, and that AMPK activity correlates with survival (Inoki *et al.*, 2003b). In a recent study it

has been shown that AMPK activation maintains NADPH anti-oxidant production via fatty acid oxidation and that this is critical for cell survival (Jeon *et al.*, 2012).

In contrast reports also show that activation of AMPK can lead to inhibition of cell growth and activation of apoptosis. One of the mechanisms by which this is achieved is a shutdown in protein translation signalled through mTORC1, leading to decreased expression of the anti-apoptotic Bcl-2 family member protein Mcl-1 (Pradelli *et al.*, 2010).

These metabolic pathways do not only cross talk into apoptotic signalling, there is growing evidence to suggest that Bcl-2 family members directly regulate cellular metabolism. An extensive review on Bad by Nika Danial (Danial, 2008) discusses that post-translational modifications, in this case serine 155 phosphorylation results in Bad assuming a metabolic role by activating glucokinase (GK). In addition, it has also been reported that the BH3 only protein Noxa, enhances glucose turnover via the PPP, and that the serine 13 phosphorylation status dictates whether it serves to promote apoptosis or regulate metabolism (Lowman *et al.*, 2010).

1.9 mTOR signalling and protein translation

The cellular nutrient sensor is mammalian target of rapamycin (mTOR), which is crucial for generating signals that tell the cell to grow and proliferate. Perhaps the most important function of mTOR is to maintain an available amino acid pool for active protein synthesis (Shimobayashi & Hall, 2014). mTOR is found in two distinct complexes, mTORC2, which contains mTOR, rapamycin insensitive companion of mTOR (Rictor), mammalian stress activated protein kinase (SAPK) interacting protein 1 (mSin1), protein observed with rictor (protor), mLST8, PRAS40 and death domain containing mTOR interacting protein (deptor) (reviewed in Showkat *et al.*, 2014). This mTOR complex is responsible for phosphorylation of Akt on S473 and thus facilitates full activation of its kinase function.

The second mTOR complex, mTORC1, contains mTOR, regulatory associated protein of mTOR (raptor), mLST8, PRAS40 and deptor (reviewed in Showkat *et al.*, 2014) (see Figure 1-11). This complex is the master regulator of cellular protein synthesis, and functions primarily by regulating the activity of eIF4E binding proteins (4EBP's) and p70S6k. Translation initiation control is mediated by the 7-methyl-GTP cap structure located at the 5' end of all mRNA's

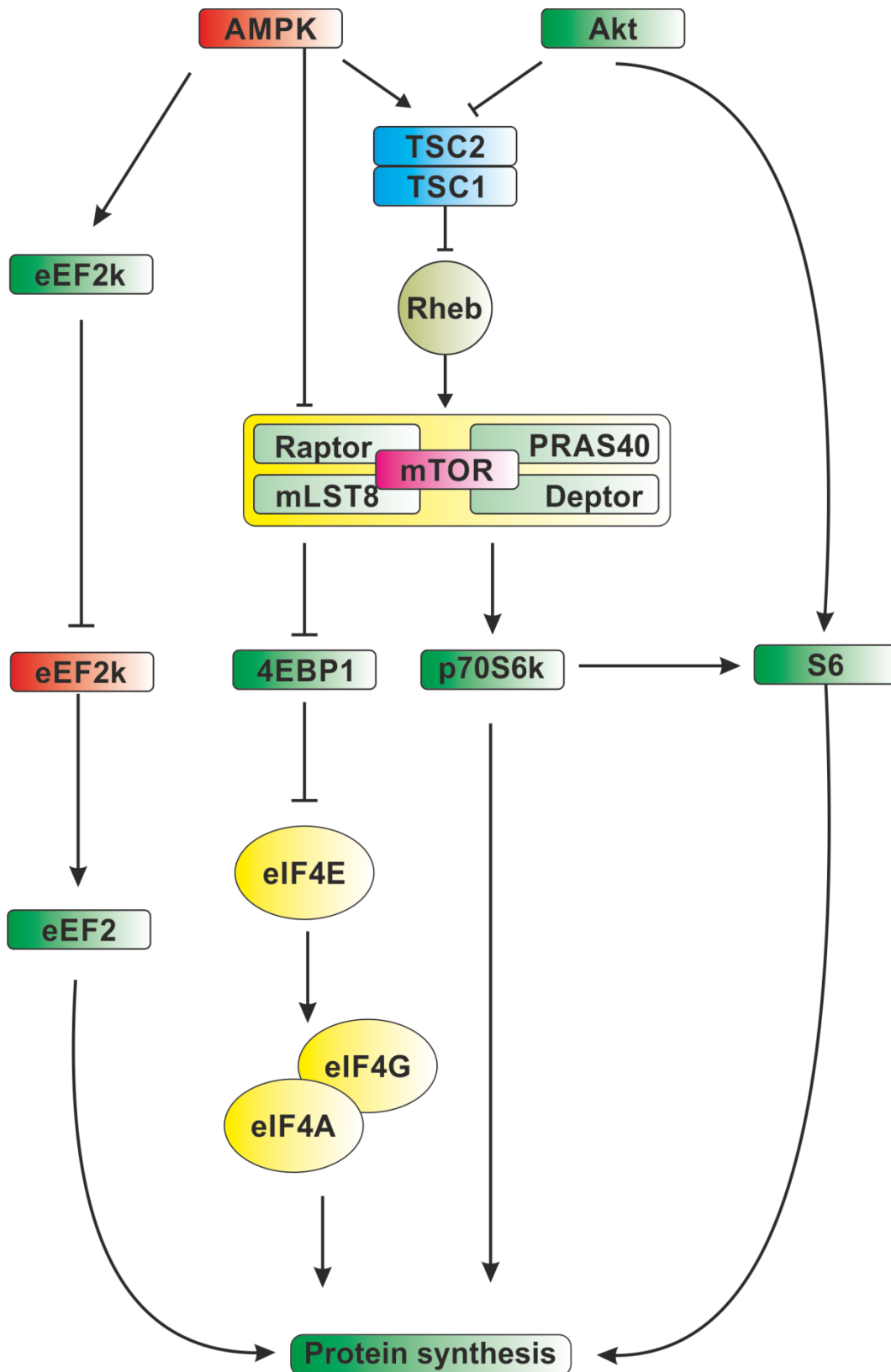


Figure 1-11 AMPK and Akt regulation of protein translation. AMPK and Akt negatively and positively regulate mTORC1 respectively. Either by regulating the upstream negative regulator TSC2, or, in the case of AMPK, additionally directly phosphorylating and inhibiting raptor. Akt can also directly activate S6, while AMPK can directly inhibit the elongation step by phosphorylation of eEF2k.

(reviewed in Showkat *et al.*, 2014). The eukaryotic initiator 4F (eIF4F) complex binds near this cap, and is comprised of the eIF4G scaffold protein, eIF4E and eIF4A, and this complex initiates translation (Pain, 1996). eIF4E binds tightly to 4EBP1 (Pause *et al.*, 1994) in the absence of an mTORC1 activation signal (i.e. Akt) or the presence of an inhibition signal (i.e. AMPK), inhibiting protein translation. mTORC1 regulates this complex, by hyper-phosphorylating 4EBP1 when mTORC1 activity is high, which results in the dissociation of 4EBP1 with eIF4E, thus allowing the eIF4F complex to form. Conversely, when activity is low or signalled for inhibition, mTORC1 does not phosphorylate 4EBP1, resulting in a hypo-phosphorylated protein that rapidly sequesters eIF4E, thus inhibiting eIF4F complex formation and protein synthesis (Gingras *et al.*, 2001).

This above process is regulated upstream of mTORC1 by two regulators of cellular homeostasis, Akt and AMPK. AMPK signals to inhibit protein translation by directly phosphorylating raptor on S722/792 or by phosphorylating TSC2 resulting in its association with TSC1 to negatively regulate protein translation (Gwinn *et al.*, 2008). Akt on the other hand phosphorylates TSC2 resulting in its dissociation from TSC1 activating protein translation (Inoki *et al.*, 2002). The TSC complex regulates protein synthesis by acting as a Rheb GAP (GTPase activating protein). Rheb GTPase binds directly to mTOR and positively regulates its kinase activity (Sancak *et al.*, 2007), activation of the TSC complex converts Rheb to an inactive GDP-bound form, which cannot activate protein synthesis (Garami *et al.*, 2003; Inoki *et al.*, 2003a); thus, dissociation of TSC2 from TSC1 by Akt phosphorylation activates protein translation through Rheb GTPase. In addition to mTORC1 regulation of 4EBP1, it also binds tightly to p70S6k and phosphorylates it at T389 (Dann *et al.*, 2007). Activation of p70S6k results in regulation of translation initiation by phosphorylating the cap binding protein eIF4B (Raught *et al.*, 2004) and inhibiting eEF2k (Wang *et al.*, 2001) (a negative regulator of elongation), it has also been reported to regulate transcription and ribosomal biogenesis by phosphorylating the transcription factor UBF-1 (Showkat *et al.*, 2014). Interestingly, p70S6k is a direct regulator of cell survival by phosphorylating both MDM2 and the Bcl-2 family member Bad (reviewed in Showkat *et al.*, 2014).

1.10 Aims

The realisation that cancer cell metabolism can be targeted with minimal off target side effects is gaining pace in academia and industry as a viable approach to modify therapeutic regimes with the aim of decreasing tumour burden. In line with this, the work in this thesis looked at how inhibiting glycolytic flux by different techniques could alter tumour cell sensitivity to traditional apoptotic stimuli, and ultimately what were the mechanisms behind the altered sensitivity.

Work previously published from our laboratory has shown that the mantle cell lymphoma derived cell line, Z138's, were less sensitive to TRAIL-induced cell killing when chronically deprived of glucose (Robinson *et al.*, 2012). The experiments described in Chapter 3 used chronic glucose deprivation (at least 7 days) as a means to study the effects of glycolytic inhibition on TRAIL-induced apoptosis in another mantle cell lymphoma derived cell line, UPN1's. The aim was to determine if glucose-deprivation also conferred resistance to TRAIL-induced apoptosis in another MCL line. UPN1 cells were maintained in glucose containing or glucose free media, and the sensitivity to TRAIL was studied using FACS analysis. In addition, the effect of glucose deprivation on the mode of cell death following TRAIL treatment was investigated and correlated with bioenergetics studies following metabolic reprogramming, along with immunoblotting analysis of key pro- and anti-apoptotic proteins.

The same study published from our laboratory showed that treating Z138 cells with 2DG for 20 h resulted in increased sensitivity to apoptotic stimuli. As cancer cells rapidly utilise glycolysis, the effects of acute glycolysis inhibition by 2DG should be far more rapid than 20 h. The experiments described in Chapter 4 aimed to delineate the kinetics and also the mechanism by which 2DG increases TRAIL and ABT-737-induced cell death. Z138 cells were maintained in glucose containing media and treated with 2DG prior to apoptosis induction by TRAIL and ABT-737, as predicted, the effects were far more rapid than previously published, with increased sensitivity observed within 2 h, which correlated with metabolic reprogramming. To characterise the mechanism by which 2DG increased sensitivity, the AMPK and Akt signal transduction pathways were examined by immunoblotting, which showed that 2DG induced a rapid and transient activation of AMPK, which was sufficient to sustain inhibition of protein translation and thus

maintain a reduced level of Mcl-1 expression. The effects of canonical activators of AMPK were examined and correlated to TRAIL and ABT-737-induced cell killing; these results showed that 2DG appears to activate AMPK independently of LKB1 and CaMKK- β

The previously published study from our laboratory and the results presented in Chapters 3 and 4 showed that inhibition of glycolysis by glucose deprivation and 2DG have profoundly different effects on sensitivity to apoptotic inducers. An alternative way to study the effects of cellular metabolism on cell death is to maintain the cells in a galactose based media, in this model, glycolysis is preserved and intermediates are still generated from the pentose phosphate pathway, however no ATP is generated from glycolysis and so the cells are reliant on mitochondrial oxidative phosphorylation. The results described in Chapter 5 used glucose and galactose cultured Z138 cells to examine the sensitivity of the cells to a panel of drugs following metabolic reprogramming with the aim of correlating this information to results obtained from glucose deprivation and 2DG studies. The degree and mode of cell death following treatment with canonical inducers of apoptosis and classical inhibitors of the mitochondrial oxidative phosphorylation system were correlated to metabolic reprogramming, which showed metabolic switching altered the mode of cell death from apoptosis to necrosis. Also, I aimed to study the mitochondrial proteome using label-free quantitative mass spectrometry to evaluate changes in protein expression, and then couple this data to bioinformatics pathway mapping. The aim was to correlate the observed altered sensitivity to apoptotic stimuli and the switch in cellular metabolism to the changes in the mitochondrial proteome, and if this methodology could be used to predict other changes that may have occurred following metabolic reprogramming.

2 Materials and Methods

2.1 Materials

Unless otherwise stated, all materials were obtained from Sigma-Aldrich (Poole, UK). Acetone, EDTA, ethanol, IMS, methanol, marvel milk powder and Sodium chloride were obtained from Fisher Scientific Ltd (Loughborough, UK). A23187, dorsomorphin dihydrochloride (compound C), thapsigargin, STO-609 and HNMPA-(AM3) were all obtained from Santa Cruz Biotechnology, Inc. (Heidelberg, Germany). Seahorse XF24 flux pak, was obtained from Seahorse bioscience (Copenhagen, Denmark). TRIS Complete™ protease inhibitor without EDTA was obtained from Roche (Sussex, UK). Cell titre Glo® Luminescent cell viability assay, passive lysis buffer 5X and sequencing grade modified trypsin were all obtained from Promega (Madison, WI, USA). Methionine and Cysteine L-[³⁵S] and scintillation fluid were obtained from PerkinElmer (Waltham, Massachusetts, USA). The pan-caspase inhibitor zVAD.fmk was obtained from MP Biomedicals (Illkirch, France). Immobilon PVDF membrane for immunoblotting was obtained from Merck Millipore Corporation (Darmstadt, Germany). Nucleofection solution SF for use with a nucleofector 4D were from Lonza Group Ltd (Verviers, Belgium). DMEM – methionine and cysteine free media, Dynabeads® protein G for immunoprecipitation, foetal calf serum, GlutaMAX™, MitoSox™ Red mitochondrial superoxide indicator, RPMI1640 without glucose, RPMI1640 with 11.1 mM D-glucose, sodium pyruvate, 4-20% TRIS-glycine mini gradient gels and 4-12% BIS-TRIS Bolt™ gels were all obtained from Life technologies (Invitrogen/Thermo Fisher Scientific) (Loughborough, UK). ECL was from GE Healthcare (Buckinghamshire, UK), Dimethyl pimelinediimidate dihydrochloride was from Fluka (poole, UK). InstantBlue™ ultrafast protein stain was from Expedeon (Cambridge, UK). AICAR was from Cell Signalling Technology (Leiden, Netherlands). Criterion 4-20% TRIS-glycine gradient gels and Bio-Rad protein assay were from Bio-Rad (Hemel-Hempstead, Hertfordshire). BD Cell-Tak™ was obtained from Becton Dickinson (Oxford, UK). A769662 and CHIR 99021 were from Tocris Bioscience (Bristol, UK). Yeast ADH1 and BSA for quantitative mass spectrometry were from Waters Corporation (Manchester, UK). ABT-737 was from SelleckChem (Munich, Germany). Recombinant Annexin-V conjugated to FITC was made in house by Dr Xiao Ming Sun. Recombinant TRAIL was made in house Prof Marion MacFarlane.

2.2 Methods

2.2.1 Tissue culture

The mantle cell lymphoma derived cell line, Z138 cells was a kind gift from Martin J.D Dyer (University of Leicester) (Estrov *et al.*, 1998). Z138 cells were cultured in RPMI 1640 media containing 11.1 mM D-glucose, supplemented with 1 mM sodium pyruvate, 2 mM glutamax and 10% foetal calf serum (FCS) and incubated in a 5% CO₂ humidified atmosphere at 37°C. Cells were seeded at either 0.1 to 0.2 x 10⁶ cells/ml and passaged every 3 to 4 days respectively.

The mantle cell lymphoma derived cell line, UPN1 cells (M'kacher *et al.*, 2003) were cultured in RPMI 1640 media containing 11.1 mM D-glucose, supplemented with 1 mM sodium pyruvate, 2 mM glutamax and 10% FCS and incubated in a 5% CO₂ humidified atmosphere at 37°C. Cells were seeded at either 0.1 to 0.2 x 10⁶ cells/ml and passaged every 3 to 4 days, respectively.

For glucose deprivation studies, glucose deprived UPN1 cells were maintained in D-glucose free RPMI 1640 media containing 2 mM L-glutamine, supplemented with 1 mM sodium pyruvate and 10% FCS. Cells were incubated in a 5% CO₂ humidified atmosphere at 37°C. Cells were seeded at either 0.1 to 0.2 x 10⁶ cells/ml and passaged every 3 to 4 days respectively. Glucose containing UPN1 cells were maintained as above.

For 2-Deoxy-D-Glucose (2DG) experiments, Z138 cells were treated with 5 mM 2DG for the indicated time points in glucose containing media as described above.

For galactose studies, Z138 cells were cultured and maintained in D-glucose free RPMI 1640 medium containing 2 mM L-glutamine, supplemented with 11.1 mM D-galactose, 1 mM sodium pyruvate and 10% FCS and incubated in a 5% CO₂ humidified atmosphere at 37°C. Glucose containing cells used for comparative studies were cultured as above. Z138 cells were kept in galactose based media for at least 7 days before experiments to allow for metabolic and proteomic reprogramming.

2.2.2 Induction of apoptosis

UPN1 Cells

UPN1 cells were seeded at 0.2×10^6 cells/ml 48 h prior to apoptosis induction and harvested between $0.8 - 1.2 \times 10^6$ cells/ml. UPN1 cells were then treated with various concentrations of wild type recombinant TRAIL, as indicated in the figure legends. For blocking apoptosis, UPN1 cells were pre-treated for 30 min with the pan-caspase inhibitor zVAD.fmk to give final concentrations of 10 – 100 μ M, followed by 200 ng/ml TRAIL for 4 h. For blocking necroptosis, UPN1 cells were pre-treated with the RIPK1 inhibitor; Necrostatin-1 (Nec-1) at 50 μ M, and zVAD.fmk at 10 μ M for 30 min, followed by 200 ng/ml TRAIL for 4 h. Cells (200 μ l) were diluted in 800 μ l Annexin buffer and cell death assessed by FACS analysis. Following drug treatments, 10^6 cell/ml were harvested and the pellet retained for assessment of caspase cleavage. Cells were centrifuged at $300 \times g$ for 3 min at 4°C, media aspirated and the cells washed twice in ice cold PBS. The pellet was snap frozen in dry ice and stored at -80°C until required.

Induction of apoptosis – comparing glucose and galactose Z138 cells

Z138 cells cultured in either glucose containing or galactose containing medium were seeded at 0.2×10^6 cells/ml 48 h prior to apoptosis induction. When confluent ($0.8 - 1.2 \times 10^6$ cells/ml), 500 μ l of Z138 cells were then treated with varying concentrations of the following drugs/chemicals for 16 h: TRAIL; ABT-737; etoposide; cisplatin; staurosporin; artusenuate; oligomycin; FCCP; rotenone; antimycin; mitomycin C; as indicated in the figures. Caspase-dependent apoptosis was inhibited by pre-treatment for 60 min with the pan-caspase inhibitor zVAD.fmk at 50 μ M, followed by varying concentrations of the above drugs/chemicals for 16 h. For blocking necroptosis, Z138 cells were pre-treated with the RIPK1 inhibitor; Nec-1 at 50 μ M, and zVAD.fmk at 50 μ M for 60 min, followed by varying concentrations of the above drugs for 16 h. The cells were then diluted 1:1 in Annexin buffer and cell death assessed by FACS analysis.

Induction of apoptosis – sensitising using AMPK activators or inhibitor

Z138 cells were seeded at 0.2×10^6 cells/ml 48 h prior to apoptosis induction and harvested between $0.8 - 1.2 \times 10^6$ cells/ml. Z138 cells were pre-treated with the

indicated concentrations of the following AMPK activators for the indicated times: 2DG; metformin; phenformin; AICAR; AMP; thapsigargin or A23187 followed by either ABT-737 or TRAIL for 4 h. For the AMPK inhibitor dorsomorphin dihydrochloride (compound C), Z138 cells were pre-treated with the indicated concentrations for 30 min, followed by combinations of 5 mM 2DG for 8 h and/or 200 ng/ml TRAIL for 4 h. Aliquots (200 µl) of cells were diluted in 800 µl of Annexin buffer and cell death assessed by FACS analysis.

2.2.3 Measuring apoptosis

Apoptotic cells undergo a variety of morphological changes that can be detected to differentiate between healthy and dying cells. Following caspase activation, phosphatidyl serine (PS) is externalised to the exoplasmic face of the plasma membrane (Fadok *et al.*, 1992). A high affinity binding protein of PS is Annexin-V, a naturally occurring protein. Recombinant Annexin-V conjugated to fluorescein Isothiocyanate (FITC), can therefore be used to fluorescently label apoptotic cells as previously described (MacFarlane *et al.*, 2002). Late stage apoptotic and necrotic cells lose plasma membrane integrity. To differentiate between early and late stage apoptosis / necrosis, propidium iodide (PI) is also added. PI is a plasma membrane impermeable fluorescent nucleic acid intercalating agent, following loss of membrane integrity PI incorporates into nucleic acids. Thus combination of Annexin-V/FITC and PI can be used to distinguish the mode and stage of cell death based on PS exposure and plasma membrane integrity, respectively, as previously described (MacFarlane *et al.*, 2002)

Control and treated Z138 and UPN1 cells were transferred to Annexin buffer (10 mM HEPES (pH 7.4), 150 mM NaCl, 5 mM KCl, 1 mM MgCl₂, 1.8 mM CaCl₂). Samples were incubated in the dark at room temperature for 30 min with 1.5 µl of diluted Annexin-V-FITC (dilution varied depending on the batch of Annexin-V-FITC used). Following incubation, PI was added at 50 µg/ml and samples placed on ice and kept in the dark. A BD FACS Calibur, using Cell Quest Pro™ was used to simultaneously analyse PS+ and PI+ cells

2.2.4 Whole cell protein expression

Whole cell protein expression was determined as described previously (Robinson *et al.*, 2012). Cells were counted using a Scharffe Casy counter, centrifuged at 200

x g for 3 min at 4°C, and the pellet washed 2 x in ice cold PBS and resuspended in 1 x Laemmli buffer, sonicated for 60 s at 5 Hz. Sonicated, solubilised cells (2.5 x 10⁵ cells) were loaded on to 4 - 20% TRIS-glycine gradient gels and protein expression was analysed by immunoblotting.

2.2.5 Preparing cell lysates

Following siRNA transfection cells were washed twice in ice cold PBS and the pellet resuspended and incubated on ice for 30 min in 1 x RIPA buffer (150 mM NaCl, 50 mM TRIS (pH 8), 1% IGEPAL CA-630, 0.5% sodium deoxycholate, 0.1% SDS). Following incubation, the lysed cells were centrifuged at 18,000 x g for 20 min at 4°C to pellet the insoluble fraction. The supernatant was aliquoted into Eppendorf tubes and the protein concentration was determined using a BioRad protein assay dye reagent concentrate (2.2.6)

2.2.6 Determining protein concentration

Cell lysates were measured using the Bio-Rad protein assay dye reagent as previously published (Bradford, 1976; Robinson *et al.*, 2012). A standard curve was generated using 0 – 8 µg/ml Bovine Serum Albumin (BSA) in appropriately diluted Bradford reagent, the standard curve samples were measured in triplicate. The experimental samples were diluted, 2 µl in 998 µl of appropriately diluted Bradford reagent and measured in duplicate. The absorbance was measured on a Beckman Coulter spectrophotometer at 595 nm and the protein concentration calculated using the standard curve. Western blotting was performed using 20 µg of protein per sample.

2.2.7 Immunoblotting

Immunoblotting was carried out as previously described (Robinson *et al.*, 2012). Briefly, using SDS-PAGE, protein samples (20 µg or 2.5 x 10⁵ cells) were separated using 4 – 20% TRIS-glycine gradient gels (Invitrogen and Biorad) in either Invitrogen sure lock X or Bio Rad criterion tanks in electrode buffer (25 mM TRIS(hydroxymethyl)aminomethane, 192 mM glycine, 10% SDS). Following electrophoresis, proteins were transferred to methanol activated PVDF in a Bio-Rad protean tetra cell kit over night at 30 V in transfer buffer (25 mM TRIS(hydroxymethyl)aminomethane, 192 mM glycine, 20% methanol). The membranes were briefly stained with Ponceau S to ensure equal protein loading

and transfer. The membranes were then blocked for at least 1 h in 5% milk in TBS-T (TBS: (+ 0.1% TWEEN-20)), then washed 3 times in TBS-T. Membranes were then probed with the indicated primary antibody overnight at 4°C (Table 2.1).

Antibody	Supplier	Dilution	Host	Catalogue No
AMPK- α	Cell Signalling	1:1000	Rabbit	5831
AMPK- β 1	Cell Signalling	1:1000	Rabbit	4150
p-AMPK- α (T172)	Cell Signalling	1:1000	Rabbit	2535
p-AMPK- α (S485)	Cell Signalling	1:1000	Rabbit	4185
p-AMPK- β 1 (S108)	Cell Signalling	1:1000	Rabbit	4181
ACC	Cell Signalling	1:1000	Rabbit	3676
p-ACC (S79)	Cell Signalling	1:1000	Rabbit	11818
Akt	Cell Signalling	1:1000	Rabbit	9272
p-Akt (T308)	Cell Signalling	1:1000	Rabbit	4056
p-Akt (S473)	Cell Signalling	1:1000	Rabbit	4058
GSK-3 β	Cell Signalling	1:1000	Rabbit	12456
p-GSK-3 β (S9)	Cell Signalling	1:1000	Rabbit	5558
GSK-3 α	Cell Signalling	1:1000	Rabbit	4337
p-GSK-3 α (S21)	Cell Signalling	1:1000	Rabbit	9316
B-Catenin	Cell Signalling	1:1000	Rabbit	8480
LKB1	Cell Signalling	1:1000	Rabbit	3050
eE2F	Cell Signalling	1:2000	Rabbit	2332
p-eE2F (T56)	Cell Signalling	1:1000	Rabbit	2331
Erk	Cell Signalling	1:1000	Rabbit	9102
p-Erk (T202/Y204)	Cell Signalling	1:1000	Rabbit	9101
STAT3	Cell Signalling	1:1000	Rabbit	8719
p-P70S6K (T389)	Cell Signalling	1:500	Mouse	9206
rS6	Cell Signalling	1:2000	Mouse	2317
p-rS6 (S240/244)	Cell Signalling	1:1000	Rabbit	5364
4EBP1	Cell Signalling	1:5000	Rabbit	9452
p-4EBP1 (S65)	Cell Signalling	1:1000	Rabbit	9451
eIF2- α	Cell Signalling	1:1000	Rabbit	9722
p-eIF2- α (S51)	Cell Signalling	1:1000	Rabbit	3597
Caspase-8	In house	1:3000	Rabbit	N/A
Caspase-9	In house	1:3000	Rabbit	N/A
Caspase-3	In house	1:3000	Rabbit	N/A
Caspase-7	In house	1:3000	Rabbit	N/A
PARP	Enzo	1:2500	Mouse	BML-5A249
α -Tubulin	Cell signalling	1:1000	Rabbit	2144
Bad	Cell Signalling	1:1000	Rabbit	9292
Bcl-2	Dako	1:1000	Mouse	Clone 124
Bcl-X _L	BD	1:1000	Rabbit	610211
Bcl2-A1	Santa cruz	1:100	Goat	Sc-6068
Puma	Cell signalling	1:1000	Rabbit	4976
Bid	Cell signalling	1:1000	Rabbit	2002
Bax	Upstate	1:1000	Rabbit	04-434
Bak	Upstate	1:1000	Rabbit	06-536
Mcl-1	Santa cruz	1:500	Rabbit	SC-819
Noxa	Calbiochem	1:250	Mouse	OP180
XIAP	Transduction labs	1:2000	Mouse	610717
RIPK1	BD	1:1000	Mouse	610458
P53	Cell signalling	1:1000	Rabbit	9282
Cyt c	Pharmlingen	1:5000	Mouse	556433

Table 2.1 Table detailing all primary antibodies used for immunoblotting, the supplier, host and the dilution required in 5% BSA.

The membranes were then probed with the corresponding secondary antibody for 2 h (Table 2.2). Immunostained membranes were then either analysed on a Li-Cor Odyssey imaging platform at the appropriate intensity or using enhanced chemiluminescence (ECL) and x-ray film.

Antibody	Supplier	Dilution	Host	Catalogue No
Anti-rabbit	Dako	1:2000	Goat	P0448
Anti-mouse	Sigma	1:2000	Goat	A8924
Anti-mouse 800cw	LiCor Bioscience	1:10000	Goat	926-32210
Anti-rabbit 800cw	LiCor Bioscience	1:10000	Goat	926-32211
Anti-Goat 800cw	LiCor Bioscience	1:10000	Donkey	926-32214
Anti-mouse 680rd	LiCor Bioscience	1:10000	Goat	926-68070
Anti-rabbit 680rd	LiCor Bioscience	1:10000	Goat	926-68071
Anti-goat 680rd	LiCor Bioscience	1:10000	Donkey	926-32224
Anti-mouse 680lt	LiCor Bioscience	1:20000	Goat	926-68020
Anti-rabbit 680lt	LiCor Bioscience	1:20000	Goat	926-68021

Table 2.2 Table detailing all secondary antibodies used for immunoblotting, the supplier, dilution, host and catalogue number. All antibodies were diluted in 5% milk (made in TBS-T)

2.2.8 Detection of mitochondrial superoxide

Detection of mitochondrial superoxide was performed using MitoSOX™ (Life Technologies). Briefly, Z138 cells were treated with MitoSOX™ to give a final concentration of 1 µM and incubated at 37°C for 10 min to allow MitoSOX™ loading. The relative intensity was then measured on BD FACS Canto flow cytometer. For 2DG and antimycin time course, a basal measure of ROS was recorded on the FACS then either 5 mM 2DG or 1 µM antimycin was added to the cells in the FACS tube and the increase in fluorescence measured against time (for 25 min).

2.2.9 siRNA transient nucleofection

Z138 cells were seeded at 0.2×10^6 cells/ml, 48 h prior to transfection in glucose containing medium. Cells were harvested between $0.8 - 1.2 \times 10^6$ cells/ml, and centrifuged at room temperature at $200 \times g$ for 5 min. The medium was aspirated and cells centrifuged again at $200 \times g$ for 3 min at room temperature, and remaining medium discarded. Z138 cells were resuspended in SF solution (LONZA) at 7.5×10^5 cells/20 µl for 16 well nucleofection strips; or 5×10^6 cells/100 µl for nucleofection cuvettes. Lyophilised siRNA was reconstituted in sterile ultrapure H₂O and added to the resuspended cells at the indicated final concentrations. Cells were then nucleofected using an Amaxa 4D nucleofector

(LONZA) on program CM119. Post transfection, cells were incubated with 4 x transfection volume recovery media (RMPI 1640 containing 11.1 mM D-glucose, no additions) at room temperature for 10 min. Transfected cells were then added to RPMI 1640 media containing 11.1 mM D-Glucose, supplemented with 1 mM Sodium pyruvate, 2 mM Glutamax; 10% FCS and incubated in a 5% CO₂ humidified atmosphere at 37°C. Samples were collected at the indicated time points for preparation of cell lysates and immunoblotting or FACS analysis of apoptosis.

2.2.10 Polysome profiling

Sucrose density gradient preparation

Polysome profiling was carried out in collaboration with Carolyn Jones from the MRC Toxicology Unit Genomics Facility as previously described (Powley *et al.*, 2009).

Gradient buffer (GB) was made as a 10x stock (3 M NaCl, 150 mM MgCl₂, 150 mM Tris-HCl (pH 7.5), 20 mM DTT, 1 mg/ml cycloheximide) and was diluted to 1 x and used to make 10%, 20%, 30%, 40% and 50% w/v sucrose solutions. To pre-washed centrifuge tubes (Sorvall PA 12 ml), 2 ml 50% sucrose was added and placed in a -80°C freezer for 30 min. From the 40% sucrose solution, 2 ml was then layered over the top and allowed to freeze at -80°C for 30 min. This process was repeated sequentially for 30, 20 and 10% sucrose solutions, and finally stored at -20°C. Prior to experimentation (16 h) the gradients were removed from the freezer and allowed to equilibrate to 4°C.

Polysome profiling

Cycloheximide (CHX) was added to control and 2DG treated Z138 cells to give a final concentration of 100 µg/ml and the samples were incubated for 3 min at 37°C in 5% CO₂ humidified atmosphere. The cells were subsequently washed twice in ice cold PBS containing 100 µg/ml CHX, cells were then centrifuged at 500 x *g* for 3 min, the supernatant aspirated and cell pellets resuspended in 1 ml polysome lysis buffer (300 mM NaCl; 15 mM MgCl₂; 15 mM TRIS-HCL (pH 7.5); 100 µg/ml CHX; 1 mg/ml heparin; 1% Triton X-100), which was centrifuged at maximum on a benchtop microfuge (approx. 18,000 x *g*). The supernatants were then gently

layered onto the pre-equilibrated 10 – 50% sucrose density gradients and centrifuged at 38,000 rpm for 2 h at 4°C. The gradients were fractionated through a Teledyne ISCO Foxy R1 fractionator with a flow rate of 1 ml/min with the absorbance continually measured at 254 nm by a Teledyne ISCO UA-6 UV-Vis detector. The absorbance values were plotted into an XY scatter plot in GraphPad Prism to generate the polysome profile trace.

2.2.11 Assessment of global protein synthesis: [³⁵S] methionine cysteine incorporation and trichloroacetic acid (TCA) protein precipitation

Z138 cells were seeded at 0.2×10^6 cells/ml 48 h prior to experiment. Cells were harvested between $0.8 - 1.2 \times 10^6$ cell/ml and treated with 5 mM 2DG at staggered intervals so that 8, 6, 4, 2, 1 and 0.5 h finished treatment at the same time. Cells were then centrifuged at $300 \times g$ for 5 min at room temperature, the supernatant aspirated and the cell pellet resuspended in 500 μ l [³⁵S] methionine and cysteine pulse labelling medium (PLM: Methionine and cysteine free DMEM, 10% (v/v) dialysed FCS and [³⁵S] methionine and cysteine at 1.43 MBq/ml) in a water bath at 37°C for 15 min, to allow incorporation of radiolabelled amino acids, tubes were inverted every 3 -5 min to keep cells resuspended. Cells were centrifuged at $18,000 \times g$ for 1 min at 4°C and the supernatant aspirated. Pellets were then washed 2 x in PBS with sequential centrifugation at $18,000 \times g$ for 1 min at 4°C and resuspended in 400 μ l passive lysis buffer (Promega) and left to incubate on ice for 10 min. Lysates were centrifuged at $18,000 \times g$ for 5 min to pellet insoluble fraction, and 300 μ l cleared lysate aliquoted into an Eppendorf tube. The remainder of the cleared lysate (~ 100 μ l) was aliquoted into an eppendorf tube for determination of protein concentration.

Whatmann 2.5 cm glass microfiber filter discs were placed on to a vacuum manifold and pre-wet with 25% TCA. To the 300 μ l of cleared lysate, 300 μ l of 25% TCA was added and incubated on ice for 30 min. The TCA-lysate solution was then spotted onto the glass microfiber filters. The filters were then washed twice in 70% IMS followed by 2 washes with acetone, left to air dry and then placed in scintillation vials containing 2 ml scintillation fluid and [³⁵S] incorporation was measured on a WALLAC WINSPECTRAL™ 1414 liquid scintillation counter.

2.2.12 Extracellular flux analysis

Extracellular flux analysis was performed as previously described (Robinson *et al.*, 2012) using a Seahorse XF24 analyser. Seahorse assay cartridges were hydrated in Seahorse calibrant 24 h prior to experimentation. Z138 or UPN1 cells were seeded at 0.2×10^6 cells/ml in appropriate RPMI 1640 media 48 h prior to experimentation. Cells were then centrifuged at $300 \times g$ for 5 min for 3 cycles, resuspending the cells in 10 ml unbuffered DMEM (pH 7.4) between each centrifugation, either containing 11.1 mM glucose, 11.1 mM galactose, 5 mM 2DG + 11.1 mM glucose or no glucose; all were supplemented with 2 mM glutamax, 1 mM sodium pyruvate and 31.6 mM NaCl. Seahorse XF24 cell culture plates were coated with 40 μ l of a Cell-Tak solution (16.6 mM NaOH, 100 mM Na₂CO₃ (pH 8), 40 μ l Cell-Tak™), and left at room temperature for 20 min, then washed 3 times in 1 ml sterile PBS. Cells were seeded at 4.5×10^5 cells/well and centrifuged at $60 \times g$ for 2 min at room temperature. Cells were then left to 'stick' to the plate for 1 h in a CO₂ free, non-humidified incubator at 37°C. This process also allowed the pH to equilibrate in un-buffered media. The final volume of unbuffered medium in each well was 675 μ l.

The ATP synthase inhibitor oligomycin was prepared in 100% ethanol to give a stock solution of 10 mM, which was further diluted to 5 μ M in unbuffered DMEM immediately prior to experimentation. The protonophore FCCP was prepared in 100% ethanol to give a stock solution of 10 mM, which was further diluted to 4 μ M in unbuffered DMEM immediately prior to experimentation. The NADH dehydrogenase inhibitor rotenone was prepared in DMSO to give a stock solution of 5 mM, which was further diluted to 10 μ M in unbuffered DMEM immediately prior to experimentation. The cytochrome *c* – oxidoreductase inhibitor antimycin was prepared in 100% ethanol to give a stock solution of 5 mM, which was further diluted to 10 μ M in unbuffered DMEM immediately prior to experimentation. All inhibitor solutions were made to pH 7.4 when diluted in the appropriate DMEM.

The mitochondrial inhibitors: oligomycin A; FCCP; rotenone and antimycin were loaded into the drug delivery ports of the hydrated assay cartridge, where ports A, B, C and D contained: 75, 83, 90 and 100 μ l respectively. Sequential injection of the desired drugs resulted in a 1:10 dilution to give the final concentrations of: oligomycin; FCCP; rotenone; antimycin were: 500 nM; 400 nM; 1 μ M and 1 μ M

respectively, unless otherwise indicated in the figure legends. Oxygen consumption rates (OCR) and extra cellular acidification rates (ECAR) were then measured in real time

2.2.13 ATP levels

ATP levels were obtained using the CellTiter-Glo® Luminescent Cell Viability Assay (Promega) following the manufacturer's instructions. Briefly, Z138 cells were treated with 5 mM 2DG or PBS (0 h control) for the indicated time points; and harvested between $0.8 - 1.2 \times 10^6$ cells/ml. Control and treated cells were diluted in culture medium to give 2×10^4 cell in 100 μ l and aliquoted into an opaque-walled 96 well plate. Control wells contained 100 μ l culture media to correct for background. CellTiter-Glo® reagent was added in a 1:1 ratio (100 μ l/well) and placed on an orbital shaker for 2 min, then left to equilibrate at room temperature for 10 min. Luminescence was recorded on a WALLAC VICTOR™ 1420 Multilable counter

2.3 Immunopurification of mitochondria for mass spectrometry

2.3.1 Subcellular fractionation

Subcellular fractionation was performed prior to immunopurification of mitochondria (2.3.4). A total of 10^9 Z138 cells cultured in either glucose, galactose, glucose free or glucose containing treated for 20 h with 5 mM 2DG were centrifuged at $600 \times g$ for 5 min at 4°C, followed by two sequential washes in ice cold PBS and centrifugation at $600 \times g$ for 5 min at 4°C. Cell pellets were resuspended in 2 x pellet cell volume (PCV) of ice cold RSB buffer (10 mM KCl; 1.5 mM MgCl₂; 10 mM HEPES-KOH; pH 7.5 with EDTA-free protease inhibitors Roche) and incubated on ice for 10 min. Resuspended cells were then mechanically homogenised using a 2 ml Dounce homogeniser for 30 strokes and added to 2 x PCV of 2.5 X MS Buffer (525 mM mannitol; 175 mM sucrose; 12.5 mM HEPES-KOH; 2.5 mM EDTA; pH 7.5 with EDTA-free protease inhibitors (Roche)) and 200 μ l of lysate sample collected. The remaining lysate was centrifuged a $900 \times g$ for 10 min at 4°C, the supernatant was removed and the pellet was resuspended in 100 μ l HIM buffer (200 mM mannitol; 70 mM sucrose; 10 mM HEPES-KOH; 1 mM EGTA; pH 7.5 with EDTA-free protease inhibitors (Roche)) (nuclei fraction 1). Supernatants were centrifuged at $1100 \times g$ for 10 min at 4°C, the supernatant collected and the pellets

were resuspended in 100 μ l HIM buffer (nuclei fraction 2). Supernatants were spun at 10000 x g for 15 min at 4°C, the supernatant was collected and stored for the cytosolic fraction. The remaining mitochondrial pellets were each resuspended in 200 μ l HIM buffer and combined into one Eppendorf tube, then centrifuged at 10000 x g for 10 min at 4°C, the supernatants were discarded and the mitochondrial fractions were resuspended in 200 μ l HIM buffer. From the mitochondrial fraction, 20 – 70 μ l of mitochondrial sample was collected and stored at -80°C at this point for immunoblotting, HIM buffer was added to the remaining mitochondrial fraction to make a final volume of 450 μ l.

2.3.2 Immobilising antibodies

Using a magnet, the holding buffer was removed from 300 μ l Dyna Protein G beads. The beads were washed sequentially 3 x in 500 μ l ice cold PBS-T (PBS + 0.05% Tween) and resuspended in 100 μ l PBS-T. TOM20 antibody (Santa Cruz) (240 μ l) was added to the beads and incubated on a roller for 1 h at 4°C. The supernatant was removed from the beads using a magnet and discarded, the beads were then cross-linked.

2.3.3 Cross-linking

The immobilised beads were washed twice in 1 ml 0.2 M triethanolamine (TES) pH 8.2 and then resuspended in 1 ml 20 mM DMP (5.4 mg/mL Dimethyl pimelinediimidate dihydrochloride in 0.2 M TEA, pH 8.2) and incubated on a roller at room temperature for 30 min. The supernatant was removed using a magnet and discarded, the beads were then resuspended in 1 ml 50 mM TRIS, pH 7.5 and incubated on a roller for 15 min at room temperature. The supernatant was removed using a magnet and discarded, and the beads then washed sequentially 3 x in 1 ml ice cold PBS-T. The beads were then resuspended in 100 μ l PBS-T and stored on ice until immunoprecipitation.

2.3.4 Immunoprecipitation

Supernatant was removed from cross-linked beads (2.3.3) and the beads resuspended with 450 μ l isolated mitochondria (2.3.1). The beads were incubated on a daisy wheel at 4°C for 2 h. The supernatant was removed using a magnet and stored in an Eppendorf tube at -20°C (flow-through). The beads were washed 3 x in 1 ml ice cold PBS, supernatant removed and discarded and the beads

resuspended in 40 μ l 2 X SDS buffer and stored at -20°C . When required for mass spectrometry analysis, the mitochondria immunopurified beads were heated to 70°C for 10 min to solubilise the mitochondria in 2 X SDS buffer. The beads were then removed from the solubilised mitochondria using a magnet, and the isolated mitochondria boiled at 99°C for 4 min. The mitochondrial samples were then loaded on to a 4-12% Bis-Tris (Invitrogen) Bolt gel and ran 3 cm into the gel to separate proteins. The gels were then stained with INSTANTBLUE™ (Expedeon) to visualise protein banding.

2.4 Mass spectrometry

2.4.1 Sample preparation

Mass spectrometry was performed in collaboration with Dr. Claudia Langlais from the MRC Toxicology Protein Profiling Group.

Coomassie stained gels from the immunoprecipitation experiment (2.3.4) were cut into 12 slices per lane. The lanes contained either glucose, galactose, glucose free or 2DG treated mitochondria. Coomassie stained slices were placed into individual wells of 96-well PCR plates, then destained with 50 mM ammonium bicarbonate / 100% acetonitrile. Following destaining, the samples were reduced with 10 mM dithiothreitol for 20 min at 56°C and alkylated with 100 mM iodoacetamide in the dark for 20 min. The samples were then washed 3 X with 50 mM ammonium bicarbonate / 100% acetonitrile. The destained, alkylated gel slices were then resuspended with 15 μ l Trypsin digestion buffer (11.11 $\mu\text{g}/\text{ml}$ in 25 mM ammonium bicarbonate; Sequencing Grade Modified Trypsin, Promega Corporation, Madison, Wisconsin, USA). The plate was sealed and incubated at 30°C overnight. To each well containing a gel slice, 80 μ l of 0.2% trifluoroacetic acid was added and the plate was incubated for 1 h at room temperature. The extracted samples were transferred to 0.5 ml Eppendorf tubes and dried for 1 h with a Savant DNA Speed Vac (Thermo Scientific, Waltham, MA, USA). The dried peptide samples were resuspended with 5% formic acid/acetonitrile (9:1), vortexed, and transferred to glass vials by combining two samples into one vial. For quantitation of protein, the samples were spiked with two internal standards, ADH1 from yeast and bovine serum albumin, to give a final concentration of 20 fmol/ μ l (MassPREP standards, Waters Corporation, Manchester, UK).

2.4.2 Mass spectrometry analysis

The peptide mixtures were analysed by nanoflow liquid chromatography coupled to a Synapt G2S mass spectrometer (NanoAcquity UPLC system and Synapt G2S mass spectrometer, Waters Corporation, Manchester, UK) using a 25 cm X 75 µm I.D., 1.7 µm, BEH130 C18 column. Samples (2 µl injections) were separated using a reversed phase 90 min solvent gradient (3% to 40% acetonitrile) at 0.3 µl/min. Mass spectrometry analysis was performed in a data-independent manner using ion mobility (HDMS^E), with IMS wave velocity set to 650 m/s in the helium cell. The mass spectrometer was programmed to step between low energy (4 eV) and elevated collision energies (20-50 eV) in the gas cell, using a scan time of 1 s and a mass range of 50-2000 *m/z*. Each biological sample was run on the mass spectrometers twice to generate technical duplicates.

2.4.3 Database search and protein identification

Raw data files were analysed using ProteinLynx Global SERVER (PLGS version 3, Waters Corporation, Manchester, UK) in combination with ISOQuant (Jörg Kuharev and Stefan Tenzer, University of Mainz, Germany, open source under: <http://www.immunologie.uni-mainz.de/isoquant/>), and TransOmics Informatics for Proteomics (version 1.1, Nonlinear Dynamics, Newcastle, UK). The human UniProt database (UniProtKB/SwissProt, release 2013_01, 06.02.2013, 20233 entries) was used for TransOmics data analysis, with a later version of the same database used in PLGS/IsoQuant, including reverse sequences (release 2014_05, 11.06.14, 20265 entries). PLGS and ISOQuant data were used for “TOP 3” absolute quantification of proteins from protein complexes, whereas TransOmics was utilised for label-free quantification of relative normalised abundancies and principal components analysis (PCA) of the whole dataset.

2.4.4 Label free quantitation using TransOmics

Raw data files were imported directly into TransOmics Informatics for Proteomics (version 1.1, Nonlinear Dynamics, Newcastle, UK) and gel slices analysed in separate data files. Samples were run in duplicate generating a total of 16 sample runs per gel slice, displayed as 2D ion intensity maps. Retention time limits were set to 15 min and 85 min. A reference run was selected automatically and runs automatically aligned, with poorly aligned runs realigned manually by inserting 4 to

8 seeding vectors. The peak picking algorithm assembled the pattern of feature outlines, which were used for normalisation correction. Samples were sorted into experimental groups and database searching performed with identical PLGS settings, with exception that the FDR was set to 4%. Identified peptides were further refined by deleting identifications with less than 2 hits and with a score of 5.5 or less. Any peptide sequence with a length of less than six amino acids was also deleted. Conflict resolution was carried out manually by assigning peptides to the protein with the highest probability score. TransOmics data files were then assembled to generate one "Multi Fraction Experiment" TransOmics data file, which was used for comparisons of relative normalised abundances and principal components analysis (PCA) of the whole dataset.

2.4.5 Ingenuity pathway analysis

From the TransOmics data generated by Dr. Claudia Langlais, the Protein Accession codes, the fold change data between glucose and galactose runs, along with the p values generated by TransOmics were copied into an excel spreadsheet. Ingenuity Pathway Analysis (<http://www.ingenuity.com/>) (QIAGEN) was launched and a new core analysis was selected. The excel spreadsheet containing fold change, p-values and accession numbers was uploaded. For the species selection tab, all were deselected except human. For the tabs: tissue and cell lines; molecule types; diseases; biofluids; biomarkers, all options were selected. The cut off value was set for $p \leq 0.05$, then a 'core analysis' was run.

In the results/analysis pane, the canonical pathways tab was selected and displayed as a stacked bar chart to show up and down regulated pathways. Metabolic and apoptotic pathways were selected manually to draw a schematic in Corel Draw X6 of alterations following metabolic reprogramming in Z138 cells cultured in galactose media (Chapter 5).

Chapter 3

3. Results Chapter 1

Glucose deprivation prevents UPN1 cells from switching to TRAIL-induced necroptosis

3.1 Introduction

In the 1920's Otto Warburg showed that cancer cells preferentially utilise aerobic glycolysis at the expense of energetically favourable mitochondrial oxidative phosphorylation (Warburg *et al.*, 1927; Warburg, 1956). Warburg ascribed this metabolic reprogramming from oxidative phosphorylation to glycolysis as a result of mitochondrial defects. Now universally known as the 'Warburg effect', metabolic reprogramming has emerged as a cancer hallmark (Hanahan & Weinberg, 2011) and there is intense ongoing academic and industrial research into its therapeutic significance. Although cancer cells do have a propensity for aerobic glycolysis, it is now known that it occurs concomitantly with mitochondrial oxidative phosphorylation (Jose *et al.*, 2011; Solaini *et al.*, 2011). Increased glycolysis results in enhanced carbon flux into subsidiary carbon shunt pathways branching from various steps in glycolysis. The most important of these for rapid uncontrollable tumour cell growth is the pentose phosphate shunt (PPP) (Reviewed in Tennant *et al.*, 2010) (see chapter 1.5). Due to the survival and growth advantages conferred by increased glycolysis, many studies have looked at the effects of glucose deprivation on cancer cell death (Robinson *et al.*, 2012; Gonin-Giraud *et al.*, 2002; Yuneva *et al.*, 2007; Lee *et al.*, 1997; Caro-Maldonado *et al.*, 2010; Zhao *et al.*, 2008; Mendivil-Perez *et al.*, 2013; Vander Heiden *et al.*, 2001; Alves *et al.*, 2006).

The extrinsic apoptotic cell death pathway is an ATP-dependent mechanism, and previous studies have shown that it is ATP levels that determine whether a cell dies via apoptosis or necrosis (Leist *et al.*, 1997). However, various studies have been published offering conflicting data, arguing that a decrease in cellular ATP levels causes a sensitization to death receptor-mediated apoptosis (Leist *et al.*, 1997; Halicka *et al.*, 1995; Munoz-Pinedo *et al.*, 2003; Nam *et al.*, 2002; Wood *et al.*, 2008). This is contrary to other reports arguing that apoptotic cells display higher ATP levels (Zamaraeva *et al.*, 2005). To complicate the issue further, ATP levels are modulated through metabolism, and some studies indicate that cells deprived of glucose are more sensitive to cell death (Pradelli *et al.*, 2010), whilst others have shown conflicting evidence to argue that certain cell lines/types are instead more resistant to cell death when deprived of glucose (Robinson *et al.*, 2012).

Apoptosis was once considered the sole form of programmed cell death, however recent evidence suggests that certain types of necrosis are also tightly regulated processes, such as 'necroptosis' (Han *et al.*, 2011). Necroptosis is thought to be an evolutionary conserved 'back-up' mechanism, used to clear viral infections that can inhibit caspase-dependent apoptosis (Cho *et al.*, 2011; Kaiser *et al.*, 2013). Necroptosis is signalled via the 'necrosome', a multi-protein complex that contains receptor interacting protein kinase-1 and -3 (RIPK1 and RIPK3) and mixed lineage kinase domain-like protein (MLKL) (Linkermann & Green, 2014). Necroptosis is inhibited by caspase activation via caspase-8 mediated cleavage of RIPK1 and RIPK3. Thus, following caspase-8 inhibition, necroptosis may occur in certain cell lines, instead of apoptosis (reviewed in Linkermann & Green, 2014)

Work previously performed in our laboratory has shown that the mantle cell lymphoma derived cell line, Z138, is resistant to both TRAIL and ABT-737-induced apoptosis when maintained in glucose-free media (Robinson *et al.*, 2012). The aims of this chapter were to determine if chronic glucose deprivation confers the same resistance to TRAIL and results in the same metabolic reprogramming in another mantle cell lymphoma derived cell line, namely, UPN1 cells. Additionally the study set out to identify if 'aerobically poisoning' the cells affects the mode of cell death following treatment with death ligands. Firstly, the time and dose-dependent apoptotic response of UPN1 cells to TRAIL was examined using Annexin-V/PI staining and flow cytometry. The modes of cell death were additionally examined by inhibiting either caspase activity with zVAD.fmk or receptor interacting protein kinase 1 (RIPK1) activity with necrostatin-1 (Nec-1). Whole cell protein expression levels were assessed for differences using immunoblotting and finally the metabolic response to glucose deprivation was analysed using a Seahorse XF24 extracellular flux analyser. The results showed that glucose deprivation resulted in a slight increase in sensitivity to TRAIL and that the mode of cell death was caspase-dependent apoptosis in both culture conditions. Strikingly though, metabolic reprogramming as a result of glucose deprivation prevented the cells from switching to TRAIL-induced necroptosis following the inhibition of caspase activity.

3.2 Results

3.2.1 Glucose deprivation alters the cell death phenotype in response to TRAIL treatment in a dose-dependent manner

Previously published work (Robinson *et al.*, 2012) has shown that chronic glucose deprivation results in resistance to TRAIL in Z138 cells. To determine if this phenomenon occurs in another mantle cell lymphoma derived cell line, UPN1 cells were cultured and maintained in the absence (glucose^{-ve}) and presence (glucose^{+ve}) of 11.1 mM glucose, as detailed in methods (2.2.1). Glucose^{+ve} and glucose^{-ve} cells were treated with increasing concentrations of TRAIL (0 – 500 ng/ml) for 4 h and cell death measured using Annexin-V-FITC and PI staining on a flow cytometer. A representative example of the FACS data from glucose^{+ve} cells treated with 100 ng/ml TRAIL is shown in Figure 3-1A, which showed a predominantly apoptotic phenotype, with cells clustered in the PS+/PI- quadrant (upper left). Interestingly, despite substantial cell death, there was minimal reduction in the size of the cells, indicated by a minor reduction in forward scatter. However, glucose^{-ve} cells (Figure 3-1B) show a predominantly primary or secondary necrotic phenotype, PS+/PI+ (upper right) (Figure 3-1 B), with significantly more cells showing a reduction in forward scatter and therefore reduction in size. Glucose^{-ve} cells were slightly more sensitive to TRAIL (Figure 3-1C), when assessing the percentage of total cell death, i.e. phosphatidyl serine positive cells (PS+), the combined values in both the upper left (PS+/PI-) and upper right (PS+/PI+) quadrants, however this was only significant at 20 and 100 ng/ml TRAIL. The TRAIL EC₅₀ in glucose^{+ve} cells was 54 ng/ml, compared to glucose^{-ve} cells, with an EC₅₀ of 34 ng/ml TRAIL; 37% lower. Strikingly the cell death phenotype appeared to be different between glucose^{+ve} and glucose^{-ve} cells. Glucose^{+ve} cells were predominantly apoptotic in phenotype, i.e. PS+/PI- (Figure 3-1C and D) from 50 to 500 ng/ml TRAIL. This was in stark contrast to glucose^{-ve} cells, which displayed a predominantly primary or secondary necrotic phenotype, i.e. PS+/PI+ (Figure 3-1E) that increased in a dose-dependent manner.

Investigation of caspase activation showed that TRAIL induced a dose-dependent cleavage and activation of caspase-8 and caspase-3 (Figure 3-1 F).

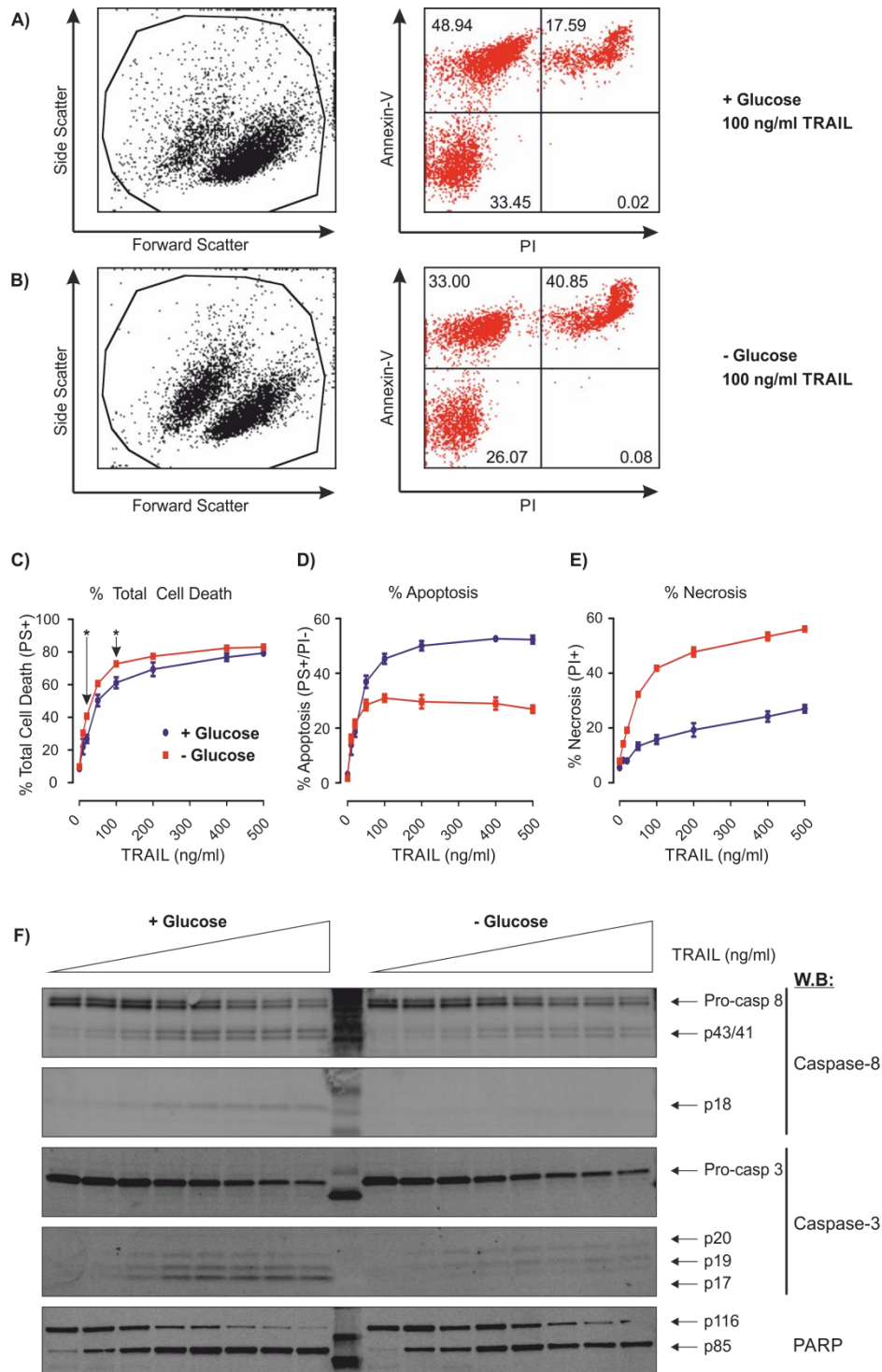


Figure 3-1 Glucose deprivation alters the cell death phenotype in response to TRAIL treatment in a dose-dependent manner. UPN1 cells were cultured in the absence (■) or presence (●) of 11.1 mM glucose, supplemented with 1 mM sodium pyruvate, 2 mM glutamax and 10% FCS. Cells were treated with 0 – 500 ng/ml TRAIL for 4 h. **A)** Glucose^{+ve} cells treated with 100 ng/ml TRAIL, representative example of forward and side scatter, additionally cells predominantly tracked to the upper left quadrant (PS+/PI-). **B)** Glucose^{-ve} cells treated with 100 ng/ml TRAIL representative example of forward and side scatter, additionally cells mainly tracked to the upper right quadrant (PS+/PI+). TRAIL dose response showing **C)** Total cell death (PS+), **D)** apoptotic cell death (PS+/PI-) and **E)** necrotic cell death (PS+/PI+). **F)** Western blot analysis of caspase-8, caspase-3 and PARP cleavage following TRAIL dose response. Experiments representative of 3 independent experiments, error bars ± SEM. Star (*) represents p < 0.05 (Students t test)

Processing of pro-caspase 8 to p43/41 was detected at 10 ng/ml TRAIL in both glucose^{+ve} and glucose^{-ve} cells. Interestingly however, the stability of the p43/41 fragments appeared to be significantly reduced in glucose^{-ve} cells compared to glucose^{+ve} cells (Figure 3-1F). Processing to the p18 fragment occurred in glucose^{+ve} cells but not in glucose^{-ve} cells; whether processing to p18 had occurred or whether the cleavage fragments were less stable remains to be determined. The dose-dependent decrease in pro-caspase-3 intensity was equal between glucose^{+ve} and glucose^{-ve} cells. Strikingly however, the caspase-3 cleavage fragments p20/19/17 were absent in glucose^{-ve} cells. This was in contrast to glucose^{+ve} cells, where the p20/19/17 cleavage fragments were clearly detectable. Processing to p17 could be seen at concentrations as low as 20 ng/ml in glucose^{+ve} cells. PARP, the caspase-3 substrate, was cleaved to the p85 subunit in both glucose^{-ve} and glucose^{+ve} cells at the lowest TRAIL concentration of 10 ng/ml, which indicated that cell death was caspase-dependent (Figure 3-1F).

3.2.2 Glucose deprivation alters the cell death phenotype in response to TRAIL within 3 h

Next, to determine if glucose^{-ve} cells first underwent apoptosis (PS+/PI-) then subsequently underwent secondary necrosis (PS+/PI+), thus tracking to the upper right quadrant, UPN1 cells were treated with 200 ng/ml TRAIL and assessed for cell death at 0,1,2,3,4,5 and 6 h. Glucose^{-ve} cells underwent cell death marginally faster than glucose^{+ve} cells. At 2 h post TRAIL treatment 30% of glucose^{+ve} cells were dead, compared to 40% cell death in glucose^{-ve} cells. (Figure 3-2A). There was no detectable cell death with Annexin-V/PI staining at 1 h post TRAIL treatment in either culture condition. The percentage of cells undergoing apoptosis (PS+/PI-) was consistently higher in glucose^{+ve} cells. (Figure 3-2B). Whereas glucose^{-ve} cells consistently contained more cells that expressed a PS+/PI+ phenotype (Figure 3-2C). Glucose^{-ve} cells predominantly expressed PS+/PI- cells at 3 h TRAIL treatment, whereas at 4 – 6 h there was a reduction in PS+/PI- cells, which indicated that glucose^{-ve} cells tracked from the PS+/PI- quadrant to the PS+/PI+ quadrant in a time-dependent manner.

Investigation of caspase activation showed that TRAIL induced a time-dependent cleavage and activation of caspase-8 and caspase-3. Processing of pro-caspase-

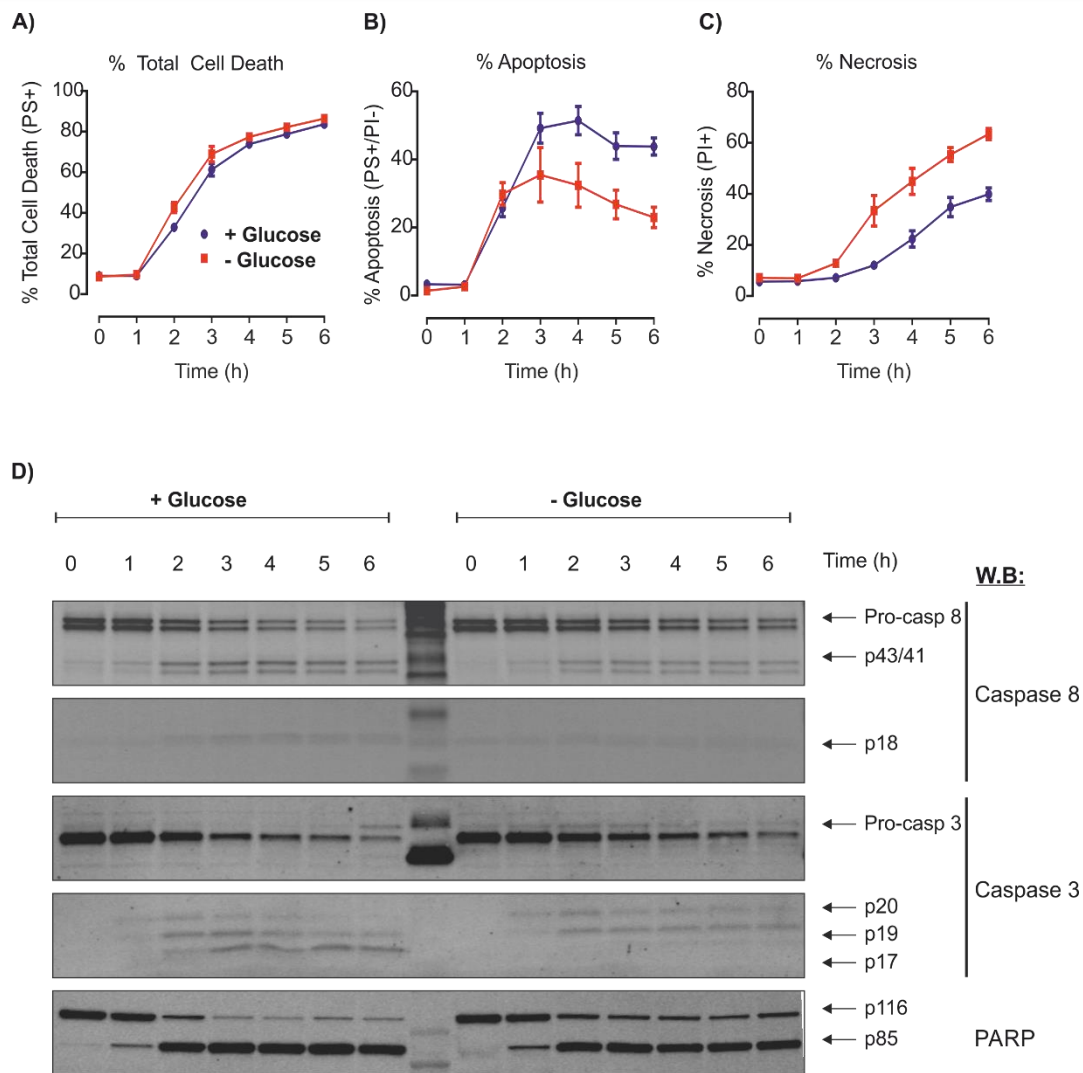


Figure 3-2 Glucose deprivation alters the cell death phenotype in response to TRAIL within 3 h. UPN1 glucose^{-ve} (■) and glucose^{+ve} (●) cells (as described in Figure 3.1) were treated with 200 ng/ml TRAIL for 0, 1, 2, 3, 4, 5 and 6 h. Annexin-V/PI analysis to show **A)** Total cell death (PS+), **B)** apoptotic cell death (PS+/PI-) and **C)** necrotic cell death (PS+/PI+). **D)** Western blot analysis of caspase-8, caspase-3 and PARP cleavage following TRAIL time course. Experiments representative of 3 independent experiments, error bars \pm SEM.

8 to p43/41 was barely detectable at 1 h post TRAIL treatment in glucose^{+ve} and glucose^{-ve} cells (Figure 3-2D). There was no detectable cleavage of pro-caspase-3 to p17 at this time, however p20 was detected in both glucose^{+ve} and glucose^{-ve} cells. Detectability of all three caspase-3 cleavage fragments p20/19/17 occurred at 2 h post TRAIL treatment in glucose^{+ve} cells. As identified in Figure 3-1F, glucose^{-ve} cells displayed minimal detectability of the caspase-3 cleavage fragment p17. Despite no PS externalisation detected at 1 h post TRAIL treatment, PARP, the downstream caspase-3 target started to show minimal cleavage from p116 to p85 subunit at 1 h post treatment in glucose^{+ve} and glucose^{-ve} cells.

3.2.3 The pan-caspase inhibitor zVAD.fmk does not completely block TRAIL-induced cell death in glucose^{+ve} cells

UPN1 glucose^{-ve} cells appeared to have a different cell death phenotype compared to glucose^{+ve} cells, with increased PI incorporation and a reduction in forward scatter (cell size) (Figure 3-1). To determine if cell death was caspase dependent, UPN1 cells were pre-treated with increasing concentrations (10 – 100 μ M) of the pan-caspase inhibitor zVAD.fmk for 30 min, followed by 200 ng/ml TRAIL for 4 h and then cell death assessed by FACS analysis. Low concentrations (10 μ M zVAD.fmk) blocked TRAIL induced apoptosis in both glucose^{+ve} and glucose^{-ve} cells (Figure 3-3A and B). Interestingly, inhibition of caspase activity with zVAD.fmk resulted in the appearance of 3 distinct PS populations, alive cells (low PS), cells with an intermediate PS exposure (circled in Figure 3.3A and B), and classical apoptotic dead cells (high PS in the upper left quadrant). Cells with intermediate PS exposure were considered to be 'alive' cells, as they resided in the lower left quadrant.

Strikingly, TRAIL-induced cell death was not completely blocked by any concentration of zVAD.fmk in glucose^{+ve} cells, 30% of the cells still underwent cell death (Figure 3-3C), compared to 15% in glucose^{-ve} cells. The phenotype of the remaining cell death in glucose^{+ve} cells was split equally between apoptotic (PS+/PI-) and secondary necrotic (PS+/PI+) (Figure 3-3D and E). At low concentrations (10 μ M zVAD.fmk), TRAIL-induced cell death was blocked in glucose^{-ve} cells, demonstrating a completely caspase-dependent apoptotic response. Investigation of caspase activation showed that zVAD.fmk blocked cleavage of pro-caspase-3, but not did not prevent processing of pro-caspase-8 (Figure 3-3F). The relative intensity of pro-caspase-8 was markedly reduced (Figure 3-3F) in glucose^{+ve} and glucose^{-ve} cells when pre-treated with zVAD.fmk followed by TRAIL. This suggested the block may have occurred down stream of initial auto-proteolytic cleavage or that zVAD.fmk induced the degradation of pro-caspase-8. The p43/41 cleavage fragments were not detected in either glucose^{+ve} or glucose^{-ve} cells following zVAD.fmk pre-treatment compared to untreated controls. Additionally, there was no reduction in total band intensity of pro-caspase-3, and the p20/19/17 cleavage fragments were not detected. Lack of cleavage of

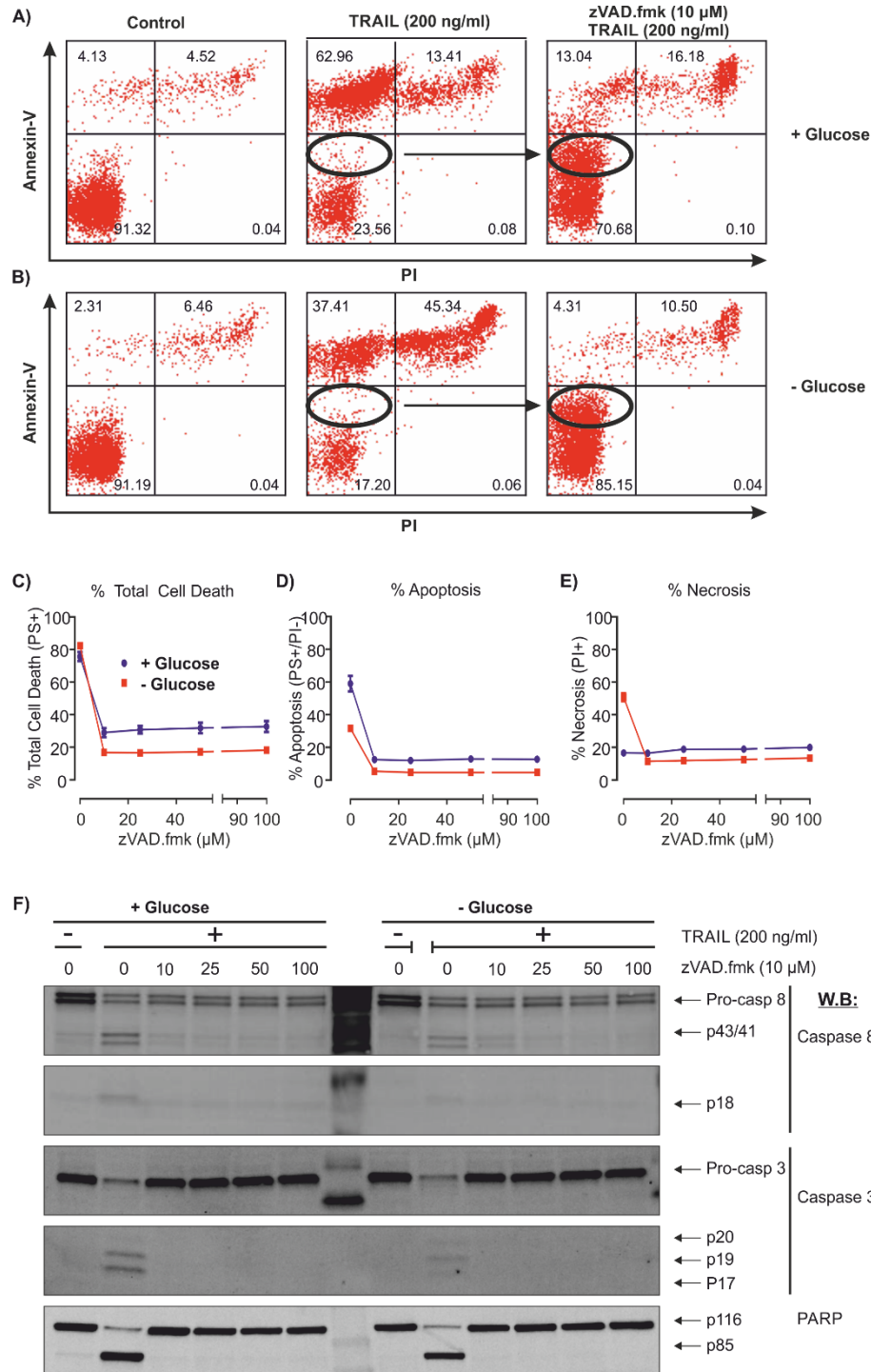


Figure 3-3 Caspase inhibition does not completely block TRAIL-induced cell death in glucose^{+ve} UPN1 cells. UPN1 glucose^{-ve} (■) and glucose^{+ve} (●) cells (as described in Figure 3.1) were pre-treated with 0 – 100 μM zVAD.fmk for 30 min followed by 200 ng/ml TRAIL for 4 h. **A)** Glucose^{+ve} cells: untreated; treated with 200 ng/ml TRAIL and 10 μM zVAD.fmk + 200 ng/ml TRAIL showed an incomplete block in PS+/PI- cells following caspase inhibition **B)** Glucose^{-ve} cells: untreated; treated with 200 ng/ml TRAIL and 10 μM zVAD.fmk + 200 ng/ml TRAIL; showed a complete block in PS+/PI- cells following caspase inhibition. Inhibition curve following zVAD.fmk and TRAIL treatment showing **C)** Total cell death (PS+), **D)** apoptotic cell death (PS+/PI-) and **E)** necrotic cell death (PS+/PI+). **F)** Western blot analysis of caspase-8, caspase-3 and PARP cleavage following zVAD.fmk inhibition of TRAIL cell death. Experiments representative of 3 independent experiments, error bars ± SEM.

pro-caspase 3 and PARP, suggested that the residual cell death in UPN1 glucose^{+ve} cells was caspase-independent.

3.2.4 Glucose^{-ve} cells are unable to switch to TRAIL-induced necroptosis

Cell death in UPN1 glucose^{+ve} cells was not completely blocked by zVAD.fmk, which has been shown to switch death ligands to activate the necroptotic pathway in certain cell lines/types (reviewed in Linkermann & Green, 2014; Dickens *et al.*, 2012b). Therefore, UPN1 cells were next pre-treated (30 min) with different combinations of 10 μ M zVAD.fmk and/or 50 μ M Necrostatin-1 (Nec-1), an inhibitor of RIPK1 and necroptosis (Degterev *et al.*, 2005), followed by 200 ng/ml TRAIL for 4 h. Figure 3-4A and C showed as in Figure 3-3A that zVAD.fmk alone did not completely block apoptosis in UPN1 glucose^{+ve} cells. The RIPK1 inhibitor, Nec-1, alone conferred no resistance to TRAIL-induced apoptosis in either glucose^{+ve} or glucose^{-ve} cells (Figure 3-4C). This was expected, since necroptosis is only activated upon inhibition of caspases; as caspase-8 cleaves RIPK1, thus inhibiting necrosome formation and subsequent activation of necroptosis (Lu *et al.*, 2011). However, combined treatment with zVAD.fmk and Nec-1 completely abrogated TRAIL-induced cell death in glucose^{+ve} cells. The combination of these results indicated that UPN1 glucose^{+ve} cells switched to necroptosis when caspases were inhibited followed by death ligand binding. In contrast, glucose deprivation conferred a type of resistance to apoptotic inducers by preventing programmed necrosis as TRAIL-induced cell death was completely dependent on caspase activity (blocked by zVAD.fmk). Interestingly, the combination of Nec-1 and zVAD.fmk pre-treatment, blocked the TRAIL-induced generation of the intermediate PS population of cells in both glucose^{+ve} and glucose^{-ve} cells. This data indicated that there was a RIPK1-dependent population of cells that displayed intermediate PS externalisation to the outer leaflet of the plasma membrane, which was independent of caspase activity.

Investigation of caspase activation (Figure 3-4D) showed that pro-caspase-8 auto-proteolytic processing was not blocked in the presence of 10 μ M zVAD.fmk in both glucose^{+ve} and glucose^{-ve} cells, however the caspase-8 cleavage fragments p43/41 were not detectable. In line with this, zVAD.fmk inhibition blocked processing of pro-caspase-3 in glucose^{+ve} and glucose^{-ve} UPN1 cells.

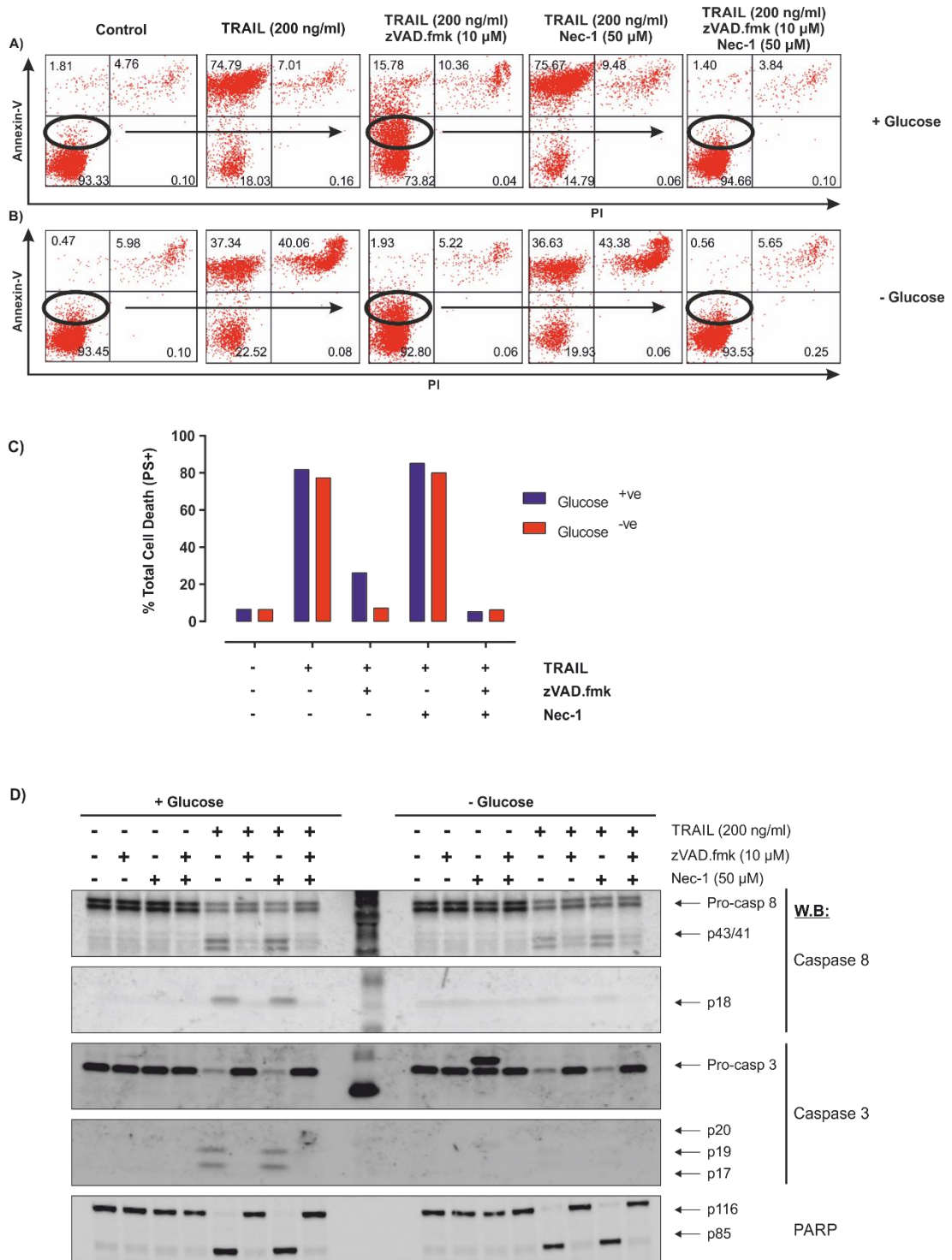


Figure 3-4 Metabolic reprogramming prevents UPN1 cells from switching to TRAIL-induced necroptosis. UPN1 glucose^{-ve} (■) and glucose^{+ve} (●) cells (as described in Figure 3.1) were pre-treated with 10 μM zVAD.fmk and/or 50 μM Nec-1 for 30 min, followed by 200 ng/ml TRAIL for 4 h. Representative examples of Annexin-V/PI FACS data from cells treated with different combinations of inhibitors in the presence of glucose **A)** showed a complete block in cell death following zVAD.fmk and Nec-1 combinatorial pre-treatment, while glucose^{-ve} cells **B)** showed a complete block in cell death following zVAD.fmk alone. **C)** Total cell death (PS+) analysis after zVAD.fmk, Nec-1 and TRAIL **D)** Western blot analysis of caspase-8, caspase-3 and PARP cleavage following zVAD.fmk and Nec-1 inhibition of TRAIL cell death. Experiments representative of 2 independent experiments.

The RIPK1 inhibitor Nec-1 did not prevent processing of either pro-caspase-8 or pro-caspase-3 when used to pre-treat the cells alone, in either glucose^{+ve} or glucose^{-ve} cells. Cell death and caspase-3 processing was completely blocked by the combination of zVAD.fmk and Nec-1. This data showed that glucose^{-ve} cells were unable to switch to necroptosis in the presence of TRAIL and that the remaining cell death in glucose^{+ve} cells was caspase-independent, but dependent on RIPK1.

3.2.5 Glucose deprivation induces minimal changes in whole cell protein expression of key anti- and pro-apoptotic proteins

As sensitivity to TRAIL and the cell death phenotype observed could be a result of differential expression of Bcl-2 family members, whole cell protein expression of a panel of key anti- and pro-apoptotic proteins was assessed by immunoblotting (Figure 3-5). There were no changes in the expression of the initiator of the intrinsic apoptosis pathway, pro-caspase-9. Additionally there were no changes in the total expression levels of the initiator of the extrinsic apoptotic pathway, pro-caspase-8. Downstream executioners' pro-caspase-3 and pro-caspase-7 additionally displayed no altered protein expression in glucose^{-ve} cells compared to glucose^{+ve} cells (Figure 3-5A). This is in contrast to the work previously published from our laboratory (Robinson *et al.*, 2012), which showed Z138 cells chronically deprived of glucose had increased pro-caspase-8 and pro-caspase-3 expression.

Profiling of BH3 only proteins (Figure 3-5B) showed minimal changes in expression, with a small reduction in expression of both Bad and Puma in glucose^{-ve} cells. There were no detectable changes in the expression of Bid, which links the extrinsic to the intrinsic apoptotic pathway (see chapter 1.4.2). Profiling of Bax and Bak protein expression (Figure 3-5B) showed there was no change in the levels of either Bax or Bak protein between glucose^{+ve} and glucose^{-ve} cells.

Additionally, profiling of anti-apoptotic proteins (Figure 3-5C) showed a reduction in protein expression of the anti-apoptotic proteins Bcl-x_L, Mcl-1 and XIAP. Previous studies published on UPN1 cells have demonstrated that there is no Bcl-2 mRNA or protein expression (Touzeau *et al.*, 2011). In line with this, immunoblotting analysis did not detect any Bcl-2 protein (data not shown). These findings correlated with the slightly increased sensitivity to TRAIL, indicating that reduction

in expression of both Bcl-x_L and XIAP may have conferred sensitivity to TRAIL-induced apoptosis.

Due to the observation that UPN1 cells were unable to switch to necroptotic cell death following TRAIL treatment in glucose^{-ve} cells, expression levels of one of the key proteins involved in necroptosis, and the target of necrostatin-1, RIPK1 was assessed (Figure 3-5 D). There were no changes in the expression of RIPK1 between glucose^{+ve} and glucose^{-ve} UPN1 cells.

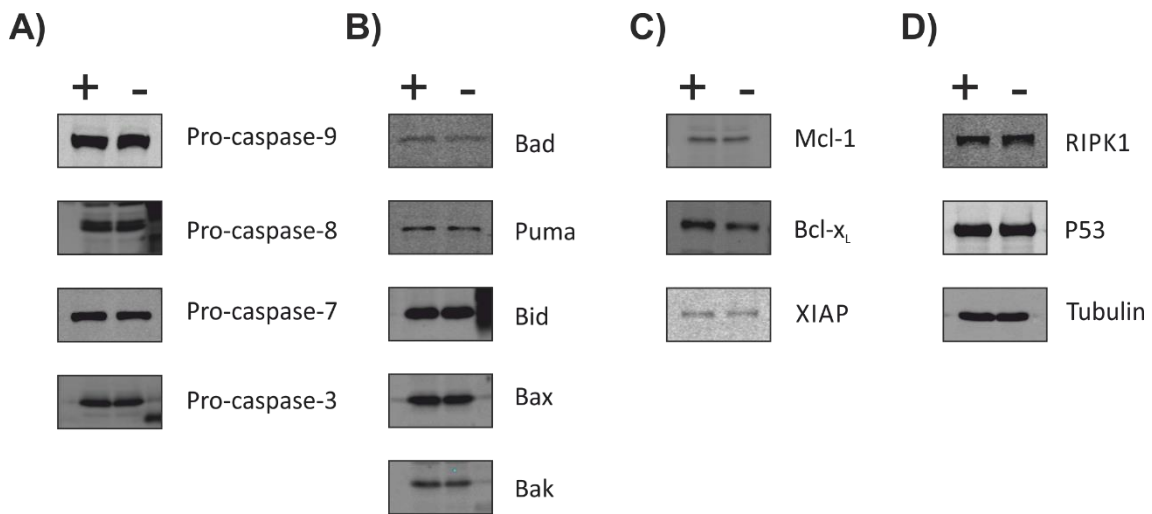


Figure 3-5 Metabolic reprogramming induces minimal changes in key pro- and anti-apoptotic proteins. UPN1 glucose^{+ve} cells (+) and glucose^{-ve} cells (—) were solubilised in sample buffer and were subjected to SDS-PAGE and immunoblotted for **A)** expression levels of pro-caspases -9, -8, -7 and -3; **B)** pro-apoptotic Bcl-2 family members; **C)** anti-apoptotic Bcl-2 family members and **D)** Nec-1 target RIPK1.

3.2.6 Glucose^{-ve} UPN1 cells undergo mitochondrial metabolic reprogramming

In Z138 cells, glucose deprivation resulted in metabolic reprogramming to up-regulate oxidative phosphorylation to compensate for ablation of glycolytic derived energy (Robinson *et al.*, 2012). Therefore, this study set out to determine if glucose deprivation in UPN1 cells resulted in the same metabolic reprogramming as seen in Z138 cells. Using a Seahorse XF24 extracellular flux analyser, measurements of oxygen consumption rates (OCR) and extracellular acidification rates (ECAR) were assessed.

UPN1 glucose^{+ve} and glucose^{-ve} cells were seeded on XF24 micro-culture plates at 4.5×10^5 cells/well, as detailed in methods (section 2.2.12). The levels of oxygen consumption were measured as real time rates; 4 initial measurements were acquired over a 30 min period to attain the basal level of OCR. The readings obtained represented the combined rates of oxygen consumed through oxidative phosphorylation and non-mitochondrial sources (see Figure 3-6A for an explanation). As shown in Figure 3-7A and B, the basal levels of oxygen consumption were 260 pmol/min/ 10^6 cells in glucose^{-ve} cells; 35% higher than glucose^{+ve} cells which had a basal OCR of 190 pmol/min/ 10^6 cells. This showed that following glucose deprivation, UPN1 cells were more dependent on mitochondrial function to maintain cellular homeostasis. The increased basal OCR in glucose^{-ve} cells was accompanied by a reduction in glycolysis (ECAR); this metabolic reprogramming is depicted by the shift and highlighted by the arrow in Figure 3-7C.

Following basal readings, the ATP synthase inhibitor oligomycin was injected to give a final concentration of 500 nM. Inhibition of ATP synthase activity blocks the import of protons from the mitochondrial inter-membrane space (IMS) to the mitochondrial matrix (see chapter 1.7), and hyperpolarises the mitochondrial membrane. The difference in OCR between the basal levels obtained and the readings generated after addition of oligomycin was representative of oxygen consumption directly attributed to ATP linked mitochondrial oxidative phosphorylation (See Figure 3-6 for an explanation). UPN1 glucose^{-ve} cells had an enhanced level of oxidative phosphorylation linked to ATP production compared to glucose^{+ve} cells with 200 pmol/min/ 10^6 cells compared to 110 pmol/min/ 10^6 cells respectively; this represented an increase of about 90% (Figure 3-7B). This data indicated that following glucose starvation, UPN1 cells underwent metabolic reprogramming to upregulate basal and ATP linked mitochondrial oxidative phosphorylation. As glycolytically derived pyruvate was absent in UPN1 glucose^{-ve} cells, mitochondrial function was maintained through exogenously supplemented pyruvate and glutamine. Glutamine is converted to glutamate then α -ketoglutarate, which feeds directly into the tricarboxylic acid (TCA) cycle (Hensley *et al.*, 2013).

After oligomycin readings were attained, FCCP was sequentially injected into each well to give a final concentration of 400 nM. FCCP is a chemical protonophore that

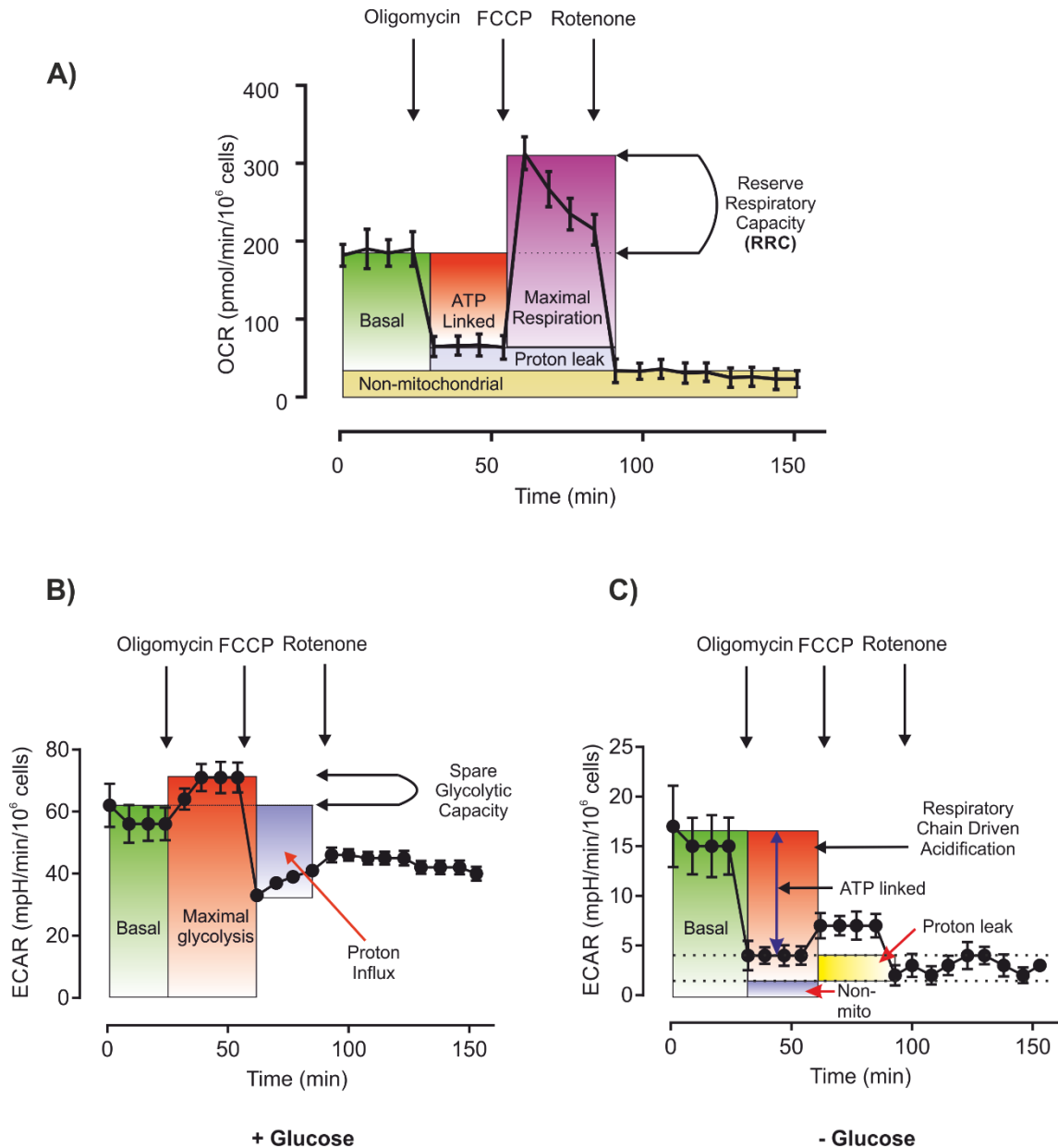


Figure 3-6 Representative examples of bioenergetics data obtained from a Seahorse XF24 analyser. UPN1 glucose^{-ve} and glucose^{+ve} cells (as described in Figure 3.1) were seeded at 4.5×10^5 cells/well. OCR and ECAR values were generated using a 24 well Seahorse extracellular flux analyser. Mitochondrial inhibitors were injected sequentially to give the following final concentrations: Oligomycin 500 nM; FCCP 400 nM and rotenone 1 μ M. **A)** Typical OCR trace after mitochondrial stress test. **B)** ECAR trace generated when cells are cultured in the presence of glucose. **C)** ECAR trace generated when cells are cultured in the absence of glucose.

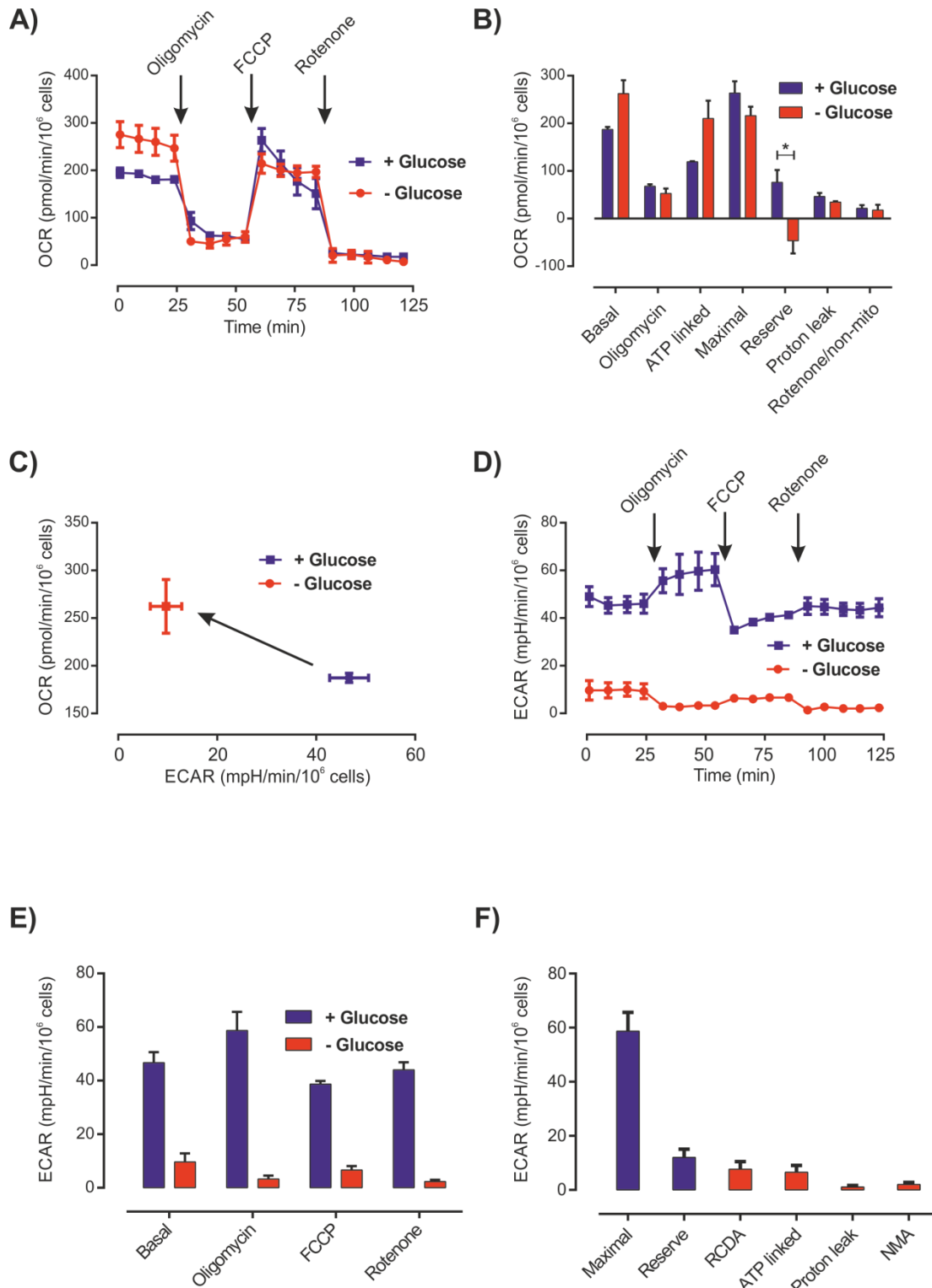


Figure 3-7 Glucose deprivation results in metabolic reprogramming of UPN1 cells. UPN1 glucose^{+ve} (blue bars) and glucose^{-ve} cells (as described in Figure 3.1) (red bars) were loaded into a Seahorse XF24 analyser. **A)** Oligomycin, FCCP and rotenone were sequentially injected to generate a mitochondrial stress test. **B)** Using Figure 3-6 bioenergetic parameters were calculated to show basal, ATP linked, maximal, reserve capacity, proton leak and non-mitochondrial OCR values. **C)** Basal OCR and ECAR values were plotted against each other to show metabolic reprogramming following glucose deprivation. **D)** Using the same injections as in (A) ECAR values were generated **E)** and plotted as a bar chart. **F)** Using Figure 3-6 the glycolytic and mitochondrial acidification rates were calculated. Experiments representative of 3 independent experiments, error bars \pm SEM. Star (*) represents $p < 0.05$ (Students t test)

uncouples the ATP synthase from the respiratory chain (See chapter 1.7). Addition of FCCP generated an OCR value representative of the theoretical maximal respiration (See Figure 3-6 for explanation). The difference between maximal respiration and basal OCR represented the reserve respiratory capacity (RRC) (See Figure 3-6 for explanation) available to the mitochondria under conditions of energetic stress. The maximal respiration of UPN1 glucose^{-ve} cells (216 pmol/min/10⁶ cells) was 18% lower than glucose^{+ve} cells (263 pmol/min/10⁶ cells) (Figure 3-7B). Additionally, glucose^{-ve} cells had a negative RRC of -46 pmol/min/10⁶ cells, while glucose^{+ve} cells had a RRC of 76 pmol/min/10⁶ cells (Figure 3-7B). These data showed that glucose^{-ve} cells were respiring maximally, in state-3 respiration. Comparatively, glucose^{+ve} UPN1 cells had the ability to up-regulate mitochondrial oxidative phosphorylation when required.

Closer analysis of the OCR trace (Figure 3-7A) showed that following FCCP stimulated respiration, OCR values dropped at each 7 min reading in glucose^{+ve} cells. This 'energetic-instability' did not occur in cells deprived of glucose. Why this phenomenon occurred is not known. Speculatively; it may have been due to the depletion of substrate (NADH), or alternatively FCCP efflux from the cell, as it can permeate through the plasma membrane. To account for this, only the first reading of the 4 generated, following FCCP injection was used to calculate the maximal and reserve values.

The final injection in Figure 3-6A was the NADH dehydrogenase (complex I) inhibitor, rotenone (see chapter 1.7), which inhibits the most upstream component of the respiratory chain. The difference in OCR values between oligomycin and rotenone addition generated a value referred to as the proton leak (See Figure 3-6 and chapter 1.7 for explanation). The proton leak in glucose^{-ve} cells was 34 pmol/min/10⁶ cells, 28% lower than in glucose^{+ve} cells which was 46 pmol/min/10⁶ cells (Figure 3-7B). These data showed that the mitochondrial electron transport chain in glucose^{-ve} cells was more tightly coupled to the ATP synthase than glucose^{+ve} cells.

Any rate of oxygen consumption generated after the addition of rotenone is from succinate and complex III or non-mitochondrial oxidation of oxygen (see Figure 3-6 for explanation), generated for example by trans-plasma membrane electron

transport occurring at the cellular plasma membrane (Herst & Berridge, 2007) or some of the many cellular oxidases. There were no significant differences in the rates of non-mitochondrial OCR between glucose^{-ve} and glucose^{+ve} cells, 18 vs 21 pmol/min/10⁶ cells respectively (Figure 3-7B).

3.2.7 Glucose deprived UPN1 cells generate an extracellular acidification rate independently of glycolysis

In Z138 cells, chronic glucose deprivation did not completely ablate extracellular acidification rates (ECAR), which is normally attributed to glycolysis (Robinson *et al.*, 2012). To determine if this phenomenon occurred in UPN1 cells, the Seahorse XF24 extracellular flux analyser was used to take real time ECAR measurements following the same stress test as in 3.2.6. UPN1 glucose^{-ve} cells had a residual basal ECAR of 10 mpH/min/10⁶ cells, 5 x lower than glucose^{+ve} cells, which had a basal ECAR of 47 mpH/min/10⁶ cells (Figure 3-7D and E), which indicated that an acidification event independent of glycolysis had occurred. The addition of mitochondrial respiratory chain inhibitors produced markedly different results in glucose^{+ve} (Figure 3-6B and Figure 3-7D) versus glucose^{-ve} UPN1 cells (Figure 3-6C and Figure 3-7D). In UPN1 glucose^{+ve} cells, the addition of oligomycin induced a burst of ECAR, referred to as the maximal level of glycolysis the cells are capable of (See Figure 3-6B for explanation), which was 59 mpH/min/10⁶ cells (Figure 3-7F). The difference between the oligomycin induced burst of ECAR and basal value is the spare glycolytic capacity (Figure 3-6B); the extra amount of glycolysis that can be used under conditions of energetic stress, such as inhibition of mitochondrial function. UPN1 glucose^{+ve} cells had a minimal spare glycolytic capacity of 12 mpH/min/10⁶ cells (Figure 3-7F).

The addition of FCCP to UPN1 glucose^{+ve} cells resulted in a reduction in ECAR to 38 mpH/min/10⁶ cells (Figure 3-7D and E). The difference between the basal rate and initial FCCP rate showed reduced acidification rates, possibly as a result of protonophore driven proton influx from the media to the cytosol (see Figure 3-6B for explanation). The following three readings showed ECAR values moderately increased in UPN1 glucose^{+ve} cells (Figure 3-6B and Figure 3-7D). This may have been a result of the protonated FCCP efflux back to the media following the initial un-coupler stimulated respiratory burst as shown in Figure 3-7A.

To gauge the rates of acidification that were generated by non-glycolytic means, UPN1 glucose^{-ve} cells were also analysed on the Seahorse XF24. As mentioned previously, there was still a basal level of ECAR of 10 mpH/min/10⁶ cells. Addition of oligomycin blocked respiratory chain function and induced a reduction in acidification rates. The difference between the basal rate and the oligomycin rate in glucose^{-ve} cells represented the rate generated by ATP linked respiratory chain driven acidification (see Figure 3-6C for explanation) which was 7 mpH/min/10⁶ cells (Figure 3-7F)

The addition of FCCP to glucose^{-ve} cells induced a burst of ECAR (Figure 3-7D) which was in contrast to the first reading obtained for glucose^{+ve} cells where FCCP reduced ECAR (Figure 3-7D). The burst in ECAR was likely due to proton extrusion from the mitochondria to the cytosol/media after uncoupling of the respiratory chain. The level of ECAR did not return to basal rates, which was likely due to the FCCP returning most of the protons to the mitochondrial matrix. The addition of rotenone completely blocks the respiratory chain at the most upstream component; any remaining ECAR observed following rotenone was non-mitochondrial and non-glycolytic acidification (NMA) (2 mpH/min/10⁶ cells). The difference between oligomycin and rotenone mediated inhibition of ECAR represented acidification generated from the mitochondrial proton leak (1 mpH/min/10⁶ cells). The addition of the ATP linked acidification and the proton leak mediated acidification represented the total ECAR attributed to respiratory chain driven acidification (RCDA) (8 mpH/min/10⁶ cells – Figure 4.7 F).

3.3 Discussion

Previous work carried out in our laboratory has shown that Z138 cells, a mantle cell lymphoma derived cell line is resistant to TRAIL and ABT-737-induced cell killing when chronically deprived of glucose (Robinson *et al.*, 2012). My study sought to determine if this phenomenon also occurs in another MCL derived cell line. As such, UPN1 cells were chronically deprived of glucose (at least 7 days before experimentation) and treated with increasing concentrations of TRAIL. Although UPN1 cells are viable in the absence of glucose, they proliferate much more slowly, owing to the ablation of carbon flux through the PPP, and therefore a reduction in macromolecules essential for proliferation. TRAIL treatment results in minimally increased total cell death in glucose deprived cells compared to cells cultured in the presence of glucose. The mode of cell death in glucose deprived UPN1 cells appears to be secondary necrosis, as observed by increased PI staining, indicative of permeabilisation of the cell plasma membrane, because cell death is completely blocked by caspase inhibition. The alternate cell death phenotype is accompanied by reduced stability of the caspase-8 cleavage fragments p43/41, and caspase-3 cleavage fragments p20/19/17. Reduced cleavage fragment detectability may be a result of targeted proteasomal degradation. A recent report has shown that TRAF2 results in K48 – linked polyubiquitination of the large caspase-8 catalytic domain targeting it for proteasomal degradation (Gonzalvez *et al.*, 2012). It may be possible that this process is increased in glucose deprived UPN1 cells. Interestingly, when trying to mimic the effects of glucose deprivation in UPN1 cells by addition of 5 mM 2DG for 20 h, UPN1 cells undergo ~60% cell death (data not shown). This highlights, like previously described (Robinson *et al.*, 2012), that 2DG and glucose deprivation cannot be used interchangeably. Why 2DG alone induces cell death in UPN1 cells is unclear and was not examined any further.

Time-dependent induction of TRAIL-induced cell death is not significantly different between UPN1 cells cultured in the presence or absence of glucose. Annexin-V/PI staining shows apoptosis induction occurs at 2 h with 100 ng/ml TRAIL. Interestingly, PARP cleavage is detected at 1 h post TRAIL treatment indicating a potential time lag between caspase-3 mediated cleavage of PARP and activation of the flippases that promote externalisation of phosphatidyl serine.

As Nec-1 does not block cell death and zVAD.fmk protects from TRAIL under both culture conditions, this would argue that cell death is caspase-dependent and not primary but secondary necrosis. This indicates that the transition in cell death from apoptosis to secondary necrosis is much more rapid in UPN1 cells deprived of glucose. In addition to this, zVAD.fmk does not completely protect UPN1 glucose^{+ve} cells from TRAIL-induced apoptosis, but when used concomitantly with Nec-1, cell death is completely abrogated (Figure 3-8). This suggests that the mode of cell death can switch to necroptosis in the glucose^{+ve} cells, but not in glucose^{-ve} cells. Interestingly, caspase inhibition with zVAD.fmk results in a third population of cells termed PS intermediate in both glucose^{+ve} and glucose^{-ve} cells. This intermediate level of PS exposure, along with high PS exposure in glucose^{+ve} cells (figure 3-3A) following zVAD.fmk and TRAIL treatment is completely blocked with the RIPK1 inhibitor Nec-1. These data suggest that activation of the necrosome complex results in partial exposure of PS to the outer leaflet of the plasma membrane, independent of the traditional caspase dependent activation of flippases. Whether the necrosome can activate flippases has yet to be described. Metabolic reprogramming therefore confers a type of resistance to TRAIL, depending on the glucose availability. Previous studies have shown that necroptosis proceeds in glucose free conditions when subjected to hypoxic conditions (oxygen glucose deprivation (OGD)) (Huang *et al.*, 2013; Chen *et al.*, 2012). Importantly, these studies used OGD to induce necroptosis in the absence of death ligands. This is the first study to identify that in certain cell lines/types, the glycolytic pathway is critically required for TRAIL-induced necroptotic signalling, highlighting a link between cell metabolism and cell death signalling in tumour cells.

Further to this, in UPN1 glucose^{-ve} cells there appears to be only minor detectable changes in total whole cell protein expression in a panel of pro- and anti- apoptotic proteins. Glucose^{-ve} cells have reduced expression of Bcl-x_L, Mcl-1 and XIAP, which correlates with the increased sensitivity to TRAIL. However, the differences in cell death phenotypes may be a result of factors upstream, such as novel interactors incorporated into the DISC. Perhaps RIPK1 and RIPK3 are present in the DISC in glucose^{+ve} cells, thus facilitating the switch to necroptosis, or there is a reduction in total levels of RIPK3 or MLKL in glucose^{-ve} cells. Moreover, if TRAF2 is

present in the DISC of glucose^{-ve} cells, this may explain the rapid degradation of caspase-8 cleavage fragments via proteasomal degradation.

As previously described in Z138 cells (Robinson *et al.*, 2012), UPN1 cells deprived of glucose have up-regulated levels of basal oxidative phosphorylation to compensate for abolished glycolysis. All of the increased basal oxidative phosphorylation is linked to mitochondrial ATP synthesis, highlighting the requirement of the mitochondria to provide ATP. The increased levels of oxidative phosphorylation are sustained by the exogenous supplementation of pyruvate that feeds directly into the TCA cycle and glutamine. Glutamine is converted to glutamate and then α -ketoglutarate, which subsequently feeds into the TCA cycle. Metabolic reprogramming to increase the OCR:ECAR ratio results in increased sensitivity to TRAIL and minor changes in the balance of pro- and anti-apoptotic proteins, directly linking cancer cell metabolism to cell survival.

Why FCCP induces markedly different results in ECAR under the different culture conditions is unclear. However, it is tempting to speculate that differential Δ pH values exist in UPN1 cells utilising different amounts of glucose, as glucose concentration has been shown to alter the pH gradient between the cytosol/IMS and matrix (Wiederkehr *et al.*, 2009). This would therefore alter the equilibrium of protonated and un-protonated FCCP depending on its subcellular localisation. Importantly, if nutrient availability alters the Δ pH, and results in metabolic reprogramming to up-regulate oxidative phosphorylation, the ratio of reduced vs oxidised cytochrome *c* (Brown & Borutaite, 2008), and indeed whole cellular redox state, may additionally differ, which could result in altered sensitivity to chemotherapeutics.

In conclusion, glucose deprivation in the mantle cell lymphoma derived cell line UPN1 results in metabolic reprogramming to upregulate mitochondrial oxidative phosphorylation to compensate for the absence of glycolytic generated ATP. This shift in the OCR:ECAR ratio moderately alters the balance of key pro- and anti-apoptotic proteins and marginally sensitises cells to TRAIL-induced cell death. The most striking findings, are that this is the first report to show that glycolytic activity and thus ATP is critically required for the initiation and execution of programmed necroptosis, and that necroptotic signalling appears to result in a partial increase in

PS externalisation, similar to canonical caspase-dependent apoptotic signalling. Observations described herein may be of therapeutic interest if this phenomenon occurs in other tumour lines/types. It is plausible that solid tumours with a hypoxic, poorly perfused necrotic core with limited nutrient availability may also demonstrate resistance to necroptosis.

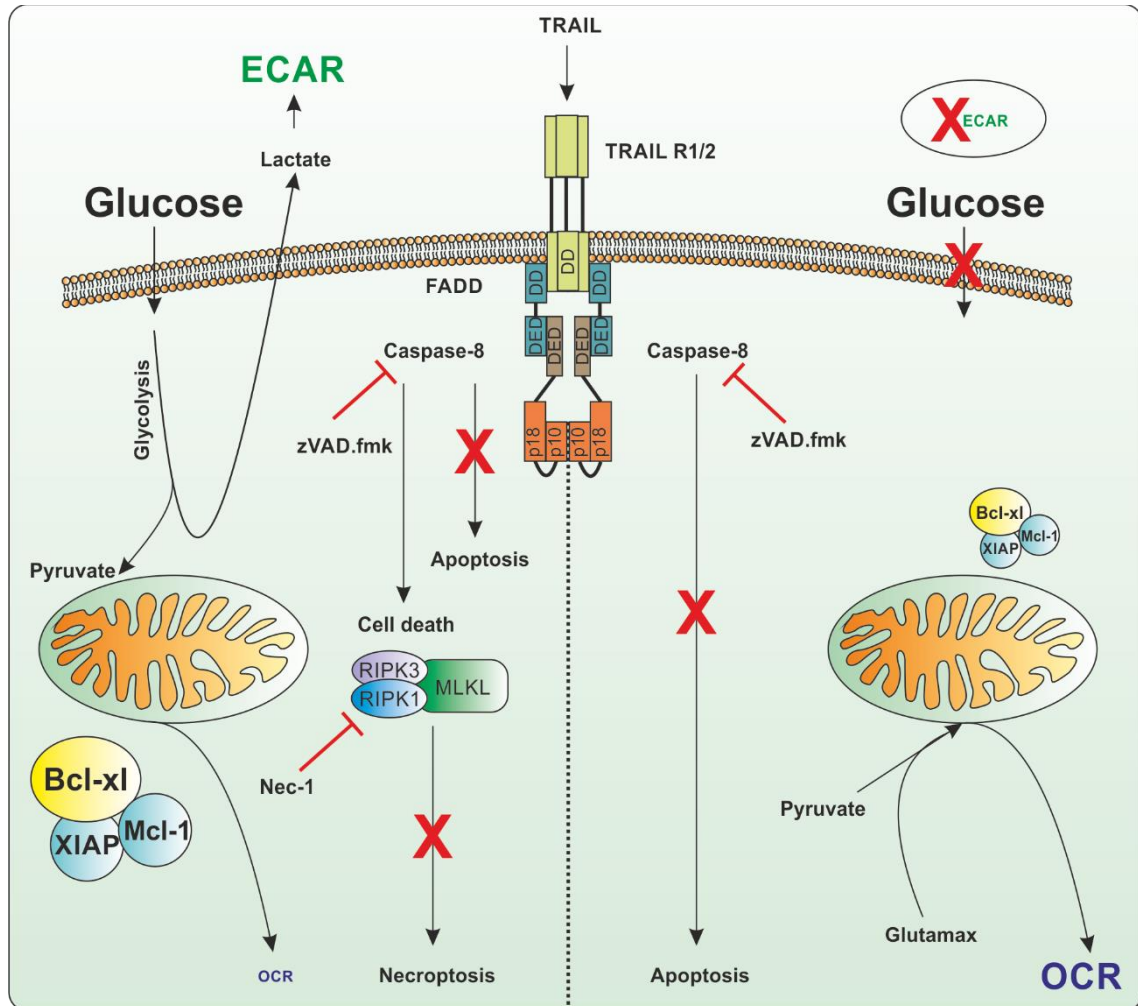


Figure 3-8 Schematic representation of changes that occur as a result of glucose deprivation. On the left, glucose cultured UPN1 cells with functional glycolysis and a low OCR:ECAR ratio, with high Bcl-x_L, Mcl-1 and XIAP expression and the ability to switch to necroptosis following caspase inhibition. On the right, glucose deprived UPN1 cells undergo metabolic reprogramming to generate a high OCR:ECAR ratio, which results in increased sensitivity to TRAIL and reduced expression of Bcl-x_L, Mcl-1 and XIAP. Metabolic reprogramming results in higher sensitivity to caspase inhibition and therefore reduced ability to switch to necroptosis following TRAIL treatment.

Chapter 4

4 Results Chapter 2

2DG rapidly and transiently activates a non-canonical AMPK signalling pathway potentiating intrinsic and extrinsic-induced cell death

4.1 Introduction

During tumorigenesis, cancer cells undergo metabolic reprogramming to upregulate carbon flux through glycolysis, shunting glucose derived carbons into the subsidiary pentose phosphate pathway and ultimately to lactate (Warburg *et al.*, 1927; Warburg, 1956). The upregulated shift to a glycolytic phenotype has been exploited diagnostically using ^{18}F -fluoro-2-deoxyglucose positron emission tomography (FDG-PET) to visualise tumours. It is possible to also exploit the Warburg effect therapeutically; like glucose, 2-deoxy-D-glucose (2DG) is imported into cancer cells by glucose transporters extremely rapidly due to the high glycolytic demand (Pelicano *et al.*, 2006). Once in the cytosol, 2DG is phosphorylated by hexokinase to produce 2-deoxy-D-glucose-6-phosphate (2DG-6-P), which cannot be further metabolised through glycolysis (Zhang *et al.*, 2014). Phosphorylation of 2DG to 2DG-6-P is additionally an ATP-dependent process; therefore 2DG is an energy dependent, glycolysis and hexokinase inhibitor, that has a relatively long intra-cellular half-life (~50 min) (Caraco *et al.*, 2000).

The 5' adenosine monophosphate kinase (AMPK) is a master regulator of cellular energy homeostasis, sensing minor changes in AMP:ATP ratios and fine tuning catabolic and anabolic processes to prevent energetic stress (Hardie, 2014). Following energetic stress, and thus an increased AMP:ATP ratio, AMP binds to the Bateman domains of the AMPK- γ subunit, which induces a conformational change that allows phosphorylation of AMPK- α T172 by LKB1 (Hardie, 2013). AMPK is also activated in response to increased cytoplasmic calcium loading by CaMKK- β -mediated phosphorylation of AMPK- α T172 (Woods *et al.*, 2005). Following activation of AMPK, mTORC1 is inhibited, thus reducing the levels of protein synthesis. Additionally, converging on mTORC1 is protein kinase B (Akt), which is a positive regulator of protein translation. Manipulating these pathways can have dramatic effects on the protein expression levels of short lived proteins.

Treatment with 2DG is well tolerated by patients, but has little therapeutic efficacy as a single agent (Mohanti *et al.*, 1996; Singh *et al.*, 2005; Stein *et al.*, 2010; Raez *et al.*, 2013). However, combining 2DG treatment with inducers of extrinsic (death receptor-mediated) or intrinsic (mitochondria-mediated) apoptosis is potentially a promising approach to cancer therapy (Yamaguchi & Perkins, 2012). 2DG has been shown to either reduce the expression of anti-apoptotic Mcl-1 (Pradelli *et al.*,

2010; Robinson *et al.*, 2012), or to displace its association with pro-apoptotic Bak (Yamaguchi *et al.*, 2011) without reducing total protein expression. Both models result in a reduction of Mcl-1 association with Bak, which either kills the cells or primes them for cell death following apoptosis induction. Mcl-1 has a very short half-life of ~30 – 120 min (Cuconati *et al.*, 2003; Craxton *et al.*, 2012), and therefore, one would predict that inhibition of glycolysis by 2DG should induce energetic stress, rapidly activate AMPK and very rapidly lower Mcl-1 protein expression.

Work previously performed in our laboratory has shown that the mantle cell lymphoma derived cell line, Z138, is sensitised to both TRAIL and ABT-737-induced cell killing following 2DG pre-treatment for 20 h (Robinson *et al.*, 2012). The rationale behind the sensitisation after 20 h was that there is a shift in the Mcl-1/Bak ratio, like previously mentioned. The aims of my study were to assess how rapidly 2DG exerted its effects on cellular metabolism and how it sensitises cells to death stimuli. The major aim was to study the molecular signalling pathways and their kinetics and how this leads to the sensitising effects of an altered Mcl-1/Bak ratio. Firstly, the time-dependent sensitisation effects of 2DG on TRAIL and ABT-737 were explored in detail using Annexin-V/PI FACS analysis and investigation of caspase activity. Then, using a Seahorse XF24 analyser, the metabolic phenotype of Z138 cells was examined following 2DG treatment at the earliest time point Z138 cells were sensitised to death (2 h). This led me to investigate the roles of both the AMPK and Akt signalling cascades that were subsequently activated following glycolytic inhibition with 2DG, and the effect the signal transduction had on global protein translation. Finally, I used activators, inhibitors or transient knockdown of the AMPK upstream kinases LKB1 and CaMKK- β to mimic or inhibit the effects of 2DG. Taken together, these results show that 2DG acts extremely rapidly, inducing metabolic reprogramming and sensitising Z138 cells to ABT-737 within 2 h. The data also show that 2DG acts very rapidly, but only transiently on AMPK, which is sufficient to sustain inhibition of protein synthesis. However, AMPK activation does not appear to be regulated by canonical kinases, and instead 2DG induces AMPK activation by a non-canonical signalling pathway.

4.2 Results

4.2.1 2DG rapidly sensitises Z138 cells to ABT-737

Previous work in our laboratory showed that 20 h pre-treatment with 2DG (5 mM) sensitised Z138 cells to ABT-737; a Bad/BH3 mimetic (Robinson *et al.*, 2012). As 2DG is an anti-glycolytic, it is likely that this sensitisation could occur far more rapidly than 20 h. My study set out to analyse the kinetics and mechanisms by which 2DG sensitises Z138 cells to ABT-737. For time-dependent studies, Z138 cells were cultured in 11.1 mM D-glucose, supplemented with 1 mM sodium pyruvate, 2 mM glutamax and 10% FCS, as detailed in methods (chapter 2.2.1), and pre-treated with 2DG (5 mM) for 0, 2, 4, 8 and 20 h, then followed by a range of concentrations (0 – 100 nM) of ABT-737. Cell death was then assessed by Annexin-V/PI incorporation and FACS analysis and caspase activation by immunoblotting, as described in Chapter 3. Firstly, pre-treatment with 2DG alone (from 0 – 8 h) resulted in no cell death (Figure 4-1A and C). However, by 20 h there was a fourfold increase in cell death from basal levels, from 5 to 20%, with cells detected in the upper left PS+/PI- quadrant (apoptosis), which then progressed to the upper right PS+/PI+ quadrant (secondary necrosis), indicative of caspase-dependent apoptosis.

Treatment with 2DG alone for 20 h was therefore slightly cytotoxic. Administration of ABT-737 following 2DG pre-treatment resulted in an apoptotic response (PS+/PI-) which progressed to secondary necrosis (PS+/PI+) with increased 2DG treatment time (Figure 4-1B), which indicated that the cell death was caspase-dependent. Treatment with ABT-737 alone (Figure 4-1D, black line) resulted in a dose-dependent increase in total cell death (PS+). There was a time-dependent increase in total cell death at all ABT-737 concentrations following 2DG pre-treatment (Figure 4-1D). Rapid sensitisation to ABT-737 occurred in the presence of 5 mM 2DG. Figure 4-1E shows that the EC₅₀ for ABT-737 was reduced by 50% from 44 nM to 22 nM by 2 h. The EC₅₀ of ABT-737 continued to decrease with increased exposure to 2DG, to 10 nM ABT-737 by 20 h 2DG pre-treatment.

As ABT-737 induces mitochondrial-mediated apoptosis, caspase-9 processing was assessed by immunoblotting. Increasing 2DG pre-treatment time resulted in increased processing of pro-caspase-9 to the p37/35 fragments in the presence of

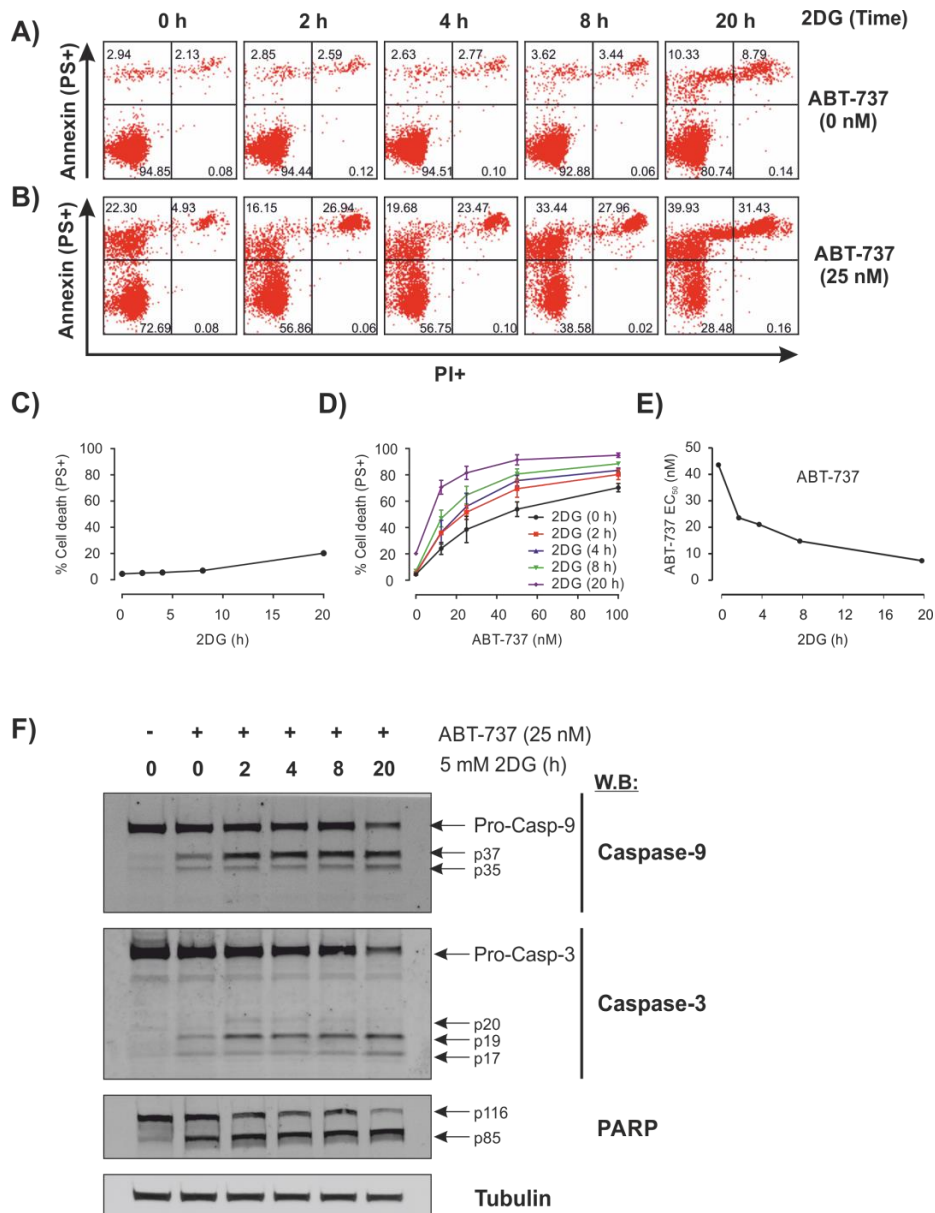


Figure 4-1 2DG rapidly sensitises Z138 cells to ABT-737. Z138 cells were cultured in 11.1 mM glucose, 1 mM sodium pyruvate, 2 mM glutamax and 10% FCS. Cells were pre-treated with 5 mM 2DG for 0 to 20 h, before adding 0 to 100 nM ABT-737 for 4 h. Cells were then analysed by FACS and immunoblotting as described in the methods section (2.2.2 and 2.2.7 respectively). **A)** Example FACS analysis of Annexin-V (PS+) labelling and propidium iodide (PI+) fluorescence are shown after treatment with 2DG for various times. **B)** Apoptotic cells (PS+/PI-) are shown in the upper left quadrant with 25 nM ABT-737, after increasing pre-treatment times with 2DG, cells progressed to the upper right quadrant (PS+/PI+), which is a measure of secondary apoptosis/necrosis. **C)** 2DG treatment alone did not induce cell death until 20 h **D)** The total cell death (PS+/PI- and PS+/PI+ herein referred to as PS+) was calculated and is shown as a concentration effect curve after increasing pre-treatment times with 2DG. **E)** EC₅₀ values were calculated from panel D and the effect of 2DG pre-treatment on the sensitivity to ABT-737-induced cell killing. **F)** Immunoblotting shows caspase-9 and caspase-3 cleavage and activation after 25 nM ABT-737 and the effect of 2DG pre-treatment times. PARP cleavage as a measure of effector caspase activity is shown in the bottom panel. FACS and immunoblotting are representative of 3 independent experiments, error bars show mean \pm SEM (n=3) for the experiments

25 nM ABT-737 treated for 4 h. Downstream effector pro-caspase-3 was additionally processed to the p19/17 cleavage fragments, although interestingly, there appeared to be very negligible amounts of the p20 fragment in ABT-737 treated cells. Although the p19 fragment showed little increase with increased 2DG pre-treatment time, the amount of pro-caspase-3 was reduced with increased exposure to 2DG. In-line with apoptosis induction, the caspase-3 downstream target PARP was also cleaved from p116 to p85 (Figure 4-1F). These data indicated that 2DG-mediated sensitisation to ABT-737-induced apoptosis was far more rapid than previously identified (Robinson *et al.*, 2012).

4.2.2 2DG rapidly sensitises Z138 cells to TRAIL

Work previously published in our laboratory has shown that 5 mM 2DG pre-treatment for 20 h sensitised Z138 cells to TRAIL (Robinson *et al.*, 2012). In agreement with the previously published data and the rapid sensitisation effects observed in 4.2.1, Z138 cells were cultured in 11.1mM D-glucose, supplemented with 1 mM sodium pyruvate, 2 mM glutamax and 10% FCS, and pre-treated with 5 mM 2DG for 2, 4, 8 and 20 h, then followed by a range of concentrations of TRAIL (0-400 ng/ml) for 3 h. Cell death was assessed by Annexin-V/PI FACS analysis and caspase cleavage by immunoblotting. Treatment with 2DG and TRAIL resulted in a primarily apoptotic phenotype (PS+/PI-) at all 2DG exposure times and TRAIL concentrations, with limited progression into the secondary necrotic, upper right quadrant (PS+/PI+) (Figure 4-2A). Pre-treatment with 2DG alone resulted in minimal cell death and the cell death phenotype appeared to be primarily apoptotic i.e. PS+/PI- as before (Figure 4-1A and D). At all TRAIL concentrations, increased 2DG pre-treatment time produced a time-dependent sensitisation to TRAIL (Figure 4-2 B), but at the earliest time (2 h), 2DG pre-treatment did not sensitise the cells to TRAIL, irrespective of the TRAIL concentration, but after 4 h 2DG treatment the EC₅₀ of TRAIL was reduced from 180 to 120 ng/ml (~ 40%) (Figure 4-2C), which showed that the effects of 2DG on TRAIL were far more rapid than previously described for Z138 cells (Robinson *et al.*, 2012).

Investigation of caspase activation following 2DG and TRAIL treatment showed pro-caspase-8 processing to the p43/41 fragments after 100 ng/ml TRAIL increased with longer exposure to 2DG. In-line with pro-caspase-8 cleavage, there was also a time-dependent increase in cleavage of the effector pro-caspase-3

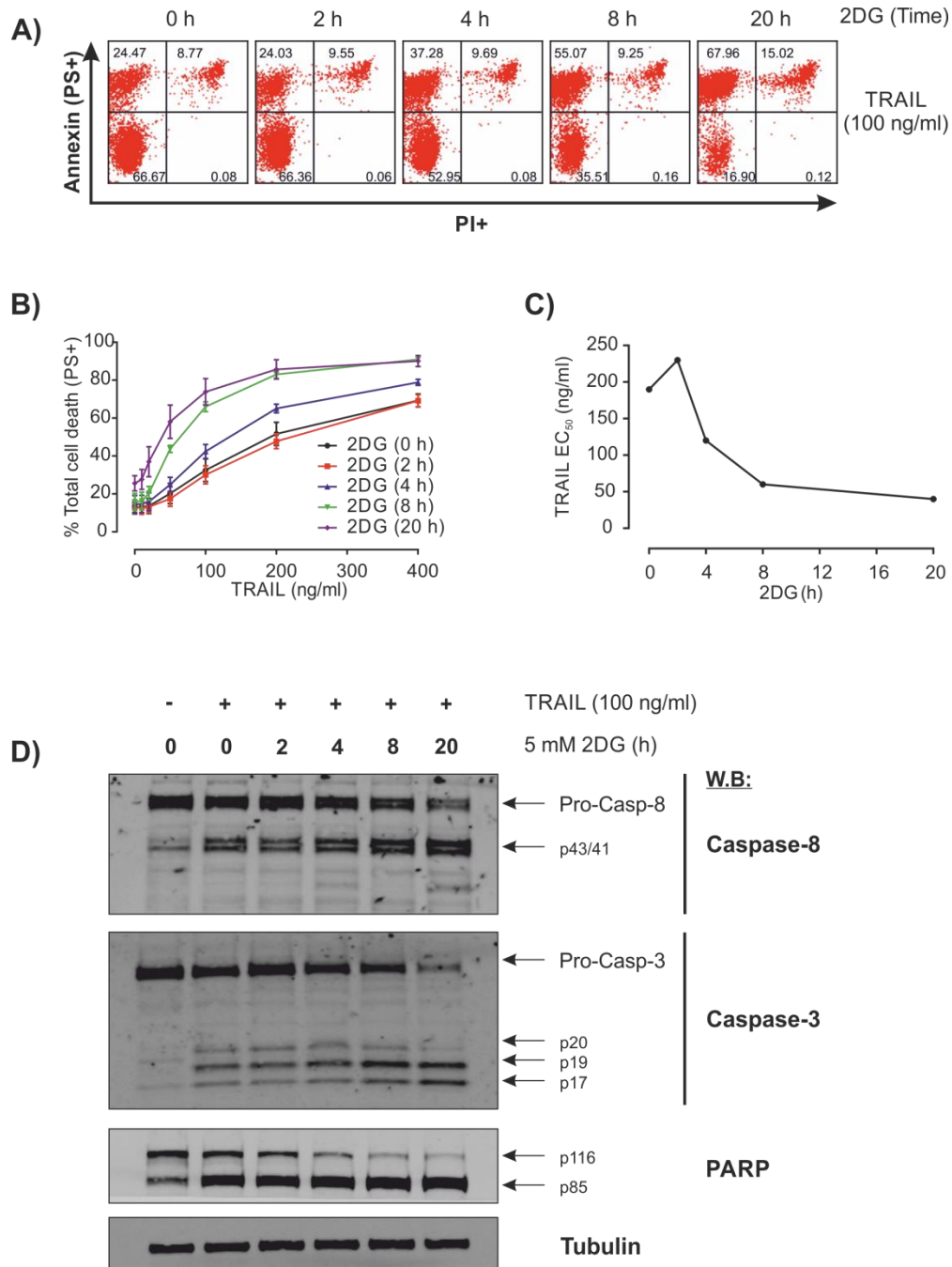


Figure 4-2 2DG rapidly sensitises Z138 cells to TRAIL. Z138 cells were cultured in standard glucose media (as described in Figure 4-1). Cells were pre-treated with 5 mM 2DG for 0 to 20 h, before adding 0 to 500 ng/ml TRAIL for 3 h. Cells were then analysed by FACS and immunoblotting as in Figure 4.1 **A)** Example FACS analysis of Annexin-V (PS+) labelling and propidium iodide (PI+) fluorescence are shown. Apoptotic cells (PS+/PI-) are shown in the upper left quadrant with 100 ng/ml TRAIL after various pre-treatment times with 2DG. The upper right quadrant (PS+/PI+) is a measure of secondary apoptosis/necrosis. **B)** The total cell death (PS+) was calculated and is shown as a concentration effect curve after increasing pre-treatment times with 2DG. **C)** EC₅₀ values were calculated from panel B and the effect of 2DG pre-treatment on the sensitivity to TRAIL-induced cell killing. **D)** Immunoblotting shows caspase-8 and caspase-3 cleavage and activation after 100 ng/ml TRAIL and the effect of 2DG pre-treatment times. PARP cleavage as a measure of effector caspase activity is shown in the bottom panel. FACS and immunoblotting are representative of 3 independent experiments, error bars show mean \pm SEM (n=3) for the experiments.

to the p20/19/17 fragments. After 20 h 2DG pre-treatment, the cleavage fragment p20 was barely detectable by immunoblotting (Figure 4-2D). There was increased amounts of the p19/17 fragments with increased 2DG treatment times. Increased 2DG exposure time followed by 100 ng/ml TRAIL resulted in increased cleavage of the downstream caspase-3 target PARP, from p116 to p85, which is used as a canonical marker of apoptosis. These data indicated that the combination of 2DG and TRAIL resulted in caspase-dependent apoptosis.

4.2.3 2DG results in metabolic reprogramming – transiently increasing oxidative phosphorylation while ablating glycolysis

As 2 h 2DG pre-treatment sensitised Z138 cells to ABT-737, I next investigated the effects of 2DG on cellular metabolism after 2 h 2DG treatment. Using a Seahorse XF24 extracellular flux analyser, the metabolic profile of Z138 cells treated with or without 5 mM 2DG for 2 h was assessed in detail. Work previously published, showed that 5 mM 2DG for 20 h induced metabolic reprogramming, to inhibit glycolysis, but additionally reduced the rates of oxidative phosphorylation (OCR) by 35% (Robinson *et al.*, 2012). As shown in the explanation Figure 3-6, the effects of 2 h 2DG treatment on Z138 cellular metabolism can be assessed. Thus, after 2DG pre-treatment, basal respiration increased by 16% from 282 ± 17 to 328 ± 11 pmol/min/ 10^6 cells. This indicated that metabolic reprogramming or switching was compensating for the effects of the anti-glycolytic, 2DG (Figure 4-3A and B). Addition of the ATP synthase inhibitor oligomycin reduced respiration in both control and 2DG treated cells to 114 ± 22 versus 114 ± 30 pmol/min/ 10^6 cells respectively. Subtraction of OCR values generated after the addition of oligomycin from the basal levels was used to calculate the extent of ATP linked oxidative phosphorylation. Thus, 2DG produced an increase in ATP linked oxidative phosphorylation (27%) in Z138 cells within 2 h of treatment with 5 mM 2DG, i.e. from 168 ± 13 to 213 ± 20 pmol/min/ 10^6 cells. This showed that the increase in OCR was due to an up-regulation of oxidative phosphorylation to generate more ATP.

After oligomycin, FCCP was added to uncouple the ATP synthase from the respiratory chain, to determine its maximal respiration. FCCP stimulated respiration was calculated by averaging the first data point generated from each individual

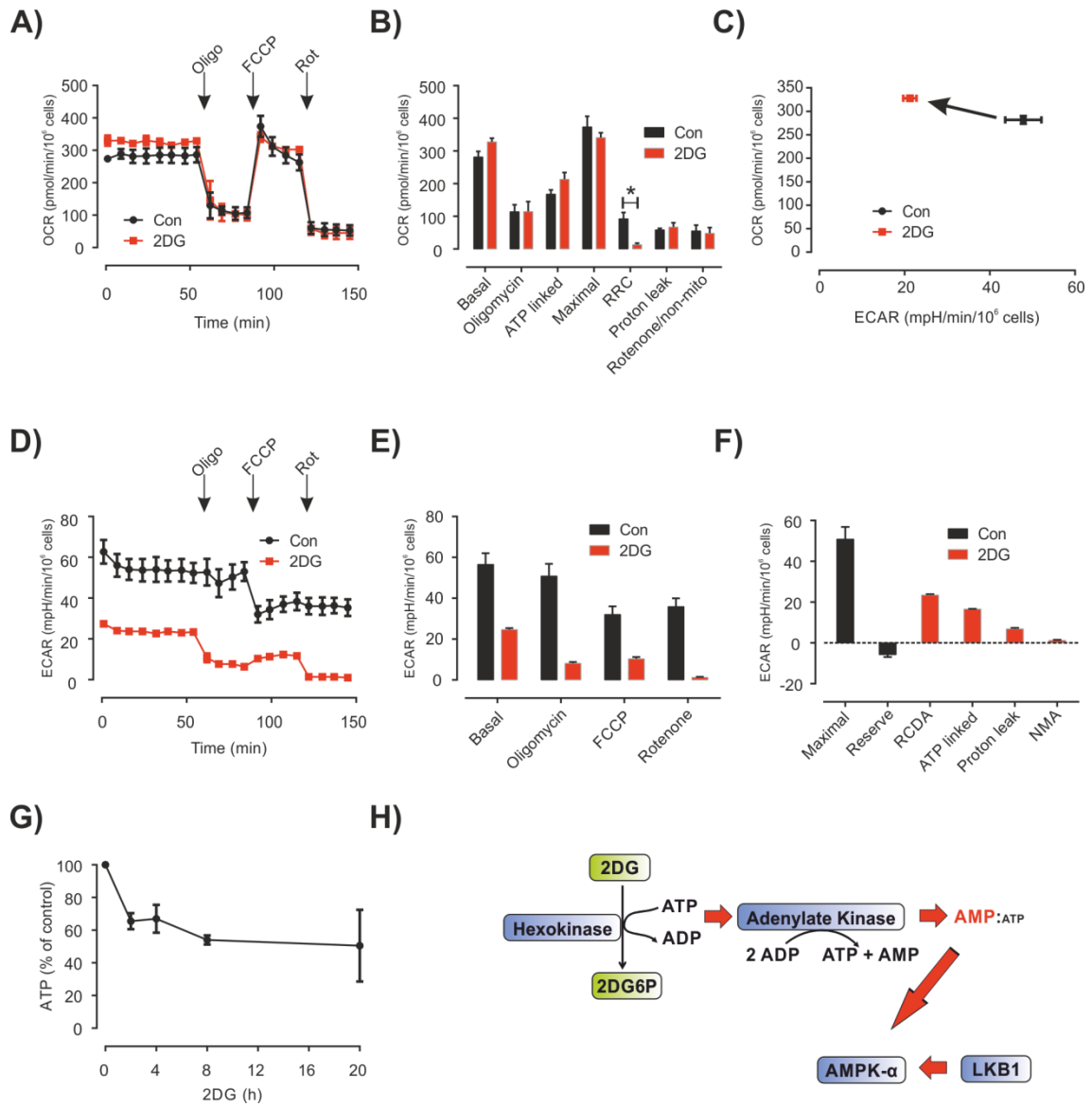


Figure 4-3 2DG treatment induces metabolic reprogramming in Z138 cells. Z138 cells were cultured standard glucose media (as described in Figure 4.1), and then 5 mM 2DG was added to the cells 2 h before analysing oxidative phosphorylation and glycolysis as described in Chapter 3. Cells were seeded at 4.5×10^5 cells/well and the indicated mitochondrial inhibitors added sequentially as shown in panel A. **A)** The OCR of control (■) and treated (2DG) (■) cells are shown as black and red symbols respectively, following a mitochondrial stress test. **B)** The various bioenergetics parameters were calculated (see Figure 3-6) to show basal, ATP linked, maximal, RRC, proton leak and non-mitochondrial OCR values. **C)** Basal OCR and ECAR values were plotted against each other to show metabolic reprogramming following 2 h treatment with 2DG. **D)** The ECAR trace of control and treated cells after the sequential injection of mitochondrial inhibitors **E)** were plotted as a bar chart to show average rates. **F)** ECAR values generated by glycolysis and the mitochondrial electron transport chain were calculated (see Figure 3-6). **G)** Z138 cells were treated with 5 mM 2DG for 0, 2, 4, 8 and 20 h, and total ATP levels calculated as a % of control. **H)** Schematic interpretation of the energetic requirements of hexokinase phosphorylation of 2DG to 2DG-6-P, and how this can lead to LKB1/AMPK activation. Panel A and D are representative traces, OCR and ECAR are shown as mean \pm SEM ($n=5$ technical repeats/wells) Panels B, C, E and F are from at least 3 independent experiments, OCR and ECAR are shown as mean \pm SEM ($n \geq 3$ biological repeats). Star (*) represents $p < 0.05$ (Students t test)

experiment. There was no significant difference in maximal respiration between control and 2DG treated Z138 cells (374 ± 32 versus 341 ± 18 pmol/min/ 10^6 cells respectively) (Figure 4-3A and B). Subtraction of the maximal values generated by FCCP stimulation from basal levels is a measure of the reserve respiratory capacity (RRC) of the cells. Control cells had an RRC of 92 ± 19 pmol/min/ 10^6 cells compared to 2DG treated cells that had an RRC of 13 ± 4 pmol/min/ 10^6 cells, an 86% reduction. These results showed that following 2DG treatment for 2 h, Z138 cells did not have a significant RRC and respired maximally under basal conditions, similar to state-3 respiration (i.e. substrates and oxygen are not limiting) (Chance & Williams, 1955). Interestingly, like UPN1 cells cultured in the presence of glucose (Figure 3-7), Z138 cells cultured in glucose were unable to maintain uncoupler stimulated respiration. Conversely, ablation of glycolysis by addition of 2DG in Z138 cells resulted in stabilisation of FCCP stimulated respiration, similar to the observed response in UPN1 cells cultured in the absence of glucose (Chapter 3). It appeared therefore, that active glycolysis prevented a sustained rate of FCCP stimulated respiration, even in the presence of exogenously supplemented pyruvate and glutamax.

Following FCCP, the NADH dehydrogenase (complex I) inhibitor rotenone ($1 \mu\text{M}$) was added to block the respiratory chain at the most upstream component. Any remaining OCR after rotenone inhibition is due to non-mitochondrial oxygen consumption or succinate. Control and 2DG treated Z138 cells did not have significantly different non-mitochondrial OCR, (55 ± 18 versus 48 ± 17 pmol/min/ 10^6 cells respectively) (Figure 4-3B). The difference in respiratory chain inhibition between oligomycin and rotenone is due to the proton leak (see Figure 3-6 for explanation and Chapter 1.7). There was no significant difference in the proton leak between control and 2DG treated Z138 cells (59 ± 5 versus 67 ± 13 pmol/min/ 10^6 cells respectively).

To ensure 5 mM 2DG was inhibiting glycolysis, (ECAR) values generated from the Seahorse XF24 were also analysed. Metabolic reprogramming or switching, to rely on mitochondrial oxidative phosphorylation following glycolysis inhibition is shown in Figure 4-3C. Representative ECAR traces generated from a standard mitochondrial stress test in control and 2DG treated (2 h) cells are shown in Figure 4-3D. Control Z138 cells had a basal ECAR of 56 ± 5 mpH/min/ 10^6 cells,

compared to 2DG treated basal rates of 25 ± 1 mpH/min/ 10^6 cells; 55% less than control cells. These results showed that after 2DG treatment for 2 h, Z138 cells generated substantial acidification which was independent of glycolysis. Addition of oligomycin to control cells decreased the ECAR from 56 ± 5 to 51 ± 6 mpH/min/ 10^6 cells, which showed that Z138 cells utilised glycolysis maximally under basal conditions (Figure 4-3D), thus oligomycin treatment resulted in a negative spare glycolysis capacity (-6 ± 1 mpH/min/ 10^6 cells) (Figure 4-3F). Addition of FCCP reduced the ECAR to 32 ± 4 mpH/min/ 10^6 cells, which may have been due to protonophore driven proton influx from the media into the cytosol/mitochondria.

In 2DG treated cells, the basal ECAR was 25 ± 1 mpH/min/ 10^6 cells, which was reduced to 8 ± 1 mpH/min/ 10^6 cells after oligomycin was added (Figure 4-3D and E), this showed that 17 ± 0.1 mpH/min/ 10^6 cells was derived from ATP linked oxidative phosphorylation. FCCP had little effect on the oligomycin inhibited ECAR, but rotenone reduced the ECAR to 1 ± 0.3 mpH/min/ 10^6 cells, this showed that 7 ± 0.5 mpH/min/ 10^6 cells was derived from the mitochondrial proton leak (Figure 4-3F). Thus, in the presence of 2DG, ECAR is due to ATP synthase derived proton extrusion and respiratory chain proton generation. Thus, 2DG completely ablates all glycolytic derived pH changes (lactic acid release), and the remaining proton extrusion is derived from the increased mitochondrial oxidative phosphorylation.

As Z138 cells treated with 2DG for 2 h had ablated glycolysis and increased basal oxidative phosphorylation; I determined the effect of 2DG on ATP levels after 0, 2, 4, 8 and 20 h 2DG exposure, to determine if metabolic reprogramming to rely on mitochondrial metabolism was sufficient to compensate for 2DG treatment and maintain ATP levels. After 2 h 2DG treatment, there was a reduction in cellular ATP levels by 35%; total ATP levels were depleted to a maximum of 50% of basal levels by 8 h (Figure 4-3G). This data indicated that the ablation of cellular ATP following 2DG treatment was extremely rapid, and that the compensatory increase in oxidative phosphorylation could not restore ATP levels to their normal level.

The effect of 2DG on cellular metabolism is more complex than simple inhibition of glycolysis via 2DG-6-P mediated inhibition of hexokinase. The conversion of 2DG to 2DG-6-P by hexokinase is an energy consuming process, whereby each 2DG molecule phosphorylated results in the consumption of one ATP, and this

potentially explains the dramatic drop in ATP levels which was not rescued by the increase in oxidative phosphorylation. Assuming that adenylate kinase functions to maintain an AMP:ATP ratio at equilibrium (reviewed in Hardie, 2013), for every two molecules of 2DG phosphorylated, two ATP molecules would be converted to two ADP molecules, which would then be enzymatically converted back to one ATP and one AMP molecule by adenylate kinase (Figure 4-3H). Thus, 2 molecules of 2DG results in the net catabolism of one ATP and anabolism of one AMP, thus increasing the AMP:ATP ratio. Increasing AMP:ATP ratios results in LKB1 mediated phosphorylation and activation of AMPK, a master regulator of cellular metabolism (Hawley *et al.*, 2003; Woods *et al.*, 2003).

4.2.4 2DG induces a rapid reduction in expression of Mcl-1

Z138 cells are type II cells, i.e. they predominantly undergo apoptosis through the mitochondrial intrinsic pathway (Robinson *et al.*, 2012). When antagonised by death receptor ligands, Z138 cells activate the mitochondrial amplification loop via cleavage of Bid to tBid (Robinson *et al.*, 2012). Additionally, it has been previously described that following treatment with 2DG, the protein expression of anti-apoptotic Mcl-1 is reduced and this was responsible for 2DG mediated sensitisation to apoptotic inducers (Pradelli *et al.*, 2010; Ramirez-Peinado *et al.*, 2011; Robinson *et al.*, 2012). To determine if the balance between pro- and anti-apoptotic proteins was altered following 2DG treatment, a panel of Bcl-2 family proteins was assessed for expression levels using immunoblotting, at 0, 2, 4, 8 and 20 h post 2DG treatment. At the early 2DG treatment time points (2, 4 and 8 h), there was no reduction in protein expression of the pro-apoptotic proteins: Cyt c; Bak; Bax; Bad or Noxa (Figure 4-4A). However, after 20 h treatment there was a significant reduction in the protein expression of the pro-apoptotic proteins, Bad Bak and Noxa.

In the case of the anti-apoptotic proteins, between 0 – 20 h, there was no significant change in protein expression of Bcl-2; Bcl-x_L was not significantly reduced between 0 – 4 h, however between 8 – 20 h, protein expression of Bcl-x_L decreased markedly (Figure 4-4B). Significantly, the levels of Mcl-1 were markedly down regulated at 2 h post 2DG treatment, and continued to decrease over the time course (Figure 4-4B). Using Li-Cor quantitative densitometry analysis of the immunoblots from 3 independent experiments of Mcl-1, it was shown that 5 mM

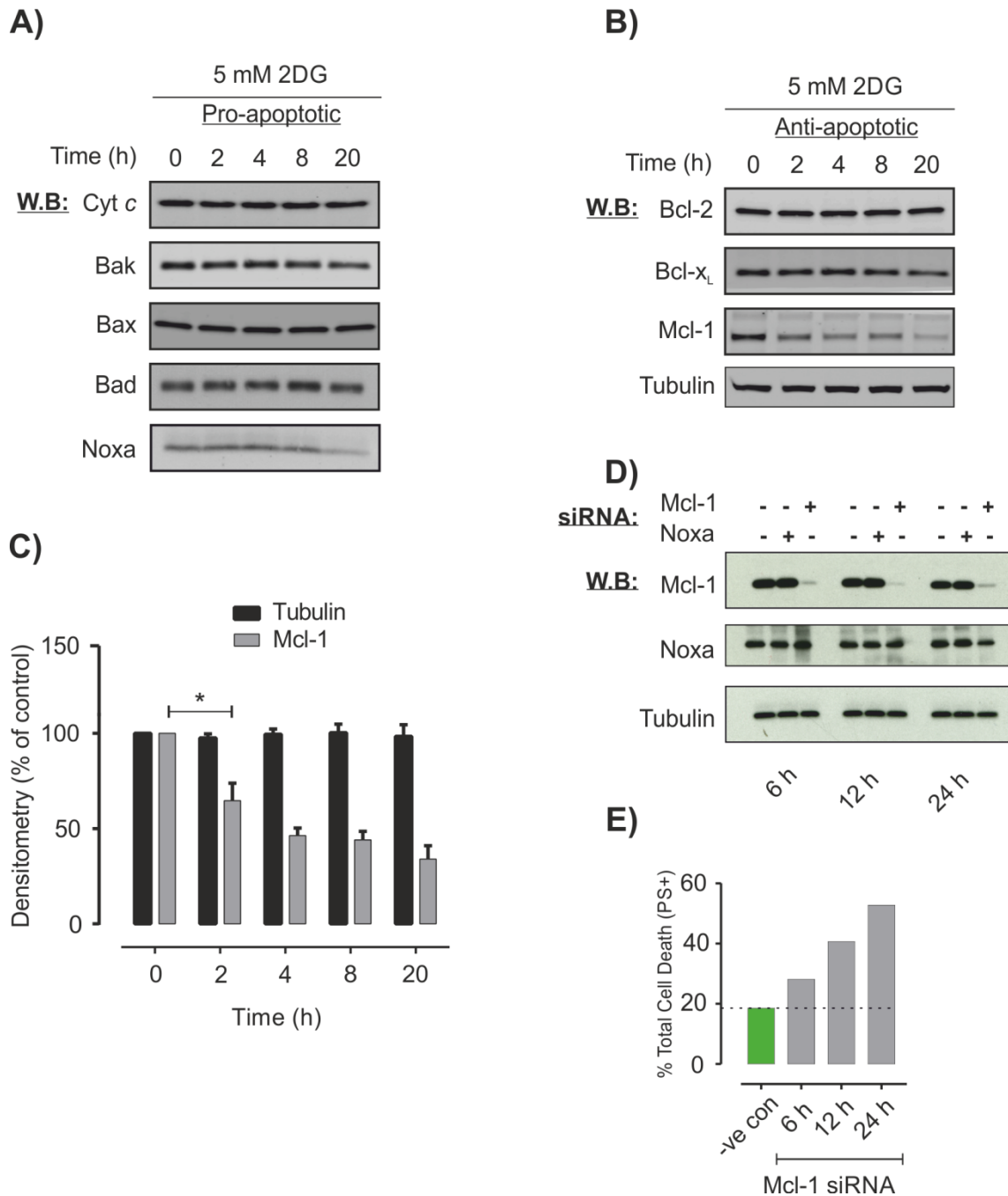


Figure 4-4 2DG rapidly reduces expression of Mcl-1 but not other Bcl-2 family members.

Z138 cells were cultured in standard glucose media (as described in Figure 4-1) and then treated with 5 mM 2DG for 0, 2, 4, 8 and 20 h. The cell pellets were solubilised and whole cell protein expression was analysed by immunoblotting. **A)** Protein expression of pro-apoptotic Cyt c; Bak; Bax; Bad and Noxa and **B)** anti-apoptotic Bcl-2; Bcl-x_L and Mcl-1 following treatment with 2DG for various times. **C)** Li-Cor quantitative densitometry analysis of Mcl-1 and tubulin immunoblots after 2DG treatment is expressed as a % of 0 h control. **D)** Immunoblots of Mcl-1 and Noxa; 6, 12 and 24 h after siRNA transfection against Mcl-1 and Noxa, respectively. Mcl-1 was rapidly depleted by siRNA, however Noxa was not. **E)** Total cell death (PS⁺) was calculated from Annexin-V/PI FACS analysis of Mcl1 knockdown cells, 6, 12 and 24 h post transfection. Immunoblots are representative of 2 – 3 independent experiments. Error bars represent mean ± SEM (n=3). Star (*) represents p < 0.05 (Students t test)

2DG induced a reduction in total Mcl-1 protein levels by 40% in 2 h and by 20 h was further reduced by 70% (Figure 4-4C), the decrease in protein expression following 2DG treatment was therefore rapid and sustained which explains the previously described results of 2DG treatment at 20 h (Robinson *et al.*, 2012).

As Mcl-1 has been previously implicated as the primary anti-apoptotic protein that is regulated by 2DG and responsible for both 2DG-induced apoptosis or sensitisation to apoptotic stimuli, I then determined if Mcl-1 knockdown replicates 2DG effects and also sensitised Z138 cells to both TRAIL and ABT-737. Knockdown of Mcl-1 by siRNA nucleofection (LONZA) resulted in almost complete ablation of Mcl-1 protein expression by 6 h, and knockdown was maintained for up to 24 h post transfection (Figure 4-4D). Mcl-1 has been reported to selectively stabilise Noxa (Craxton *et al.*, 2012); therefore following loss of Mcl-1, Noxa expression is also reduced. However, there was no detectable difference in Noxa protein expression until 20 h post treatment. Knockdown of Noxa by siRNA transfection was assessed by immunoblotting. There was no reduction in protein expression of Noxa following knockdown, which indicated that the presumed band may have been non-specific (Figure 4-4D). Conversely however, following proteasome inhibition (Appendix Figure 7-1A) with MG132, there was a rapid and marked increase in 'Noxa' expression. Additionally, following inhibition of protein translation with cycloheximide (CHX), there was rapid decrease in 'Noxa' expression with a half-life of ~30 min (Appendix Figure 7-1B), consistent with previously published data (Craxton *et al.*, 2012). These data indicated that the band in Figure 4-4D was likely Noxa; it was therefore possible that the Mcl-1:Noxa ratio may have been implicated in the sensitisation effects observed following 2DG treatment. 2DG-induced down regulation of Mcl-1 and a corresponding up-regulation in Noxa has previously been described as an essential component in 2DG-induced cell death in rhabdomyosarcomas (Ramirez-Peinado *et al.*, 2011).

However, knockdown of Mcl-1 alone resulted in 30% total cell death (PS+) by 6 h post knock down (transfection alone induced 18% cell death), which increased to 55% total cell death (PS+) by 24 h post transfection, without the addition of any apoptotic inducers (Figure 4-4E). Therefore Z138 cells appeared to be already 'primed' for cell death and Mcl-1 was the gatekeeper preventing apoptosis. Strikingly, despite the presence of both Bcl-2 and Bcl-x_L, which are believed to

provide redundancy for each other and Mcl-1 (Eichhorn *et al.*, 2014), this was not the case. Z138 cells appeared to be addicted to Mcl-1, because transient transfection induced substantial knockdown of Mcl-1, which induced 55% total cell death. It was striking therefore that ablation of Mcl-1 protein expression by 2DG treatment alone did not induce significant apoptosis in Z138 cells, even at 20 h post 2DG treatment there was only 20% cell death (Figure 4-1A).

4.2.5 2DG results in AMPK- α T172 de-phosphorylation and Akt S473 phosphorylation

Two master regulators of cellular metabolism are the 5' adenosine monophosphate kinase (AMPK) and protein kinase B (Akt), which function to maintain a balance between catabolic and anabolic processes upon minor changes to energy supply and demand (reviewed in Schultze *et al.*, 2012). It has previously been shown that 2DG can activate both the AMPK (Hawley *et al.*, 2010; Jeon *et al.*, 2012; Xi *et al.*, 2013; Pradelli *et al.*, 2010) and Akt (Zhong *et al.*, 2009; Zhong *et al.*, 2008) pathways following 2DG treatment. AMPK is a negative regulator of protein synthesis while Akt is positive regulator. Upon activation, they phosphorylate TSC2 to either activate or inhibit its activity (Figure 4-5A), which results in inhibition or activation of protein synthesis respectively (see chapter 1.9). The downstream proteins 4EBP1 and p70S6k are therefore good markers of both protein synthesis status and AMPK/Akt activity. Firstly, phosphorylation of the catalytic AMPK subunit; AMPK- α T172 was assessed by immunoblotting after 0, 2, 4, 8 and 20 h 2DG treatment. There was no significant detectable change in the total AMPK- α level until a decrease 20 h post treatment. Interestingly however, contrary to the above published literature, there was a de-phosphorylation of AMPK- α T172 by 2 h, which continued to decrease up to 20 h. There was no detectable difference in the total levels of the regulatory subunit AMPK- β 1, however there appeared to be a minor increase in S108 phosphorylation up to 8 h, which was dramatically reduced by 20 h. Phosphorylation of AMPK- β S108 appears to be required for the AMPK heterotrimer activity (Warden *et al.*, 2001). Downstream of AMPK is tuberous sclerosis 2 (TSC2), there was a detectable phosphorylation of TSC2 S1387 up to 4 h, which decreased from 8 - 20 h and mirrored the changes in total TSC2 levels. Additionally, there was a rapid decrease in phosphorylation of p70S6k T389, which indicated a shut down in protein translation. This indicated that following 2DG

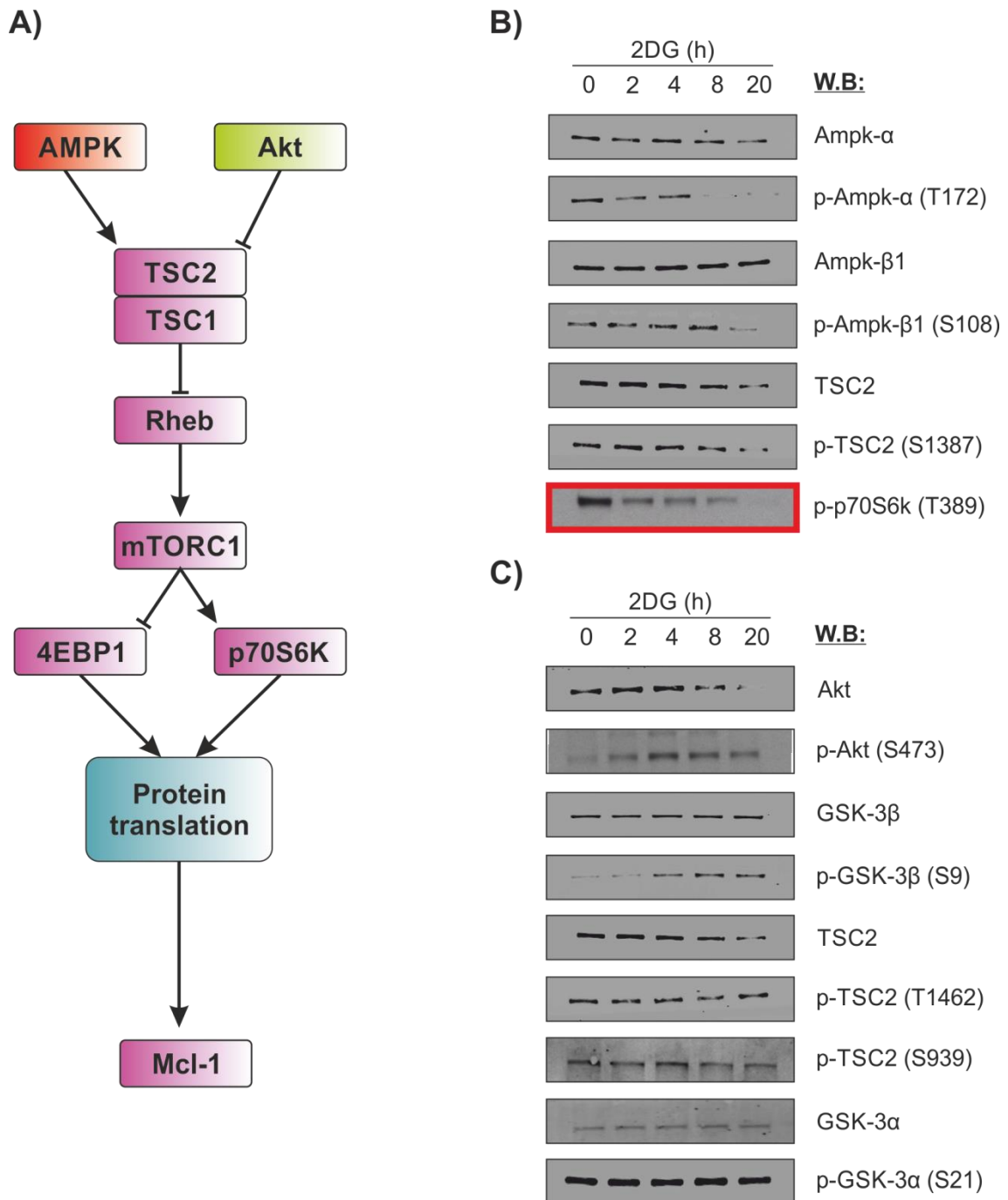


Figure 4-5 2DG results in AMPK de-phosphorylation and Akt phosphorylation.

A) Schematic representation of how AMPK and Akt regulate protein translation and thus Mcl-1 protein expression. Z138 cells were cultured in standard glucose media (as described in Figure 4-1) and then treated with 5 mM 2DG for 0, 2, 4, 8 and 20 h, the cell pellets were the solubilised and whole cell protein expression was analysed by immunoblotting for markers of AMPK activation **B)** AMPK-α; p-AMPK-α T172, AMPK-β1, p-AMPK-β1 S108, TSC2, p-TSC2 S1387 and p-p70S6k T389. **C)** Additionally, markers of Akt activation: Akt, p-Akt S473, GSK-3β, p-GSK-3β S9, TSC2, p-TSC2 T1462 and S939; GSK-3α and GSK-3α S21. Western blots are representative of at least 2 independent experiments.

treatment, AMPK appeared to be activated independently of AMPK- α T172 phosphorylation and inhibition of protein translation appeared to start prior to the 2 h time point analysed, as indicated by the rapid de-phosphorylation of p70S6k (Figure 4-5B).

Akt is a positive regulator of protein synthesis, and it was possible this would be deactivated following 2DG treatment as p70S6k T389 was de-phosphorylated. Interestingly however, total Akt protein expression increased up to 2 h and then reduced from 8 – 20 h. Furthermore, Akt S473 was increasingly phosphorylated from 2 h to 4 h, after which it was de-phosphorylated between 8 and 20 h (Figure 4-5C). In-line with this activation event, phosphorylation of glycogen synthase kinase-3 β (GSK-3 β) S9 occurred with similar kinetics to Akt S473 phosphorylation. There was no difference in total levels of GSK-3 β at any time point. Interestingly, phosphorylation of Akt downstream targets TSC2 T1462/S939 was not detected, which indicated that Akt may have a selective substrate repertoire following 2DG treatment. There was no detectable difference in phosphorylation of GSK-3 α S21 indicating that this isoform was not post translationally regulated following 2DG treatment at any time (Figure 4-5C). These results suggested that Akt was not signalling to activate protein translation following S473 hyper-phosphorylation and that AMPK was likely to be the dominant kinase responsible for inhibition of translation.

4.2.6 2DG treatment induces a rapid AMPK activation event

There was no detectable AMPK activity at 0 – 20 h (4.2.5) when assessed by immunoblotting of AMPK- α T172, but there was a rapid de-phosphorylation of p70S6k T389 within 2 h. This suggested that a signalling event earlier than 2 h had likely occurred and resulted in translation inhibition; therefore AMPK activity was assessed at 0, 5, 10, 15, 30 and 60 min following 2DG treatment. This showed that there was a very rapid and transient phosphorylation of AMPK- α T172 that occurred at 5 min post 2DG treatment, which was maintained until 15 – 30 min (Figure 4-6A) and then phosphorylation decreased to below basal levels. A functional read out of AMPK activity was assessed by immunoblotting for phosphorylated Acetyl Coenzyme-A Carboxylase (ACC) S79. ACC was phosphorylated following 2DG treatment with similar kinetics to AMPK- α T172 phosphorylation, however phosphorylation remained up to 60 min post treatment

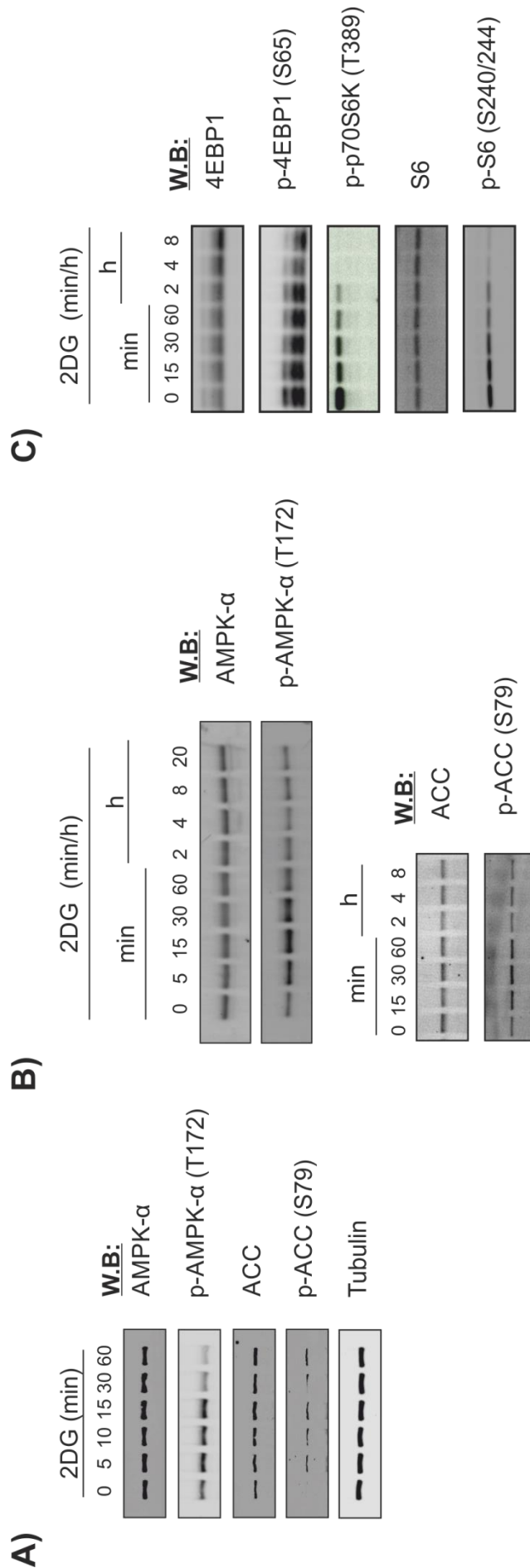


Figure 4-6 2DG induces a rapid and transient AMPK event. Z138 cells were cultured in standard glucose media (as described in Figure 4-1) and then treated with 5 mM 2DG for various times, the cell pellets were then solubilised and whole cell protein expression was analysed by immunoblotting for **A)** AMPK- α , p-AMPK- α T172, ACC and p-ACC (S79). To confirm the transient AMPK- α T172, and examine its kinetics at early as well as longer 2DG treatment times Z138 cells were treated with 5 mM 2DG for 0, (5), 15, 30, 60 min and 2, 4, (20) h and then the expression levels analysed for **B)** AMPK- α , p-AMPK T172, ACC and p-ACC S79. To determine if AMPK transient activation was inhibiting protein synthesis, solubilised cell pellets were also immunoblotted for **C)** 4EBP1, p-4EBP1 S65, p-p70S6k T389, S6 and p-S6 S240/244. The immunoblots are representative of at least 2 independent experiments.

after AMPK phosphorylation had dissipated (Figure 4-6A) and then returned to basal levels from 2 – 8 h (Figure 4-6B).

As there was a rapid and transient AMPK activation, downstream markers of protein translation were analysed at 0, 15, 30, 60 min and 2, 4 and 8 h. There was a very rapid decrease in p70S6k T389 expression, which occurred at the earliest time point (15 min). Expression of p70S6k T389 continued to decrease with increased 2DG exposure until it was no longer detectable at 4 h. Expression of total protein levels of the p70S6k downstream target S6, did not change, but phosphorylation of S6 S240/244 decreased with similar kinetics to p70S6k T389 de-phosphorylation. Also, 2DG treatment produced a rapid de-phosphorylation of 4EBP1 S65 (Figure 4-6C). 4EBP1 is phosphorylated at multiple residues resulting in its inhibition, de-phosphorylation results in binding to eIF4E and inhibition of protein translation (chapter 1.9). Three bands were visible, the γ top band, which represented hyper-phosphorylation, the β middle band and the bottom α , hypo-phosphorylated band. Detectability of 4EBP1 γ reduced by 15 min. Interestingly, in all of the repeats, 4EBP1 S65 expression of all three bands was markedly reduced at the 4 h time point, followed by an increase in the hypo-phosphorylated α band at 8 h; in agreement with the Akt S473 phosphorylation seen in Figure 4-5C.

4.2.7 2DG results in Akt de-phosphorylation before hyper-phosphorylation

It has been previously reported that 2DG can induce Akt survival signalling in certain cancer cell types/lines (Zhong *et al.*, 2008; Zhong *et al.*, 2009); and Akt was shown to be phosphorylated at S473 following 2DG treatment (Figure 4-5C). Next, Akt signalling was analysed by immunoblotting at 0, 15, 30 60 min and 2, 4 and 8 h. There was no detectable difference in total Akt expression or Akt T308 phosphorylation (Figure 4-7A). Interestingly however, 2DG induced a transient and rapid decrease in Akt S473 phosphorylation as early as 15 min post treatment, which returned to basal levels by 60 min and became hyper-phosphorylated by 2h. There appeared to be a bi-phasic relationship between AMPK signalling and Akt signalling. Akt is a positive regulator of protein synthesis, via TSC2 and mTORC1. Activation of Akt under normal circumstances should result in stimulation of protein synthesis (reviewed in Showkat *et al.*, 2014). Immunoblots from Figure 4-6C showed that Akt hyper-phosphorylation was not sufficient to reactivate protein

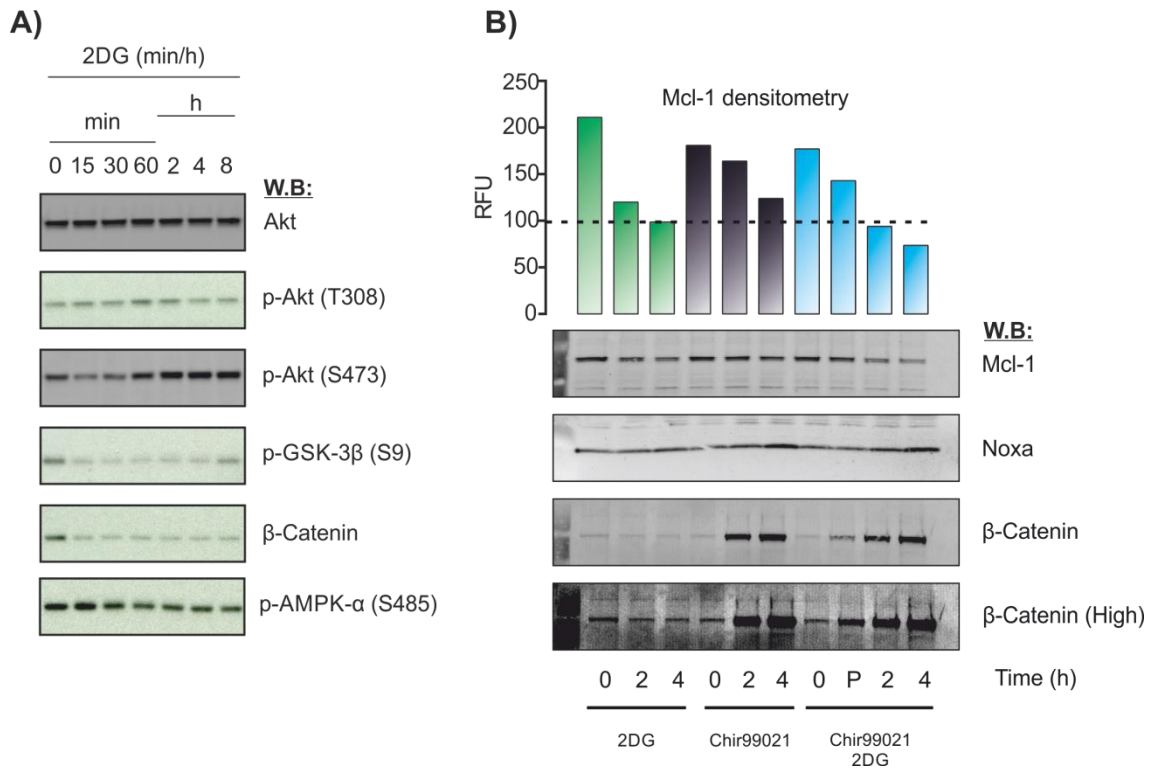


Figure 4-7 2DG induces Akt de-phosphorylation before hyper-phosphorylation. Z138 cells were cultured in standard glucose media (as described in Figure 4-1) and then treated with 5 mM 2DG for 0, 15, 30 and 60 min; 2, 4 and 8 h, the cell pellets were solubilised and whole cell protein expression analysed by immunoblotting for **A)** Akt, p-Akt T308, p-Akt S473, p-GSK-3 β , β -catenin and p-AMPK- α S485. **B)** Z138 cell were treated with either 5 mM 2DG, 5 μ M Chir99021 or pre-treated with 5 μ M Chir99021 followed by 5 mM 2DG for 0, 2, 4 h. Lane P represents 30 min Chir99021 pre-treatment before addition of 2DG. The cell pellets were then harvested, solubilised and immunoblotted for Mcl-1, Noxa and β -catenin. The bar graph depicts the raw data obtained from Li-Cor densitometry of Mcl-1 protein expression; the dotted line shows the level of Mcl-1 protein expression after 4 h 2DG treatment. The Immunoblots are representative of at least 2 independent experiments

translation after the initial AMPK activation. AMPK- α T172 and Akt S473 phosphorylation status were inversely correlated with each other.

To investigate the activity of Akt, downstream targets were assessed by immunoblotting. Akt phosphorylates GSK-3 β S9 (Cross *et al.*, 1995) and de-phosphorylation of GSK-3 β occurred with similar kinetics to Akt S473 de-phosphorylation, with GSK-3 β S9 recovering to basal levels within 8 h (Figure 4-7A). Additionally, AMPK- α S485 is a direct downstream target of Akt (Ning *et al.*, 2011), which was de-phosphorylated by 30 min, concordant with the loss of Akt activity. A second wave of re-phosphorylation was not detected at any time point analysed. As GSK-3 β has been implicated in the regulation of Mcl-1 via

proteasome-mediated degradation (Ding *et al.*, 2007), the activation status of GSK-3 β was analysed by assessing the activity of the destruction complex, which actively targets β -catenin for degradation in the presence of activated GSK-3 β (reviewed in Stamos & Weis, 2013). Total protein expression of β -catenin was analysed by immunoblotting and β -catenin expression was reduced as soon as GSK-3 β was activated (de-phosphorylation at S9), i.e. 15 min post 2DG treatment. Expression of β -catenin did not recover at any of the time points analysed; even though Akt S473 was phosphorylated at the later time points (Figure 4-7A).

GSK-3 β has been shown to regulate Mcl-1 protein expression by phosphorylating Mcl1 on S159, which targets it for proteasome degradation (Maurer *et al.*, 2006). To ascertain whether GSK-3 β was responsible for the rapid reduction in Mcl-1 protein expression (Figure 4-4B), Z138 cells were treated with the GSK-3 β inhibitor Chir99021, with and without 2DG (Figure 4-7B), with the expectation that inhibition of GSK-3 β would prevent Mcl-1 phosphorylation and subsequent degradation. Inhibition of GSK-3 β resulted in a rapid accumulation of β -catenin (Figure 4-7B), which indicated successful GSK-3 β inhibition. Interestingly however, using Li-COR quantitative densitometry of the immunoblots, it was observed that GSK-3 β inhibition did not prevent the reduction of Mcl-1 protein expression. In fact, there was a reduction in Mcl-1 protein expression when treated with Chir99021 in the absence of 2DG (Figure 4-7B black bars). When Z138 cells were pre-treated with Chir99021 followed by 2DG, there was a synergistic effect, which resulted in a greater reduction in Mcl-1 expression than 2DG alone at both 2 and 4 h post treatment. These results indicated that GSK-3 β inhibition instead of activation, may function as a novel mechanism to post-translationally regulate Mcl-1 protein expression in certain cell lines/types. However, because GSK-3 β was activated following 2DG treatment it is possible that the regulation of Mcl-1 by 2DG is independent of the conventionally described GSK-3 β pathway (Maurer *et al.*, 2006). Interestingly, inhibition of GSK-3 β resulted in increased expression of Noxa in both the presence and absence of 2DG, which highlighted that GSK-3 β may be a potential regulatory kinase common between both Mcl-1 and Noxa.

4.2.8 2DG rapidly inhibits global protein synthesis

It has been shown previously that 2DG abrogates protein translation (Pradelli *et al.*, 2010; Robinson *et al.*, 2012), presumably by inhibiting p70S6k T389 phosphorylation (Figure 4-6C). To characterise how protein synthesis was inhibited by 2DG, two independent functional readouts for assessing inhibition of protein synthesis were used. Firstly, Z138 cells were treated with 2DG (5 mM) for 0, 1, 2, 4 and 20 h, then incubated for 3 min with CHX, centrifuged and the pellet lysed in polysome lysis buffer and then centrifuged again (as detailed in Chapter 2.2.10), the supernatant was carefully layered over the top of pre-prepared sucrose density gradients and centrifuged for 2 h to separate the polysomes and sub-polysomes. Depending on the density of the gradient, differential separation occurred with high molecular weight actively translating polysomes sedimenting towards the 50% sucrose layer and with the sub-polysomes sedimenting at the top towards the 10% sucrose layer (Figure 4-8A). By 1 h, 2DG treatment induced a shift in the actively translating polysome fraction (Figure 4-8B, right of graph) to the sub-polysomes (left of graph). There was a rapid time-dependent increase in the extent of the shift from the polysomes to sub-polysomes after 2DG treatment, which was maximal between 2 and 4 h, which indicated that translation was inhibited in a time-dependent manner (Figure 4-8B).

To determine the extent to which total protein synthesis was inhibited by 2DG treatment, global protein synthesis was determined by ³⁵S methionine/cysteine incorporation in cellular proteins which were precipitated with TCA then analysed by scintillation counting. At the earliest time point assessed (30 min), there was a 40% reduction in total protein synthesis, and this level of inhibition was sustained up to at least 4 h (Figure 4-8C). As the maximal reduction in protein translation was ~40% of control, this may have indicated a selective shut down in protein translation after 2DG treatment.

To determine if 2DG and inhibition of protein translation alone induced the same changes to protein expression of Bcl-2 family members; Z138 cells were treated with the protein synthesis inhibitor CHX and protein expression levels of key pro- and anti-apoptotic levels were analysed by immunoblotting. The protein expression of pro-apoptotic: Cyt c; Bad; Bak and Bax did not change following CHX treatment

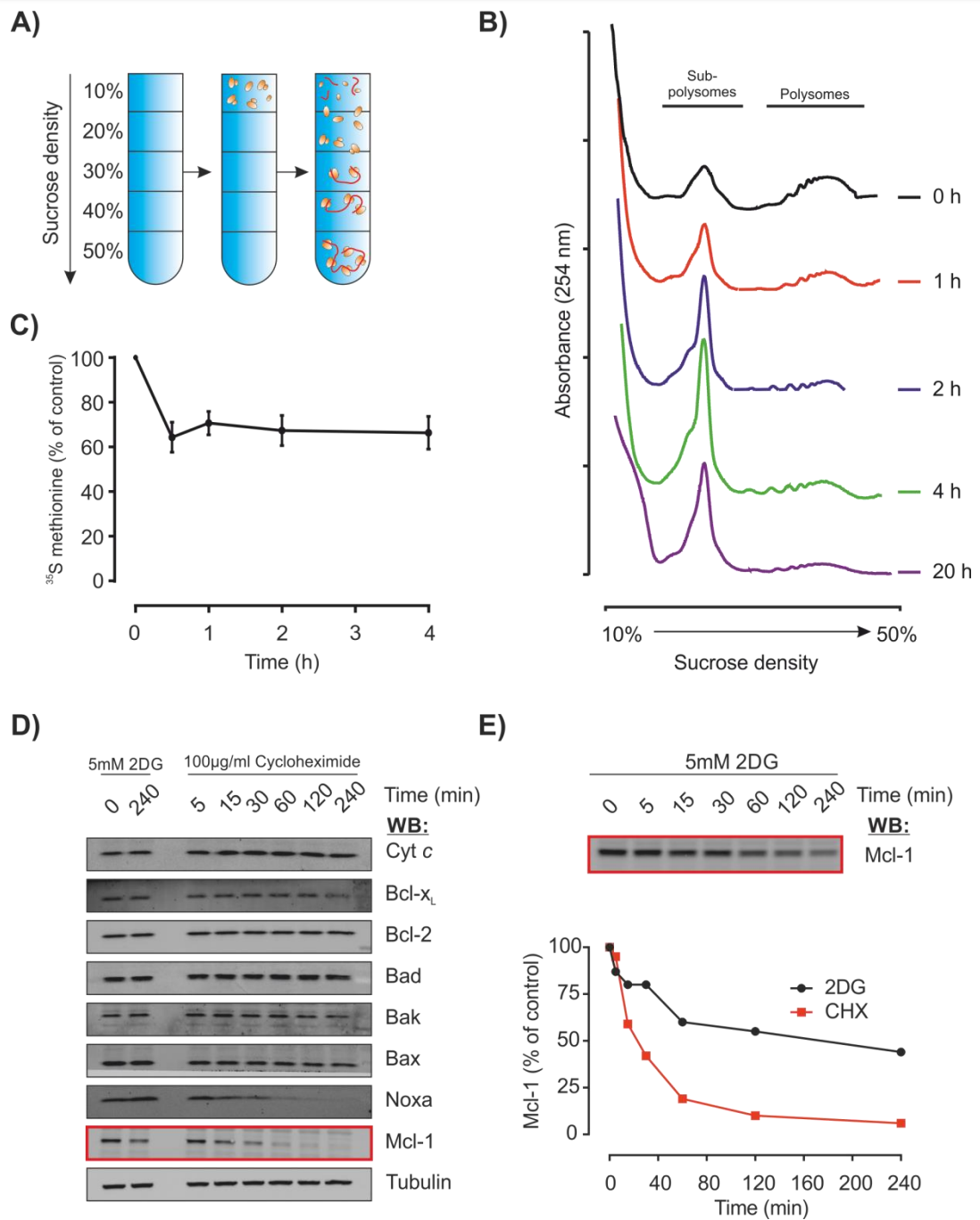


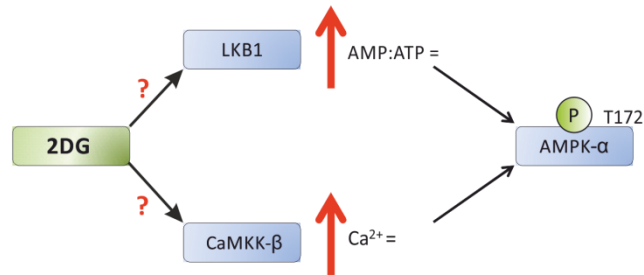
Figure 4-8 2DG treatment rapidly reduces global protein synthesis. Z138 cells were cultured in standard glucose media (as described in Figure 4-1) and then treated with 5 mM 2DG for 0, 1, 2, 4 and 20 h. The cells were then treated briefly with CHX (see Chapter 2.2.10), lysed and layered on a sucrose density gradient and centrifuged to separate actively translating polysomes and non-translating sub-polysomes as depicted in panel **A**). Gradient fractionation was assessed by continuous monitoring of the absorbance at 254 nm **B**) where actively translating polysomes appear as a peak on the right side of the graph (50% sucrose), and sub-polysomes appear as a peak on the left (10% sucrose). **C**) Z138 cells were also treated with 5 mM 2DG for 0, 0.5, 1, 2 and 4 h, followed by the addition of ^{35}S methionine, TCA protein precipitation and scintillation counting was used to determine the extent of global protein synthesis inhibition. **D**) Cells were treated with 100 $\mu\text{g}/\text{ml}$ CHX for the indicated times, the cell pellets were then analysed by immunoblotting for: Cyt c, Bcl- x_L , Bcl-2, Bad, Bak, Bax, Noxa and Mcl-1. **E**) Z138 cells were treated with 5 mM 2DG for the indicated times and immunoblotted for Mcl-1, the graph shows Li-Cor quantitative densitometry of Mcl-1 treated with CHX vs 2DG (expressed as a % of control), densitometry is the average of two gels.

up to the longest time point analysed (4 h). Additionally, there was no change in protein expression of anti-apoptotic: Bcl-x_L or Bcl-2 (Figure 4-8D). As expected, the expression of Mcl-1 following total inhibition of protein synthesis was markedly reduced with a half-life of 15 - 30 min; additionally, the half-life of Noxa was also ~15 min (Appendix 7-1B). To determine if 2DG treatment induced a reduction of Mcl-1 with similar kinetics to CHX, protein expression of Mcl-1 after 2DG treatment was also analysed at the same time points. There was a rapid reduction of Mcl-1 protein expression following 2DG treatment; however, it did not occur at the same rate as CHX (Figure 4-8E). Additionally, the expression of Mcl-1 in 2DG treated cells did not drop to the same levels as CHX treatment. These results showed that inhibition of protein synthesis by 2DG resulted in a reduction in expression of Mcl-1 to an extent. The remaining Mcl-1 protein following 2DG treatment was probably residual translation from the incomplete inhibition. It was striking however, that inhibition of translation by 2DG did not reduce Noxa expression but CHX did. This indicated that the Mcl-1:Noxa ratio may be critical for 2DG-mediated sensitisation to both TRAIL and ABT-737 in Z138 cells.

4.2.9 Canonical AMPK activators do not induce phosphorylation of AMPK- α T172

2DG induced a rapid and transient activation of AMPK that resulted in a rapid and partial inhibition of protein translation. Previous studies identified the mechanism to be via phosphorylation of AMPK- α T172 by LKB1 (Corradetti *et al.*, 2004), which is activated through increasing AMP:ATP ratios, CaMKK- β activation which results from increased cytoplasmic calcium loading (Xi *et al.*, 2013) (Figure 4-9A), or an unidentified mechanism independent of both (Jeon *et al.*, 2012). I therefore investigated whether in Z138 cells activation of AMPK was either due to LKB1 or CaMKK- β following 2DG treatment. Subsequently, to determine if activation of AMPK was the initial signal that resulted in the sensitisation to both TRAIL and ABT-737-induced cell killing. Therefore, Z138 cells were treated with the AMPK activators: metformin, phenformin, AICAR, AMP, thapsigargin and A23187, and the AMPK activity analysed by immunoblotting, the results of which are summarised in Figure 4-9B. The effects of these compounds on TRAIL and ABT-737-induced cell killing were assessed by Annexin-V/PI FACS analysis. Z138 cells were pre-treated with the highest concentration used for each drug (detailed in Figure 4-9B) for 4

A)



B)

Compound	Function	[Max]	Effect on AMPK	Effect on TRAIL	Effect on ABT-737
Metformin	Complex 1 Inhibitor	1 mM	No effect	No effect	No effect
Phenformin	Inhibitor of cellular Respiration	1 mM	No effect (200 μ M) De-phosphorylation (1 mM)	No effect (4 h) toxic (20 h)	No effect (4 h) toxic (20 h)
AICAR	AMP analogue	2 mM	Dephosphorylation	Sensitised/ toxic	Sensitised/ toxic
AMP	N/A	5 mM	No effect	No effect	No effect
Thapsigargin	SERCA Inhibitor	5 μ M	Dephosphorylation	Cytotoxic	Cytotoxic
A23187	Calcium Ionophore	5 μ M	Dephosphorylation	Cytotoxic	Cytotoxic
2DG	Glycolytic and Hexokinase Inhibitor	5 mM	Phosphorylation/ Activation	Sensitise	Sensitise

Figure 4-9 Traditional AMPK activators do not induce AMPK- α T172 phosphorylation.

A) Schematic to show the canonical routes by which 2DG can activate AMPK, through either LKB1 or CaMKK- β . **B)** Table summarises: the activators used (column 1) how they function to activate AMPK (column 2), the maximum concentration used (column 3), the effect they had on AMPK- α T172 phosphorylation (column 4), the effect they had on TRAIL (column 5) and the effect they had on ABT-737 (column 6). Z138 cells were cultured in standard glucose media (as described in Figure 4-1) and then treated for various times with the activators, the cell pellets were then harvested, solubilised and analysed by immunoblotting for AMPK and p-AMPK- α T172 to determine AMPK activity (see Appendix 7-2). To determine the effect of the compounds on TRAIL and ABT-737-induced cell killing, Z138 cells were pre-treated with each activator at [max] for 4 and 20 h, followed by 200 ng/ml TRAIL or 25 nM ABT-737 for 4 h, cell death was analysed using Annexin-V/PI FACS analysis (see Appendix 7-3)

and 20 h, followed by TRAIL (200 ng/ml) or ABT-737 (25 nM) for 4 h, the results of which are summarised in Figure 4-9B.

The biguanides metformin and phenformin are anti-diabetic medications used to reduce blood sugar levels (phenformin retracted from market due to high incidences of lactic acidosis). They also activate AMPK by incompletely understood mechanisms, although it is likely by indirectly inhibiting the NADH dehydrogenase (complex I) of the mitochondrial respiratory chain (Wheaton *et al.*, 2014). Inhibition of complex I prevents mitochondrial oxidative generation of ATP and thus should increase the AMP:ATP ratio. Treatment with metformin (1 mM) did not induce AMPK- α T172 phosphorylation at any time point analysed (Appendix 7-2). Treatment with metformin (1 mM) for 4 and 20 h did not induce cell death alone. Additionally, pre-treatment with metformin for 4 and 20 h did not sensitise Z138 cells to either TRAIL or ABT-737 (Appendix 7-3). Treatment with phenformin (200 μ M or 1 mM) did not induce AMPK- α T172 phosphorylation at any time point analysed (Appendix 7-2), in fact, 1 mM phenformin resulted in de-phosphorylation of AMPK- α T172 by 30 min. Treatment with phenformin (1 mM) for 4 h did not induce any cell death and did not sensitise Z138 cells to TRAIL or ABT-737. Treatment with ABT-737 alone induced 37% cell death and TRAIL induced 55% cell death. By 20 h, phenformin (1 mM) alone was cytotoxic and induced 33% cell death. Pre-treatment, followed by ABT-737 resulted in 51% cell death and pre-treatment followed by TRAIL resulted in 59% cell death. The combined cell death values of phenformin alone and TRAIL/ABT-737 alone (33% + 37% and 33% + 55%, respectively) were higher than the combinatorial treatment, which indicated that phenformin had an additive effect to cell death, not synergistic, and the mechanism of action was therefore likely to not be the same as 2DG (Appendix 7-3).

AICAR is a cell permeable compound, which upon entry into the cell is phosphorylated to ZMP, an AMP analogue, and thus activator of AMPK. Treatment with AICAR (2 mM) did not induce AMPK- α T172 phosphorylation at any time point analysed. Like phenformin, AICAR treatment resulted in a rapid de-phosphorylation of AMPK- α T172 (Appendix 7-2). AICAR (2 mM) alone was cytotoxic to Z138 cells and resulted in cell death at 4 h (24%) and 20 h (40%) post treatment (Appendix 7-3). When combined with ABT-737 or TRAIL after 4 h pre-treatment, cell death was

increased to 76% and 90% respectively. When combined with ABT-737 or TRAIL after 20 h pre-treatment, cell death was increased to 79% and 83% respectively, AICAR appeared to sensitise Z138 cells to both TRAIL and ABT-737. However, because AICAR resulted in a de-phosphorylation of AMPK- α T172, it was likely that this effect was independent of AMPK signalling. AICAR has previously been reported to induce cell death in an AMPK independent manner in certain cell lines/types (Santidrian *et al.*, 2010).

Next, Z138 cells were treated with AMP (0.2 and 5 mM), direct addition of AMP did not induce phosphorylation of AMPK- α T172 at any time point analysed (Appendix 7-2). Treatment with AMP (5 mM) for 4 and 20 h did not induce cell death alone compared to control cells. Additionally, pre-treatment with AMP for 4 and 20 h did not sensitise Z138 cells to either TRAIL or ABT-737 (Appendix 7-3).

Thapsigargin is a sarcoplasmic- endoplasmic reticulum calcium ATPase inhibitor (SERCA), which results in Ca^{2+} efflux from the ER increasing the cytosolic $[\text{Ca}^{2+}]$ (Wictome *et al.*, 1992). Increased cytosolic calcium loading can activate AMPK by activating the upstream kinase CaMKK- β independently of the AMP:ATP ratio (Woods *et al.*, 2005). Treatment with thapsigargin (5 μM) resulted in a rapid de-phosphorylation of AMPK- α T172 at all of the time points analysed (Appendix 7-2). Additionally, treatment with thapsigargin (5 μM) was extremely cytotoxic, which resulted in 100% cell death at both 4 and 20 h treatment (Appendix 7-3). Treatment with the calcium ionophore A23187 (5 μM) resulted in a rapid de-phosphorylation of AMPK- α T172 at all of the time points analysed (Appendix 7-2). Additionally, treatment with A23187 (5 μM) was extremely cytotoxic, and resulted in 100% cell death at both 4 and 20 h treatment (Appendix 7-3).

As the AMPK activators used did not result in AMPK phosphorylation, I hypothesised that the AMPK inhibitor compound C would reverse the 2DG-mediated sensitisation to TRAIL. Therefore, Z138 cells were pre-treated with compound C (5, 10 and 30 μM) for 30 min, followed by 2DG (5 mM) for 4 h and TRAIL (200 ng/ml) for 4 h (total time for compound C treatment alone was therefore 8.5 h). Unexpectedly, compound C resulted in dose-dependent cell death, more strikingly however, compound C-induced cell death was protected by 2DG treatment. When compound C and TRAIL were used in combination, there

was an additive effect on cell death with 10 and 30 μ M compound C, increasing cell death. When compound C, 2DG and TRAIL were all used together, there was a compound C dose-dependent decrease in cell death. Strikingly therefore, this data indicated that 2DG actually protected against TRAIL and compound C synergism (Appendix 7-4)

4.2.10 Inhibition of AMPK kinase CaMKK- β with STO-609 and transient knockdown of LKB1 does not prevent 2DG-mediated phosphorylation of AMPK- α T172

To further rule out the involvement of LKB1 and CaMKK- β in 2DG-mediated AMPK activation in Z138 cells, CaMKK- β was inhibited with STO-609 and LKB1 was knocked down with siRNA. Strikingly, when Z138 cells were treated with the CaMKK- β inhibitor STO-609, basal levels of AMPK phosphorylation were almost completely ablated (Figure 4-10A left panel). The immunoblots also showed that ACC S79 phosphorylation was abolished by STO-609. Treatment with STO-609 did not induce a marked down regulation of protein synthesis alone at early time points, however at later time points (4 h), there appeared to be a minor inhibition of protein translation (S6 S240/244 de-phosphorylation and an increase in the 4EBP1 α band). The minor inhibition in protein synthesis was not sufficient to reduce protein expression of Mcl-1. This data indicated that under basal conditions Z138 cells had a high level of endogenous AMPK signalling that was regulated by CaMKK- β and therefore through calcium and calmodulin flux.

Pre-treatment with STO-609 for 30 min (Figure 4-10A, right panel, lane P) did not prevent 2DG induced transient phosphorylation of AMPK- α T172 and additionally ACC S79 phosphorylation still occurred. There was no difference in the phosphorylation patterns of downstream protein translation markers between 2DG alone or with STO-609 pre-treatment (Figure 4-10A, compare middle panel with right panel). Additionally, Mcl-1 protein expression was reduced with the same kinetics between the two treatment conditions. These results demonstrated that 2DG was regulating the activity of AMPK and expression of Mcl-1 independently of CaMKK- β .

To determine if 2DG activated AMPK by LKB1 via AMP:ATP ratio changes, LKB1 protein levels were reduced using siRNA transient knock down.

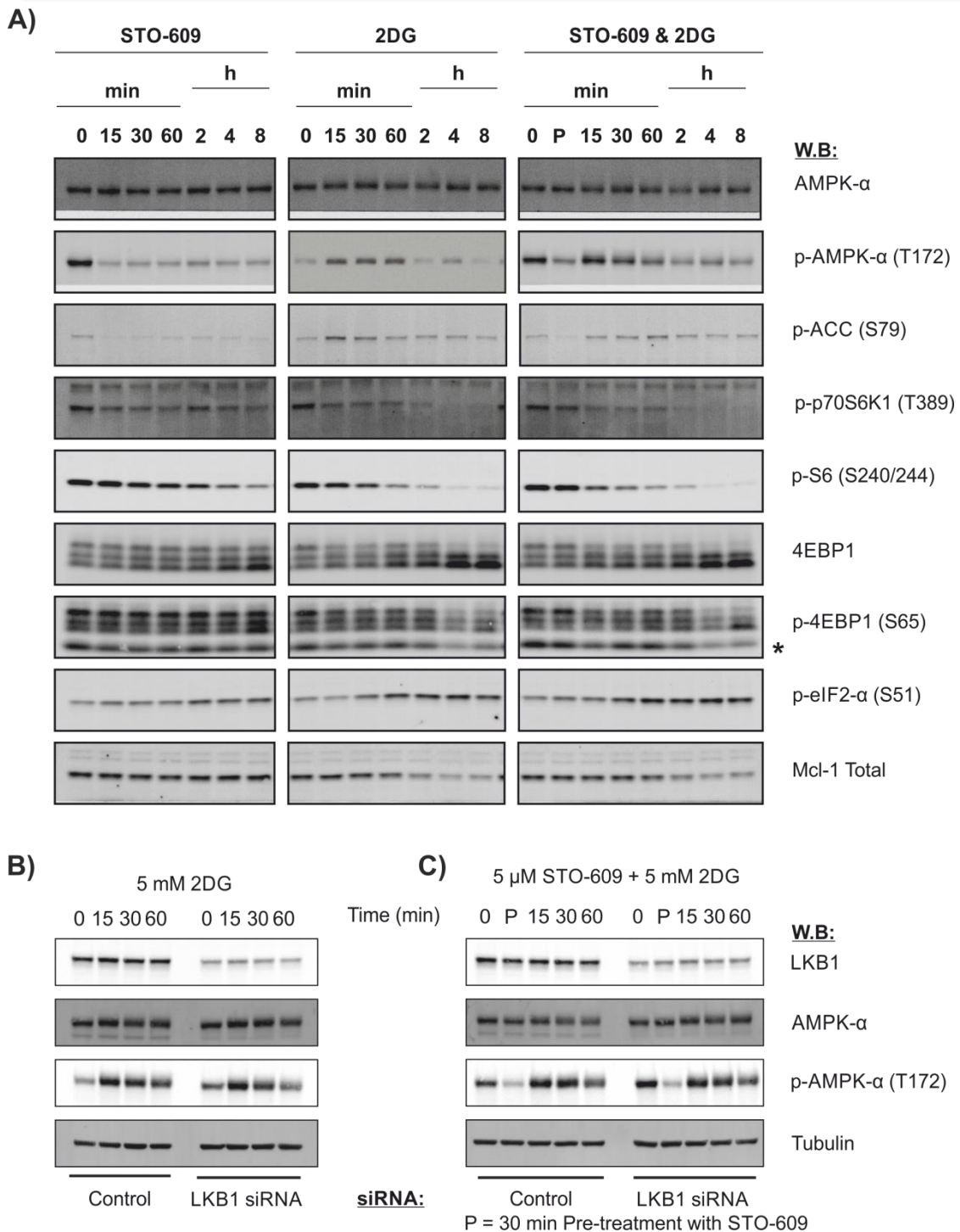


Figure 4-10 Inhibition of AMPK kinase CaMKK-β and knockdown of LKB1 does not prevent 2DG-mediated phosphorylation of AMPK-α T172. Z138 cells were cultured in standard glucose media (as described in Figure 4-1) and then treated with either **A)** 5 μM STO-609, 5 mM 2DG, or pre-treated with 5 μM STO-609 for 30 min followed by 5 mM 2DG for the indicated times. P represents 30 min STO-609 pre-treatment alone before the addition of 2DG. Cell pellets were collected, solubilised and protein expression analysed by immunoblotting with the indicated antibodies. **B)** Z138 cells were transfected with STK11 siRNA (LKB1 gene name), the cells were harvested 24 h post transfection then treated with 5 mM 2DG for 0, 15, 30 and 60 min or **C)** pre-treated with 5 μM STO-609 for 30 min (P), followed by 15, 30 and 60 min 5 mM 2DG, then immunoblotted for LKB1, AMPK-α T172, p-AMPK-α T172 or tubulin. Immunoblots are representative of at least 2 independent experiments.

siRNA of LKB1 resulted in a 60% reduction in protein expression (Li-Cor densitometry, data not shown). 2DG treatment for 0, 15, 30 and 60 min showed that reduction in LKB1 protein expression was not sufficient to inhibit transient phosphorylation of AMPK- α T172 (Figure 4-10B).

Next, to determine if there was redundancy between LKB1 and CaMKK- β following 2DG treatment, LKB1 was knocked down in combination with STO-609 pre-treatment prior to treatment with 2DG. Ablating both AMPK kinases was insufficient to inhibit 2DG mediated phosphorylation of AMPK- α T172. This data, alongside the inability of AMPK activators to activate AMPK, indicated that it was unlikely that 2DG was activating AMPK and inhibiting protein synthesis through either LKB1 or CaMKK- β and there may be a third mechanism to activate AMPK in Z138 cells. However, LKB1 cannot be completely excluded as it is not rate-limiting and even 90% knockdown of LKB1 is sufficient to activate AMPK (Sakamoto *et al.*, 2005).

4.3 Discussion

4.3.1 2DG rapidly reprograms metabolism and sensitises Z138 cells to apoptosis

In this study I have shown that inhibiting glycolysis with the anti-glycolytic 2DG rapidly sensitises the mantle cell lymphoma derived Z138 cells to intrinsic and extrinsic apoptotic inducers. The sensitisation to ABT-737-induced cell killing is far more rapid than has previously been reported (Robinson *et al.*, 2012) with the EC_{50} of ABT-737 being reduced by 50% as quickly as 2 h following glycolysis inhibition with 2DG (Figure 4-1). Additionally 2DG pre-treatment reduces the EC_{50} of TRAIL by 40% in 4 h (Figure 4-2). The mode of cell death in combinatorial treatment is caspase-dependent apoptosis, which can be seen by increasing phosphatidyl serine exposure to the outer leaflet of the plasma membrane (as measured by FACS analysis) with increasing 2DG exposure times in both ABT-737 and TRAIL-induced apoptosis (Figure 4-1 and 4-2). Additionally, immunoblots of the initiator caspases-8 and -9, and executioner caspase-3 confirms that 2DG rapidly sensitises TRAIL and ABT-737 to caspase-dependent apoptosis.

Using real time measurements of oxidative phosphorylation and glycolysis, I have shown that 2DG treatment for 2 h results in metabolic reprogramming or switching

to increase oxidative phosphorylation by ~16% which is all directly linked to generating ATP, and forces the cells to respire maximally similar to state-3 respiration (Chance & Williams, 1955). Treatment with 2DG completely ablates glycolysis; however, extracellular acidification is only reduced by ~55% (Figure 4-3). This is contrary to work previously performed in our laboratory on Z138 cells after 20 h treatment with 2DG (Robinson *et al.*, 2012), where 20 h treatment results in reduction of oxidative phosphorylation and near complete ablation of extracellular acidification. It highlights that in the early stages of treatment with 2DG, exogenous supplementation of pyruvate and glutamax is sufficient to sustain mitochondrial metabolism and is possibly why Z138 cells do not start undergoing cell death following 2DG treatment alone until 20 h (Figure 4-1). Comparing these two studies indicates that the metabolic reprogramming induced by 2DG is transient, but more importantly, at 2 h post treatment, the remaining acidification that is not observed at 20 h post treatment is linked to mitochondrial metabolism, not glycolysis. Treatment with 2DG for 2 h highlights that 45% of the acidification generated by Z138 cells is respiratory chain driven acidification, 70% of which is directly linked to ATP production and the remaining 30% derived from the mitochondrial proton leak. It is not possible with the data presented to determine if untreated cells also undergo mitochondrial-mediated acidification or if it is induced by 2DG. It would be interesting however to study this phenomenon further, to determine to what extent mitochondrial metabolism plays a role in generating an acidic tumour micro-environment, which is largely attributed to the 'Warburg effect'; increased glycolysis and lactate efflux (reviewed in Kato *et al.*, 2013). Additionally, to determine if 2DG is in fact inducing the mitochondrial-mediated acidification, or just unmasking its presence would be of important clinical significance to ensure treatment with 2DG is not generating a survival advantage by increasing the acidity of the tumour micro-environment. Despite the increase in oxidative phosphorylation following 2DG treatment, there is still a ~40% reduction in cellular ATP levels by 2 h. This reduction in ATP is likely due to the energetic requirements of phosphorylating 2DG to 2DG-6-P, shown in Figure 4-3 (schematic).

It has been previously described that Mcl-1 is the primary anti-apoptotic protein down regulated following 2DG treatment (Pradelli *et al.*, 2010; Robinson *et al.*, 2012). These studies however, have looked at the cell death mechanisms after late

time points (16 – 20 h). In this study, the early initiating events that lead to rapid sensitisation are explored in detail. Perhaps one of the most striking findings is that Mcl-1 is rapidly down-regulated, 13% by 5 min (Figure 4-8), and 40% by 2 h (Figure 4-4). This rapid disappearance is not shared between any of the other pro- or anti-apoptotic proteins, not even Noxa, which does not start to show reduced expression until 8 – 20 h, despite the short half-life of ~30 min (Craxton *et al.*, 2012). Bak, Bad and Bcl-x_L do not start to show reduced detectability by immunoblotting until 8 h post 2DG treatment (Figure 4-4). There are two parallel theories as to how 2DG manipulates Mcl-1 to sensitise cells to apoptotic inducers. The first being a reduction in expression of Mcl-1, as seen in Z138 cells and my data support this theory. The second is that 2DG reduces the association of Mcl-1 with Bak, in the absence of reduced Mcl-1 expression, thus liberating Bak to initiate mitochondrial outer membrane permeabilisation (Yamaguchi *et al.*, 2011). Although this second mechanism cannot be ruled out in my study, it seems unlikely as Mcl-1 is so dramatically down regulated following 2DG treatment in Z138 cells. An additional striking observation, is that Z138 cells appear to be addicted to Mcl-1, as siRNA knockdown induces substantial cell death, the lack of complete knock down of Mcl-1 following 2DG treatment is likely the reason Z138 cells are resistant to 2DG-induced cell death until 20 h (Figure 4-1). At this time point, the reduced ATP levels, oxidative phosphorylation and abolished glycolysis described by Robinson *et al.*, 2012 likely synergise with the reduced Mcl-1 expression levels to engage apoptosis.

4.3.2 2DG activates both AMPK and Akt

It has been previously described that 2DG can activate AMPK (Pradelli *et al.*, 2010), an effect that appears to be maintained. My study however, identifies a rapid and transient increase in AMPK- α T172 phosphorylation, which is completely ablated by 60 min (Figure 4-6), even in the presence of a sustained reduction in ATP levels (Figure 4-3). Assuming that the adenylate kinase reaction is functional in this system, it would attempt to maintain an AMP:ATP equilibrium by converting two ADP to one each of AMP and ATP (Hardie, 2013). This reaction would therefore increase the AMP:ATP ratio in the presence of the sustained reduced levels of ATP following 2DG treatment. The increased AMP should bind to the AMPK- γ regulatory sub-unit, inducing a conformational change allowing LKB1 to

phosphorylate AMPK- α T172. Considering the sustained reduction in ATP levels, it is therefore striking that the phosphorylation of AMPK- α T172 is only transient.

Additionally, transient activation of AMPK appears to be sufficient to maintain partial inhibition of protein synthesis (Figure 4-8). Inhibition of protein synthesis, specifically by de-phosphorylation and inactivation of p70S6K induces a feed-back loop that activates Akt through the IRS-1/PI3K signalling axis (reviewed in Martelli *et al.*, 2010). It is however, unlikely that this feed-back loop is responsible for the Akt survival signal, as the insulin receptor tyrosine kinase inhibitor HNMPA-(AM)3 does not prevent 2DG-mediated induction of Akt signalling (Appendix 7-5A), which is in agreement with other reports that Akt activation by 2DG is independent of AMPK signalling (Zhong *et al.*, 2008). The reduction in expression of Mcl-1 appears to be independent of GSK-3 β signalling, which is activated following the initial 2DG-mediated inhibition of Akt. In-fact, GSK-3 β inhibition results in a decrease in total Mcl-1 protein expression, which is contrary to previously published reports (Ding *et al.*, 2007). There is a bi-phasic relationship between AMPK and Akt signalling, whereby either one or the other is activated, but not both together following 2DG treatment, which is not surprising as they induce opposing effects on catabolic and anabolic pathways. It is interesting though that Akt activation appeared to be insufficient to re-activate protein synthesis after the initial inhibitory signal generated through AMPK.

It is puzzling that the panel of activators used in Figure 4-9 to stimulate an AMPK activation response did not produce the results expected. It is even more striking that four of six compounds (phenformin, AICAR, thapsigargin and A23187) actually induced a de-phosphorylation of AMPK- α T172. It is possible that endogenous AMPK activity is stimulated maximally by CaMKK- β , which is why no further phosphorylation is observed following thapsigargin and A23187. It may also be that the compounds are so extremely cytotoxic, that Z138 cells are dying much more rapidly than the time points assessed, which may explain the rapid de-phosphorylation. As four of the six activators induce AMPK activation through LKB1, and Z138 cells did not respond, it agrees with the argument in 4.3.1, whereby a sustained reduction in ATP levels should maintain AMPK activation, but it did not. This suggests that 2DG mediated activation of AMPK is probably independent of LKB1 signalling. Further to this, transient knockdown of LKB1 alone

did not prevent 2DG from activating AMPK (Figure 4-10). More interestingly, inhibition of CaMKK- β with STO-609 almost completely ablated basal AMPK- α T172, but did not prevent 2DG from inducing transient AMPK activation. Combining LKB1 knockdown and CaMKK- β inhibition additionally did not prevent 2DG from transiently activating AMPK. Similar results have been previously described by Jeon *et al.*, 2012, who could not identify the kinase responsible for 2DG-mediated activation of AMPK, but did implicate hexokinase as the critical factor. Z138 cells express both Hexokinase I and II (Appendix 7-5B), so knockdown/out of these proteins followed by 2DG treatment to determine if hexokinases are implicated in 2DG-induced AMPK- α T172 transient phosphorylation would be interesting.

Inhibition of AMPK with compound C alone induces cell death, additionally, it was extremely difficult to knock down the AMPK- α subunits (maximal knock down 35%, data not shown), and therefore, it appears that AMPK is critically required for the survival of Z138 cells. AMPK therefore acts as a two edge sword – activation can sensitise cells to apoptosis, but ablation of function/expression is lethal, and is therefore both a survival signal and a death signal depending on the context. To more definitively conclude the necessity of AMPK on Z138 cell survival, complete genetic ablation of AMPK would be required. This is because compound C is the only AMPK inhibitor and unfortunately is very unspecific (Bain *et al.*, 2007), cell death may therefore have been a result of inhibition of other key kinases. A summary of the key findings are depicted in Figure 4.11.

In summary, my study shows that the biological effects of 2DG on cell death, metabolism and cell signalling are far more rapid and complex than has been previously examined. The major contributing protein to 2DG's sensitisation to cell death is the anti-apoptotic protein Mcl-1 and reduction of expression of Mcl-1 is controlled translationally by AMPK. However the mechanism that 2DG induces to activate AMPK transiently in Z138 cells remains unknown. My results suggest that it is highly unlikely to be either LKB1 or CaMKK- β , however as previously stated, LKB1 is not rate limiting for AMPK activation, and the 60% knockdown achieved in my studies may not have been sufficient to completely ablate its kinase activity. Conversely, AMPK activators that function through LKB1 do not result in AMPK- α T172 phosphorylation in Z138 cells, suggesting an LKB1 independent role. Activating AMPK pharmacologically to reduce Mcl-1 and sensitise cancers to

therapeutics is an active area of cancer research. If alternative mechanisms of AMPK activation exist, which this study suggests is a probability; then characterising them could be of clinical significance. Additionally, because 2DG can activate AMPK by LKB1 and CaMKK- β in certain cell lines/types, identifying a third route of activation would make 2DG a powerful, well-tolerated clinical agent to sensitise a wide range of tumours to cell death. An example being the ongoing studies in our laboratory that have successfully sensitised notoriously resistant primary mesothelioma cells (patient derived cells and *ex plants*) to cell death by combinatorial treatment with 2DG.

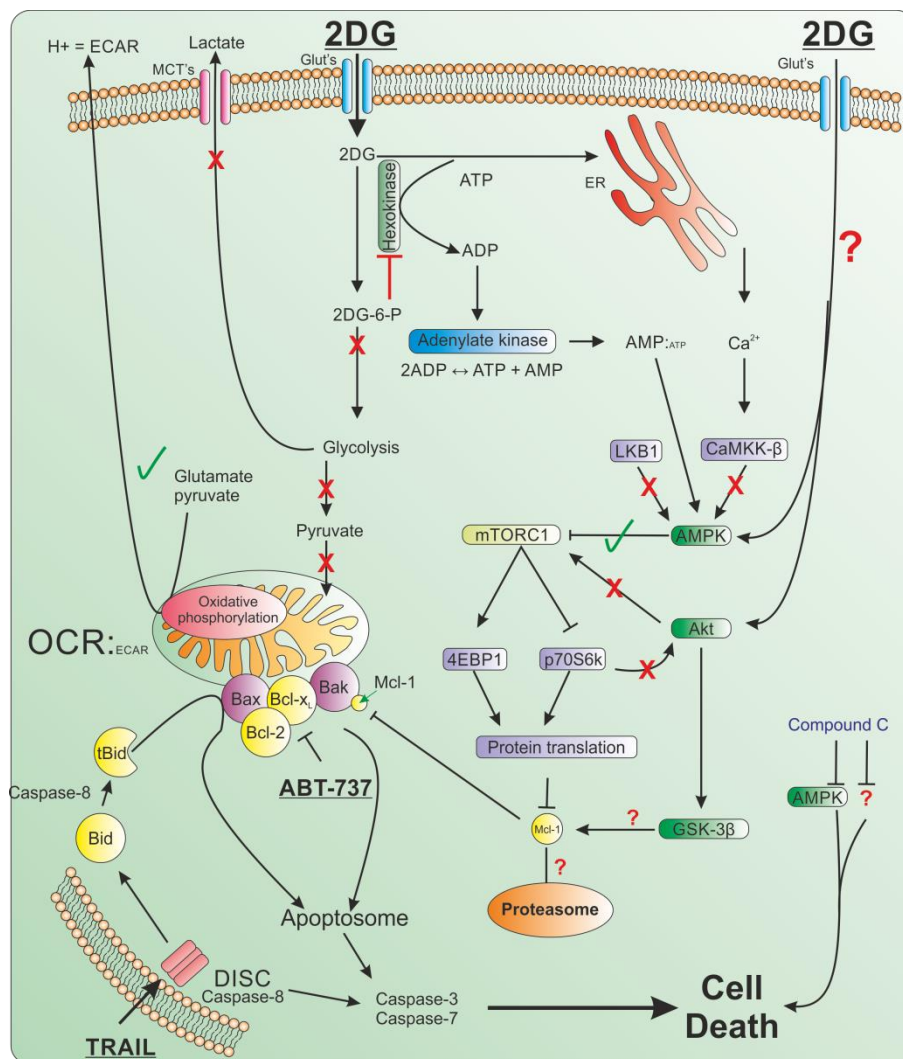


Figure 4-11 Model of the identified results following 2DG treatment. 2DG resulted in metabolic reprogramming which resulted in the transient phosphorylation and activation of AMPK independently of LKB1 and CaMKK- β , which resulted in the inhibition of protein translation and a reduction in Mcl-1. 2DG-induced Akt activity was insufficient to reactivate protein synthesis, and the initial Akt de-activation activated GSK-3 β , although this appeared to not regulate Mcl-1 expression. Z138 cells critically rely on AMPK for survival, inhibition with compound C induced cell death. The reduction in Mcl-1 was the major determinant of sensitivity to both TRAIL and ABT-737-induced cell killing

Chapter 5

5. Results Chapter 3

Galactose grown cells as an *in vitro* model for investigating drug-induced mitochondrial toxicity

5.1 Introduction

Cancer cells preferentially utilise aerobic glycolysis instead of the energetically favourable oxidative phosphorylation pathway (Warburg, 1956), resulting in increased rates of glycolysis and carbon-flux into the pentose-phosphate-pathway (PPP), enhancing production of macro-molecular precursors and facilitating hypertrophy and hyperplasia (Jiang *et al.*, 2014; Patra & Hay, 2014). As a result of this diminished reliance on mitochondrial oxidative phosphorylation, agents/treatments which target glycolysis can have profound effects on cell survival. The realisation that metabolic status can modulate the cell response to chemicals can also have important consequences for predicting adverse toxicity, particularly in respect to unexpected drug-induced mitochondrial dysfunction.

Drug-induced mitochondrial toxicity tends to be directed against highly energetic and mitochondria rich organs (such as the heart, liver, kidneys), and has been implicated as a major factor in adverse drug reactions and subsequent withdrawal of drugs from the market, for example troglitazone and cerivastatin were withdrawn in 1997 and 2001 respectively (Will & Dykens, 2014). Mitochondria rich organs require high rates of blood flow and thus are exposed to high levels of circulating xenobiotics and so are more susceptible to mitochondrial toxins, which has resulted in the need for high through put *in vitro* predictive models to identify potential drugs that induce mitochondrial dysfunction at an early stage in development

Glucose^{-ve} Z138 cells have a completely ablated glycolytic pathway and up-regulated oxidative phosphorylation to compensate, while glycolysis is also ablated in 2DG treated cells. The conversion of 2DG to 2DG-6-P is an energy consuming process, and this results in different sensitisation effect to TRAIL and ABT-737 induced cell killing (Robinson *et al.*, 2012). An additional way to study the effects of altered cancer cell metabolism on cell killing is by maintaining cells in glucose-free media, supplemented with galactose, which switches the cells to rely on oxidative phosphorylation. In this model galactose is still metabolised through glycolysis and intermediates are still fed into the PPP, but at the expense of 2 Pi (1 Pi and 1 UTP; see chapter 1.6), in addition to the ATP used in glycolysis, so a net gain of energy can only be generated from mitochondrial oxidative phosphorylation. Moreover, GLUT's have a much lower affinity for galactose than glucose and so it is imported

into the cell at a much slower rate (Wagner *et al.*, 1991); once in the cell, galactose is metabolised 8 fold slower than glucose by the rate limiting galactokinase (Kase *et al.*, 2013). Cells that are dependent on oxidative phosphorylation are more susceptible to drug-induced mitochondrial toxicity (Marroquin *et al.*, 2007; Rana *et al.*, 2011) and may potentially provide a useful high through put model to investigate drug-induced mitochondrial liabilities at an early stage in development.

I have investigated this interplay between cell death and metabolism using a mantle cell lymphoma derived cell line, Z138, with the aim of investigating what the effects of galactose metabolism are on TRAIL and ABT-737-induced cell death, additionally how this model affects cell death following treatment with classical mitochondrial poisons. To investigate this, cell metabolism was switched so that cells relied on mitochondrial oxidative. Firstly, the metabolic profile of Z138 cells grown on galactose media was assessed using a Seahorse XF24 and analysed in detail to demonstrate successful metabolic reprogramming. Then, Z138 cells were treated with classical inhibitors of the mitochondrial oxidative phosphorylation system (namely oligomycin, rotenone and antimycin), in the presence or absence of cell death inhibitors. Cell death was then analysed by Annexin-V/PI FACS analysis to determine the degree and mode of cell death, which showed that classical mitochondrial poisons resulted in necrosis in galactose^{+ve} cells. Cells were then treated with metformin and phenformin, complex I inhibitors, metformin was not toxic in Z138 cells, but phenformin, a more potent inhibitor of the respiratory chain (Wheaton *et al.*, 2014), recapitulated the necrotic response observed with canonical inhibitors. The effect of culturing cells in galactose on TRAIL and ABT-737-induced cell killing was also evaluated, which showed that metabolic reprogramming decreased the sensitivity to both, however, ABT-737 induced necrosis in the presence of zVAD.fmk in galactose^{+ve} cells. Dose response curves for rotenone and antimycin were generated using the Seahorse XF24 which showed that sensitivity to respiratory chain inhibition was decreased following metabolic reprogramming.

I next investigated if the observed differences in cell death between glucose^{+ve} and galactose^{+ve} cells, following treatment with the drugs and mitochondrial poisons could be explained by analysing the mitochondrial proteome from glucose^{+ve} and galactose^{+ve} cells. Additionally, because drug-induced mitochondrial dysfunction

can present as more than direct inhibition of the oxidative phosphorylation system, such as changes in protein expression or the increase in certain species of ROS for example, immunopurified mitochondria from glucose^{+ve} and galactose^{+ve} cultured cells were analysed by label-free quantitative mass spectrometry. The aim was to investigate if mass spectrometry coupled to bioinformatics programs could identify proteomic changes at the level of the mitochondrial proteome and to use pathway mapping software to predict any changes in cellular homeostasis as a result of the metabolic switch from the mitochondrial proteome data. These results identified that the majority of the proteins involved in the respiratory chain were up-regulated in galactose^{+ve} cells, which potentially explains the decreased sensitivity to rotenone and antimycin-induced respiratory chain inhibition. Moreover, pathway and network mapping in Ingenuity successfully predicted the inhibition of Bak, Bax, and protein synthesis and the activation of Akt survival signalling.

5.2 Results

5.2.1 Galactose^{+ve} Z138 cells undergo metabolic reprogramming

Work previously described in our laboratory (Robinson *et al.*, 2012 and Chapter 4) has shown that inhibiting glycolysis by chronic glucose deprivation or treatment with the anti-glycolytic 2DG can have opposing effects on both cellular metabolism and sensitivity to cell death. An alternative means of reprogramming cells to rely on oxidative phosphorylation *in vitro* is to culture them in glucose free media, supplemented with galactose, whereby they have a fully functional glycolytic capacity but generate a net of 0 ATP from glycolysis (see Chapter 1.6); therefore, all energy is produced by the mitochondria. I investigated the effects of galactose based media on cellular metabolism using a Seahorse XF24 extra cellular flux analyser. The metabolic profile of Z138 cells cultured in galactose medium was assessed after culturing the cells in glucose free media, supplemented with 11.1 mM D-galactose, 1 mM sodium pyruvate, 2 mM glutamax and 10% FCS for at least 7 days before experimentation. Glucose^{+ve} and galactose^{+ve} cells were seeded at 4.5×10^5 cells/well in Seahorse culture plates and OCR and ECAR was evaluated to generate the metabolic parameters as detailed in Figure 3-6. Z138 glucose^{+ve} cells had a basal oxidative phosphorylation of 313 ± 16 pmol/min/ 10^6 cells, which was up-regulated by 69% in galactose^{+ve}

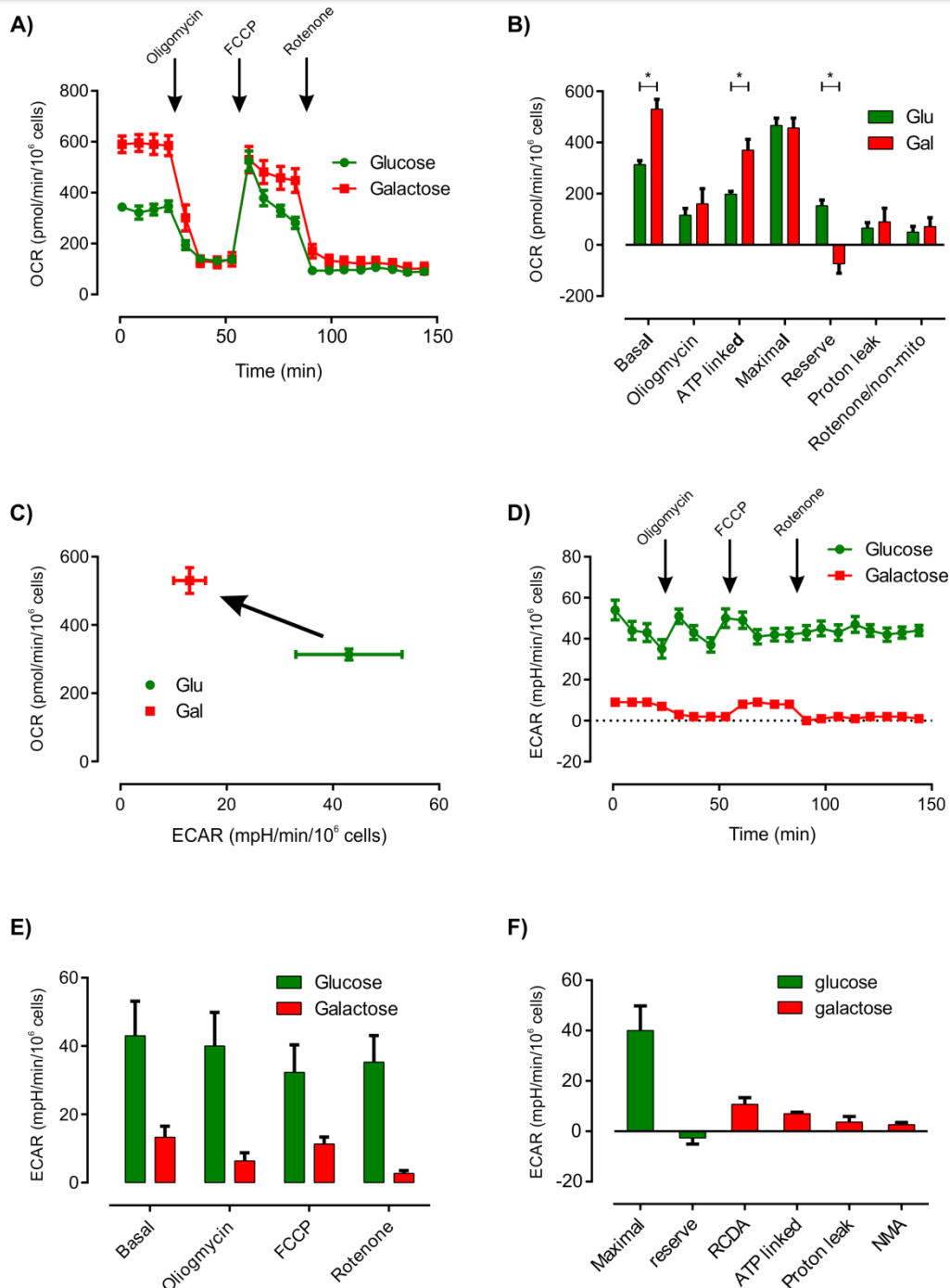


Figure 5-1 Culturing Z138 cells in galactose induces metabolic reprogramming. Z138 cells were cultured in 11.1 mM glucose (green symbols) or 11.1 mM galactose (red symbols) supplemented with, 1 mM sodium pyruvate, 2 mM glutamax and 10% FCS and then oxidative phosphorylation and glycolysis were analysed as described in Chapter 3. Cells were seeded at 4.5×10^5 cells/well and the indicated inhibitors added sequentially as shown in panel A. **A)** The OCR of glucose^{+ve} (●) and galactose^{+ve} (■) cells are shown as green and red symbol respectively, following a mitochondrial stress test. **B)** Various bioenergetics parameters were calculated (see Figure 3-6) to show basal, ATP linked, maximal, RRC, proton leak and non-mitochondrial OCR values. **C)** Basal OCR and ECAR values were plotted against each other to show metabolic reprogramming of galactose^{+ve} cells. **D)** The ECAR trace of glucose^{+ve} and galactose^{+ve} cells after sequential injection of mitochondrial inhibitors **E)** were plotted as a bar chart to show the average rates. **F)** ECAR values generated by glycolysis and the mitochondrial electron transport chain were calculated (see Figure 3-6). Data representative of 3 independent experiments, error bars represent mean \pm SEM. Error bars are \pm SEM. Star (*) represents $p < 0.05$ (Students t test)

cells to 530 ± 38 pmol/min/ 10^6 cells. These results indicated that metabolic reprogramming or switching to an oxidative metabolism was induced by culturing the cells in galactose (Figure 5-1A and B). The ATP synthase inhibitor oligomycin reduced the respiration in glucose^{+ve} and galactose^{+ve} cells, to 115 ± 27 versus 161 ± 59 pmol/min/ 10^6 cells, respectively. ATP linked OCR was not completely ablated after the first reading taken by the Seahorse, however by the second reading (14 min) oligomycin reduced the OCR to the same extent in both glucose^{+ve} and galactose^{+ve} cells. These results showed that the up-regulated basal oxidative phosphorylation in galactose^{+ve} cells was entirely linked to ATP synthesis, which was 70% higher in galactose^{+ve} cells (370 ± 42 pmol/min/ 10^6) compared to glucose^{+ve} cells (198 ± 11 pmol/min/ 10^6 cells) (Figure 5-1B)

After oligomycin, FCCP was added to uncouple the ATP synthase from the respiratory chain to determine the cells maximal respiration rate. FCCP stimulated respiration was calculated by averaging the first data point generated from each individual experiment. There was no difference in the maximal respiration rate between galactose^{+ve} and glucose^{+ve} cells (457 ± 39 versus 466 ± 29 pmol/min/ 10^6 cells respectively) (Figure 5-1B). Subtracting the maximal respiration from the basal respiration is a measure of the RRC (see Figure 3-6). Glucose^{+ve} cells had an RRC of 153 ± 22 pmol/min/ 10^6 cells, which meant that under conditions of energetic stress the cells could up-regulate oxidative phosphorylation. In contrast, galactose^{+ve} cells had an RRC of -74 ± 37 pmol/min/ 10^6 cells, these results showed they were respiring maximally, similar to state-3 respiration (Chance & Williams, 1955). Interestingly, galactose^{+ve} cells sustained FCCP stimulated respiration (Figure 5-1A), similar to the results observed in Chapters 3 and 4, where inhibition of glycolysis by glucose deprivation or 2DG, respectively, sustained uncoupler stimulated respiration

Following FCCP, the NADH dehydrogenase (complex I) inhibitor rotenone (1 μ M) was added to block the respiratory chain at the most upstream component. Any remaining OCR after rotenone inhibition is due to non-mitochondrial oxygen consumption or from succinate metabolised at complex II, which was 41% higher in galactose^{+ve} cells (71 ± 35 pmol/min/ 10^6 cells) compared to glucose^{+ve} cells (50 ± 23 pmol/min/ 10^6 cells), however this difference was not statistically significant ($p = 0.634$, t-test). The difference in respiratory chain inhibition between oligomycin and

rotenone is due to the mitochondrial proton leak, which was similar between galactose^{+ve} and glucose^{+ve} cells (89 ± 53 versus 66 ± 21 pmol/min/ 10^6 cells respectively)

Metabolic reprogramming or switching the cells to rely on mitochondrial oxidative phosphorylation is shown in Figure 5-1C. Representative ECAR traces generated from a standard mitochondrial stress test in glucose^{+ve} and galactose^{+ve} cells are shown in Figure 5-1D. Galactose^{+ve} cells had a basal ECAR of 14 ± 3 mpH/min/ 10^6 cells, 70% less than glucose^{+ve} cells (43 ± 10 mpH/min/ 10^6 cells). Since galactose is metabolised through the glycolysis pathway, the effects the mitochondrial inhibitors had on ECAR were analysed to determine if the basal ECAR in galactose^{+ve} cells was glycolytic acidification (lactic acid efflux) or respiratory chain driven acidification (mitochondrial H⁺ efflux). Oligomycin did not significantly affect the ECAR in glucose^{+ve} cells, which indicated that glycolysis was maximal under basal conditions (Figure 5-1F), as such there was no spare glycolytic capacity available to the cells (-3 ± 2 mpH/min/ 10^6 cells)

In galactose^{+ve} cells, the basal ECAR was 14 ± 3 mpH/min/ 10^6 cells, which was reduced to 6 ± 2 mpH/min/ 10^6 cells following oligomycin (Figure 5-1D and E), which showed that 7 ± 0.5 mpH/min/ 10^6 cells was derived from ATP linked mitochondrial oxidative phosphorylation. FCCP increased the ECAR to 11 ± 2 mpH/min/ 10^6 cells in galactose^{+ve} cells, which was attributable to respiratory chain derived proton extrusion from uncoupler stimulated respiration. Rotenone reduced the ECAR to 3 ± 0.8 mpH/min/ 10^6 cells, which showed that 4 ± 2 mpH/min/ 10^6 cells may have been derived from the mitochondrial proton leak (Figure 5-1F). Thus, in Z138 cells grown in galactose, 11 ± 3 mpH/min/ 10^6 cells was from respiratory chain driven acidification generated from ATP synthase derived proton extrusion and respiratory chain proton generation. The remaining 3 ± 0.8 mpH/min/ 10^6 cells was a combination of non-mitochondrial acidification and possibly glycolytically generated lactic acid. These results showed that the metabolised galactose was probably being converted to pyruvate and diverted into the TCA cycle to up-regulate and sustain mitochondrial oxidative phosphorylation, and not converted to lactic acid and expelled from the cell.

5.2.2 Oligomycin may induce non-canonical programmed cell death in galactose^{+ve} cells

It has been previously shown that cells cultured on a galactose based medium are more susceptible to drug-induced mitochondrial toxicities in hepatocellular carcinoma HepG2, H9c2 cardiac and L6 skeletal muscle cells (Marroquin *et al.*, 2007; Dykens *et al.*, 2008; Rana *et al.*, 2011; Dott *et al.*, 2014). However this has not been tested in a hematopoietic cell line before. Therefore, glucose^{+ve} and galactose^{+ve} Z138 cells were pre-treated with or without different combinations of the caspase inhibitor zVAD.fmk (50 μ M) and the RIPK1 inhibitor Nec-1 (50 μ M) for 60 min, and then treated with a range of oligomycin (ATP synthase inhibitor) concentrations (0 – 1000 nM) for 16 h, and cell death assessed using Annexin-V/PI FACS analysis. FACS dot plots from glucose^{+ve} cells treated with 1000 nM oligomycin in the presence or absence of different cell death inhibitors are shown in Figure 5-2A. Oligomycin did not induce any total cell death (PS+/PI- and PS+/PI+, herein referred to as PS+) at any oligomycin concentration (Figure 5-2C).

Conversely, galactose^{+ve} cells underwent ~60% total cell death at the lowest oligomycin concentration (31.25 nM). The degree of cell death did not increase above ~60% at any of the higher oligomycin concentrations (Figure 5-2C). The cell death phenotype appeared to be apoptotic, as ~50% of the cells underwent phosphatidyl serine externalisation while maintaining plasma membrane integrity i.e. PS+/PI- (top left quadrant, Figure 5-2B and D). Interestingly however, inhibition of caspases with zVAD.fmk alone or in combination with Nec-1 did not prevent cell death, and the phenotype remained 'apoptotic' (PS+/PI-). It was therefore unlikely that cell death following oligomycin was canonical caspase-dependent apoptosis, or necrosis (PS+/PI+). It appeared therefore, that oligomycin-induced cell death in galactose^{+ve} cells may be a form of programmed cell death, independent of both caspases and RIPK1 signalling.

5.2.3 Rotenone induces necrosis in galactose^{+ve} cells

The results from 5.2.2 showed that galactose^{+ve} cells were susceptible to oligomycin-induced cell death, and that the cell death phenotype was caspase-independent, and potentially a non-canonical form of programmed cell death. I next investigated whether this phenomenon occurred in the presence of another

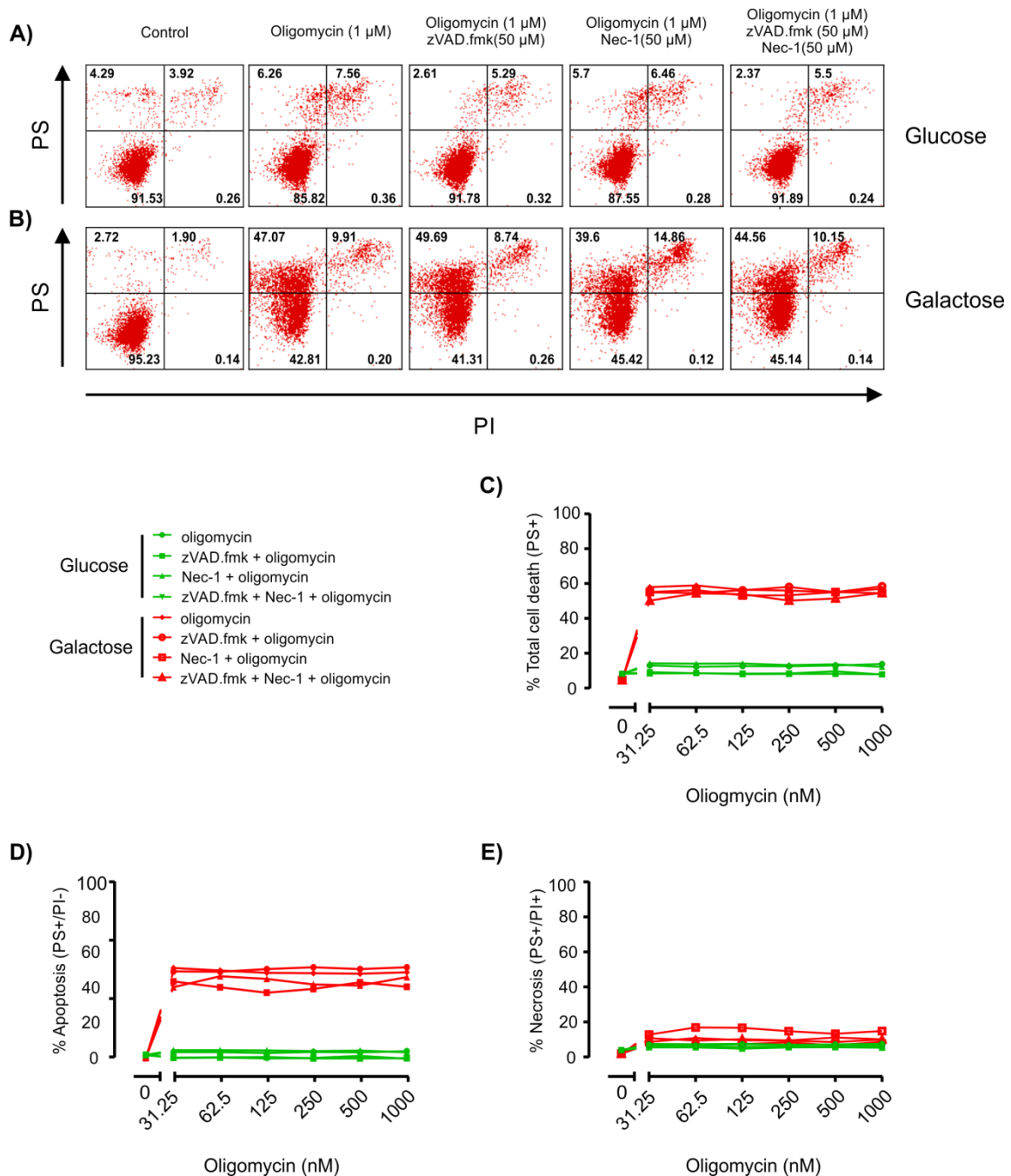


Figure 5-2 Galactose⁺ cells are sensitive to oligomycin-induced cell death. Galactose⁺ and glucose⁺ Z138 cells were pre-treated with 50 μ M zVAD.fmk and 50 μ M Nec-1 alone or in combination for 60 min followed by oligomycin (0 – 1000 nM). **A)** Example FACS analysis of Annexin-V (PS+) labelling and propidium iodide (PI) fluorescence in glucose⁺ cells after treatment with oligomycin (1000 nM) following different combinations of death inhibitors shows that cells are alive in the bottom left quadrant (PS-/PI-). **B)** Galactose⁺ cells treated with oligomycin (1000 nM) underwent cell death with most of the cells detected in the apoptotic quadrant (PS+/PI-), even in the presence of zVAD.fmk and Nec-1. **C)** The total cell death (PS+/PI+ and PS+/PI+, herein referred to as PS+) was calculated and plotted as a concentration effect curve. **D)** Concentration effect curve of apoptotic cell death (PS+/PI-). **E)** Concentration effect curve of necrotic cell death (PS+/PI+). Data are a representative example from 2 independent experiments.

classical mitochondrial poison, rotenone. Therefore galactose^{+ve} and glucose^{+ve} cells (as described in 5.2.2) were pre-treated with or without different combinations of zVAD.fmk (50 μ M) Nec-1 (50 μ M) for 60 min, and then treated with a range of rotenone (NADH dehydrogenase inhibitor) concentrations (0 – 1000 nM) for 16 h, and cell death assessed using Annexin-V/PI FACS analysis. FACS dot plots from glucose^{+ve} cells treated with 1000 nM rotenone in the presence or absence of different cell death inhibitors is shown in Figure 5-3A, and shows that rotenone did not induce cell death at any of the concentrations used (Figure 5-3A and C).

Conversely, galactose^{+ve} cells showed a concentration effect response to rotenone (Figure 5-3C); total cell death increased to a maximum (~80%) at 500 nM. With increasing rotenone concentrations the cell death phenotype increased equally between the apoptotic (Figure 5-3D) and the secondary apoptotic/necrotic quadrants (Figure 5-3E). Pre-treatment with the caspase inhibitor zVAD.fmk did not significantly ablate rotenone-induced cell killing at any rotenone concentration. Additionally, pre-treatment with combinations of zVAD.fmk and Nec-1 or Nec-1 alone did not prevent rotenone-induced cell death (Figure 5-3C). Interestingly, analysis of the FACS dot plots from galactose^{+ve} cells after different pre-treatments followed by rotenone (1000 nM), showed that the mode of cell death appeared to be primarily necrosis with the dead cells detected in the necrotic quadrant, which indicated of loss of plasma membrane integrity in the absence of phosphatidyl serine exposure. Dead cells in the apoptotic quadrant were also progressing diagonally, and were also likely to be undergoing necrosis. Both oligomycin (5.2.2) and rotenone induced cell death in galactose^{+ve} cells, while glucose^{+ve} cells were resistant to these classical mitochondrial poisons, which confirmed that Z138 grown in galactose media were extremely sensitive to mitochondrial toxins.

5.2.4 Antimycin induces necrosis in galactose^{+ve} cells

It was striking that two classical inhibitors of mitochondrial oxidative phosphorylation, namely oligomycin (5.2.2) and rotenone (5.2.3) resulted in different cell death phenotypes in galactose^{+ve} cells. It appeared, therefore that inhibition of the ATP synthase complex induced a different form of cell death to that induced by inhibition of the respiratory chain. To test this, Z138 galactose^{+ve}

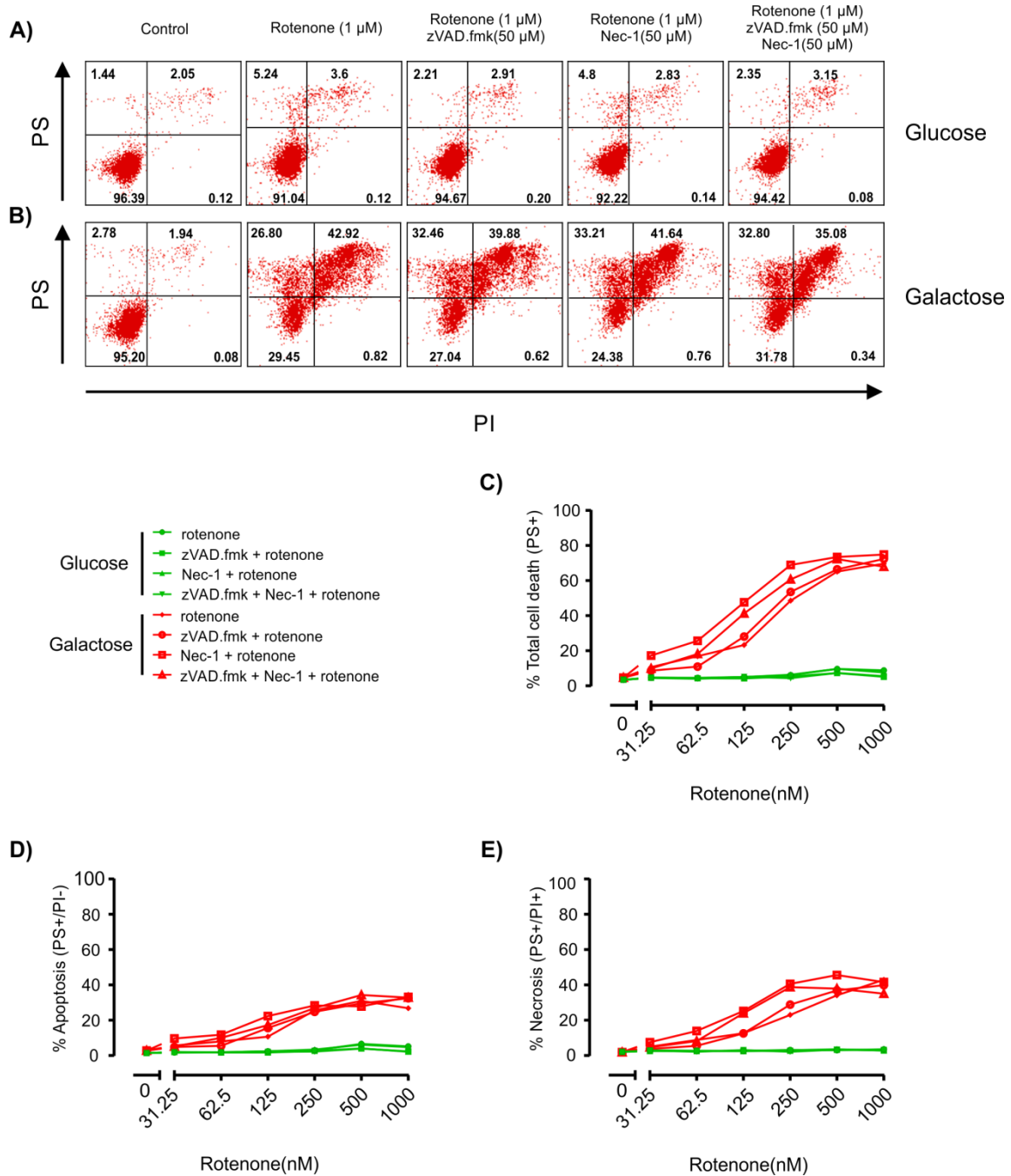


Figure 5-3 Rotenone induces necrosis in galactose^{+ve} cells. Galactose^{+ve} and glucose^{+ve} Z138 cells were pre-treated with 50 μ M zVAD.fmk and 50 μ M Nec-1 alone or in combination for 60 min followed by rotenone (0 – 1000 nM). **A)** Example FACS analysis of PS⁺ labelling and propidium iodide (PI⁺) fluorescence in glucose^{+ve} cells after treatment with rotenone (1000 nM) following different combinations of death inhibitors, alive cells were detected in the bottom left quadrant **B)** Galactose^{+ve} cells treated with rotenone (1000 nM) were detected in the apoptotic and necrotic quadrants. **C)** The total cell death was calculated and plotted as a concentration effect curve. **D)** Concentration effect curve of apoptotic cell death. **E)** Concentration effect curve of necrotic cell death. Data are a representative example from 2 independent experiments.

and glucose^{+ve} cells (as described in 5.2.2) were pre-treated with or without different combinations zVAD.fmk (50 μ M) and Nec-1 (50 μ M) for 60 min, and then treated with a range of antimycin (Q-cytochrome *c* oxidoreductase [complex III] inhibitor) concentrations (0 – 1000 nM) for 16 h, and cell death assessed using Annexin-V/PI FACS analysis. FACS dot plots from glucose^{+ve} cells treated with 1000 nM antimycin in the presence or absence of different cell death inhibitors is shown in Figure 5-4A and shows that antimycin did not induce any death following any antimycin concentrations used (Figure 5-4A and C), similar to the response observed with oligomycin and rotenone.

Conversely, galactose^{+ve} cells were sensitive to antimycin-induced cell killing, and underwent 50% total cell death at the lowest antimycin concentration (31.25 nM) which increased to ~70% total cell death by 1000 nM antimycin. The mode of cell death appeared to primarily secondary apoptosis/necrosis (Figure 5-4B and E), with only a small degree of apoptotic cell death (Figure 5-4D), which was maximal (~20%) following 1000 nM antimycin. Analysis of the FACS dot plots from galactose^{+ve} cells after different pre-treatments followed by antimycin (1000 nM), showed that the mode of cell death appeared to be primarily necrosis (Figure 5-4B). Like rotenone, antimycin-induced cell death resulted in a direct shift in dead cells to the necrotic quadrant, which was indicative of loss of plasma membrane integrity in the absence of phosphatidyl serine exposure. The results obtained with oligomycin, rotenone and antimycin showed that inhibition at different points of the oxidative phosphorylation system produced different forms of cell death.

5.2.5 Galactose^{+ve} cells are less sensitive to respiratory chain inhibition

A previously published study has shown that the skeletal muscle cell line, L6, cultured in galactose did not have altered sensitivity to antimycin-induced respiratory chain inhibition compared to glucose cultured controls, as determined by Seahorse analysis (Dott *et al.*, 2014). To investigate if this occurred in Z138 cells, glucose^{+ve} and galactose^{+ve} cells (as described in 5.2.2) were seeded at 4.5×10^5 cells/well in Seahorse culture plates and a standard mitochondrial stress test was performed (oligomycin, FCCP then rotenone or antimycin). The OCR was evaluated following a rotenone or antimycin dose response (0 to 100 nM – 2 fold serial dilutions). Glucose^{+ve} cells were extremely sensitive to rotenone at all concentrations (Figure 5-5A); the OCR was inhibited by 50% of basal levels

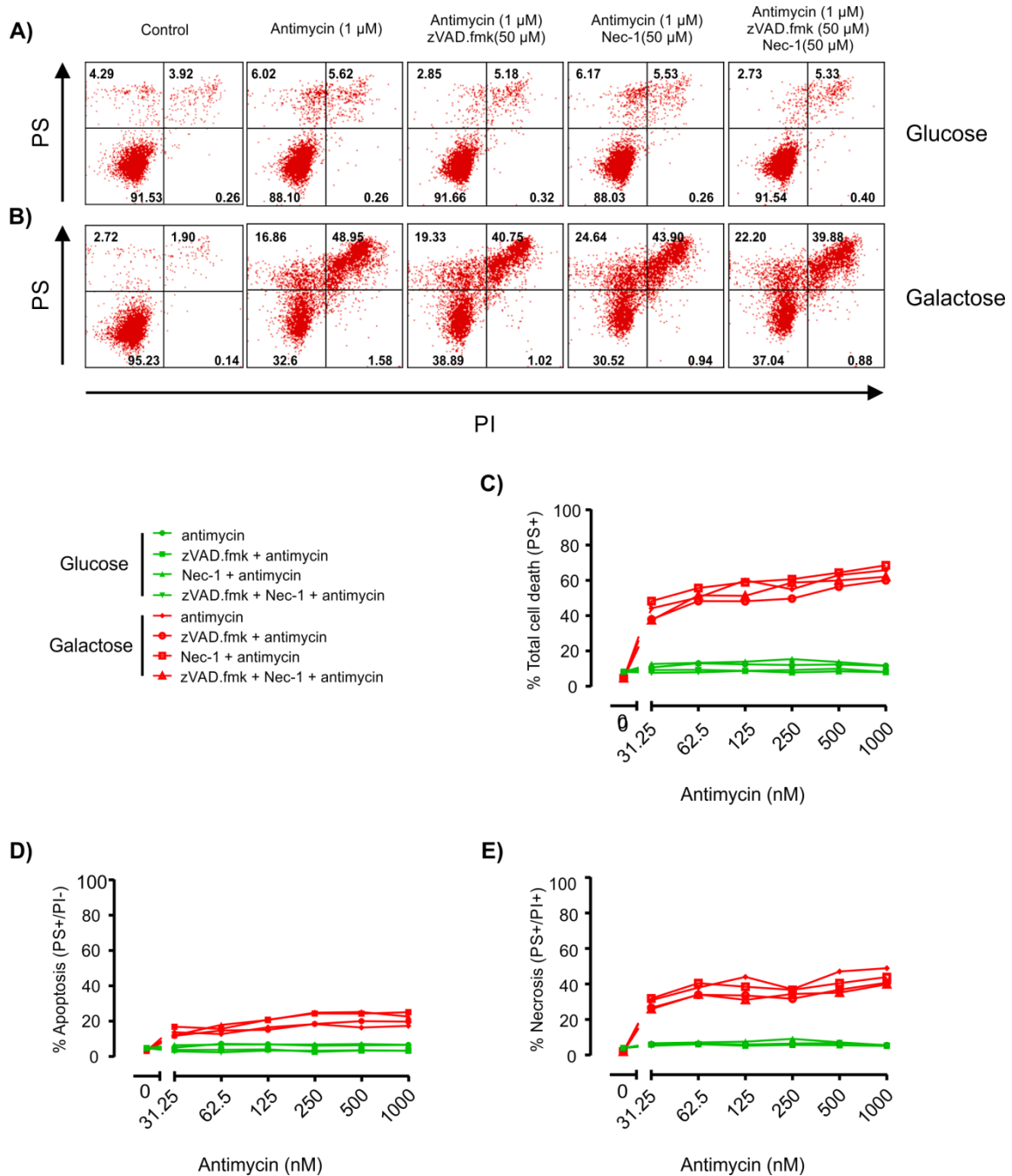


Figure 5-4 Antimycin induces necrosis in galactose⁺ cells. Galactose⁺ and glucose⁺ Z138 cells were pre-treated with 50 μ M zVAD.fmk and 50 μ M Nec-1 alone or in combination for 60 min followed by antimycin (0 – 1000 nM). **A)** Example FACS analysis of PS⁺ labelling and propidium iodide (PI⁺) fluorescence in glucose⁺ cells after treatment with antimycin (1000 nM) following different combinations of death inhibitors, alive cells were detected in the bottom left quadrant **B)** Galactose⁺ cells treated with antimycin (1000 nM) were mainly detected in the necrotic quadrant. **C)** The total cell death was calculated and plotted as a concentration effect curve. **D)** Concentration effect curve of apoptotic cell death **E)** Concentration effect curve of necrotic cell death. Data are a representative example from 2 independent experiments.

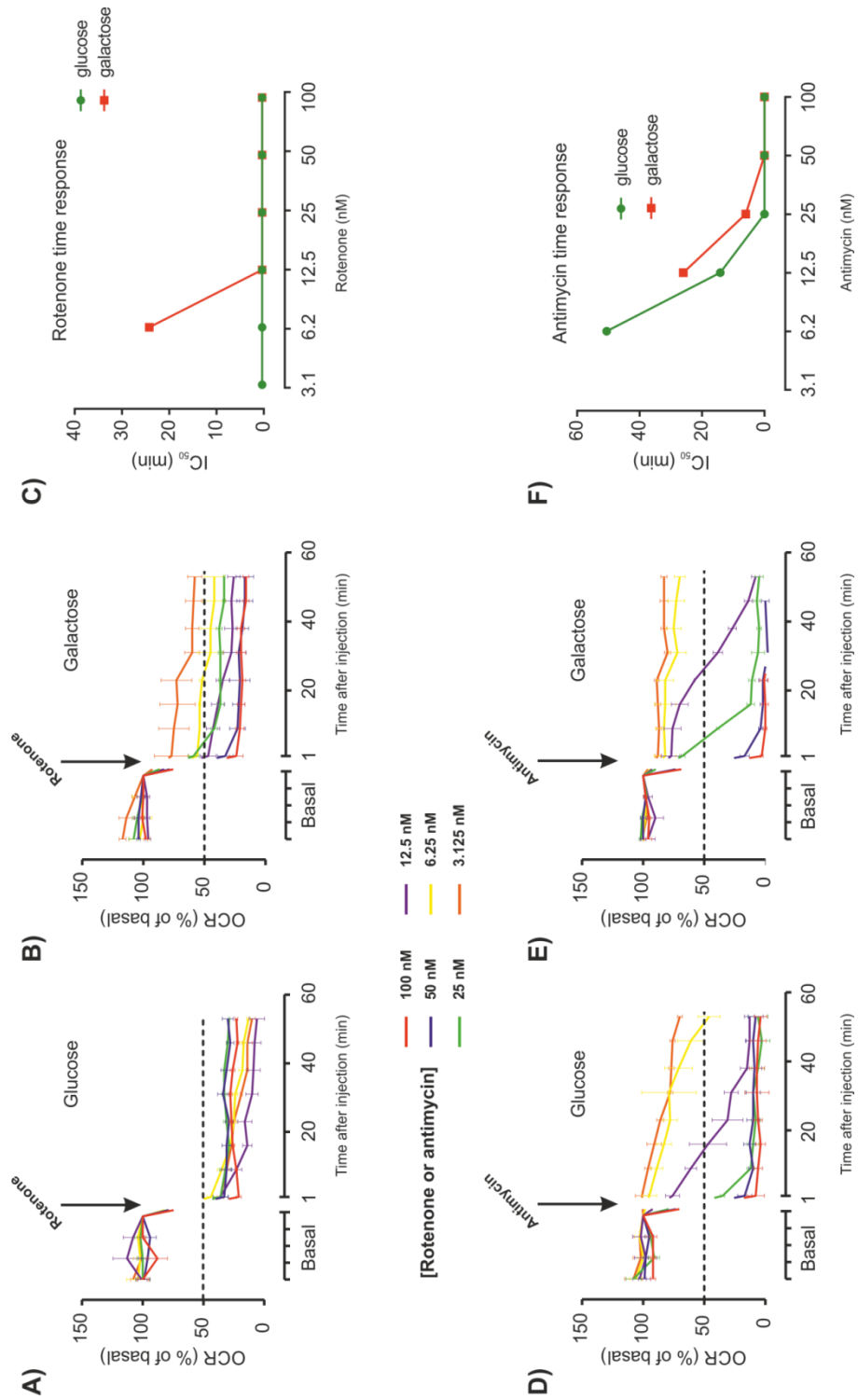


Figure 5-5 Galactose^{+ve} cells are less sensitive to respiratory chain inhibition. Z138 cells were cultured in standard glucose or galactose media (as described in Figure 5-1) then the oxidative phosphorylation and glycolysis were analysed as described in Chapter 3. Cells were seeded at 4.5×10^5 cells/well and then oligomycin, FCCP and rotenone/antimycin were added sequentially, the oligomycin and FCCP effects on OCR were removed from the graphs and only the effect of rotenone or antimycin is shown as % inhibition of basal rate. Rotenone and antimycin were injected in at a range of concentrations (3.125 – 100 nM). **A)** Glucose^{+ve} cells were sensitive to rotenone at all concentrations. **B)** Galactose^{+ve} cells were less sensitive to rotenone-induced inhibition of the respiratory chain **C)** The time (min) to reach the IC₅₀ at each rotenone concentration used, if there are no data points then the IC₅₀ was not achieved with that concentration. **D)** Concentration effect of antimycin on the OCR in glucose^{+ve} cells **E)** Concentration effect of antimycin on the OCR in galactose^{+ve} cells. **F)** The time (min) to reach the IC₅₀ at each antimycin concentration used, if there are no data points then the IC₅₀ was not achieved with that concentration. Data are a representative example from 2 independent experiments.

immediately at all concentrations (3.125 – 100 nM). Conversely, galactose^{+ve} cells were less sensitive to rotenone-induced respiratory chain inhibition; rotenone (12.5 – 100 nM) inhibited the OCR by 50% immediately (Figure 5-5B). However, rotenone (6.25 nM) inhibited the respiratory chain by 50% in 24 min (IC₅₀ min), and the lowest concentration of rotenone (3.125 nM) did not achieve 50% inhibition of the OCR even after 55 min with the inhibitor (Figure 5-5B and C). These results indicated that the up-regulated basal oxidative phosphorylation observed in galactose^{+ve} cells (5.2.1) may have been due to increased expression of complex I, because rotenone binds non-competitively to the NADH dehydrogenase ubiquinone binding site at the iron sulphur cluster in NDUFS2 (Fendel *et al.*, 2008), and therefore it is possible that increased expression of complex I was also responsible for reduced sensitivity to rotenone-induced inhibition of the respiratory chain.

In glucose^{+ve} cells, inhibition of OCR by antimycin was both time and concentration-dependent. At the higher concentrations (25 – 100 nM) antimycin produced 50% inhibition of the OCR immediately, whereas at the lower concentration (12.5 nM), 50% inhibition of the OCR was achieved within 14 min, which increased to 50 min following 6.25 nM antimycin. (Figure 5-5D and F). Galactose^{+ve} cells were less sensitive to respiratory chain inhibition by antimycin compared to glucose^{+ve} cells. Antimycin (50 -100 nM) produced 50% inhibition of OCR immediately; however lower concentrations of antimycin (25 nM) inhibited the OCR by 50% within 6 min, which increased to 26 min in the presence of 12.5 nM of antimycin. The two lowest concentrations (3.125 – 6.25 nM) of antimycin did produce 50% inhibition even after 55 min of incubation with the inhibitor (Figure 5-5 E and F). Antimycin binds specifically to the quinone reduction site in the complex III (Huang *et al.*, 2005); and therefore the decreased sensitivity to antimycin-induced inhibition of oxidative phosphorylation and the up-regulated basal OCR seen in 5.2.1, may be due to up-regulated expression the cytochrome *c* oxidoreductase complex.

5.2.6 Phenformin induces necrosis in galactose^{+ve} cells

Z138 cells cultured in galactose were extremely sensitive to the mitochondrial toxicity caused by three classic potent inhibitors of the mitochondrial oxidative phosphorylation system, namely oligomycin, rotenone and antimycin, as

determined by assessing the degree and mode of cell death with Annexin-V/PI FACS analysis. I next determined if galactose^{+ve} Z138 cells could be used to identify drug-induced mitochondrial toxicity with non-specific inhibitors of mitochondrial function. Therefore, glucose^{+ve} and galactose^{+ve} cells (as detailed in 5.2.2) were pre-treated with zVAD.fmk (50 μ M) with or without Nec-1 (50 μ M) for 60 min, followed by a range of concentrations (0 – 1000 μ M) of the biguanides metformin or phenformin. Metformin and phenformin are believed to inhibit the respiratory chain at complex I, although the mechanism is not fully understood (Wheaton *et al.*, 2014). Metformin did not induce cell death any concentration in glucose^{+ve} or galactose^{+ve} cells, irrespective of pre-treatment with the inhibitors (Appendix Figure 7-6).

Similarly, glucose^{+ve} cells treated with 1000 μ M phenformin in the presence or absence of different cell death inhibitors did not produce any cell death (Figure 5-6A and C). However, galactose^{+ve} cells were resistant to phenformin-induced cell death from 0 – 250 μ M, but from 500 – 1000 μ M, the cells exhibited a concentration effect response in the presence of phenformin (Figure 5-6B and C). Total cell death increased in a concentration-dependent manner up to a maximum of ~60% following 1000 μ M. The mode of cell death appeared to be primarily secondary apoptosis/necrosis (Figure 5-6B and E). Pre-treatment with the caspase inhibitor zVAD.fmk did not significantly ablate phenformin-induced cell killing at any concentration. Additionally, the combination of zVAD.fmk and Nec-1 did not inhibit phenformin-induced cell death (Figure 5-6C). Interestingly, analysis of the FACS dot plots from galactose^{+ve} cells after different death inhibitor pre-treatments followed by phenformin (1000 μ M), confirmed that the mode of cell death appeared to be primarily necrosis, as dead cells were detected in the upper right quadrant. This was similar to the results observed with inhibition of complex I with rotenone (5.2.3) and antimycin (5.2.4).

5.2.7 Galactose^{+ve} cells are less sensitive to TRAIL-induced cell killing, and have a limited capacity to switch to TRAIL-induced necroptosis

Using galactose cultured cells is a powerful tool to study the effect of cellular metabolism on drug-induced cancer cell death. Work previously published from our laboratory (Robinson *et al.*, 2012) and the results presented in

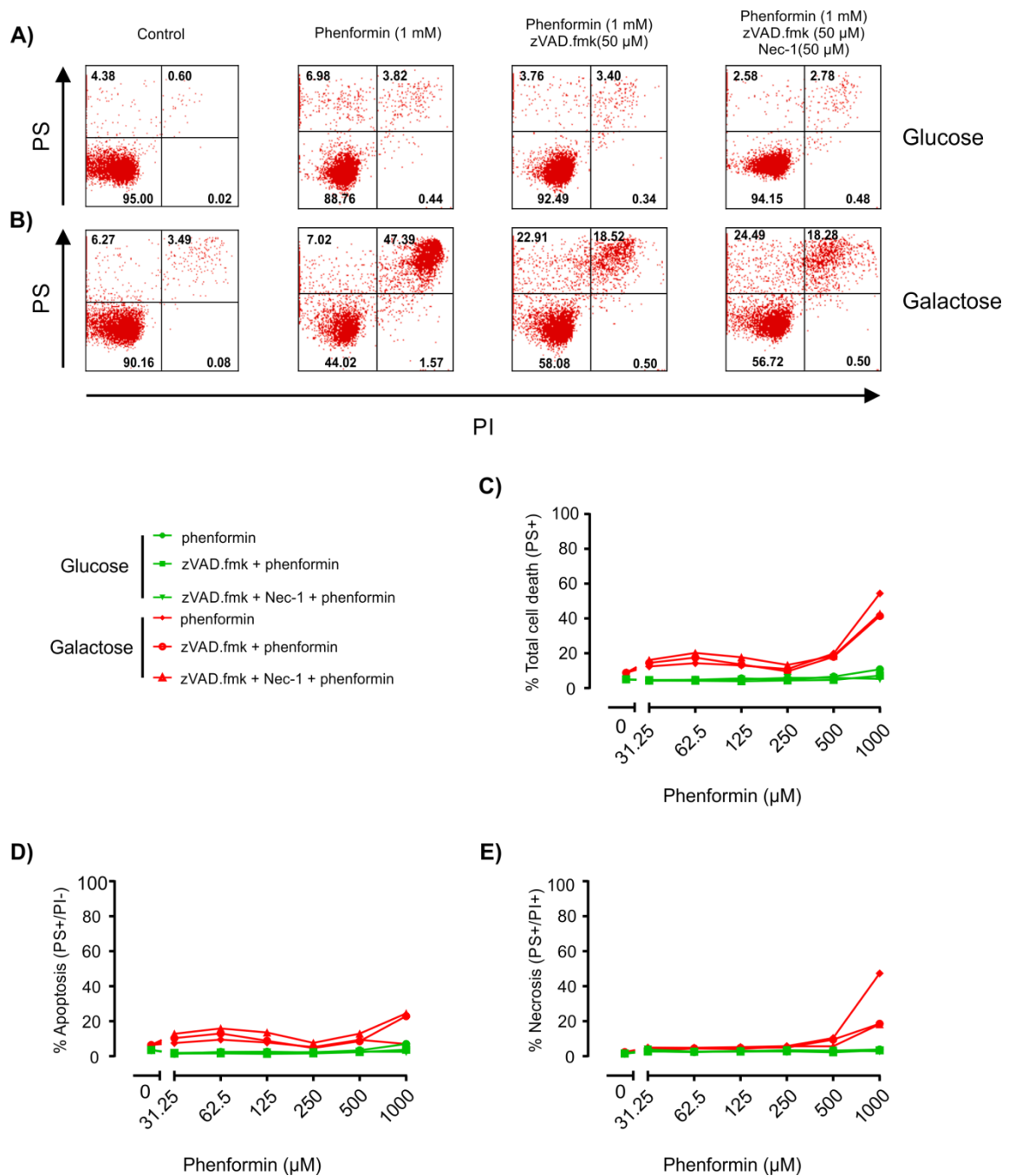


Figure 5-6 Galactose^{+ve} cells are sensitive to phenformin-induced cell death. Galactose^{+ve} and glucose^{+ve} Z138 cells were pre-treated with 50 μ M zVAD.fmk and 50 μ M Nec-1 alone or in combination for 60 min followed by phenformin (0 – 1000 μ M). **A)** Example FACS analysis of PS+ labelling and propidium iodide (PI+) fluorescence in glucose^{+ve} cells after treatment with phenformin (1000 μ M) following different combinations of death inhibitors, alive cells were detected in the bottom left quadrant **B)** Galactose^{+ve} cells treated with phenformin (1000 μ M) were mainly detected in the necrotic quadrant. **C)** The total cell death was calculated and plotted as a concentration effect curve. **D)** Concentration effect curve of apoptotic cell death **E)** Concentration effect curve of necrotic cell death Data are a representative example from 2 independent experiments.

Chapters 3 and 4 have shown that inhibition of glycolysis by chronic glucose deprivation or treatment with the anti-glycolytic 2DG can dramatically alter the cells response following TRAIL and ABT-737-induced cell death. Glucose deprivation completely ablates glycolysis with no energetic demand; conversely, 2DG ablates glycolysis at the expense of ATP (see Figure 4-3). I next investigated the effect of culturing cells in galactose on TRAIL-induced cell death, therefore glucose^{+ve} and galactose^{+ve} cells (as described in 5.2.2) were pre-treated with or without different combinations of zVAD.fmk (50 μ M) and Nec-1 (50 μ M) for 60 min, and then treated with a range of TRAIL concentrations (0 – 1000 ng/ml) for 16 h, and cell death assessed using Annexin-V/PI FACS analysis.

In glucose^{+ve} cells, TRAIL-induced cell killing was primarily apoptotic at all concentrations (Figure 5-7A, C and D). The concentration effect response on total cell death is shown in Figure 5-7C. TRAIL-induced apoptosis was maximal (100%) following 250 ng/ml. TRAIL-induced cell death was partially inhibited by the pan-caspase inhibitor zVAD.fmk (60% cell death with 1000 ng/ml), however, similar to glucose^{+ve} UPN1 cells (Chapter 3, Figure 3-3) inhibition of TRAIL-induced cell death resulted in an intermediate PS+ population of cells. Addition of zVAD.fmk in combination with Nec-1 completely ablated all TRAIL-induced cell killing. These results demonstrated that Z138 cells can switch to TRAIL-induced necroptosis, and that the intermediate PS+ population of cells was RIPK1-dependent, similar to the results obtained with UPN1^{+ve} cells in Chapter 3.

Glucose deprived Z138 cells have been shown to be less sensitive to TRAIL-induced cell death (Robinson *et al.*, 2012); galactose^{+ve} cells were also less sensitive to TRAIL-induced cell killing (Figure 5-7C). Like glucose^{+ve} cells, galactose^{+ve} cells primarily underwent apoptotic cell death (Figure 5-7B, D and E), as shown by the FACS dot plots following 1000 ng/ml TRAIL (Figure 5-7B). Pre-treatment with zVAD.fmk completely blocked TRAIL-induced cell killing at low TRAIL concentrations (31.25 – 62.5 ng/ml), however, at higher concentrations (125 – 1000 ng/ml), zVAD.fmk did not completely inhibit cell death (Figure 5-7C). Despite the incomplete block of cell death, galactose^{+ve} cells were more sensitive to zVAD.fmk-mediated inhibition of TRAIL-induced cell death (30% cell death at 1000 ng/ml). Similar to glucose^{+ve} cells, galactose^{+ve} cells pre-treated with

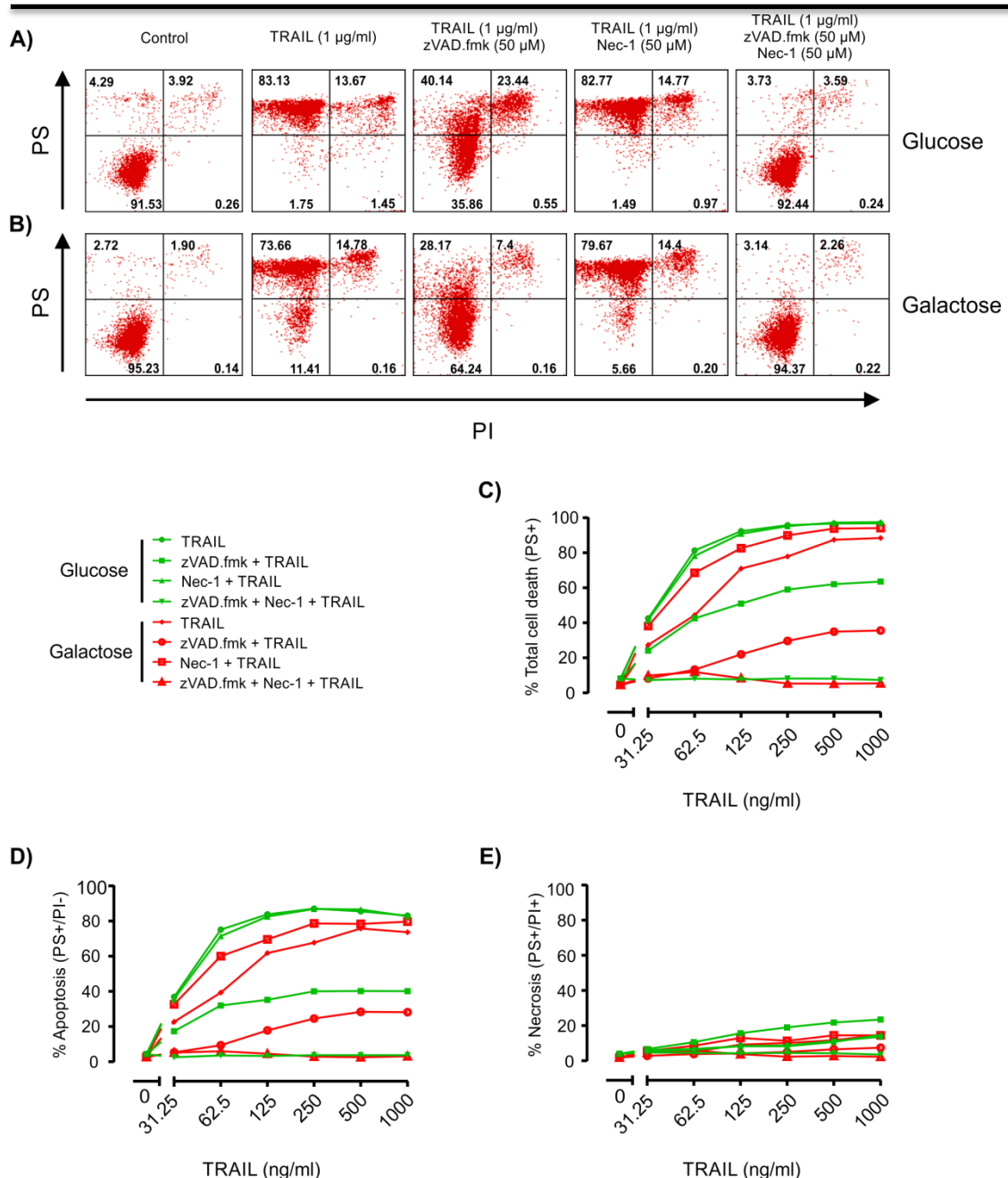


Figure 5-7 Galactose^{+ve} cells are less able to switch to TRAIL-induced necroptosis. Z138 cells cultured in standard glucose or galactose media were pre-treated with 50 µM zVAD.fmk and 50 µM Nec-1 alone or in combination for 60 min followed by increasing concentrations of TRAIL (0 – 1000 ng/ml). **A)** Example FACS analysis PS⁺ labelling and PI⁺ fluorescence in glucose^{+ve} cells after treatment with TRAIL (1000 ng/ml) following different combinations of death inhibitors shows that glucose^{+ve} cells are extremely sensitive TRAIL. TRAIL-induced cell death was partially inhibited by zVAD.fmk, and completely inhibited by both zVAD.fmk and Nec-1. **B)** Galactose^{+ve} cells treated with TRAIL (1000 ng/ml) underwent cell death which was partially inhibited by zVAD.fmk, and completely inhibited by both zVAD.fmk and Nec-1. **C)** Total cell death was calculated and plotted as a concentration effect curve and shows that galactose^{+ve} cells are less sensitive to TRAIL compared to glucose^{+ve}. **D)** Apoptotic cell death was plotted to show that most of the TRAIL-induced cell death in galactose^{+ve} and glucose^{+ve} cells was apoptotic cell death at all concentrations, and that zVAD.fmk switched to mode of cell death to necroptosis in both glucose^{+ve} and galactose^{+ve} cell. **E)** Necrotic cell death was plotted to show that TRAIL-induced cell death in glucose^{+ve} and galactose^{+ve} cells induced a typical apoptotic phenotype. Data are a representative example from 2 independent experiments.

zVAD.fmk followed by TRAIL resulted in an intermediate PS⁺ population of cells, which was completely inhibited by combinatorial pre-treatment of zVAD.fmk and Nec-1. These results showed that both glucose^{+ve} and galactose^{+ve} cells could switch to TRAIL-induced necroptosis; however, to a far lesser extent in galactose^{+ve} cells. This is in agreement with the results presented in Chapter 3, which showed that glycolysis is critically required for TRAIL-induced necroptosis. It would be interesting to determine if chronic glucose deprivation in Z138 cells can completely ablate TRAIL-induced necroptosis.

5.2.8 Galactose^{+ve} cells are less sensitive to the Bcl-2/Bcl-x_L inhibitor ABT-737.

Inhibition of glycolysis by glucose deprivation has been shown to confer resistance to ABT-737, while 2DG treatment can sensitise Z138 cells to ABT-737-induced cell death (Chapter 4 and Robinson *et al.*, 2012). ABT-737 is designed to stop Bcl-2 and Bcl-x_L from inhibiting Bak and Bax mediated apoptosis, and therefore acts directly at the mitochondria to induced intrinsic-apoptosis. As glucose deprivation and galactose cultured cells both resulted in resistance to TRAIL-induced cell killing, and glucose deprivation induced resistance to ABT-737, I next investigated if galactose^{+ve} cells were more sensitive to ABT-737. Therefore glucose^{+ve} and galactose^{+ve} cells (as described in 5.2.2) were pre-treated with or without different combinations of zVAD.fmk (50 µM) and Nec-1 (50 µM) for 60 min, followed by a range of ABT-737 concentrations (0 – 1000 nM) for 16 h, and cell death assessed using Annexin-V/PI FACS analysis.

In glucose^{+ve} cells ABT-737-induced cell death was concentration-dependent and was maximal (100%) following 500 nM ABT-737 (Figure5-8C), with dead cells primarily detected in the apoptotic quadrant (Figure5-8A and D). ABT-737-induced cell killing was completely inhibited by zVAD.fmk alone which showed that the mode of cell death was completely caspase-dependent apoptosis. The RIPK1 inhibitor had no effect on ABT-737-induced cell killing which again indicated that cell death was caspase-dependent and RIPK1-independent.

Galactose^{+ve} cells treated with ABT-737 primarily underwent apoptotic cell death (Figure 7-8E), with a small amount progressing to secondary apoptosis/necrosis at

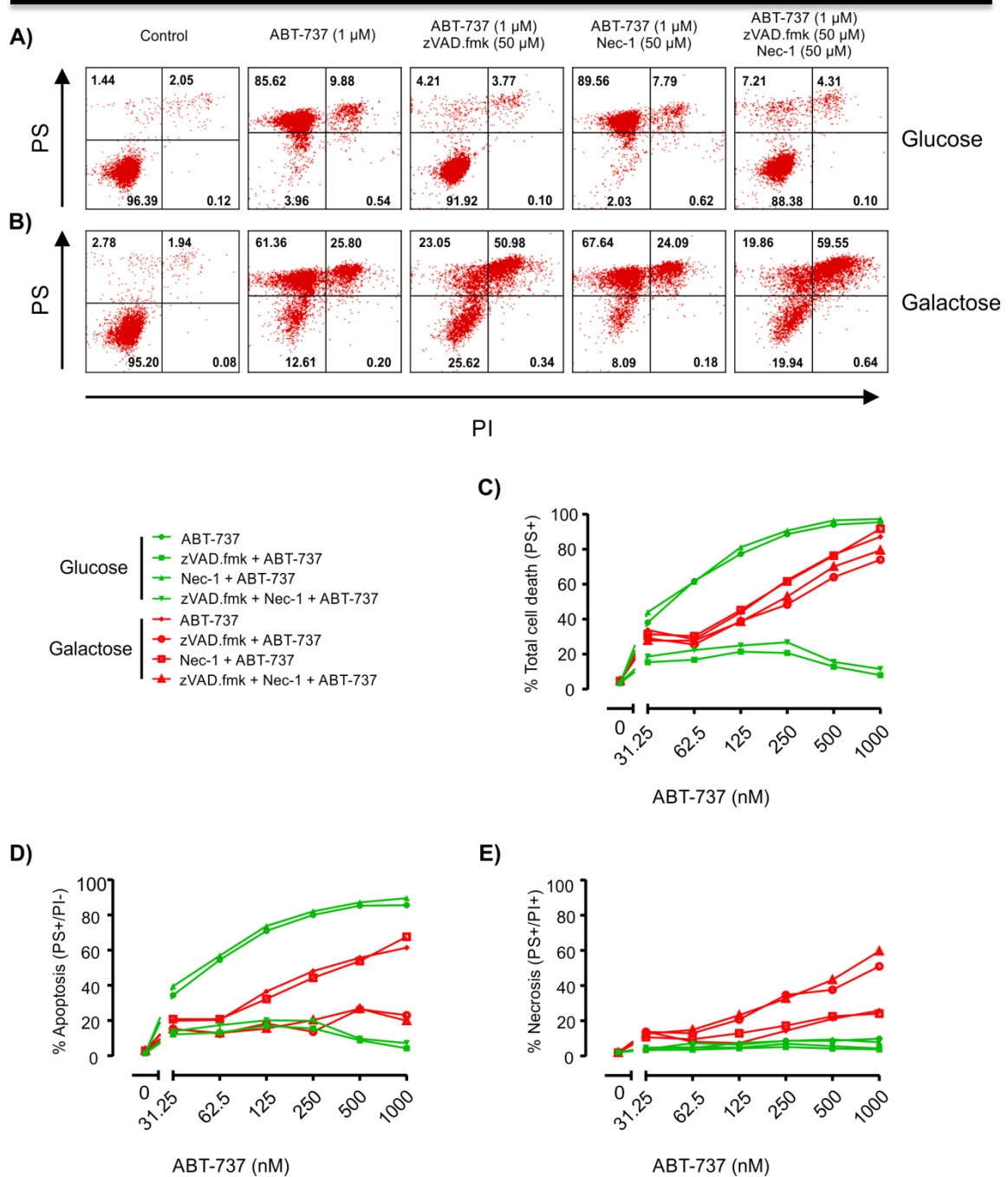


Figure 5-8 ABT-737 induces apoptosis. Z138 cells cultured in standard glucose or galactose media were pre-treated with 50 μ M zVAD.fmk and 50 μ M Nec-1 alone or in combination for 60 min followed by ABT-737 (0 – 1000 nM). **A)** FACS analysis PS+ labelling and PI+ fluorescence in glucose^{+ve} cells after ABT-737 (1000 nM) following different combinations of death inhibitors shows that glucose^{+ve} cells were extremely sensitive ABT-737 which was completely inhibited by zVAD.fmk alone **B)** Galactose^{+ve} cells treated with ABT-737 (1000 nM) underwent apoptotic cell death, which was not inhibited by zVAD.fmk alone or in combination with Nec-1, inhibition of caspase activity resulted in ABT-737-induced necrosis. **C)** Total cell death shows that galactose^{+ve} cells are less sensitive to ABT-737 compared to glucose^{+ve} **D)** Apoptotic cell death shows that all of the ABT-737-induced cell death in glucose^{+ve} cells was located in the apoptotic quadrant at all concentrations, whereas in galactose^{+ve} cells, 60% of the dead cells were located in the apoptotic quadrant, in the absence of zVAD.fmk **E)** Necrotic cell death was plotted to show that ABT-737-induced cell death in glucose^{+ve} and galactose^{+ve} cells was not necrotic and typical apoptosis, however in galactose^{+ve} cells, zVAD.fmk followed by ABT-737 resulted in a typical necrotic phenotype. Data are a representative example from 2 independent experiments.

the highest ABT-737 concentrations (250 – 1000 nM), which indicated that the mode of cell death was caspase-dependent apoptosis (Figure 7-8B, D and E).

Interestingly, total cell death (Figure 7-8C) was consistently lower in galactose^{+ve} cells compared to glucose^{+ve} cells, which showed that galactose^{+ve} cells were less sensitive to ABT-737-induced cell death. However, pre-treatment with zVAD.fmk alone or in combination with Nec-1 did not prevent galactose^{+ve} cells from undergoing cell death. Strikingly, the mode of cell death switched from apoptosis to completely necrotic, as shown in Figure 5-8B and E. Galactose^{+ve} cells probably switched to necrosis in the presence of zVAD.fmk and ABT-737 because initiation of the intrinsic apoptotic pathway by mitochondrial outer membrane permeabilisation precedes caspase-9 activation at the apoptosome, and thus the mitochondria are likely to be too damaged to maintain oxidative phosphorylation. In agreement with this hypothesis, ABT-737 at high concentrations (250 - 500 nM) completely ablates the mitochondrial respiratory chain within 10 min in glucose^{+ve} cells, low concentrations also completely inhibit the respiratory chain, an effect that is not rescued by inhibition of caspases in glucose^{+ve} cells (Appendix Figure 7-7).

5.2.9 Etoposide induces necrosis at low concentrations in galactose^{+ve} cells

Etoposide has previously been shown to induce apoptosis by inhibiting nuclear topoisomerases at low doses, while directly targeting the mitochondria at higher doses (Robertson *et al.*, 2000), and therefore may be considered an indirect mitochondrial toxin at higher doses. As classical mitochondrial inhibitors of the oxidative phosphorylation system and ABT-737 induced necrosis, I investigated if high concentrations of etoposide also induced necrosis. Glucose^{+ve} and galactose^{+ve} cells were pre-treated with or without zVAD.fmk (50 µM) and Nec-1 (50 µM) for 60 min, followed by etoposide (0 – 1000 nM) for 16 h, and cell death assessed using Annexin-V/PI FACS analysis.

Etoposide induced apoptotic cell death at all concentrations in glucose^{+ve} cells (Figure 5-9A, D and E), which were extremely sensitive to etoposide-induced killing; the lowest concentration (31.25 nM) induced 95% total cell death (Figure 5-9C). Total cell death was almost completely inhibited by zVAD.fmk (~20% cell death remaining), which showed that the mode of cell death was primarily

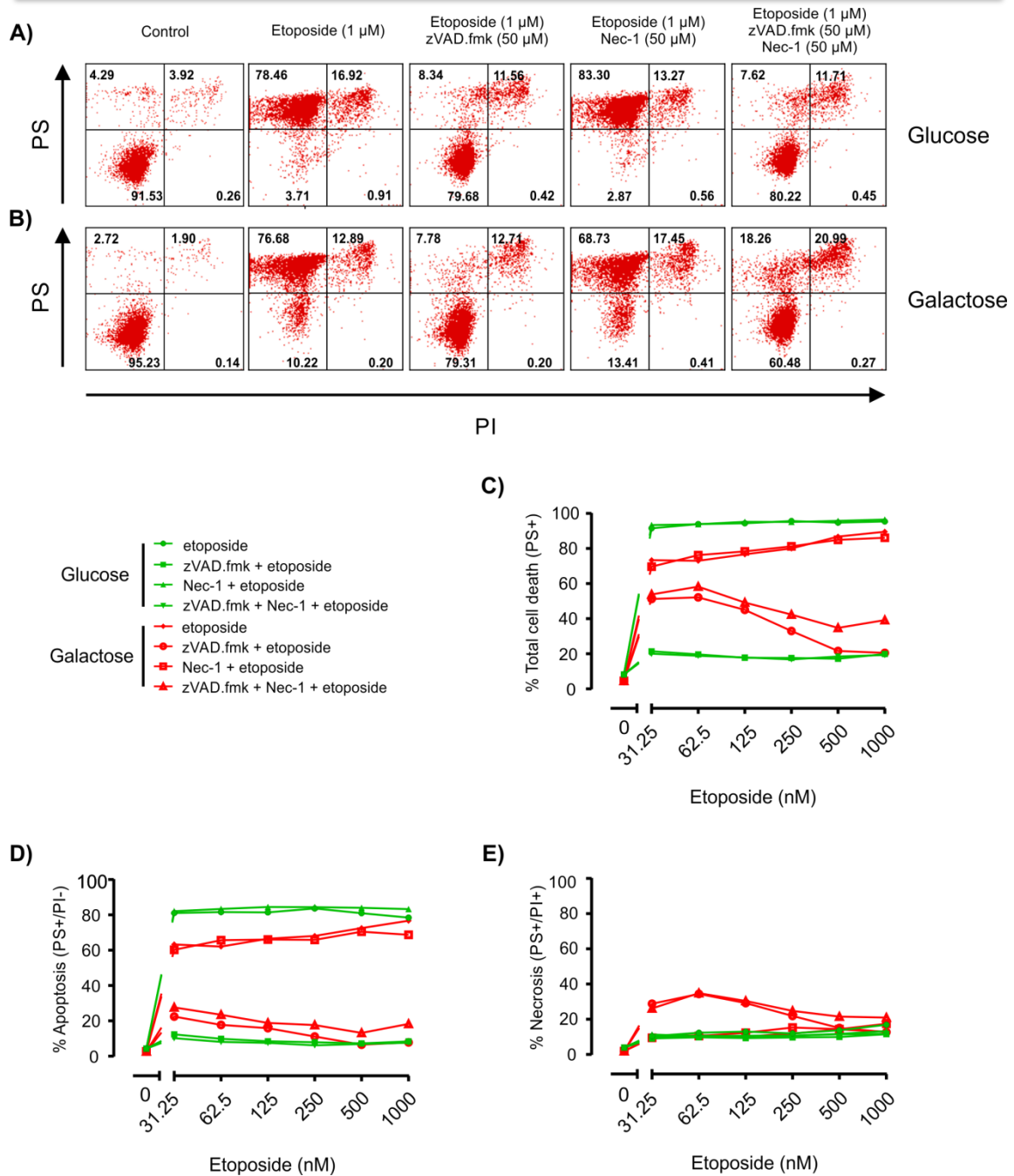


Figure 5-9 Etoposide induces necrosis at low concentrations in galactose^{+ve} cells. Z138 cells cultured in standard glucose or galactose media were pre-treated with 50 μ M zVAD.fmk and 50 μ M Nec-1 alone or in combination for 60 min followed by etoposide (0 – 1000 nM). **A)** FACS analysis of PS⁺ labelling and PI⁺ fluorescence in glucose^{+ve} cells after etoposide (1000 nM) following different combinations of death inhibitors showed that glucose^{+ve} cells were extremely sensitive etoposide, which was almost completely inhibited by zVAD.fmk. **B)** Galactose^{+ve} cells treated with etoposide (1000 nM) also underwent apoptosis, which was almost completely inhibited by zVAD.fmk. **C)** Total cell death was plotted as a concentration effect curve and shows that galactose^{+ve} cells are less sensitive to etoposide compared to glucose^{+ve}. **D)** Apoptotic cell death was plotted to show that most of the etoposide-induced cell death in galactose^{+ve} and glucose^{+ve} cells was apoptotic at all concentrations in the absence of zVAD.fmk. **E)** Necrotic cells were plotted to show that etoposide-induced cell death in galactose^{+ve} cells induced a typical necrotic phenotype at low concentrations (31.25 – 125 nM). Data are a representative example from 2 independent experiments.

caspase-dependent apoptosis. Nec-1 had no effect on etoposide-induced cell killing which indicated that cell death was primarily caspase-dependent and RIPK1-independent.

Galactose^{+ve} cells were also very sensitive to etoposide at all concentrations, however total cell death was lower compared to glucose^{+ve} cells, which showed that galactose^{+ve} cells were less sensitive to etoposide-induced cell killing (Figure 5-9C). Cell death in the absence of death inhibitors was primarily apoptotic at all concentrations (Figure 5-9D). Interestingly, in the presence of zVAD.fmk, cell death was not blocked at the lower etoposide concentrations (31.25 – 125 nM); however, increased etoposide concentrations resulted in cell death that was inhibited by zVAD.fmk (Figure 5-9C). Following low etoposide concentrations (31.25 nM) in galactose^{+ve} cells, dead cells were detected equally in the apoptotic and necrotic quadrants (Figure 5-9D and E). These results were the opposite of what was expected, and showed that in Z138 cells, low concentrations of etoposide induced necrosis in a caspase-independent and RIPK1-independent manner. Moreover, higher concentrations appear to target the cell for death through a caspase-dependent route, which was likely to be independent of the mitochondrial intrinsic pathway, as activation of MOMP, as seen with ABT-737 induces necrosis in the presence of zVAD.fmk

5.2.10 Characterisation of the mitochondrial proteome by label-free quantitative mass spectrometry

Switching Z138 cells to rely on mitochondrial oxidative phosphorylation can have profound effects on sensitivity to apoptotic stimuli and mitochondrial poisons. I next used a proteomic and bioinformatics approach to characterise the mitochondrial proteome using quantitative label-free mass spectrometry coupled to bioinformatics, with the aim of determining if changes to the mitochondrial proteome could be quantitatively detected, additionally, if these changes to cellular metabolism and altered sensitivity to apoptotic stimuli could be explained using this technique.

In collaboration with Dr Claudia Langlais, of the MRC Toxicology Unit Protein Profiling group, subcellular fraction followed by immunopurification of the mitochondria from 1×10^9 cells from glucose^{+ve}, galactose^{+ve}, glucose^{-ve} and 20h

2DG treated Z138 cells was carried out (as detailed in chapter 2.3). This was carried out 4 times to generate 4 biological repeats (n=4), which were all run as a technical duplicates on the mass spectrometers. Yeast ADH1 and BSA were spiked-in to each sample at known fmol concentrations to allow for accurate quantitation. The mass spectrometry data were then processed using TransOmics for bioinformatics to generate quantitative relative normalised abundance values. The values generated were expressed as a fold change of glucose^{+ve} controls, with an ANOVA p value. The data in this chapter only assesses the changes identified in galactose^{+ve} cells compared to glucose^{+ve} controls. The fold change data generated from TransOmics was then imported into Ingenuity™ (Qiagen) where pathway analysis and differences were analysed.

The mass spectrometry data generated 2280 quantifiable proteins, of these, 707 (31%) were known mitochondrial proteins and of the 2280 identified proteins, 555 proteins in galactose^{+ve} cells were significantly different from the glucose^{+ve} controls. This striking difference is depicted as a principal component analysis (Figure 5-10). The grey cloud represents all identified proteins, with glucose^{+ve} cells (deep blue spots) spatially separated from galactose^{+ve} cells (light blue spots) beneath. The variation in the 2nd principal component (y axis), which spatially separates the two conditions indicates there is statistically significant differences.

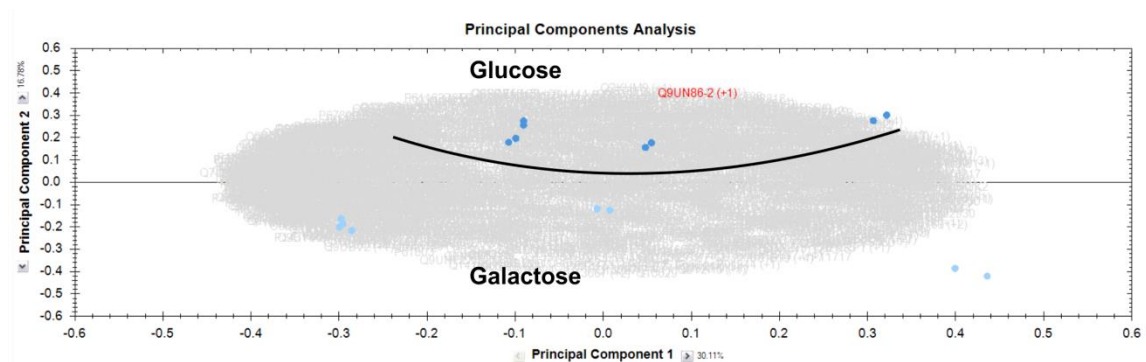


Figure 5-10 Principal component analysis from the mitochondrial proteome data. The differences observed between glucose^{+ve} and galactose^{+ve} cells is easily distinguished, with glucose^{+ve} cells (deep blue) clustered above and galactose^{+ve} cells (light blue) clustered below, separated by the black line.

Firstly, because galactose^{+ve} cells had an up-regulated basal oxidative phosphorylation (Figure 5-1) and were less sensitive to rotenone and antimycin-induced inhibition of the respiratory chain (Figure 5-5); the mass spectrometry data were used to analyse the amount of identifications and expression of the

mitochondrial oxidative phosphorylation system, the TCA cycle and the pyruvate dehydrogenase complex (129 proteins). A total of 93 proteins were identified (76%), which are depicted in Figure 5-11; the inner pie represents the total amount of proteins per complex, while the outer pie shows the amount of proteins that were identified in this study per complex (underlined number), or could not be detected by mass spectrometry (not underlined). As a large majority of the proteins that comprise the oxidative phosphorylation system were identified, Ingenuity was used to generate a schematic of the respiratory chain, which identified where these proteins were located in the ETC and ATP synthase complex; also to determine if expression was up- or down-regulated. Figure 5-12 shows all the proteins identified bordered in pink, and from those identified in the NAD dehydrogenase complex, only 4 were down-regulated, while the rest were up-regulated (red represents up-regulation, and green represents down-regulations). Importantly, the subunit that rotenone binds to (NDUFS2) was up-regulated (circled in red), which potentially explains the reduced sensitivity to rotenone-induced inhibition of the respiratory chain.

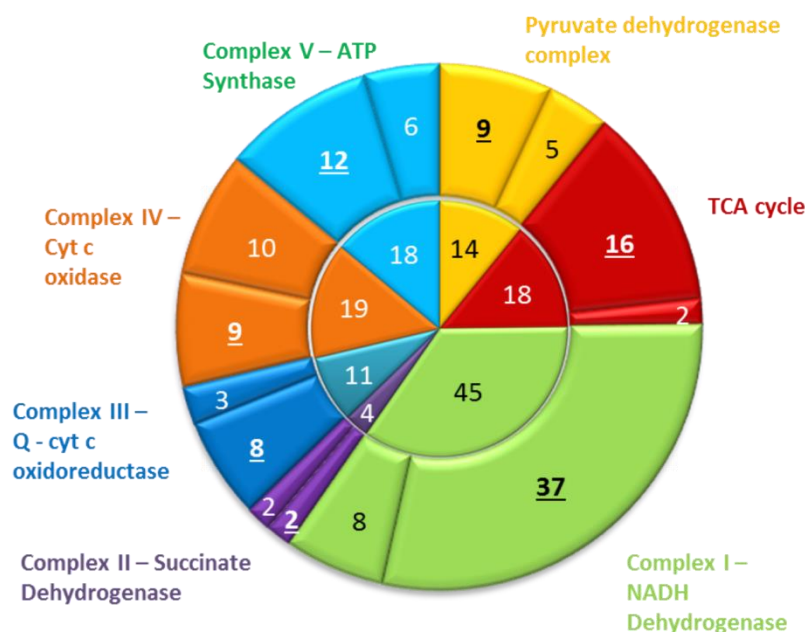


Figure 5-11 Mass spectrometry analysis of immunopurified mitochondria can identify 76% of the proteins involved in oxidative phosphorylation. Z138 cells were cultured in standard glucose and galactose media, subcellular fractionated and mitochondria immunopurified as detailed in the methods. The inner pie represents the total number of proteins that compose the corresponding respiratory chain complex or TCA cycle. The underlined numbers in the outer pie represents the amount of those proteins identified by mass spectrometry. The numbers in the outer pie that are not underlined represents the amount of proteins that were not identified by mass spectrometry.

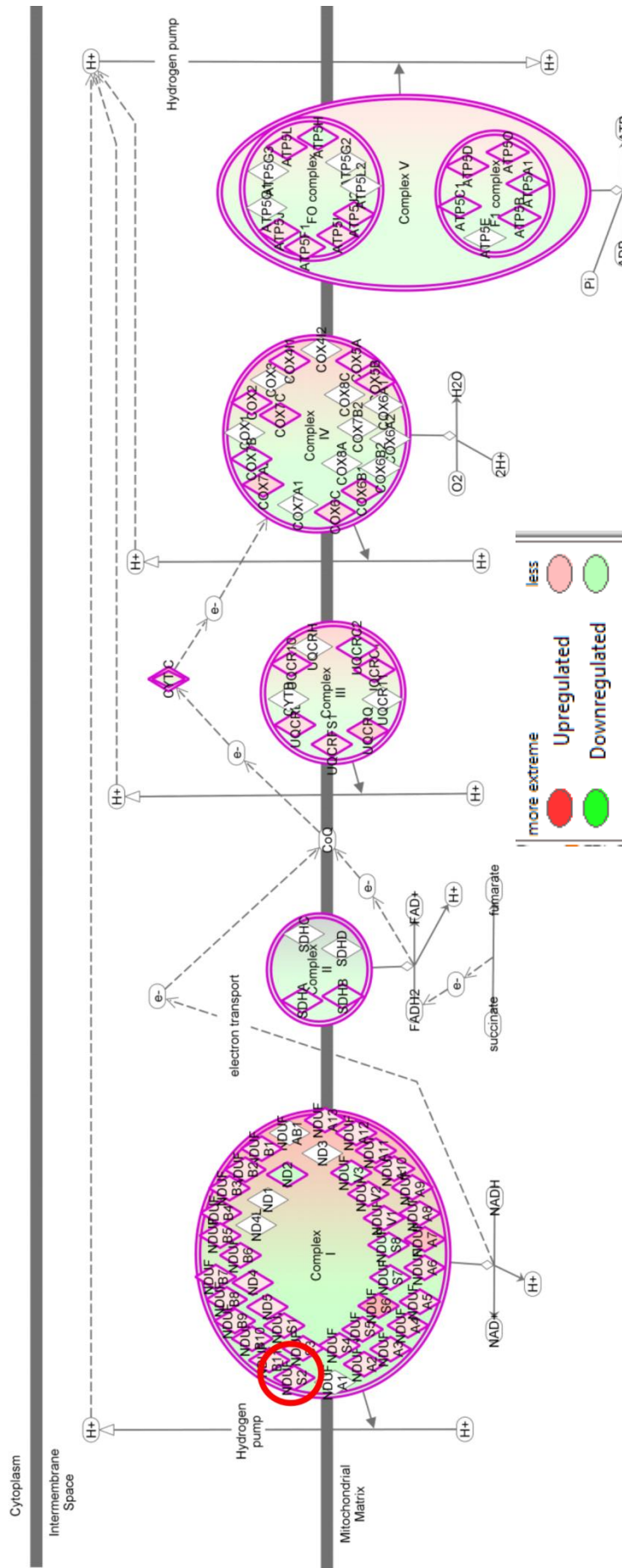


Figure 5-12 Proteins in the mitochondrial respiratory chain are up-regulated in galactose⁺ Z138 cells. Z138 cells were cultured in standard glucose and galactose media, subcellular fractionated and mitochondria immunopurified as detailed in Chapter 2.3. The data was then normalised using TransOmics and imported into Ingenuity™ where the data was analysed. The Figure is directly exported from Ingenuity™ and shows the identified proteins of the respiratory chain (bordered in pink) coloured in either red or green, unidentified proteins are not bordered in pink. Red represents up-regulation and green represents down-regulations. The rotenone binding site is located in NDUFS2, circled in red, which was up-regulated. The majority of the proteins identified were up-regulated in galactose⁺ cells.

Succinate dehydrogenase is comprised of 4 subunits, 2 were identified and found to be down-regulated, which indicated that complex I may be the dominant apical respiratory complex, perhaps utilising NADH from exogenous glutamax and pyruvate, or pyruvate generated from the metabolism of galactose. Q-cytochrome *c* oxidoreductase only had one down-regulated protein, the rest were up-regulated, which may explain the reduced sensitivity to antimycin-induced inhibition of the respiratory chain in galactose^{+ve} cells. Additionally, all cyt *c* oxidase proteins were up-regulated in galactose^{+ve} cells, except one. These results showed that metabolic reprogramming to rely on oxidative phosphorylation may have been a result of up-regulated protein expression of the respiratory chain.

As galactose^{+ve} cells were less sensitive to TRAIL and ABT-737-induced cell killing, the protein expression of a panel of pro- and anti-apoptotic Bcl-2 family proteins was evaluated using the mass-spectrometry data, and then additionally analysed by immunoblotting. Mass spectrometry analysis identified Bax and Bak to be down-regulated in galactose^{+ve} cells (Figure 5-13A), which was confirmed by immunoblotting (Figure 5-13B). In addition, immunoblotting also showed that pro-apoptotic Puma, Noxa, Bid, Bad and cyt *c* were also reduced in galactose^{+ve} cells. Mass spectrometry identified the anti-apoptotic protein Bcl-2 as being up-regulated (Figure 5-13A), which was confirmed by immunoblotting (Figure 5-13C). In addition, immunoblotting of Bcl-x_L and Mcl-1 demonstrated reduced expression in galactose^{+ve} cells. The significant reduction in expression of Bax and Bak, and only moderate reduction in Mcl-1 altered the Mcl-1/Bak/Bax ratio, which potentially explains the reduced sensitivity to ABT-737-induced cell killing in galactose^{+ve} cells. There appeared to be no significant reduction in expression of pro-caspase-8, -9 or -3 (Figure 5-13D); it may be possible that the reduced sensitivity to TRAIL-induced apoptosis was due to the down-regulation of Bid, and thus limited the caspase-8 – Bid-mediated mitochondrial amplification loop.

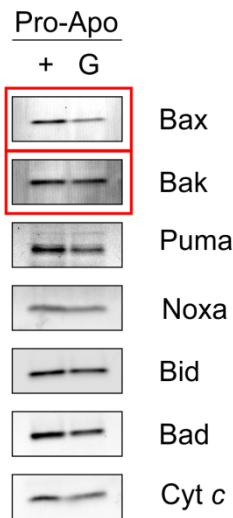
5.2.11 Ingenuity analysis predicts Akt survival signalling is switched on in galactose^{+ve} cells

The mitochondrial proteome was used to map signal transduction pathways and responses, based on the fold change data of the 2280 identified proteins that precipitated with the mitochondria and were imported into the software. It was predicted that Akt survival signalling was activated in galactose^{+ve} cells (Appendix

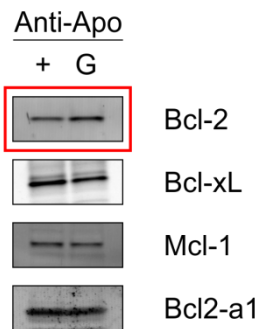
A)

Accession	Protein	p value	fold change	glucose mean	galactose mean
Q16611	Bak	0.0193	-1.78	4451	2498
Q07812	Bax	0.04	-1.73	24864	14347
P10415	Bcl-2	0.0005	1.88	26062	48956

B)



C)



D)

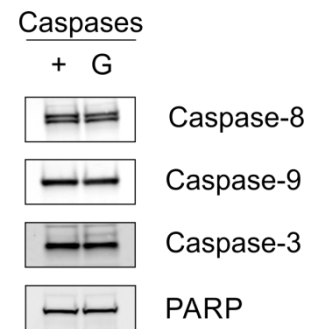


Figure 5-13 Quantitative label-free mass spectrometry can accurately predict changes in the protein expression from the mitochondrial proteome. Z138 cells were cultured in standard glucose and galactose media, subcellular fractionated and mitochondria immunopurified as detailed in Chapter 2.3. The data was then normalised using TransOmics, **A)** Three Bcl-2 family proteins were identified by mass spectrometry, Bax, Bak and Bcl-2, the p value, fold change compared to glucose^{+ve} and means are shown. Bak and Bax were down-regulated and Bcl-2 was up-regulated. To validate the data and additionally profile other key Bcl-2 family proteins in galactose^{+ve} cells, whole cells were solubilised and immunoblotted for **B)** Bax and Bak, to validate the mass spectrometry data, which it did, additionally, the pro-apoptotic proteins Puma, Noxa, Bid, Bad and Cyt c were all down-regulated in galactose^{+ve} cells. **C)** Anti-apoptotic Bcl-2 was found to be up-regulated, in agreement with panel A, Expression of Bcl-x_L and Mcl-1 were slightly reduced, and there was no change in the expression of Bcl2-a1. **D)** There was no significant detectable change in the expression of pro-caspase-8, -9 or -3 or PARP. Immunoblots are representative examples from 2 independent experiments.

Figure 7-8). Akt did not precipitate with the mitochondria; the activation prediction was based on a variety of the identified proteins that have been reported to be either up- or down-stream of Akt regulation. Interestingly however, Ingenuity identified 88 proteins involved in eIF2 signalling, 52 of which were up-regulated, which indicated an activation of eIF2 and potential inhibition of protein synthesis (see Appendix Table7-1 for an example of the amount of proteins Ingenuity uses to make activation/inhibition predictions). Moreover, 53 proteins involved in mTOR

signalling were identified, 34 of which were down-regulated, which also indicated a potential inhibition of protein synthesis (see Appendix Figure 7-9). Activation of Akt should lead to activation of protein synthesis (see Chapter 1.8.2), therefore immunoblotting was performed on Akt and p-Akt S473, along with downstream markers of protein translation. The immunoblot results showed that in galactose^{+ve} cells, Akt was phosphorylated at S473 (Figure 5-14A), in agreement with the Ingenuity prediction that Akt was activated. Interestingly, markers of mTOR signalling, p-p70S6k T389 and p-S6 S240/244 showed reduced phosphorylation, which indicated a reduction in protein translation, in agreement with the Ingenuity data, which predicted an inhibition of mTOR signalling based on the expression profile of 53 proteins. 4EBP1 had increased expression of the hypo-phosphorylated α -band, which indicated a reduction in protein translation. Moreover, p-eIF2- α S51 was phosphorylated to greater extent in galactose^{+ve} cells compared to glucose^{+ve} cells (Figure 5-14B). These results showed that even in the presence of increased Akt signalling, protein translation appeared to be repressed in galactose^{+ve} cells, these results were accurately predicted using the results generated from the mitochondrial proteome data.

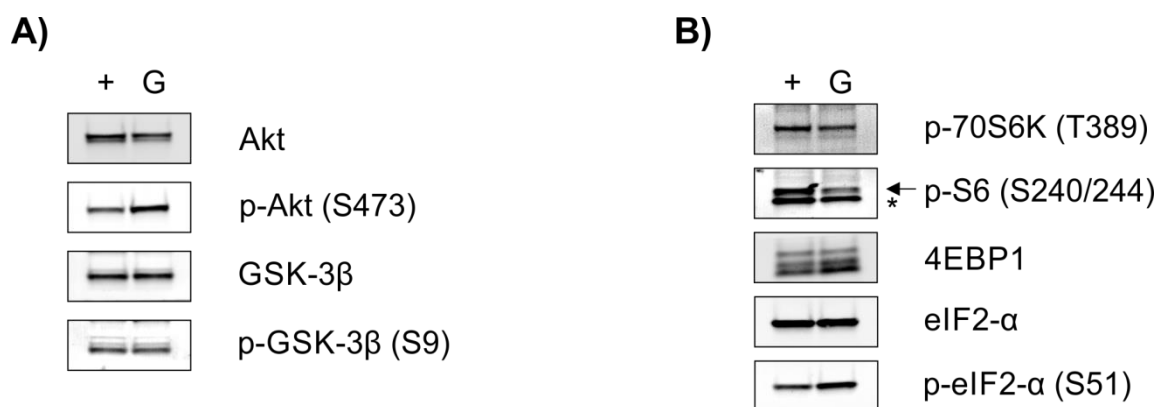


Figure 5-14 Ingenuity can accurately predict signal transduction events from mitochondrial proteome data. To validate the Ingenuity™ predictions, Z138 cells were cultured in standard glucose or galactose media. Whole cell pellets were solubilised and subjected to SDS-PAGE, then immunoblotted for **A)** Total Akt, p-Akt S473, and downstream targets GSK-3 β and p-GSK-3 β S9. As predicted by Ingenuity™ Akt was found to be phosphorylated/activated. **B)** Immunoblot analysis of p-p70S6k T389, p-S6 S240/244, 4EBP1, eIF2- α and p-eIF2- α S51 additionally validated the Ingenuity™ results that galactose^{+ve} cells had down-regulated protein synthesis compared to glucose^{+ve} controls, despite activated Akt – a positive regulator of protein translation. Immunoblots are representative examples from 2 independent experiments.

5.2.12 Galactose^{+ve} cells have elevated basal superoxide levels and are less able to convert glucose to lactic acid.

The mitochondrial respiratory chain is the major source of cellular superoxide (Drose & Brandt, 2012), and because galactose^{+ve} cells had up-regulated basal oxidative phosphorylation and respiratory chain components, mitochondrial superoxide was measured using MitoSOX™ to determine if galactose^{+ve} cells had an elevated level of ROS. Z138 cells were cultured in standard glucose and galactose media and loaded with MitoSOX™ (1 μM) for 30 min, then the fluorescence was measured by FACS analysis. Figure 5-15 shows that basal levels of superoxide are elevated in galactose^{+ve} cells by ~30% compared to glucose^{+ve} cells.

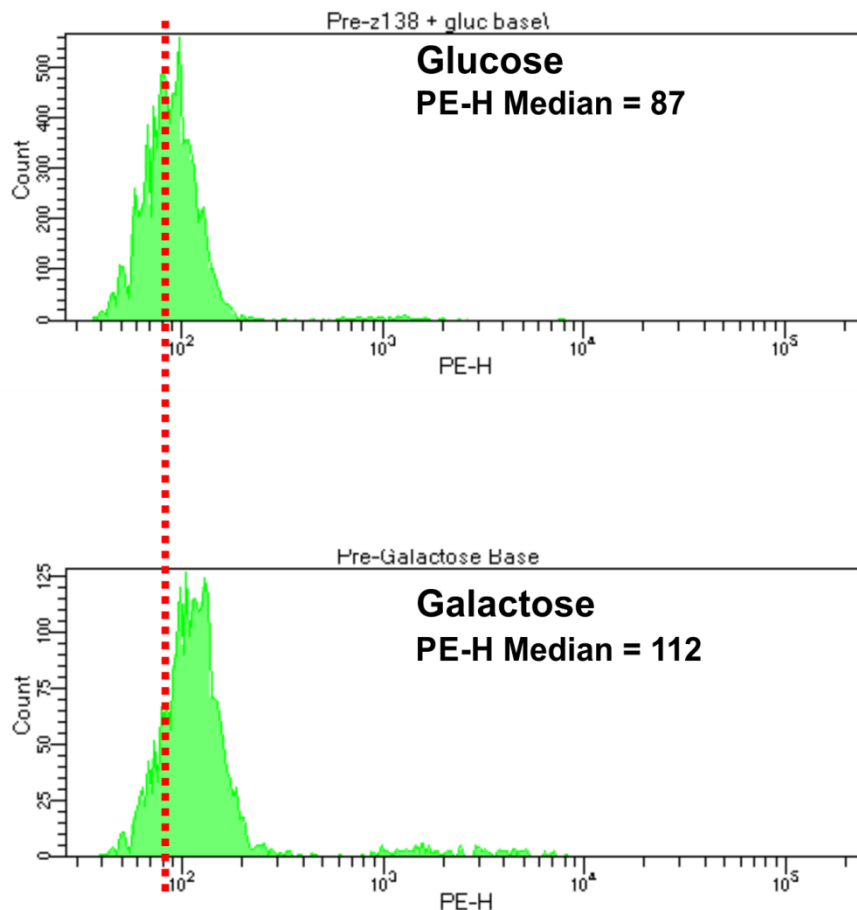


Figure 5-15 Z138 cells cultured in galactose have elevated mitochondrial superoxide. Z138 cells were cultured in standard glucose and galactose media and were loaded with MitoSOX™ (1 μM) for 30 min, then MitoSOX™ fluorescence was measured on a FACS Calibur. Galactose^{+ve} cells displayed 30% more mitochondrial superoxide than glucose^{+ve} cells under basal conditions. Data are a representative example generated from 2 independent experiments.

In addition, the mass spectrometry data detected that galactose^{+ve} cells had reduced levels of mitochondrial associated lactate dehydrogenase A and B (LDHA and LDHB) (Figure 5-16A and B), which may have been why the metabolised galactose was not converted into lactic acid (Figure 5-1D and F). I next investigated this by moving the glucose^{+ve} and galactose^{+ve} cells into glucose free unbuffered DMEM (as detailed in Chapter 2.2.12), and then measured the ECAR on a Seahorse XF24, with sequential injections of D-glucose (50 mM), oligomycin (500 nM) and 2DG (50mM). Moving glucose^{+ve} and galactose^{+ve} cells to glucose free media ablated the basal ECAR values to similar levels, i.e no glycolysis (Figure 5-16D). Addition of glucose generates a rate that represents glycolysis (see Figure 5-16C for an explanation), which increased the ECAR in glucose^{+ve} cells to 67 ± 16 mpH/min/ 10^6 cells, double the glycolysis galactose^{+ve} cells were capable of (35 ± 6 mpH/min/ 10^6 cells) (Figure 5-16D and E). These results showed that galactose^{+ve} cells were less able to convert glucose into lactic acid, and that the metabolised glucose was likely being converted into pyruvate and shunted into the TCA cycle for mitochondrial metabolism. Addition of oligomycin increases glycolysis to its maximal capacity, and the difference between oligomycin stimulated ECAR and the glucose stimulated ECAR is the spare glycolytic capacity (SGC) (see Figure 5-16C for an explanation). Oligomycin did not markedly affect the ECAR in galactose^{+ve} cells; however it resulted in a drop in ECAR in glucose^{+ve} cells which indicated that cells were utilising glycolysis maximally and had no SGC. The addition of 2DG inhibits all glycolytically derived ECAR; the remaining ECAR is non-glycolytic. Adding 2DG reduced the ECAR in glucose^{+ve} and galactose^{+ve} cells to similar levels (10.5 ± 4.5 versus 9 ± 2 mpH/min/ 10^6 cells respectively), which showed that glucose^{+ve} and galactose^{+ve} cells both generated a small amount of ECAR that was independent of glycolysis.

A summary of some of the changes identified by the mass spectrometry analysis and mapped with Ingenuity are depicted in Figure 5-17. The schematic was drawn by collating a variety of events that were statistically significant in the Ingenuity mapping software. These changes were used to try and explain the differences observed in relation to sensitivity to apoptotic stimuli, or metabolic reprogramming. Up-regulated proteins are coloured green, and down-regulated proteins are coloured red. The schematic shows the up-regulated oxidative phosphorylation

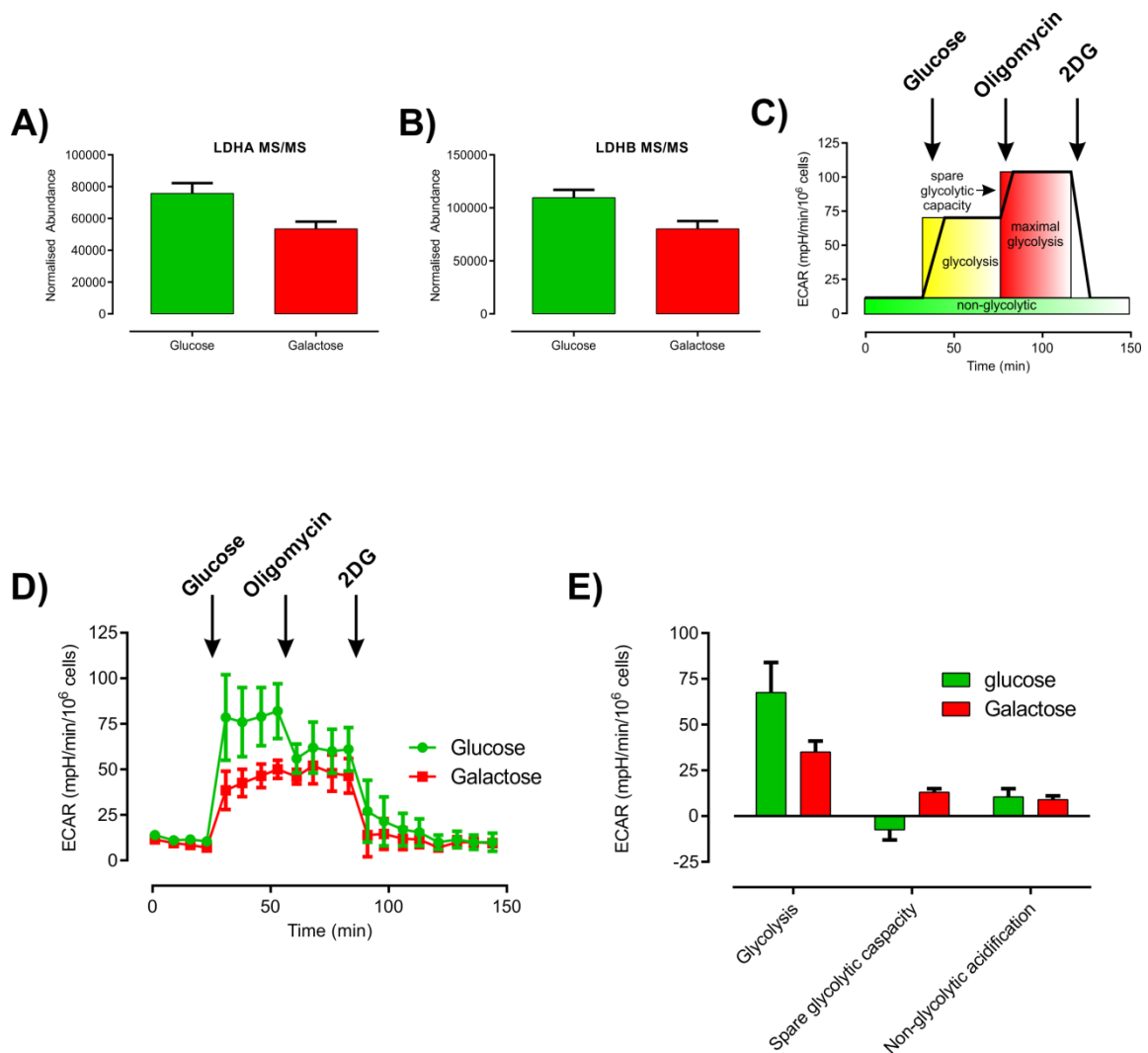


Figure 5-16 Galactose^{+ve} cells cannot divert as much glucose into lactic acid compared to glucose^{+ve} cells. Relative normalised abundance values generated from TransOmics for **A)** LDHA and **B)** LDHB. **C)** Schematic of a typical glycolysis test from a Seahorse XF24, which details how to interpret the results. Z138 cells were cultured in standard glucose and galactose media and seeded at 4.5×10^5 cells/well. Prior to loading into the Seahorse XF24, the media was changed to glucose-free unbuffered DMEM (see Chapter 2.2.12) for both glucose^{+ve} and galactose^{+ve} cells, and the indicated inhibitors added sequentially as shown in panel (C) and ECAR measured. **D)** Addition of glucose (50 mM) to glucose^{+ve} cells induced a large increase in ECAR which was significantly greater than that achieved by galactose^{+ve} cells. Oligomycin (500 nM) reduced the ECAR in glucose^{+ve} cells but had no effect on galactose^{+ve} cells. 2DG (50 mM) ablated ECAR in glucose^{+ve} and galactose^{+ve} cells to the same extent. **E)** The mean value generated after the addition of glucose represents glycolytic ECAR. Subtraction of oligomycin from basal the values represents the spare glycolytic capacity (SGC). Any remaining ECAR after the addition of 2DG is non-glycolytic ECAR. Seahorse data are representative of 3 independent experiments.

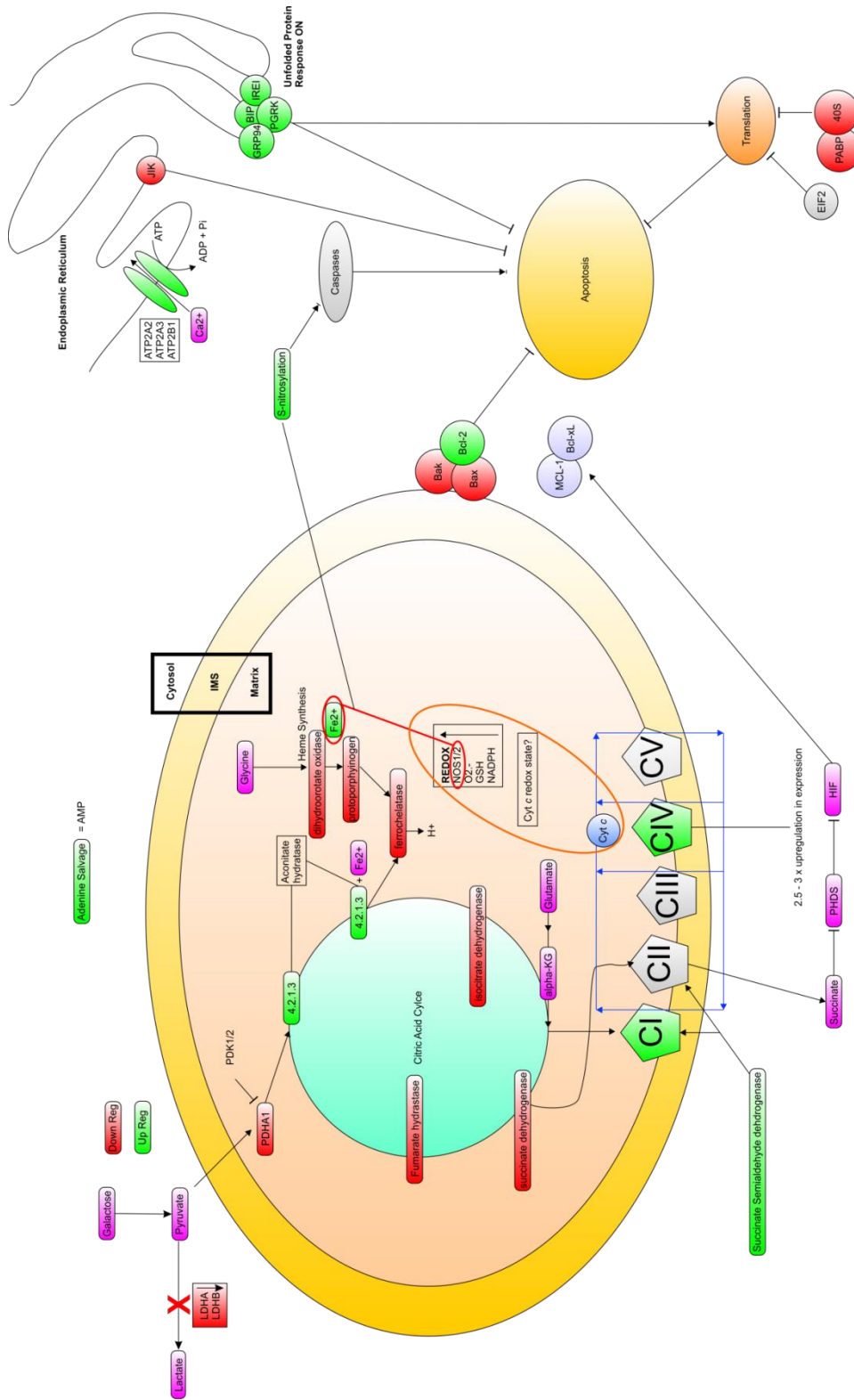


Figure 5-17. Schematic representation of a selection of changes in galactose^{+ve} cells that were predicted by TransOmics coupled to Ingenuity™. It was used to predict that ROS levels were up in galactose^{+ve} cells, and that galactose^{+ve} cells would be less able to divert glucose into lactic acid following the addition of glucose. The mass spectrometry data coupled to TransOmics quantified mitochondrial protein expression, significantly, the respiratory chain and apoptotic related proteins. It predicted that galactose media would confer resistance to apoptotic inducers (right side) by a variety of mechanisms, which was proven by a conferred resistance to intrinsic and extrinsic death stimuli (ABT-737 and TRAIL respectively). There were 555 significantly different proteins, only a selection was manually mapped to this schematic.

system, the prediction of increased levels of ROS, reduced expression of Bak and Bax, and increased expression of Bcl-2. These changes were mapped to show an inhibition of apoptosis, or resistance to drugs. In addition, there was a predicted increase in the unfolded protein response, which was predicted to additionally inhibit apoptosis signalling.

5.3 Discussion

5.3.1 The mode of cell death, not the degree, appears to be critical for identifying drug-induced mitochondrial toxicity

In this study I have shown that culturing cells in galactose supplemented media resulted in metabolic reprogramming or switching, forcing the cells to rely on mitochondrial oxidative phosphorylation, as previously shown (Robinson *et al.*, 1992; Gohil *et al.*, 2010). Switching cells to a galactose based media increased the level of basal oxidative phosphorylation by 69%, from 313 ± 16 to 530 ± 38 pmol/min/ 10^6 cells, thus 370 ± 42 pmol/min/ 10^6 cells of basal OCR was committed to mitochondrial ATP synthesis. Additionally, switching the cells to oxidative phosphorylation in galactose medium resulted in an uncoupler-induced maximal respiratory capacity of 457 ± 39 pmol/min/ 10^6 cells which resulted in a negative RRC of -74 ± 37 pmol/min/ 10^6 cells, these results showed that galactose^{+ve} Z138 cells were respiring maximally under basal conditions similar to state-3 respiration (Figure 5-1) (Chance & Williams, 1955). These results were similar to the results obtained by chronically depriving Z138 cells of glucose (Robinson *et al.*, 2012), and showed the cells were completely dependent on oxidative phosphorylation for ATP generation and thus survival, despite the preservation of the PPP in galactose^{+ve} cells.

In addition, galactose^{+ve} cells were less sensitive to rotenone and antimycin-induced inhibition of oxidative phosphorylation, which suggested that the up-regulated basal oxidative phosphorylation may have been attributed to increased expression of respiratory chain proteins. Despite being dependent on mitochondrial oxidative phosphorylation, galactose^{+ve} cells still generated an ECAR of 14 ± 3 mpH/min/ 10^6 cells, 70% lower than glucose^{+ve} cells; of this 11 ± 3 mpH/min/ 10^6 cells was derived from respiratory chain driven acidification generated from ATP

synthase derived proton extrusion and respiratory chain proton generation, the remaining 3 ± 0.8 mpH/min/ 10^6 cells may have been from lactic acid derived from the glycolytic metabolism of galactose and non-glycolytic acidification. These results, taken together with the OCR data showed that galactose^{+ve} cells were completely dependent on their mitochondria for ATP generation and survival.

It has recently been reported that hippocampal HT22 cells are extremely sensitive to ATP synthase inhibition by oligomycin in the presence of galactose instead of glucose (Pfeiffer *et al.*, 2014). Thus, after successfully confirming that galactose^{+ve} cells had undergone metabolic reprogramming to be dependent on oxidative phosphorylation, Z138 cells were treated with increasing concentrations of classical mitochondrial poisons, namely oligomycin, rotenone and antimycin (0 – 1000 nM); glucose^{+ve} cells were completely resistant to the poisons and did not undergo any cell death. In contrast, galactose^{+ve} cells underwent cell death in the presence of all the oxidative phosphorylation inhibitors. The mode of cell death following oligomycin treatment was not inhibited by the inhibition of caspases or RIPK1, which suggested oligomycin-induced cell killing, was necrotic. Strikingly though, analysis of the FACS data (Figure 5-2) showed that the cells were dying with a PS+/PI- phenotype, which is a hallmark of canonical caspase-dependent apoptosis, or possibly an unidentified novel RIPK1-dependent mechanism as described in Chapter 3. This was in contrast to rotenone and antimycin-induced cell death, which drove the cells into necrosis in the absence of phosphatidyl serine externalisation. High concentrations of zVAD.fmk (50 μ M) and Nec-1 (50 μ M) alone or in combination did not block cell death following any classical poison in galactose^{+ve} cells. These results suggest that oligomycin may induce a potentially novel caspase-independent, RIPK1-independent form of programmed cell death which was not recapitulated with rotenone and antimycin. Moreover, even in the presence of rotenone or antimycin, glucose cells survived extremely high levels of mitochondrial superoxide production (data not shown), which has been shown to induce apoptosis in HT1080 cells (Li *et al.*, 2003b).

It is puzzling that direct inhibition of the electron transport chain results in a different mode of cell death to direct inhibition of the ATP synthase. The only difference between the two classes of inhibitors is that following ATP synthase inhibition, the electron transport chain can still function, albeit slowly, to produce

the mitochondrial proton leak, which is not coupled to the ATP synthase, whereas ETC inhibition does not. These results suggested that maintenance of the mitochondrial proton leak may have been involved in executing the 'programmed' cell death observed following oligomycin treatment. Galactose^{+ve} cells were next used to test if the biguanides metformin and phenformin, compounds that inhibit complex I through unknown mechanisms (Wheaton *et al.*, 2014), induce necrosis in cells dependent on mitochondrial oxidative phosphorylation. Although recent evidence does support the notion that metformin acts directly at the mitochondria (Andrzejewski *et al.*, 2014), metformin did not induce cell death at any concentration (0 – 1000 μ M) after 16 h, it is possible that 1000 μ M was insufficient to completely ablate respiration in Z138 cells; because 5 mM metformin for 24 h only reduced OCR ~60% in MCF7 cells (Andrzejewski *et al.*, 2014). Bioenergetics data generated from a Seahorse analyser would be essential to verify these findings. In contrast, treatment with the more potent phenformin (1000 μ M) resulted in necrotic cell death in galactose^{+ve} cells. These results were similar to the findings with rotenone, the classical complex I inhibitor which induced necrosis in galactose^{+ve} cells (Figure 5-3). The differences observed between metformin and phenformin may be because metformin is a poor inhibitor of the respiratory chain compared to phenformin, or that phenformin is more cell-permeable, as it appears to be less dependent on organic cation transport 1 (OCT1) to enter the cell (Hawley *et al.*, 2010). The necrotic phenotype observed following phenformin treatment highlighted that galactose^{+ve} Z138 cells can be used to investigate drug-induced mitochondrial toxicity, by analysing the degree and also the mode of cell death.

To explore the effect of galactose metabolism on canonical inducers of apoptosis, glucose^{+ve} and galactose^{+ve} cells were treated with TRAIL and ABT-737. TRAIL is an initiator of apoptosis through death receptor-mediated extrinsic pathway, and can be blocked by caspase inhibition. ABT-737 induces apoptosis through the intrinsic mitochondrial pathway resulting in mitochondrial outer membrane permeabilisation before caspase activation. Interestingly, galactose^{+ve} cells were less sensitive to ABT-737-induced cell death, which is similar to work previously published from our laboratory using glucose deprived cells (Robinson *et al.*, 2012). However, pre-treatment with the pan-caspase inhibitor zVAD.fmk and the RIPK1

inhibitor Nec-1 did not prevent cell death, and changed the mode from caspase-dependent apoptosis to necrosis (Figure 5-8). These results agree with the conclusion that the mode of cell death following drug treatment can be used to investigate if the drug induces mitochondrial dysfunction.

TRAIL-induced cell death was completely blocked by zVAD.fmk and Nec-1 in combination in both glucose^{+ve} and galactose^{+ve} cells. However, TRAIL-induced cell death was not completely blocked by zVAD.fmk alone in either glucose^{+ve} or galactose^{+ve} cells, which suggests that Z138 cells switch to TRAIL-induced necroptosis following caspase inhibition. Galactose^{+ve} cells still underwent ~35% cell death at 1000 ng/ml TRAIL (Figure 5-7), which was in contrast to glucose^{+ve} cells (~65%), these results validated the findings in Chapter 3, in which UPN1^{-ve} cells were unable to switch to necroptosis. It therefore appears that an active glycolytic pathway and glycolytically generated ATP are critical for TRAIL-induced necroptosis; it is possible that galactose^{+ve} cells still undergo necroptosis as glycolysis is still active in this model, but not energetically competent. To verify these results, the ability of Z138 cells to switch to necroptosis in glucose and galactose free conditions would need to be assessed. Moreover, this study also recapitulated the findings in Chapter 3, which show that RIPK1-dependent TRAIL-induced necroptosis results in an intermediate PS⁺ population of cells, and therefore partial externalisation of phosphatidyl serine.

Etoposide has been shown to directly act at the mitochondria at high doses (Robertson *et al.*, 2000), whilst engaging apoptosis by inhibiting nuclear topoisomerases at low doses. As such galactose^{+ve} and glucose^{+ve} cells were treated with a range of etoposide concentrations (0 – 1000 nM) (Figure 5-9), with the expectation that high doses would result in necrosis similar to the results obtained with the classical poisons, ABT-737 and phenformin. Glucose^{+ve} cells were extremely sensitive to etoposide, which resulted at ~90 – 95% cell death at the lowest concentration (31.25 nM), the cell death in glucose^{+ve} cells was inhibited by zVAD.fmk which showed caspase-dependent apoptosis at all concentrations. Interestingly, galactose^{+ve} cells were less sensitive to etoposide compared to glucose^{+ve} cells at all concentrations. Strikingly however, it appeared that low concentrations of etoposide (31.25 – 125 nM) induced necrosis and may be acting at the mitochondria, whilst high concentrations (0.25 – 1 μ M) were not, as low

concentrations induced caspase-dependent apoptosis that was inhibited by zVAD.fmk. Etoposide has been shown to result in mitochondrial biogenesis by activating ATM which results in an increase in the mitochondrial membrane potential, mass and mtDNA (Fu *et al.*, 2008); speculatively, it may have been possible that high doses of etoposide increased the membrane potential and somehow prevented its direct action on the mitochondria, thus preventing the cells from undergoing necrosis at the higher concentrations.

5.3.2 The mitochondrial proteome can accurately be evaluated by mass spectrometry

Switching Z138 cells to rely on mitochondrial oxidative phosphorylation has profound effects on sensitivity to apoptotic stimuli and classical mitochondrial inhibitors. I therefore investigated if a proteomic and bioinformatics approach to characterise the whole mitochondrial proteome using quantitative label-free mass spectrometry, could accurately identify changes in the mitochondrial proteome. In addition, the changes that were identified were analysed by pathway mapping software with the aim of predicting the effect of metabolic reprogramming on sensitivity to apoptotic stimuli. Drug-induced mitochondrial toxicity can present in forms other than direct inhibition of oxidative phosphorylation, such as inhibition of substrate oxidation, inhibition of mitochondrial biogenesis or the inhibition of mtDNA and biomass (reviewed in Wallace, 2008), these forms of drug-induced mitochondrial toxicity may not completely ablate the respiratory chain, and therefore *in vitro* functional readouts for investigating the toxicity may not work, and so this approach could possibly be used as an endpoint study for identifying drug-induced mitochondrial toxicity in a more relevant model.

Glucose^{+ve} and galactose^{+ve} Z138 cells were fractionated and the mitochondria immunopurified and analysed by label-free quantitative mass spectrometry, there were 2280 quantifiable proteins identified, of those, 555 were significantly different between glucose^{+ve} and galactose^{+ve}. From the oxidative phosphorylation system, 76% of the proteins were identified, and most of them were found to be up-regulated in galactose^{+ve} cells. These results may explain the decreased sensitivity to rotenone and antimycin-induced inhibition of oxidative phosphorylation. Moreover, results shown in Figures 5-10, 5-11 and 5-12 highlighted the accuracy of the mass spectrometers in identifying changes in protein concentration; and

therefore may be a powerful tool to evaluate off-target drug effects that reduce synthesis/expression of the respiratory chain (or indeed other mitochondrial proteins), but not completely ablate expression, and therefore functional readouts of the respiratory capacity or sensitivity to cell killing may not detect.

Mass spectrometry analysis coupled to bioinformatics pathway mapping in Ingenuity, accurately predicted that galactose^{+ve} cells may be partially resistant to ABT-737 (in the absence of caspase inhibition), by accurately quantifying the key proteins involved in sensitivity to ABT-737, Bak, Bax and Bcl-2 (Figure 5-13), these results were confirmed by immunoblotting. As the identification rate was so high (2280 proteins), Ingenuity can additionally map changes in cellular signal transduction events based on the expression of targets both up- and down-stream of the protein in question, this study showed an example of that. Galactose^{+ve} cells were predicted to activate Akt, but counterintuitively inhibit protein synthesis. Evaluation of whole cell protein expression by immunoblotting validated these results (Figure 5-14); Akt S473 was phosphorylated in galactose^{+ve} cells. However the phosphorylation status of p70S6k T389, S6 S240/244 and 4EBP1 all agreed with an inhibition of protein translation. Phosphorylation of eIF2 α was predicted to occur from 88 different proteins, which was validated by immunoblotting (Figure 5-14). These results demonstrate that analysis of the mitochondrial proteome coupled to bioinformatics pathway mapping can accurately identify changes in mitochondrial protein expression but additionally predict cellular signal transduction events. This may be a powerful tool for investigating off-target drug-induced mitochondrial toxicity, but also, for example, if cancer therapeutics produce off-target survival signalling, in which case this system could potentially be used to select a combinatorial therapy to counter that signal.

In addition to identifying protein changes and alterations in signal transduction events, analysing changes in the mitochondrial proteome can be used to predict changes in the superoxide levels, which were increased in galactose^{+ve} cells, even though it has been shown previously that in certain cell lines galactose^{+ve} cells have significantly less superoxide than glucose^{+ve} cells (Dott *et al.*, 2014). In agreement with this prediction, Figure 5-15 shows that galactose^{+ve} cells generate 30% more superoxide under basal conditions compared to glucose^{+ve} cells. As

there was so many significantly different changes (555) it is beyond the scope of this thesis to analyse all of them. However, as I have tried to depict in Figure 5-17, this methodology can be used to generate a ‘map’ of a variety of proteomic and functional changes, which would aid in identifying the mechanisms of altered sensitivity to apoptotic stimuli, or possibly to help predict drug-induced mitochondrial toxicities in a more relevant model.

In conclusion, galactose^{+ve} cells decreased the sensitivity to canonical inducers of apoptosis, but increased sensitivity to classical mitochondrial poisons. This occurred as a result of the switch to mitochondrial oxidative phosphorylation, which induced changes in the balance of key pro- and anti-apoptotic Bcl-2 proteins. An unexpected finding was that TRAIL-induced necroptosis was partially ablated in galactose^{+ve} cells, highlighting the necessity for an active glycolytic pathway to switch to this mode of cell death, as described in Chapter 3. The analysis of the mitochondrial proteome is still in early development, but the sensitivity of the mass spectrometers coupled to bioinformatics proved to be extremely accurate, and requires testing further. It provides a sensitive platform to investigate the effects of metabolic reprogramming on drug-induced cell death and aid in the identification of the location and possibly mechanism of action.

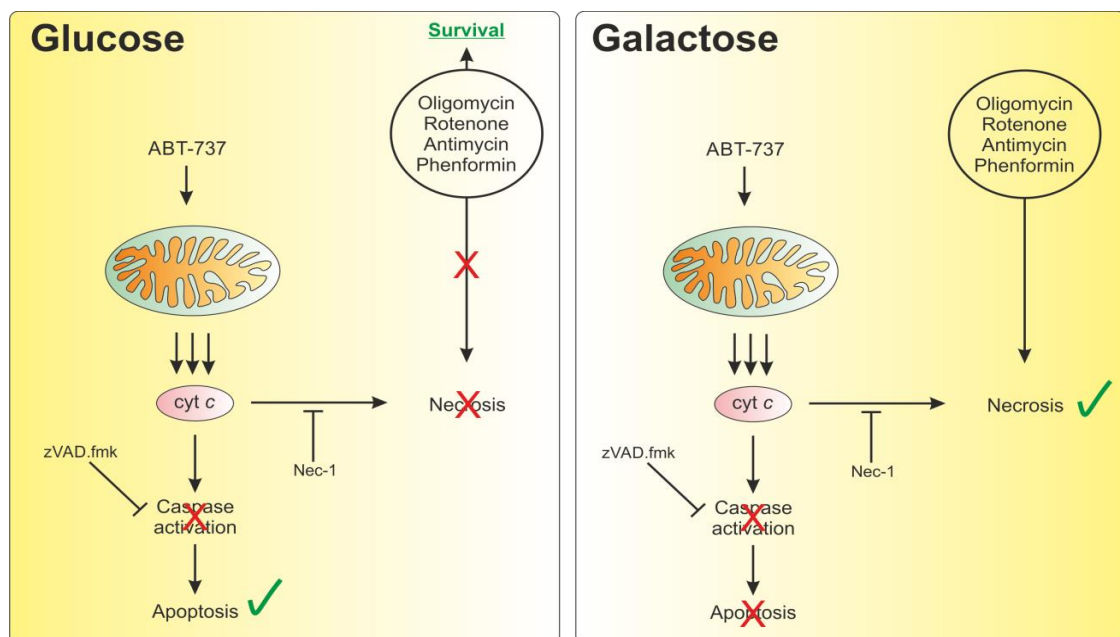


Figure 5-18 Galactose^{+ve} cells undergo necrosis when the mitochondria are compromised. Schematic showing that glucose^{+ve} cells are resistant to inhibitors of the oxidative phosphorylation system, and following ABT-737 treatment undergo classical caspase-dependent apoptosis. Conversely, galactose^{+ve} cells undergo caspase-independent necrosis after the mitochondria are damaged or oxidative phosphorylation is blocked.

6. Final Discussion

6.1 Overview

The aim of the research presented in this thesis was to investigate how metabolic status, using three different methods of modulating glycolytic flux, can alter tumour cell sensitivity to apoptotic stimuli. This was achieved by chronic glucose deprivation, galactose supplemented media and treatment with the anti-glycolytic 2DG, in the mantle cell lymphoma derived cell lines, UPN1 and Z138. The results have provided evidence for an important role of glycolysis in regulating necroptosis, a recently published novel form of programmed necrosis, and additionally that RIPK1 mediated cell death results in the partial externalisation of phosphatidyl serine to the outer leaflet of the plasma membrane. Moreover, targeting glycolysis with anti-glycolytic compounds in combination with traditional inducers of apoptosis is potentially a means to increase tumour cell sensitivity to cell death. The study in Chapter 4 examined the kinetics and mechanisms of the anti-glycolytic 2DG on cellular metabolism, cell death and signal transduction pathways in detail, and provided evidence for an LKB1 – CaMKK- β -independent route of AMPK activation and sensitisation to both intrinsic (ABT-737) and extrinsic (TRAIL) apoptotic stimuli. A summary of the findings is depicted in Figure 6-1.

6.2 Metabolism and (programmed) necrosis

Most tumour cells undergo metabolic reprogramming to increase dependence on aerobic glycolytic metabolism (Warburg *et al.*, 1927; Warburg, 1956). Recent advances in the field of tumour cell metabolism have shown that this switch promotes tumorigenesis and survival advantages, so neoplastic cells can survive otherwise un-survivable environments (reviewed in Coller, 2014). An additional advantage of this switch is that cellular metabolism is regulated by upstream signal transduction cascades, and thus, up-regulation of these signals to increase aerobic glycolysis also results in the generation of additional survival signalling, which happens to confer resistance to intrinsic and extrinsic mediated apoptosis (reviewed in Ganapathy-Kanniappan & Geschwind, 2013).

Although a lot is now known about the role of tumour cell metabolism on survival signalling, little is still known about the role of cellular metabolism on the regulation of cell death. Work from our laboratory has shown that inhibition

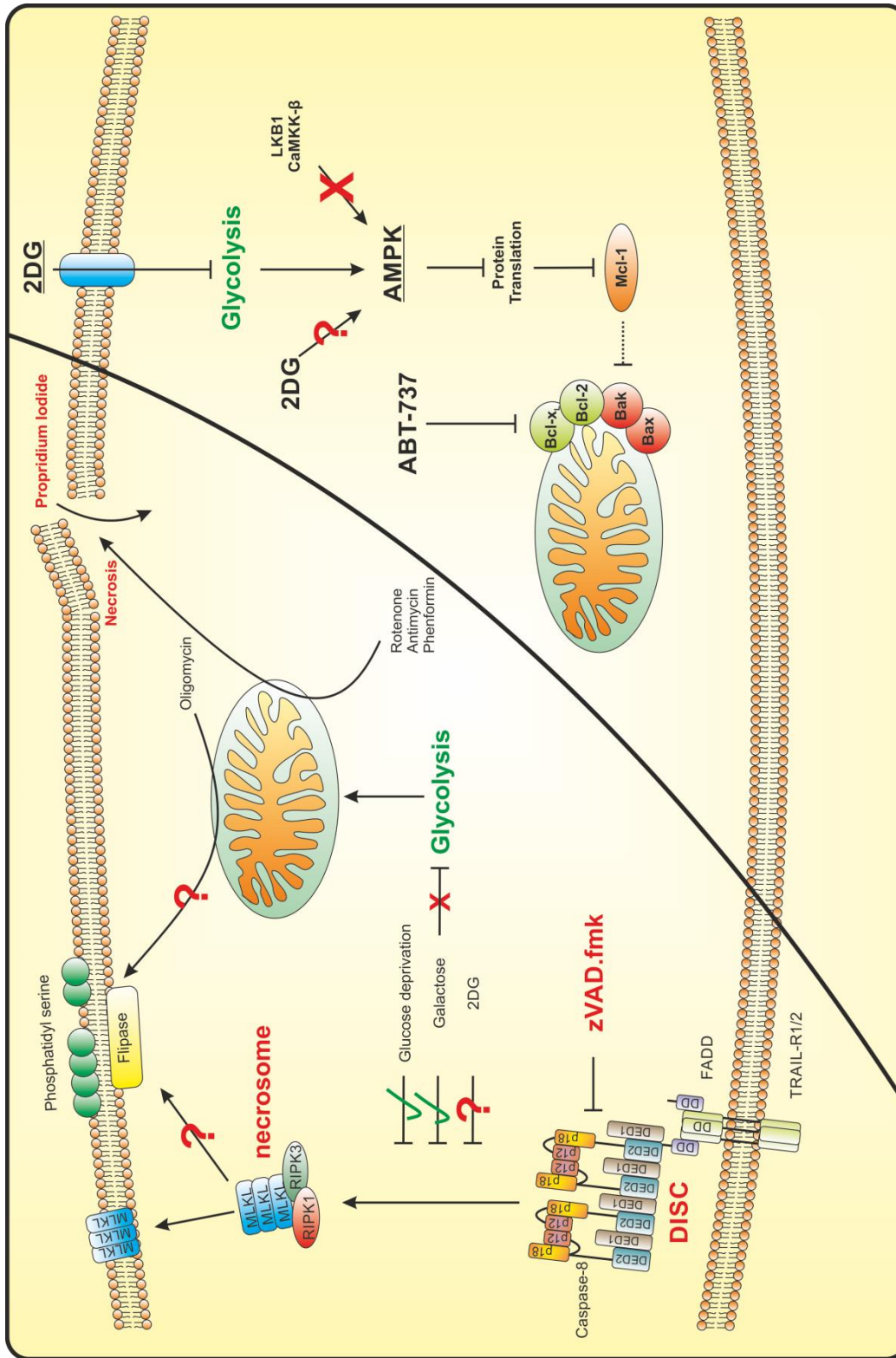


Figure 6-1 Glucose deprivation and galactose supplemented media inhibits TRAIL-induced necroptosis, and 2DG activates AMPK independently of LKB1 and CaMKK-β . On the left, glucose deprivation and galactose cultured cells inhibit TRAIL-induced necroptosis signalling. Necroptosis results in the partial externalisation of phosphatidyl serine through unknown mechanisms, this also occurs following oligomycin treatment in galactose^{+/ve} cells, but results in plasma membrane rupture following complex I or III inhibition with rotenone, phenformin or antimycin, respectively. On the right, 2DG activates AMPK independently of the known canonical kinases LKB1 and CaMKK-β, however the mechanism remains unknown. This results in the rapid and significant down regulation of Mcl-1, thus potentiating intrinsic and extrinsic cell death.

of glycolysis by glucose deprivation confers resistance to TRAIL and ABT-737-induced cell death (Robinson *et al.*, 2012), contradictory to other studies; we have yet to determine if this switch in sensitivity is the result of ablated glycolysis or increased mitochondrial oxidative phosphorylation. Similarly, the role of cancer cell metabolism on necroptosis has not been investigated, and the results presented in this thesis demonstrated that TRAIL-induced necroptosis is ablated following glucose deprivation and is significantly reduced in the presence of galactose.

Necroptosis is a novel form of programmed cell death that has been identified in a variety of pathological diseases such as atherosclerosis (Lin *et al.*, 2013), pancreatitis (Wu *et al.*, 2013), inflammatory bowel disease (Welz *et al.*, 2011) and myocardial infarction (Smith *et al.*, 2007). Activation of necroptosis results in the formation of the necrosome, a multi-protein complex composed of RIPK3, RIPK1 and MLKL (reviewed in Linkermann & Green, 2014). Activation of necroptosis occurs following activation of death receptors in the presence of caspase-8 inhibition (or removal), thus resulting in a classical necrotic phenotype (reviewed in Dickens *et al.*, 2012b; Linkermann & Green, 2014). Moreover, these results also demonstrated that in mantle cell lymphoma derived cell lines, necroptosis induces a RIPK1-dependent partial externalisation of phosphatidyl serine to the outer plasma membrane, which is not typical of the oncosis to necrosis mode of cell death. These results further confirm that necroptosis is a programmed form of cell death, however the end result may not be typical necrosis (plasma membrane rupture), but instead programmed removal, similar to apoptosis. Cellular metabolism appears to be critical for the engagement of necroptosis, but, like the altered sensitivity to intrinsic and extrinsic apoptotic stimuli, it is yet to be determined if this requirement is glycolytic or mitochondrial. The mitochondrial phosphatase phosphoglycerate mutase (PGAM5) has been implicated in necroptosis (Wang *et al.*, 2012), but this is yet to be recapitulated by other laboratories.

Another key question that remains is, how does necroptosis result in the possible activation of flippases externalising phosphatidyl serine? And why does this occur in haematopoietic Z138 and UPN1 cells? A limitation of these studies is that cell death *in vitro* will ultimately lead to secondary apoptosis (plasma membrane rupture) and cannot be differentiated from primary necrosis, as such; the

significance of the partial externalisation of phosphatidyl serine following TRAIL-induced necroptosis remains unknown. Phosphatidyl serine is an 'eat me' signal, typically associated with apoptotic cell death to clear the cells in the absence of inflammation and autoimmunity (reviewed in Hochreiter-Hufford & Ravichandran, 2013), and may indicate that necroptosis *in vivo* in certain conditions may not be inflammatory. Although necroptosis has not been shown to result in phosphatidyl serine exposure before, another programmed necrotic pathway, pyroptosis does externalise 'eat me' signals (Wang *et al.*, 2013)

There are a variety of regulated necrotic pathways that have recently started to emerge, ferroptosis, pyroptosis, PARP-1 mediated regulated necrosis, NADPH-oxidase-mediated regulated necrosis, lysosomal membrane permeabilisation (reviewed in Linkermann & Green, 2014) and there may be more to come in this emerging field of cell death. The fact that oligomycin induces PS externalisation in the absence of caspase activity suggests a programmed form of cell death. RIPK1, the target of Nec-1 is not always critically required for engagement of necroptosis, and so, will inhibiting MLKL with necrosulfonimide prevent oligomycin-induced cell killing? Moreover, why are cells maintained in glucose resistant to this form of death?

The mechanisms of necrotic cell death following treatment with classical mitochondrial poisons when maintained in galactose media remains to be investigated. Programmed necrosis through the mitochondrial permeability transition pore (mPTP) needs to be assessed in detail when switching cells to rely on oxidative phosphorylation. The mPTP appears to be critically dependent on cyclophilin D for execution (Bernardi, 2013), however on going work in our laboratory has shown that primary patient CLL tumours do not express it, whereas cell lines do (C Langlais, K Cain *et al.*, unpublished data), and it remains to be determined if this is a common alteration among other tumour types, and thus a viable therapeutic target or not.

6.3 Targeting cancer cell metabolism as a therapeutic strategy

Inhibiting cancer cell metabolism, specifically glycolysis, alters the balance between pro- and anti-apoptotic proteins by modulating the balance between AMPK and Akt, master regulators of cellular homeostasis (discussed in

MacFarlane *et al.*, 2012). Inhibiting glycolysis by 2DG in Z138 cells results in a rapid and transient activation of AMPK that appears to be a dominant signal over a subsequent Akt activation event (Chapter 4). This rapidly alters the balance in the Mcl-1/Bak ratio thus potentiating TRAIL and ABT-737-induced cell killing within 2 h. The relevance of this is that leukaemias and many epithelial tumours are resistant to TRAIL-induced apoptosis (MacFarlane *et al.*, 2002). Targeting altered cancer cell metabolism therefore may be a means to enhance the efficacy of this cytokine. In agreement with 2DG being a powerful tool to sensitise tumours to cell death, primary mesothelioma *ex plants* and cells, which are notoriously resistant to chemotherapeutics (Hudson *et al.*, 2014), can be significantly sensitised to ABT-737-induced cell killing (X M Sun, M MacFarlane *et al.*, unpublished work), however the mechanism of action appears to be different between the two models. 2DG has been shown to activate AMPK through both the LKB1 (Corradetti *et al.*, 2004) and CaMKK- β (Xi *et al.*, 2013) pathways. It was a striking finding that in Z138 cells, 2DG appears to activate AMPK independently of these two canonical kinases through a hitherto unknown signalling mechanism. If 2DG can activate AMPK through multiple signals, it would be an extremely powerful combinatorial drug to sensitise tumours to chemotherapeutics through regulating the balance between pro- and anti-apoptotic proteins.

Targeting glycolysis with 2DG results in Akt activation and the activation of other survival signals (Chapter 4 and Zhong *et al.*, 2008; Zhong *et al.*, 2009). The significance of these signals has not been studied, and the effect they have on mitochondrial metabolism following 2DG-induced survival signalling has been largely ignored. Ongoing bioinformatics analysis I am performing on immunopurified mitochondria treated with 2DG for 20 h will hopefully address some of these issues. I showed in Chapter 5 that bioinformatics methodologies can be used to predict the generation of survival signalling from the mitochondrial proteome data. Furthermore, this approach can be used to identify common alterations between the 'same' tumour types that could potentially be targeted therapeutically. In line with this, immunopurified mitochondria from CLL patients show large inter-patient differences in their mitochondrial proteome (C Langlais, K Cain *et al.*, unpublished work), which may confer resistance to therapeutics.

The effect of inhibiting tumour cell glycolytic metabolism needs to be further studied in terms of retrograde signalling. This is process whereby a signal emanating from the mitochondria ultimately leads to a signal being delivered to the nucleus (reviewed in da Cunha *et al.*, 2015), thus changing the cells transcriptional and translational output. Increasing mitochondrial oxidative phosphorylation by targeting glycolysis is likely to lead to a retrograde response, and the significance of these needs to be evaluated as it may be a contributing factor to the change in balance between pro- and anti-apoptotic proteins, this is currently been evaluated using mass spectrometry data from immunopurified mitochondria from glucose deprived, glucose containing, galactose grown and 2DG treated Z138 cells.

Additionally, the role of autophagy has not been examined in this thesis, which is co-ordinately regulated alongside apoptosis by Mcl-1. Loss of Mcl-1 appears to activate a robust autophagic response in cortical neurons (Germain *et al.*, 2011). Conversely, Mcl-1-deficient cardiac myocytes are incapable of undergoing autophagy (reviewed in Thomas & Gustafsson, 2013). Mcl-1 regulation of autophagy therefore appears to be cell type dependent, and thus the rapid depletion of Mcl-1 following 2DG in Z138 cells may either increase or decrease autophagic flux

6.4 Future work

From the data presented in this thesis, important questions still remain and future work needs to focus on these questions. The importance of glycolysis versus oxidative phosphorylation in regulating programmed necroptosis needs to be explored further to determine which (or both) is critical for successful necroptosis signalling. Additionally, the significance of the partial externalisation of phosphatidyl serine to the outer leaflet of the plasma membrane needs to be studied in more detail, to determine if necroptosis can potentially result in an inflammation free mode of cell death.

The results have shown that inhibition of glycolysis can switch the mode of cell death from apoptosis to necrosis, and this needs to be investigated further in the 2DG model to determine if the sensitisation to TRAIL and ABT-737 is via apoptosis or necrosis. Also, the mechanisms by which 2DG activates AMPK remain to be determined, and the involvement of phosphatase regulation needs to be ruled out

before determining the upstream kinase. More importantly, the relevance of these findings in a clinical setting needs to be assessed. Additionally, the possible involvement of the mPTP on rotenone and antimycin-induced cell death needs to be evaluated using cyclosporine A in galactose^{+ve} cells, as the mass spectrometry data showed that Cyclophilin D is present in Z138 cells.

7 Appendix

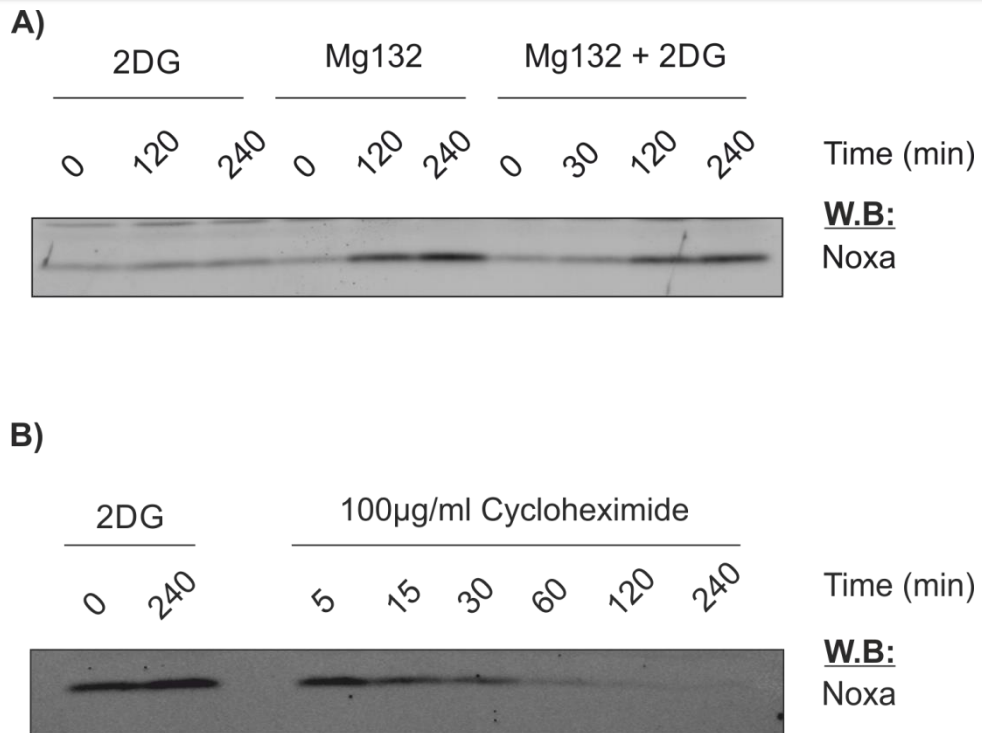


Figure 7-1 Noxa has a half-life of ~30 min. Z138 cells were cultured in standard glucose media (as described in Figure 4.1). Cells were treated with **A)** 5 mM 2DG, 20 µM MG132, or pre-treated with 20 µM MG132 for 30 min (lane 9) followed by 5 mM 2DG for the indicated times. cell pellets were then solubilised and immunoblotted for Noxa. **B)** Cells were treated with 5 mM 2DG or 100 µg/ml cycloheximide for the indicated times and then pellets solubilised and immunoblotted for Noxa.

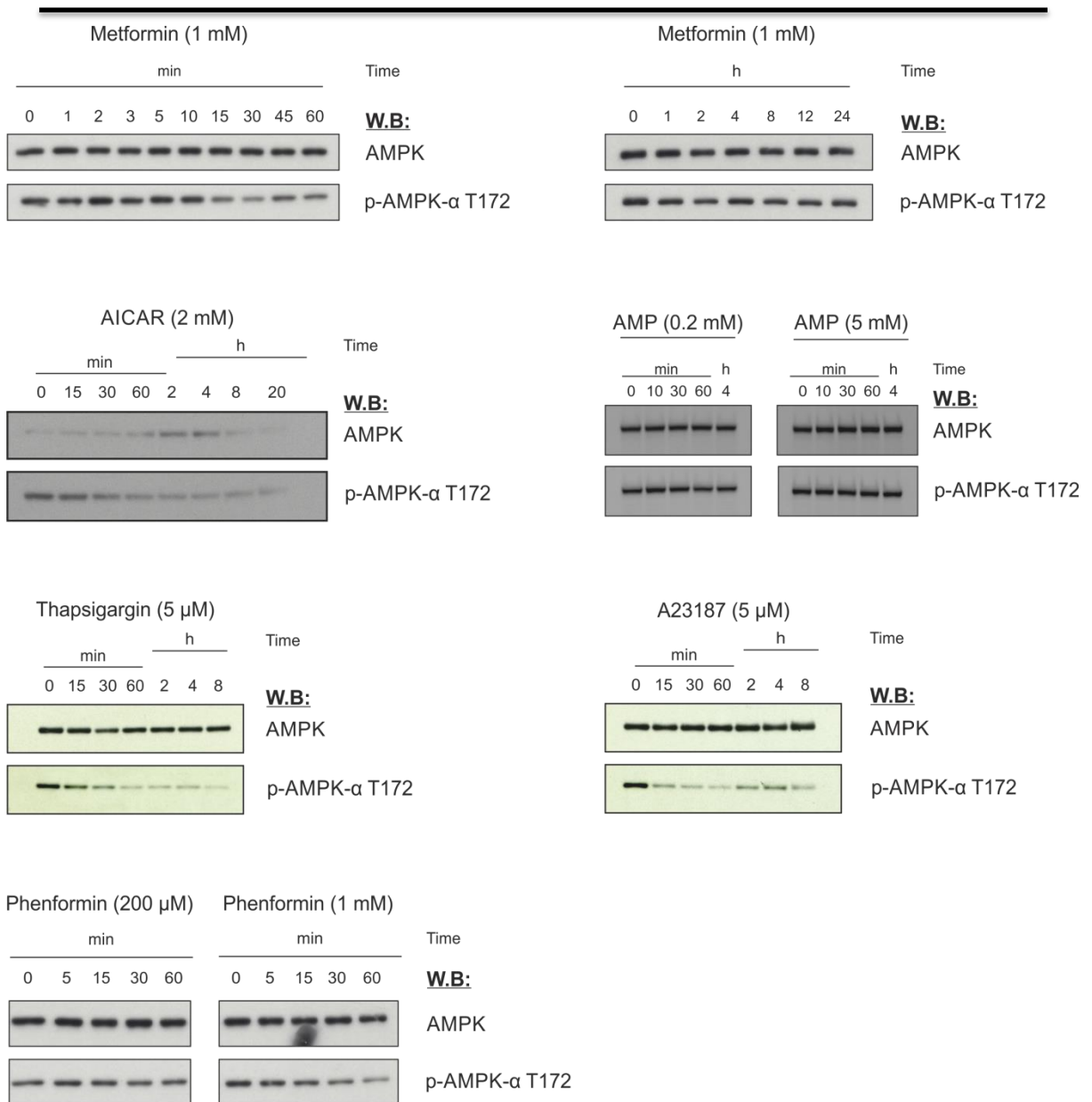


Figure 7-2 AMPK activators do not activate AMPK in Z138 cells. Z138 cells were cultured in standard glucose media (as described in Figure 4.1). Cells were then treated with metformin (1 mM); AICAR (2 mM); AMP (0.2 and 5 mM); thapsigargin (5 μM); A23187 (5 μM) or phenformin (200 μM and 1 mM) for the indicated times. Cell pellets were harvested and solubilised, and then immunoblotted for AMPK-α and p-AMPKα T172. Immunoblots representative of at least 2 independent experiments.

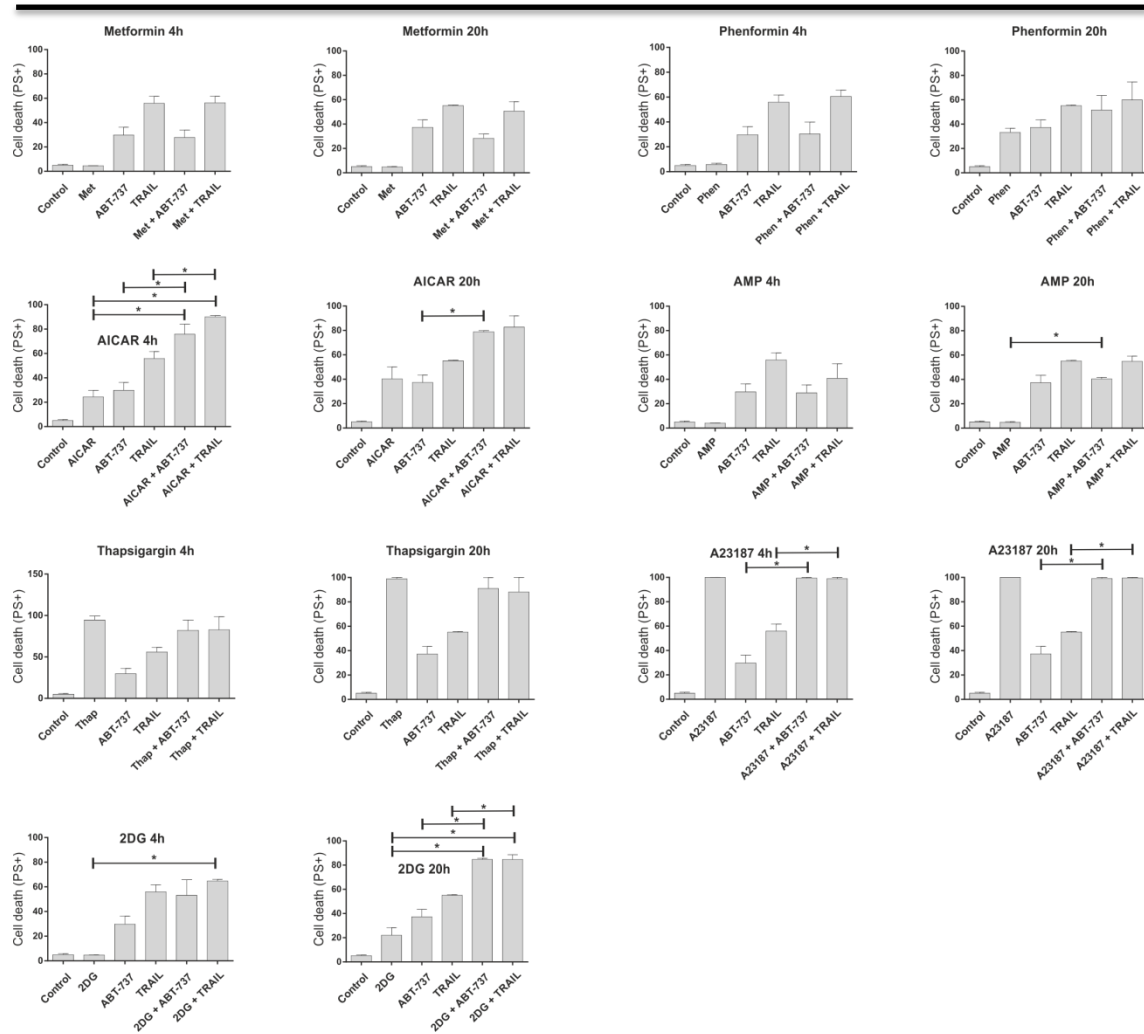


Figure 7-3 AMPK activators do not sensitise Z138 cells to TRAIL or ABT-737. Z138 cells were cultured in standard glucose media (as described in Figure 4.1). Cells were pre-treated with: metformin; phenformin; AICAR; AMP; thapsigargin; A23187 or 2DG with the [max] concentration detailed in Figure 4.9 for either 4 or 20 h, with or without 25 nM ABT-737 or 200 ng/ml TRAIL for 4 h after initial pre-treatment. Cell death was analysed by Annexin-V/PI FACS analysis. The data is presented as a % of total cell death (PS+). Data are from 3 independent experiments. Error bars are \pm SEM. Star (*) represents $p < 0.05$ (Students t test)

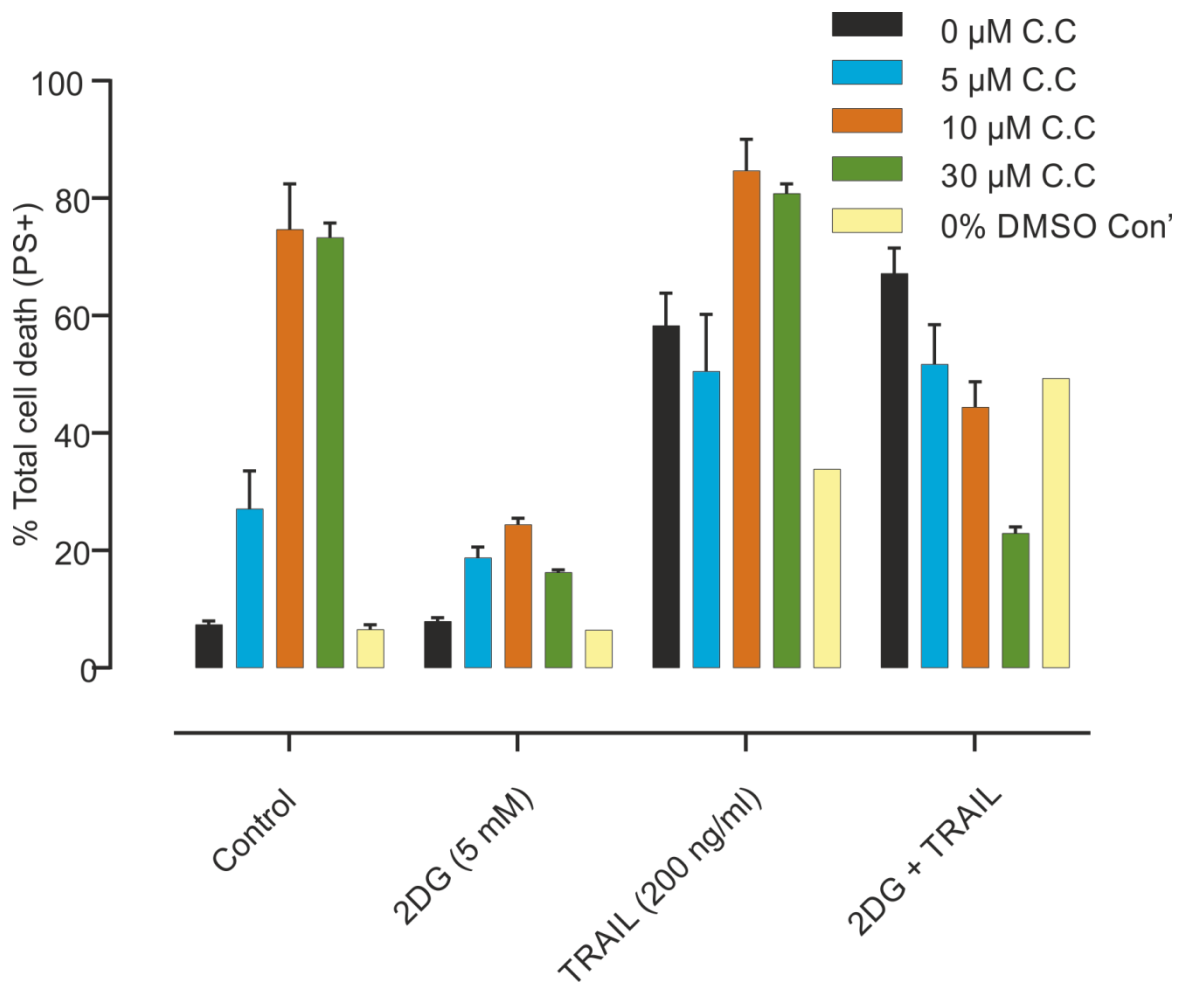


Figure 7-4 AMPK inhibition with compound C is toxic to Z138 cells. Z138 cells were cultured in standard glucose media (as described in Figure 4.1). Cells were pre-treated with: 0.1% DMSO (0 μ M); compound C (5, 10 and 30 μ M) or PBS (0% DMSO con') for 30 min, followed by: (from left to right) PBS for 8 h, 5mM 2DG for 8 h, 200 ng/ml TRAIL for 4 h or 5 mM 2DG for 4 h then an additional 4 h with 200 ng/ml TRAIL. Cell death was analysed with Annexin-V/PI FACS analysis, the data is presented as the % of total cell death (PS+). The data is from at least 3 independent experiments. Error bars are \pm SEM.

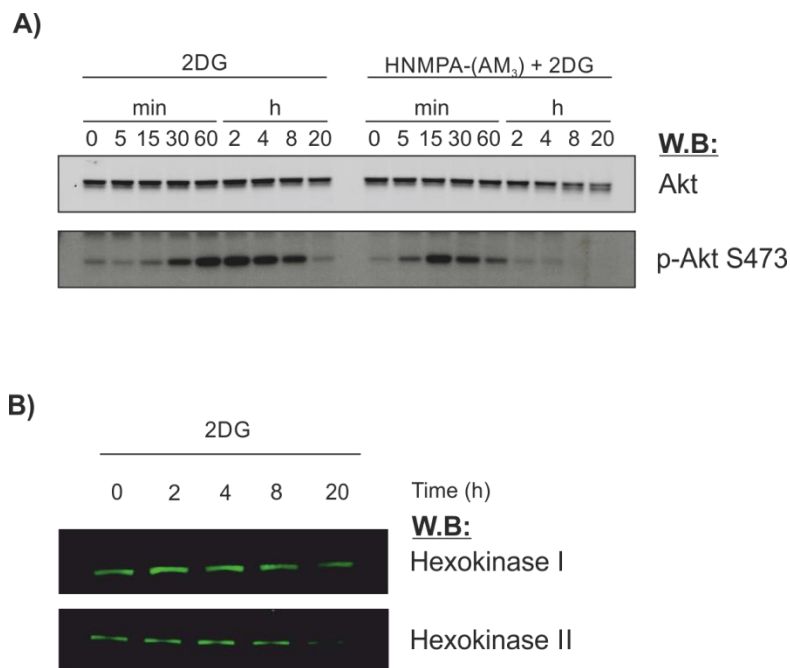


Figure 7-5 Insulin receptor tyrosine kinase inhibition does not prevent Akt activation following 2DG treatment. Z138 cells express both hexokinase I and II. Z138 cells were cultured in standard glucose media (as described in Figure 4.1). **A)** Cells were treated with 5 mM 2DG for the indicated times or pre-treated with 500 μ M HNMPA-(AM₃) for 30 min followed by 5 mM 2DG for the indicated times. The cell pellets were harvested and solubilised, then immunoblotted for Akt and p-Akt S473. **B)** Z138 cells were pre-treated with 5 mM 2DG for 0, 2, 4, 8 and 20 h, the pellets were solubilised and then immunoblotted for hexokinase I and hexokinase II.

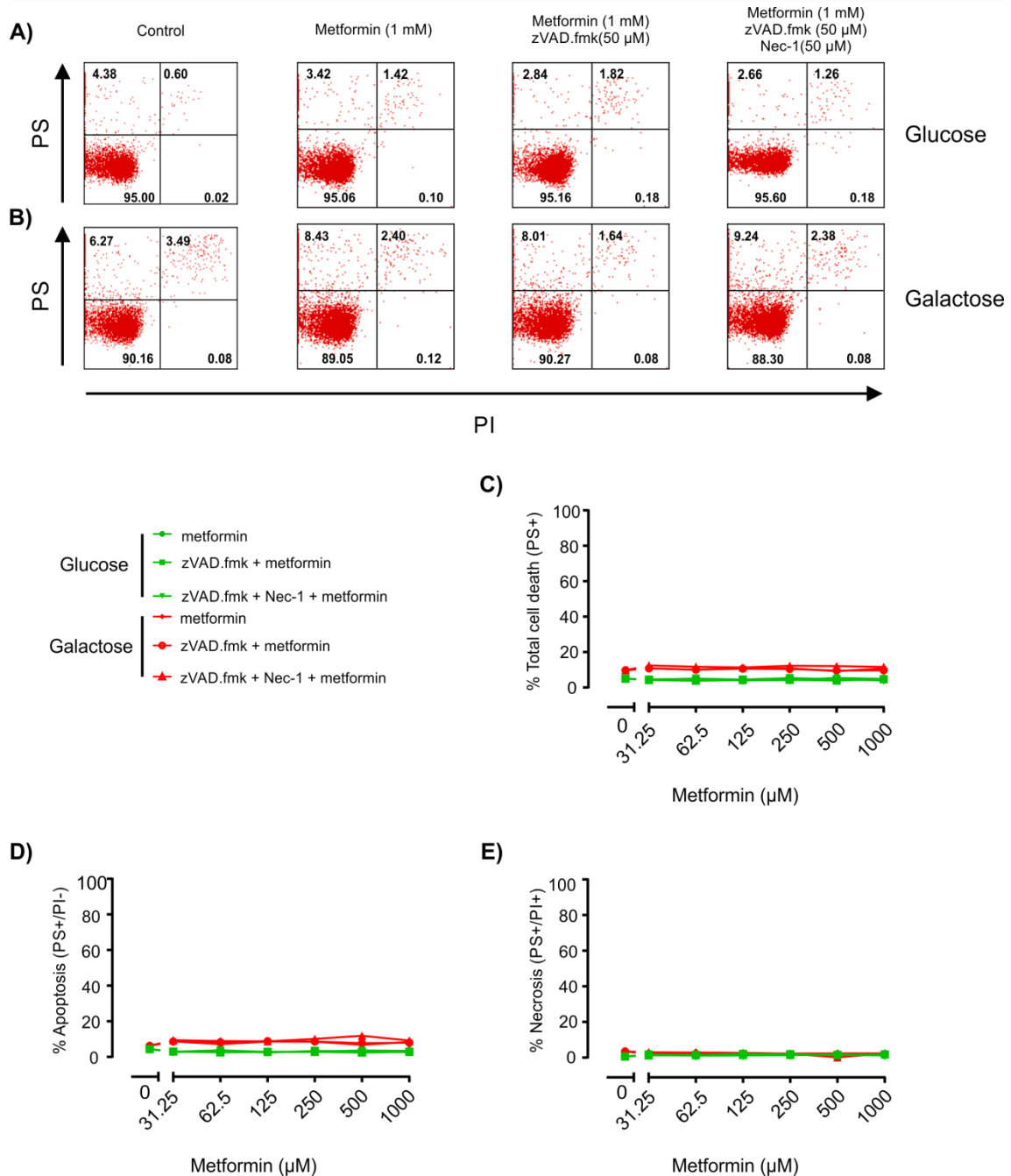


Figure 7-6 Z138 cells cultured in both glucose and galactose are resistant to metformin. Z138 cells were cultured in standard glucose or galactose media (as described in Figure 5-1) and were then pre-treated with 50 μ M zVAD.fmk and 50 μ M Nec-1 alone or in combination for 60 min followed by increasing concentrations of metformin (0 – 1 mM). **A)** Example FACS analysis of Annexin-V (PS⁺) labelling and propidium iodide (PI⁺) fluorescence in glucose⁺ cells after treatment with metformin (1000 μ M) shows that the cells are resistant **B)** Galactose⁺ cells treated with metformin (1000 μ M) were also resistant to death. **C)** The total cell death (PS⁺) was calculated and plotted as a concentration effect curve and shows metformin did not induce cell death at any concentration. **D)** There was no apoptotic cell death (PS⁺/PI⁻) at any concentration. **E)** There was no necrotic cell death (PS⁺/PI⁺) at any concentration. Data is a representative example from 2 independent experiments.

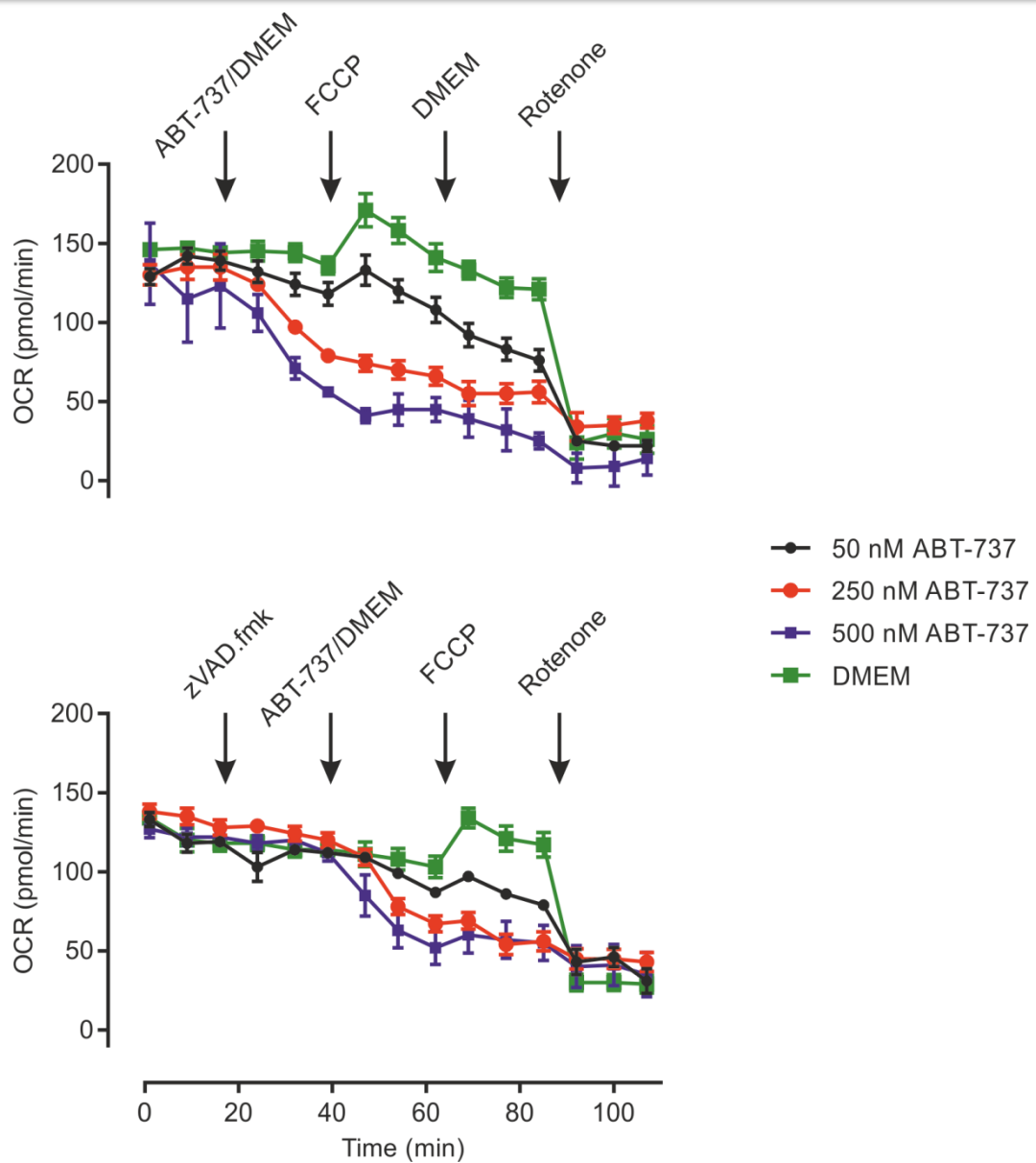


Figure 7-7 ABT-737 inhibits the mitochondrial respiratory chain. Z138 cells were cultured in 11.1 mM glucose as described in Chapter 2.2.1. OCR values were analysed after sequential injections of the indicated compounds/inhibitors. Top panel shows that ABT-737 inhibits the mitochondrial respiratory chain at concentrations as low as 50 nM. The bottom panel shows that mitochondrial respiratory chain inhibition by ABT-737 is not inhibited by pre-treatment with zVAD.fmk (50 μ M). Experiments are a representative example from 2 independent experiments.

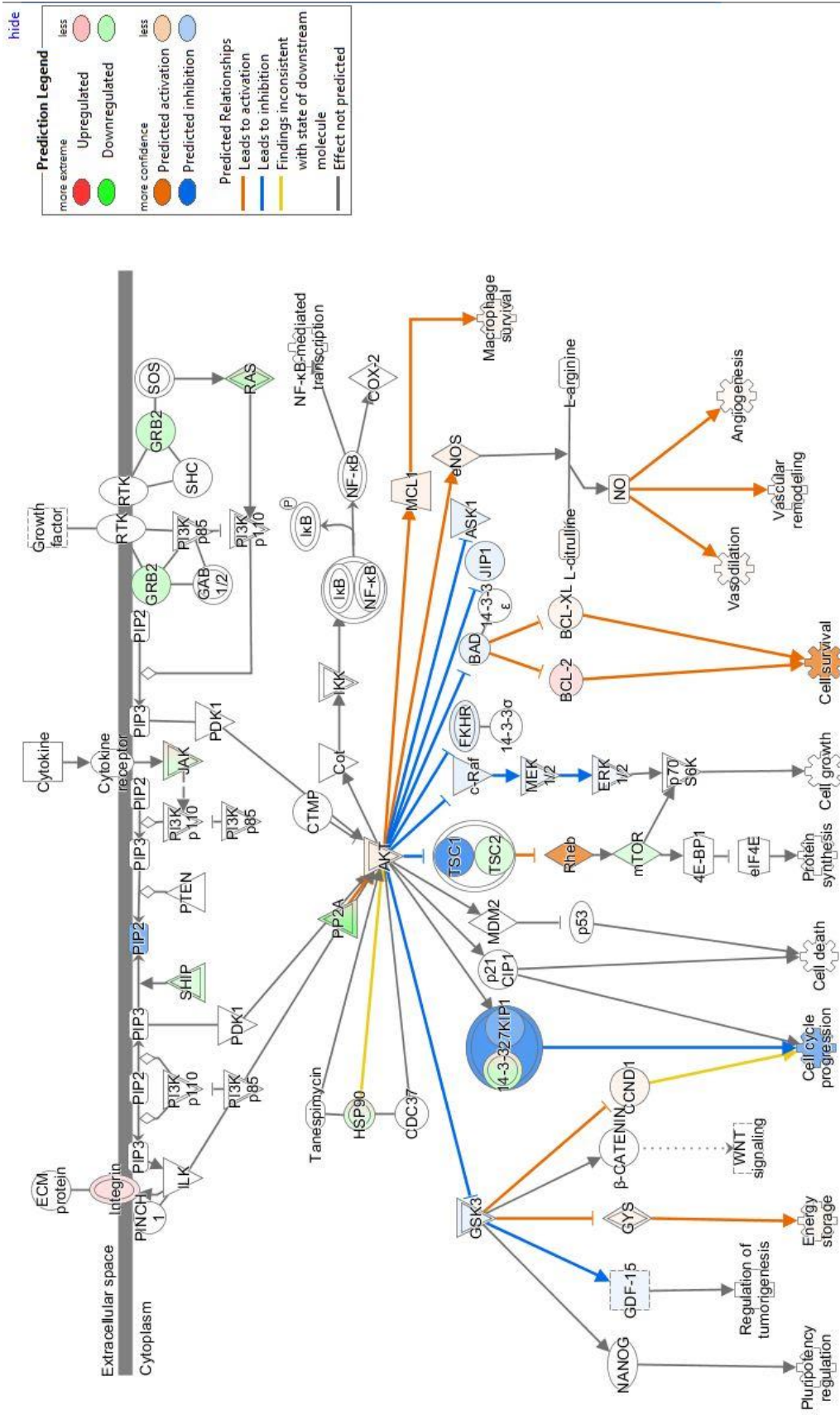


Figure 7-8 Ingenuity™ can successfully predict the activation status of signal transduction pathways. Schematic from Ingenuity™ that predicted Akt activation based on the normalised abundance data generated from TransOmics. Red proteins are up-regulated, green proteins are down-regulated. Blue proteins and arrows indicate inhibition while orange indicates activation.

© 2000-2015 QIAGEN. All rights reserved.							
Symbol	Entrez Gene Name	UniProt Accession	p-value	Fold Change	Location	Type(s)	Entrez Gene ID for Human
EIF2A	eukaryotic translation initiation factor 2A, 65kDa	Q9BY44	4.01E-01	-2.892	Cytoplasm	translation regulator	83939
EIF2AK3	eukaryotic translation initiation factor 2-alpha kinase 3	Q9NZJ5	2.22E-02	1.327	Cytoplasm	kinase	9451
EIF2S1	eukaryotic translation initiation factor 2, subunit 1 alpha, 35kDa	P05198	5.35E-01	1.049	Cytoplasm	translation regulator	1965
EIF3A	eukaryotic translation initiation factor 3, subunit A	Q14152	6.23E-02	-1.165	Cytoplasm	other	8661
EIF3B	eukaryotic translation initiation factor 3, subunit B	P55884	6.09E-02	-1.269	Cytoplasm	translation regulator	8662
EIF3C	eukaryotic translation initiation factor 3, subunit C	Q99613	6.91E-02	-1.317	Other	translation regulator	8663
EIF3J	eukaryotic translation initiation factor 3, subunit J	O75822	1.10E-01	-1.508	Cytoplasm	translation regulator	8669
EIF4A1	eukaryotic translation initiation factor 4A1	P60842	5.23E-01	-1.365	Cytoplasm	translation regulator	1973
EIF4A2	eukaryotic translation initiation factor 4A2	Q14240	9.26E-01	-1.324	Cytoplasm	translation regulator	1974
EIF4A3	eukaryotic translation initiation factor 4A3	P38919	5.69E-01	1.070	Nucleus	enzyme	9775
EIF4G1	eukaryotic translation initiation factor 4 gamma, 1	Q04637	7.75E-02	-1.362	Cytoplasm	translation regulator	1981
FAU	--	P62861	9.75E-01	1.367	Other	other	
GRB2	growth factor receptor-bound protein 2	P62993	7.83E-01	-1.772	Cytoplasm	other	2885
INSR	insulin receptor	P06213	1.09E-01	1.132	Plasma Membrane	kinase	3643
KRAS	Kirsten rat sarcoma viral oncogene homolog	P01116	2.72E-02	-2.425	Cytoplasm	enzyme	3845
NRAS	neuroblastoma RAS viral (v-ras) oncogene homolog	P01111	1.33E-01	1.861	Plasma Membrane	enzyme	4893
PABPC1	poly(A) binding protein, cytoplasmic 1	P11940	2.82E-03	-1.830	Cytoplasm	translation regulator	26986
PPP1CA	protein phosphatase 1, catalytic subunit, alpha isozyme	P62136	2.54E-01	-1.063	Cytoplasm	phosphatase	5499
PPP1CC	protein phosphatase 1, catalytic subunit, gamma isozyme	P36873	1.01E-01	-7.742	Nucleus	phosphatase	5501
RPL3	--	P39023	1.05E-03	1.289	Other	other	
RPL4	ribosomal protein L4	P36578	1.14E-02	-1.270	Cytoplasm	enzyme	6124
RPL5	ribosomal protein L5	P46777	3.61E-02	1.185	Cytoplasm	other	6125
RPL6	--	Q02878	8.50E-01	1.030	Other	other	
RPL7	ribosomal protein L7	P18124	5.82E-01	1.054	Nucleus	transcription regulator	6129
RPL8	ribosomal protein L8	P62917	5.18E-01	1.114	Other	other	6132
RPL9	--	P32969	3.14E-01	1.224	Other	other	
RPL10	ribosomal protein L10	P27635	9.96E-01	1.007	Cytoplasm	other	6134
RPL11	ribosomal protein L11	P62913	2.45E-02	1.284	Cytoplasm	other	6135
RPL12	ribosomal protein L12	P30050	2.93E-01	1.411	Nucleus	other	6136
RPL13	--	P26373	5.94E-01	-1.034	Other	other	
RPL14	ribosomal protein L14	P50914	8.60E-01	-1.012	Cytoplasm	other	9045
RPL15	ribosomal protein L15	P61313	5.63E-01	1.034	Cytoplasm	other	6138
RPL17	ribosomal protein L17	P18621	6.78E-01	1.067	Cytoplasm	other	6139
RPL18	ribosomal protein L18	Q07020	6.01E-01	1.085	Cytoplasm	other	6141
RPL19	ribosomal protein L19	P84098	1.93E-01	-1.192	Cytoplasm	other	6143
RPL21	--	P46778	2.18E-01	1.432	Other	other	
RPL22	ribosomal protein L22	P35268	2.65E-02	1.630	Nucleus	other	6146
RPL23	ribosomal protein L23	P62829	3.78E-01	1.710	Cytoplasm	other	9349
RPL24	ribosomal protein L24	P83731	4.48E-01	-1.097	Cytoplasm	other	6152
RPL26	ribosomal protein L26	P61254	8.86E-01	1.055	Cytoplasm	other	6154

RPL27	--	P61353	1.06E-04	1.451	Other	other	
RPL28	--	P46779	2.16E-01	1.467	Other	other	
RPL29	ribosomal protein L29	P47914	6.51E-01	-1.273	Cytoplasm	other	6159
RPL30	ribosomal protein L30	P62888	1.50E-01	1.519	Cytoplasm	other	6156
RPL31	ribosomal protein L31	P62899	4.68E-01	1.378	Cytoplasm	other	6160
RPL34	ribosomal protein L34	P49207	1.45E-01	1.210	Cytoplasm	other	6164
RPL35	ribosomal protein L35	P42766	6.92E-01	1.477	Cytoplasm	other	11224
RPL38	ribosomal protein L38	P63173	8.20E-01	1.223	Cytoplasm	other	6169
RPL10A	ribosomal protein L10a	P62906	6.17E-01	1.083	Nucleus	other	4736
RPL13A	ribosomal protein L13a	P40429	1.75E-01	1.167	Cytoplasm	other	23521
RPL18A	ribosomal protein L18a	Q02543	3.71E-01	1.160	Cytoplasm	other	6142
RPL23A	ribosomal protein L23a	P62750	3.63E-02	1.485	Other	other	6147
RPL27A	--	P46776	7.18E-02	1.211	Other	other	
RPL35A	ribosomal protein L35a	P18077	2.20E-03	2.404	Cytoplasm	other	6165
RPL36AL	ribosomal protein L36a-like	Q969Q0	3.04E-01	15.929	Cytoplasm	other	6166
RPL37A	ribosomal protein L37a	P61513	9.36E-01	1.123	Cytoplasm	other	6168
RPL7A	--	P62424	5.56E-01	1.059	Other	other	
RPLP0	--	P05388	7.19E-01	1.064	Other	other	
RPLP1	ribosomal protein, large, P1	P05386	7.46E-01	1.318	Cytoplasm	other	6176
RPLP2	ribosomal protein, large, P2	P05387	3.41E-01	2.003	Cytoplasm	other	6181
RPS2	--	P15880	1.03E-04	-1.693	Other	other	
RPS3	ribosomal protein S3	P23396	7.09E-01	1.137	Cytoplasm	enzyme	6188
RPS5	ribosomal protein S5	P46782	3.79E-03	-1.586	Cytoplasm	other	6193
RPS6	ribosomal protein S6	P62753	1.35E-03	-1.511	Cytoplasm	other	6194
RPS7	ribosomal protein S7	P62081	1.27E-01	-1.272	Cytoplasm	other	6201
RPS8	--	P62241	1.11E-02	-1.537	Other	other	
RPS9	ribosomal protein S9	P46781	6.21E-02	-1.730	Cytoplasm	translation regulator	6203
RPS10	ribosomal protein S10	P46783	1.73E-01	-1.270	Cytoplasm	other	6204
RPS11	ribosomal protein S11	P62280	8.28E-01	1.036	Cytoplasm	other	6205
RPS12	--	P25398	9.83E-01	1.640	Other	other	
RPS13	ribosomal protein S13	P62277	6.47E-01	1.025	Other	other	6207
RPS14	ribosomal protein S14	P62263	4.98E-01	1.352	Cytoplasm	translation regulator	6208
RPS16	ribosomal protein S16	P62249	8.84E-01	1.147	Cytoplasm	other	6217
RPS17	ribosomal protein S17	P0CW22	2.87E-01	-1.237	Cytoplasm	other	6218
RPS18	ribosomal protein S18	P62269	3.38E-02	-1.405	Cytoplasm	other	6222
RPS19	--	P39019	5.10E-01	-1.047	Other	other	
RPS20	ribosomal protein S20	P60866	9.69E-01	1.031	Cytoplasm	other	6224
RPS23	--	P62266	4.27E-01	1.074	Other	other	
RPS24	ribosomal protein S24	P62847	5.03E-01	1.386	Cytoplasm	other	6229
RPS25	ribosomal protein S25	P62851	3.05E-01	-1.212	Cytoplasm	other	6230
RPS26	ribosomal protein S26	P62854	3.66E-01	1.537	Cytoplasm	other	6231
RPS27	ribosomal protein S27	P42677	3.33E-02	-1.328	Cytoplasm	other	6232
RPS28	ribosomal protein S28	P62857	3.78E-01	-1.274	Cytoplasm	other	6234
RPS15A	ribosomal protein S15a	P62244	9.93E-01	1.172	Cytoplasm	other	6210
RPS3A	ribosomal protein S3A	P61247	2.11E-01	-1.125	Nucleus	other	6189
RPS4X	ribosomal protein S4, X-linked	P62701	4.24E-03	-1.686	Cytoplasm	other	6191
RPSA	ribosomal protein SA	P08865	4.88E-04	-1.844	Cytoplasm	translation regulator	3921
UBA52	ubiquitin A-52 residue ribosomal protein fusion product 1	P62987	4.52E-01	-1.043	Cytoplasm	enzyme	7311

Table 7-1 An example of the data Ingenuity uses to predict activation or inhibition of 1 protein. This table lists the TransOmics data that Ingenuity used to determine that eIF2- α would be activated. There are a total of 88 proteins used.

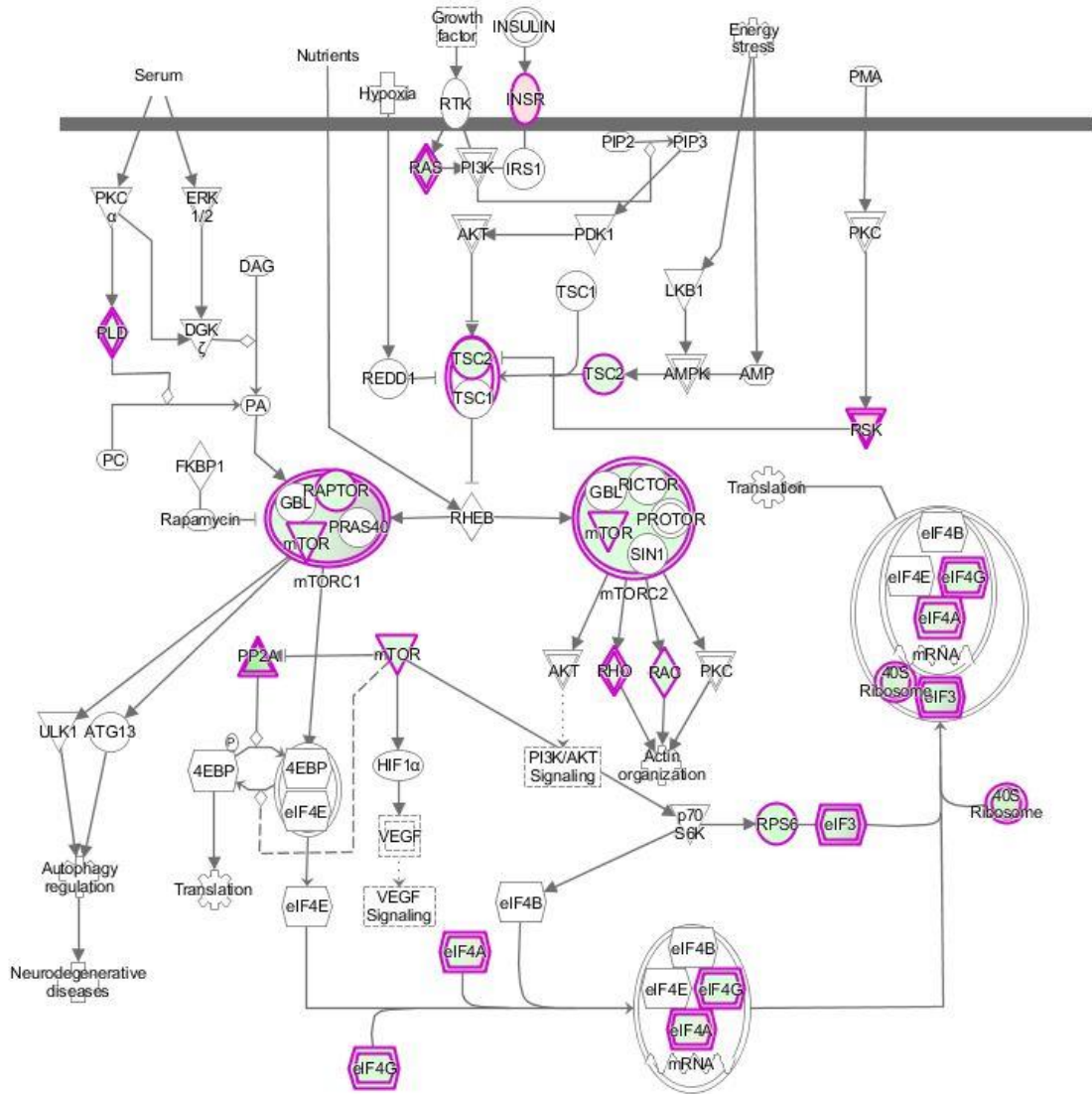


Figure 7-9 Proteins involved in protein synthesis are down-regulated. Based on 55 quantifiable proteins from TransOmics, Ingenuity successfully determined that protein translation would be reduced in galactose^{+ve} cells compared to glucose^{+ve} controls despite activated Akt.

8 References

-
- Acehan, D., Jiang, X., Morgan, D.G., Heuser, J.E., Wang, X., Akey, C.W., 2002. Three-dimensional structure of the apoptosome: implications for assembly, procaspase-9 binding, and activation. *Molecular Cell*. **9**, 423-432.
- Agarwal, E., Brattain, M.G., Chowdhury, S., 2013. Cell survival and metastasis regulation by Akt signaling in colorectal cancer. *Cellular Signalling*. **25**, 1711-1719.
- Alves, N.L., Derks, I.A., Berk, E., Spijker, R., van Lier, R.A., Eldering, E., 2006. The Noxa/Mcl-1 axis regulates susceptibility to apoptosis under glucose limitation in dividing T cells. *Immunity*. **24**, 703-716.
- Andrzejewski, S., Gravel, S.P., Pollak, M., St-Pierre, J., 2014. Metformin directly acts on mitochondria to alter cellular bioenergetics. *Cancer & Metabolism*. **2**, 12-3002-2-12. eCollection 2014.
- Bain, J., Plater, L., Elliott, M., Shpiro, N., Hastie, C.J., McLauchlan, H., Klevernic, I., Arthur, J.S., Alessi, D.R., Cohen, P., 2007. The selectivity of protein kinase inhibitors: a further update. *The Biochemical Journal*. **408**, 297-315.
- Barthel, A., Okino, S.T., Liao, J., Nakatani, K., Li, J., Whitlock, J.P., Jr, Roth, R.A., 1999. Regulation of GLUT1 gene transcription by the serine/threonine kinase Akt1. *The Journal of Biological Chemistry*. **274**, 20281-20286.
- Ben Sahra, I., Laurent, K., Giuliano, S., Larbret, F., Ponzio, G., Gounon, P., Le Marchand-Brustel, Y., Giorgetti-Peraldi, S., Cormont, M., Bertolotto, C., Deckert, M., Auberger, P., Tanti, J.F., Bost, F., 2010. Targeting cancer cell metabolism: the combination of metformin and 2-deoxyglucose induces p53-dependent apoptosis in prostate cancer cells. *Cancer Research*. **70**, 2465-2475.
- Bensinger, S.J. & Christofk, H.R., 2012. New aspects of the Warburg effect in cancer cell biology. *Seminars in Cell & Developmental Biology*. **23**, 352-361.
- Bernardi, P., 2013. The mitochondrial permeability transition pore: a mystery solved? *Frontiers in Physiology*. **4**, 95.
- Berthelet, J. & Dubrez, L., 2013. Regulation of Apoptosis by Inhibitors of Apoptosis (IAPs). *Cells*. **2**, 163-187.
- Billard, C., 2013. BH3 mimetics: status of the field and new developments. *Molecular Cancer Therapeutics*. **12**, 1691-1700.
- Boatright, K.M. & Salvesen, G.S., 2003. Mechanisms of caspase activation. *Current Opinion in Cell Biology*. **15**, 725-731.
- Boroughs, L.K. & DeBerardinis, R.J., 2015. Metabolic pathways promoting cancer cell survival and growth. *Nature Cell Biology*. **17**, 351-359.

-
- Bradford, M.M., 1976. A rapid and sensitive method for the quantitation of microgram quantities of protein utilizing the principle of protein-dye binding. *Analytical Biochemistry*. **72**, 248-254.
- Brand, M.D., Brindle, K.M., Buckingham, J.A., Harper, J.A., Rolfe, D.F., Stuart, J.A., 1999. The significance and mechanism of mitochondrial proton conductance. *International Journal of Obesity and Related Metabolic Disorders : Journal of the International Association for the Study of Obesity*. **23 Suppl 6**, S4-11.
- Brand, M.D., Pakay, J.L., Ocloo, A., Kokoszka, J., Wallace, D.C., Brookes, P.S., Cornwall, E.J., 2005. The basal proton conductance of mitochondria depends on adenine nucleotide translocase content. *The Biochemical Journal*. **392**, 353-362.
- Brand, M. & Nicholls, D., 2011. Assessing mitochondrial dysfunction in cells. *Biochemical Journal*. **435**, 297-312.
- Bremer, E., 2013. Targeting of the tumor necrosis factor receptor superfamily for cancer immunotherapy. *ISRN Oncology*. **2013**, 371854.
- Brown, G.C. & Borutaite, V., 2008. Regulation of apoptosis by the redox state of cytochrome c. *Biochimica Et Biophysica Acta*. **1777**, 877-881.
- Burgering, B.M. & Coffey, P.J., 1995. Protein kinase B (c-Akt) in phosphatidylinositol-3-OH kinase signal transduction. *Nature*. **376**, 599-602.
- Cai, Z., Jitkaew, S., Zhao, J., Chiang, H.C., Choksi, S., Liu, J., Ward, Y., Wu, L.G., Liu, Z.G., 2014. Plasma membrane translocation of trimerized MLKL protein is required for TNF-induced necroptosis. *Nature Cell Biology*. **16**, 55-65.
- Cain, K., Bratton, S.B., Cohen, G.M., 2002. The Apaf-1 apoptosome: a large caspase-activating complex. *Biochimie*. **84**, 203-214.
- Cairns, R.A., Harris, I.S., Mak, T.W., 2011. Regulation of cancer cell metabolism. **11**, 85-95.
- Campo, E. & Rule, S., 2015. Mantle cell lymphoma: evolving management strategies. *Blood*. **125**, 48-55.
- Cantor, J.R. & Sabatini, D.M., 2012. Cancer cell metabolism: one hallmark, many faces. *Cancer Discovery*. **2**, 881-898.
- Cao, X., Fang, L., Gibbs, S., Huang, Y., Dai, Z., Wen, P., Zheng, X., Sadee, W., Sun, D., 2007. Glucose uptake inhibitor sensitizes cancer cells to daunorubicin and overcomes drug resistance in hypoxia. *Cancer Chemotherapy and Pharmacology*. **59**, 495-505.
- Caraco, C., Aloj, L., Chen, L.Y., Chou, J.Y., Eckelman, W.C., 2000. Cellular release of [¹⁸F]2-fluoro-2-deoxyglucose as a function of the glucose-6-

-
- phosphatase enzyme system. *The Journal of Biological Chemistry*. **275**, 18489-18494.
- Caro-Maldonado, A., Tait, S.W., Ramirez-Peinado, S., Ricci, J.E., Fabregat, I., Green, D.R., Munoz-Pinedo, C., 2010. Glucose deprivation induces an atypical form of apoptosis mediated by caspase-8 in Bax-, Bak-deficient cells. *Cell Death and Differentiation*. **17**, 1335-1344.
- Certo, M., Del Gaizo Moore, V., Nishino, M., Wei, G., Korsmeyer, S., Armstrong, S.A., Letai, A., 2006. Mitochondria primed by death signals determine cellular addiction to antiapoptotic BCL-2 family members. *Cancer Cell*. **9**, 351-365.
- Chance, B. & Williams, G.R., 1955. Respiratory enzymes in oxidative phosphorylation. I. Kinetics of oxygen utilization. *The Journal of Biological Chemistry*. **217**, 383-393.
- Chen, L., Willis, S.N., Wei, A., Smith, B.J., Fletcher, J.I., Hinds, M.G., Colman, P.M., Day, C.L., Adams, J.M., Huang, D.C.S., 2005. Differential Targeting of Prosurvival Bcl-2 Proteins by Their BH3-Only Ligands Allows Complementary Apoptotic Function. *Molecular Cell*. **17**, 393-403.
- Chen, W.W., Yu, H., Fan, H.B., Zhang, C.C., Zhang, M., Zhang, C., Cheng, Y., Kong, J., Liu, C.F., Geng, D., Xu, X., 2012. RIP1 mediates the protection of geldanamycin on neuronal injury induced by oxygen-glucose deprivation combined with zVAD in primary cortical neurons. *Journal of Neurochemistry*. **120**, 70-77.
- Chen, X., Li, W., Ren, J., Huang, D., He, W.T., Song, Y., Yang, C., Li, W., Zheng, X., Chen, P., Han, J., 2014. Translocation of mixed lineage kinase domain-like protein to plasma membrane leads to necrotic cell death. *Cell Research*. **24**, 105-121.
- Cho, Y.S., McQuade, T., Zhang, H., Zhang, J., Chan, F.K.M., 2011. RIP1-Dependent and Independent Effects of Necrostatin-1 in Necrosis and T Cell Activation. *PLoS ONE*. **6**, e23209. doi:10.1371/journal.pone.0023209.
- Coller, H.A., 2014. Is Cancer a Metabolic Disease? *The American Journal of Pathology*. **184**, 4-17.
- Corradetti, M.N., Inoki, K., Bardeesy, N., DePinho, R.A., Guan, K.L., 2004. Regulation of the TSC pathway by LKB1: evidence of a molecular link between tuberous sclerosis complex and Peutz-Jeghers syndrome. *Genes & Development*. **18**, 1533-1538.
- Craxton, A., Butterworth, M., Harper, N., Fairall, L., Schwabe, J., Ciechanover, A., Cohen, G.M., 2012. NOXA, a sensor of proteasome integrity, is degraded by 26S proteasomes by an ubiquitin-independent pathway that is blocked by MCL-1. *Cell Death and Differentiation*. **19**, 1424-1434.

-
- Cross, D.A., Alessi, D.R., Cohen, P., Andjelkovich, M., Hemmings, B.A., 1995. Inhibition of glycogen synthase kinase-3 by insulin mediated by protein kinase B. *Nature*. **378**, 785-789.
- Cuconati, A., Mukherjee, C., Perez, D., White, E., 2003. DNA damage response and MCL-1 destruction initiate apoptosis in adenovirus-infected cells. *Genes & Development*. **17**, 2922-2932.
- Czabotar, P.E., Lessene, G., Strasser, A., Adams, J.M., 2014. Control of apoptosis by the BCL-2 protein family: implications for physiology and therapy. *Nature Reviews.Molecular Cell Biology*. **15**, 49-63.
- da Cunha, F.M., Torelli, N.Q., Kowaltowski, A.J., 2015. Mitochondrial Retrograde Signaling: Triggers, Pathways, and Outcomes. *Oxidative Medicine and Cellular Longevity*.
- Dagon, Y., Avraham, Y., Berry, E.M., 2006. AMPK activation regulates apoptosis, adipogenesis, and lipolysis by eIF2alpha in adipocytes. *Biochemical and Biophysical Research Communications*. **340**, 43-47.
- Dagon, Y., Avraham, Y., Magen, I., Gertler, A., Ben-Hur, T., Berry, E.M., 2005. Nutritional status, cognition, and survival: a new role for leptin and AMP kinase. *The Journal of Biological Chemistry*. **280**, 42142-42148.
- Danial, N.N., 2008. BAD: undertaker by night, candyman by day. *Oncogene*. **27 Suppl 1**, S53-70.
- Dann, S.G., Selvaraj, A., Thomas, G., 2007. mTOR Complex1-S6K1 signaling: at the crossroads of obesity, diabetes and cancer. *Trends in Molecular Medicine*. **13**, 252-259.
- Datta, S.R., Dudek, H., Tao, X., Masters, S., Fu, H., Gotoh, Y., Greenberg, M.E., 1997. Akt Phosphorylation of BAD Couples Survival Signals to the Cell-Intrinsic Death Machinery. *Cell*. **91**, 231-241.
- Davids, M.S. & Letai, A., 2012. Targeting the B-cell lymphoma/leukemia 2 family in cancer. *Journal of Clinical Oncology : Official Journal of the American Society of Clinical Oncology*. **30**, 3127-3135.
- Degterev, A., Huang, Z., Boyce, M., Li, Y., Jagtap, P., Mizushima, N., Cuny, G.D., Mitchison, T.J., Moskowitz, M.A., Yuan, J., 2005. Chemical inhibitor of nonapoptotic cell death with therapeutic potential for ischemic brain injury. *Nature Chemical Biology*. **1**, 112-119.
- Deprez, J., Vertommen, D., Alessi, D.R., Hue, L., Rider, M.H., 1997. Phosphorylation and activation of heart 6-phosphofructo-2-kinase by protein kinase B and other protein kinases of the insulin signaling cascades. *The Journal of Biological Chemistry*. **272**, 17269-17275.

-
- Dickens, L.S., Boyd, R.S., Jukes-Jones, R., Hughes, M.A., Robinson, G.L., Fairall, L., Schwabe, J.W., Cain, K., Macfarlane, M., 2012a. A death effector domain chain DISC model reveals a crucial role for caspase-8 chain assembly in mediating apoptotic cell death. *Molecular Cell*. **47**, 291-305.
- Dickens, L.S., Powley, I.R., Hughes, M.A., MacFarlane, M., 2012b. The 'complexities' of life and death: death receptor signalling platforms. *Experimental Cell Research*. **318**, 1269-1277.
- Ding, Q., He, X., Hsu, J.M., Xia, W., Chen, C.T., Li, L.Y., Lee, D.F., Liu, J.C., Zhong, Q., Wang, X., Hung, M.C., 2007. Degradation of Mcl-1 by I²-TrCP Mediates Glycogen Synthase Kinase 3-Induced Tumor Suppression and Chemosensitization. *Molecular and Cellular Biology*. **27**, 4006-4017.
- Dondelinger, Y., Declercq, W., Montessuit, S., Roelandt, R., Goncalves, A., Bruggeman, I., Hulpiau, P., Weber, K., Sehon, C., Marquis, R., Bertin, J., Gough, P., Savvides, S., Martinou, J., Bertrand, M.M., Vandenameele, P., 2014. MLKL Compromises Plasma Membrane Integrity by Binding to Phosphatidylinositol Phosphates. *Cell Reports*. **7**, 971-981.
- Donepudi, M. & Grutter, M.G., 2002. Structure and zymogen activation of caspases. *Biophysical Chemistry*. **101-102**, 145-153.
- Dott, W., Mistry, P., Wright, J., Cain, K., Herbert, K.E., 2014. Modulation of mitochondrial bioenergetics in a skeletal muscle cell line model of mitochondrial toxicity(). *Redox Biology*. **2**, 224-233.
- Drose, S. & Brandt, U., 2012. Molecular mechanisms of superoxide production by the mitochondrial respiratory chain. *Advances in Experimental Medicine and Biology*. **748**, 145-169.
- Durante, P., Gueuning, M., Darville, M.I., Hue, L., Rousseau, G.G., 1999. Apoptosis induced by growth factor withdrawal in fibroblasts overproducing fructose 2,6-bisphosphate. *FEBS Letters*. **448**, 239-243.
- Dykens, J.A., Jamieson, J.D., Marroquin, L.D., Nadanaciva, S., Xu, J.J., Dunn, M.C., Smith, A.R., Will, Y., 2008. In vitro assessment of mitochondrial dysfunction and cytotoxicity of nefazodone, trazodone, and buspirone. *Toxicological Sciences : An Official Journal of the Society of Toxicology*. **103**, 335-345.
- Eichhorn, J.M., Alford, S.E., Sakurikar, N., Chambers, T.C., 2014. Molecular analysis of functional redundancy among anti-apoptotic Bcl-2 proteins and its role in cancer cell survival. *Experimental Cell Research*. **322**, 415-424.
- Elmore, S., 2007. Apoptosis: a review of programmed cell death. *Toxicologic Pathology*. **35**, 495-516.
- Estrov, Z., Talpaz, M., Ku, S., Harris, D., Van, Q., Beran, M., Hirsch-Ginsberg, C., Huh, Y., Yee, G., Kurzrock, R., 1998. Z-138: a new mature B-cell acute

-
- lymphoblastic leukemia cell line from a patient with transformed chronic lymphocytic leukemia. *Leukemia Research*. **22**, 341-353.
- Evan, G.I. & Vousden, K.H., 2001. Proliferation, cell cycle and apoptosis in cancer. *Nature*. **411**, 342-348.
- Fadok, V.A., Voelker, D.R., Campbell, P.A., Cohen, J.J., Bratton, D.L., Henson, P.M., 1992. Exposure of phosphatidylserine on the surface of apoptotic lymphocytes triggers specific recognition and removal by macrophages. *Journal of Immunology (Baltimore, Md.: 1950)*. **148**, 2207-2216.
- Fedorenko, A., Lishko, P.V., Kirichok, Y., 2012. Mechanism of fatty-acid-dependent UCP1 uncoupling in brown fat mitochondria. *Cell*. **151**, 400-413.
- Fendel, U., Tocilescu, M.A., Kerscher, S., Brandt, U., 2008. Exploring the inhibitor binding pocket of respiratory complex I. *Biochimica Et Biophysica Acta*. **1777**, 660-665.
- Ferlay, J., Soerjomataram, I., Dikshit, R., Eser, S., Mathers, C., Rebelo, M., Parkin, D.M., Forman, D., Bray, F., 2015. Cancer incidence and mortality worldwide: sources, methods and major patterns in GLOBOCAN 2012. *International Journal of Cancer. Journal International Du Cancer*. **136**, E359-86.
- Fernandes-Alnemri, T., Litwack, G., Alnemri, E.S., 1994. CPP32, a novel human apoptotic protein with homology to *Caenorhabditis elegans* cell death protein Ced-3 and mammalian interleukin-1 beta-converting enzyme. *The Journal of Biological Chemistry*. **269**, 30761-30764.
- Fu, X., Wan, S., Lyu, Y.L., Liu, L.F., Qi, H., 2008. Etoposide induces ATM-dependent mitochondrial biogenesis through AMPK activation. *PloS One*. **3**, e2009.
- Fuentes-Prior, P. & Salvesen, G., 2004. The protein structures that shape caspase activity, specificity, activation and inhibition. *Biochemical Journal*. **384**, 201-232.
- Galluzzi, L., Kepp, O., Kroemer, G., 2014. MLKL regulates necrotic plasma membrane permeabilization. *Cell Research*. **24**, 139-140.
- Gambhir, S.S., 2002. Molecular imaging of cancer with positron emission tomography. *Nature Reviews. Cancer*. **2**, 683-693.
- Ganapathy-Kanniappan, S. & Geschwind, J.F., 2013. Tumor glycolysis as a target for cancer therapy: progress and prospects. *Molecular Cancer*. **12**, 152-4598-12-152.
- Garami, A., Zwartkuis, F.J., Nobukuni, T., Joaquin, M., Rocco, M., Stocker, H., Kozma, S.C., Hafen, E., Bos, J.L., Thomas, G., 2003. Insulin activation of Rheb, a mediator of mTOR/S6K/4E-BP signaling, is inhibited by TSC1 and 2. *Molecular Cell*. **11**, 1457-1466.

Germain, M., Nguyen, A.P., Le Grand, J.N., Arbour, N., Vanderluit, J.L., Park, D.S., Opferman, J.T., Slack, R.S., 2011. MCL-1 is a stress sensor that regulates autophagy in a developmentally regulated manner. *The EMBO Journal*. **30**, 395-407.

Ghielmini, M. & Zucca, E., 2009. How I treat mantle cell lymphoma. *Blood*. **114**, 1469-1476.

Giammarioli, A.M., Gambardella, L., Barbati, C., Pietraforte, D., Tinari, A., Alberton, M., Gnessi, L., Griffin, R.J., Minetti, M., Malorni, W., 2012. Differential effects of the glycolysis inhibitor 2-deoxy-D-glucose on the activity of pro-apoptotic agents in metastatic melanoma cells, and induction of a cytoprotective autophagic response. *International Journal of Cancer. Journal International Du Cancer*. **131**, E337-47.

Gillies, R.J., Robey, I., Gatenby, R.A., 2008. Causes and consequences of increased glucose metabolism of cancers. *Journal of Nuclear Medicine : Official Publication, Society of Nuclear Medicine*. **49 Suppl 2**, 24S-42S.

Gingras, A.C., Raught, B., Gygi, S.P., Niedzwiecka, A., Miron, M., Burley, S.K., Polakiewicz, R.D., Wyslouch-Cieszynska, A., Aebersold, R., Sonenberg, N., 2001. Hierarchical phosphorylation of the translation inhibitor 4E-BP1. *Genes & Development*. **15**, 2852-2864.

Gohil, V.M., Sheth, S.A., Nilsson, R., Wojtovich, A.P., Lee, J.H., Perocchi, F., Chen, W., Clish, C.B., Ayata, C., Brookes, P.S., Mootha, V.K., 2010. Nutrient-sensitized screening for drugs that shift energy metabolism from mitochondrial respiration to glycolysis. **28**, 249-255.

Gonin-Giraud, S., Mathieu, A.L., Diocou, S., Tomkowiak, M., Delorme, G., Marvel, J., 2002. Decreased glycolytic metabolism contributes to but is not the inducer of apoptosis following IL-3-starvation. *Cell Death and Differentiation*. **9**, 1147-1157.

Gonzalvez, F., Lawrence, D., Yang, B., Yee, S., Pitti, R., Marsters, S., Pham, V.C., Stephan, J.P., Lill, J., Ashkenazi, A., 2012. TRAF2 Sets a threshold for extrinsic apoptosis by tagging caspase-8 with a ubiquitin shutoff timer. *Molecular Cell*. **48**, 888-899.

Gorrini, C., Harris, I.S., Mak, T.W., 2013. Modulation of oxidative stress as an anticancer strategy. **12**, 931-947.

Gowans, G., Hawley, S., Ross, F., Hardie, D. ., 2013. AMP Is a True Physiological Regulator of AMP-Activated Protein Kinase by Both Allosteric Activation and Enhancing Net Phosphorylation. *Cell Metabolism*. **18**, 556-566.

Grun, B.R., Berger, U., Oberdorfer, F., Hull, W.E., Ostertag, H., Keppler, D., 1990. In vivo metabolism and UTP-depleting action of 2-deoxy-2-fluoro-D-galactose. *Advances in Enzyme Regulation*. **30**, 231-242.

-
- Gwinn, D.M., Shackelford, D.B., Egan, D.F., Mihaylova, M.M., Mery, A., Vasquez, D.S., Turk, B.E., Shaw, R.J., 2008. AMPK phosphorylation of raptor mediates a metabolic checkpoint. *Molecular Cell*. **30**, 214-226.
- Hajdуч, E., Alessi, D.R., Hemmings, B.A., Hundal, H.S., 1998. Constitutive activation of protein kinase B alpha by membrane targeting promotes glucose and system A amino acid transport, protein synthesis, and inactivation of glycogen synthase kinase 3 in L6 muscle cells. *Diabetes*. **47**, 1006-1013.
- Halicka, H.D., Ardelt, B., Li, X., Melamed, M.M., Darzynkiewicz, Z., 1995. 2-Deoxy-D-glucose enhances sensitivity of human histiocytic lymphoma U937 cells to apoptosis induced by tumor necrosis factor. *Cancer Research*. **55**, 444-449.
- Han, J., Zhong, C., Zhang, D., 2011. Programmed necrosis: backup to and competitor with apoptosis in the immune system. *Nature Immunology*. **12**, 1143-1149.
- Hanahan, D. & Weinberg, R.A., 2011. Hallmarks of cancer: the next generation. *Cell*. **144**, 646-674.
- Happo, L., Strasser, A., Cory, S., 2012. BH3-only proteins in apoptosis at a glance. *Journal of Cell Science*. **125**, 1081-1087.
- Hardie, D.G., 2015. AMPK: positive and negative regulation, and its role in whole-body energy homeostasis. *Current Opinion in Cell Biology*. **33**, 1-7.
- Hardie, D.G., 2014. AMP-activated protein kinase: maintaining energy homeostasis at the cellular and whole-body levels. *Annual Review of Nutrition*. **34**, 31-55.
- Hardie, D.G., 2013. AMPK: a target for drugs and natural products with effects on both diabetes and cancer. *Diabetes*. **62**, 2164-2172.
- Hardie, D.G., 2011. AMP-activated protein kinase: an energy sensor that regulates all aspects of cell function. *Genes & Development*. **25**, 1895-1908.
- Hardie, D.G., 2007. AMP-activated/SNF1 protein kinases: conserved guardians of cellular energy. *Nature Reviews. Molecular Cell Biology*. **8**, 774-785.
- Hart, J.R. & Vogt, P.K., 2011. Phosphorylation of AKT: a Mutational Analysis. *Oncotarget*. **2**, 467-476.
- Hawley, S.A., Boudeau, J., Reid, J.L., Mustard, K.J., Udd, L., Makela, T.P., Alessi, D.R., Hardie, D.G., 2003. Complexes between the LKB1 tumor suppressor, STRAD alpha/beta and MO25 alpha/beta are upstream kinases in the AMP-activated protein kinase cascade. *Journal of Biology*. **2**, 28.
- Hawley, S.A., Ross, F.A., Chevtzoff, C., Green, K.A., Evans, A., Fogarty, S., Towler, M.C., Brown, L.J., Ogunbayo, O.A., Evans, A.M., Hardie, D.G., 2010.

Use of cells expressing gamma subunit variants to identify diverse mechanisms of AMPK activation. *Cell Metabolism*. **11**, 554-565.

Hemminki, A., Markie, D., Tomlinson, I., Avizienyte, E., Roth, S., Loukola, A., Bignell, G., Warren, W., Aminoff, M., Hoglund, P., Jarvinen, H., Kristo, P., Pelin, K., Ridanpaa, M., Salovaara, R., Toro, T., Bodmer, W., Olschwang, S., Olsen, A.S., Stratton, M.R., de la Chapelle, A., Aaltonen, L.A., 1998. A serine/threonine kinase gene defective in Peutz-Jeghers syndrome. *Nature*. **391**, 184-187.

Hensley, C.T., Wasti, A.T., DeBerardinis, R.J., 2013. Glutamine and cancer: cell biology, physiology, and clinical opportunities. *The Journal of Clinical Investigation*. **123**, 3678-3684.

Herst, P.M. & Berridge, M.V., 2007. Cell surface oxygen consumption: a major contributor to cellular oxygen consumption in glycolytic cancer cell lines. *Biochimica Et Biophysica Acta*. **1767**, 170-177.

Hochreiter-Hufford, A. & Ravichandran, K.S., 2013. Clearing the dead: apoptotic cell sensing, recognition, engulfment, and digestion. *Cold Spring Harbor Perspectives in Biology*. **5**, a008748.

Holoch, P.A. & Griffith, T.S., 2009. TNF-related apoptosis-inducing ligand (TRAIL): a new path to anti-cancer therapies. *European Journal of Pharmacology*. **625**, 63-72.

Hsu, P.P. & Sabatini, D.M., 2008. Cancer cell metabolism: Warburg and beyond. *Cell*. **134**, 703-707.

Hu, C.J., Wang, L.Y., Chodosh, L.A., Keith, B., Simon, M.C., 2003. Differential Roles of Hypoxia-Inducible Factor 1 α (HIF-1 α) and HIF-2 α in Hypoxic Gene Regulation. *Molecular and Cellular Biology*. **23**, 9361-9374.

Huang, C.Y., Kuo, W.T., Huang, Y.C., Lee, T.C., Yu, L.C., 2013. Resistance to hypoxia-induced necroptosis is conferred by glycolytic pyruvate scavenging of mitochondrial superoxide in colorectal cancer cells. *Cell Death & Disease*. **4**, e622.

Huang, L.S., Cobessi, D., Tung, E.Y., Berry, E.A., 2005. Binding of the respiratory chain inhibitor antimycin to the mitochondrial bc1 complex: a new crystal structure reveals an altered intramolecular hydrogen-bonding pattern. *Journal of Molecular Biology*. **351**, 573-597.

Hudson, A.L., Weir, C., Moon, E., Harvie, R., Klebe, S., Clarke, S.J., Pavlakis, N., Howell, V.M., 2014. Establishing a panel of chemo-resistant mesothelioma models for investigating chemo-resistance and identifying new treatments for mesothelioma. *Cell*. **4**, 6152.

Hughes, M.A., Harper, N., Butterworth, M., Cain, K., Cohen, G.M., MacFarlane, M., 2009. Reconstitution of the Death-Inducing Signaling Complex Reveals a

Substrate Switch that Determines CD95-Mediated Death or Survival. *Molecular Cell*. **35**, 265-279.

Hüttemann, M., Pecina, P., Rainbolt, M., Sanderson, T.H., Kagan, V.E., Samavati, L., Doan, J.W., Lee, I., 2011. The multiple functions of cytochrome c and their regulation in life and death decisions of the mammalian cell: from respiration to apoptosis. *Mitochondrion*. **11**, 369-381.

Inoki, K., Li, Y., Xu, T., Guan, K.L., 2003a. Rheb GTPase is a direct target of TSC2 GAP activity and regulates mTOR signaling. *Genes & Development*. **17**, 1829-1834.

Inoki, K., Zhu, T., Guan, K.L., 2003b. TSC2 mediates cellular energy response to control cell growth and survival. *Cell*. **115**, 577-590.

Inoki, K., Li, Y., Zhu, T., Wu, J., Guan, K., 2002. TSC2 is phosphorylated and inhibited by Akt and suppresses mTOR signalling. *Nature Cell Biology*. **4**, 648-657.

Inuzuka, H., Shaik, S., Onoyama, I., Gao, D., Tseng, A., Maser, R.S., Zhai, B., Wan, L., Gutierrez, A., Lau, A.W., Xiao, Y., Christie, A.L., Aster, J., Settleman, J., Gygi, S.P., Kung, A.L., Look, T., Nakayama, K.I., DePinho, R.A., Wei, W., 2011. SCF(FBW7) regulates cellular apoptosis by targeting MCL1 for ubiquitylation and destruction. *Nature*. **471**, 104-109.

Jares, P., Colomer, D., Campo, E., 2012. Molecular pathogenesis of mantle cell lymphoma. *The Journal of Clinical Investigation*. **122**, 3416-3423.

Jastroch, M., Divakaruni, A.S., Mookerjee, S., Treberg, J.R., Brand, M.D., 2010. Mitochondrial proton and electron leaks. *Essays in Biochemistry*. **47**, 53-67.

Jenne, D.E., Reimann, H., Nezu, J., Friedel, W., Loff, S., Jeschke, R., Muller, O., Back, W., Zimmer, M., 1998. Peutz-Jeghers syndrome is caused by mutations in a novel serine threonine kinase. *Nature Genetics*. **18**, 38-43.

Jeon, S.M., Chandel, N.S., Hay, N., 2012. AMPK regulates NADPH homeostasis to promote tumour cell survival during energy stress. *Nature*. **485**, 661-665.

Jiang, P., Du, W., Wu, M., 2014. Regulation of the pentose phosphate pathway in cancer. *Protein & Cell*. **5**, 592-602.

Joost, H.G., Bell, G.I., Best, J.D., Birnbaum, M.J., Charron, M.J., Chen, Y.T., Doege, H., James, D.E., Lodish, H.F., Moley, K.H., Moley, J.F., Mueckler, M., Rogers, S., Schurmann, A., Seino, S., Thorens, B., 2002. Nomenclature of the GLUT/SLC2A family of sugar/polyol transport facilitators. *American Journal of Physiology. Endocrinology and Metabolism*. **282**, E974-6.

Joost, H.G. & Thorens, B., 2001. The extended GLUT-family of sugar/polyol transport facilitators: nomenclature, sequence characteristics, and potential

function of its novel members (review). *Molecular Membrane Biology*. **18**, 247-256.

Jornayvaz, F.R. & Shulman, G.I., 2010. Regulation of mitochondrial biogenesis. *Essays in Biochemistry*. **47**, 69-84.

Jose, C., Bellance, N., Rossignol, R., 2011. Choosing between glycolysis and oxidative phosphorylation: A tumor's dilemma? *Biochimica Et Biophysica Acta (BBA) - Bioenergetics*. **1807**, 552-561.

Kaiser, W.J., Upton, J.W., Mocarski, E.S., 2013. Viral modulation of programmed necrosis. *Current Opinion in Virology*. **3**, 296-306.

Kase, E.T., Nikolic, N., Bakke, S.S., Bogen, K.K., Aas, V., Thoresen, G.H., Rustan, A.C., 2013. Remodeling of oxidative energy metabolism by galactose improves glucose handling and metabolic switching in human skeletal muscle cells. *PLoS One*. **8**, e59972.

Kato, Y., Ozawa, S., Miyamoto, C., Maehata, Y., Suzuki, A., Maeda, T., Baba, Y., 2013. Acidic extracellular microenvironment and cancer. *Cancer Cell International*. **13**, 89-2867-13-89.

Kefas, B.A., Cai, Y., Ling, Z., Heimberg, H., Hue, L., Pipeleers, D., Van de Casteele, M., 2003a. AMP-activated protein kinase can induce apoptosis of insulin-producing MIN6 cells through stimulation of c-Jun-N-terminal kinase. *Journal of Molecular Endocrinology*. **30**, 151-161.

Kefas, B.A., Heimberg, H., Vaulont, S., Meisse, D., Hue, L., Pipeleers, D., Van de Casteele, M., 2003b. AICA-riboside induces apoptosis of pancreatic beta cells through stimulation of AMP-activated protein kinase. *Diabetologia*. **46**, 250-254.

Kerr, J.F., Wyllie, A.H., Currie, A.R., 1972. Apoptosis: a basic biological phenomenon with wide-ranging implications in tissue kinetics. *British Journal of Cancer*. **26**, 239-257.

Kianercy, A., Veltri, R., Pienta, K.J., 2014. Critical transitions in a game theoretic model of tumour metabolism. *Interface Focus*. **4**, 20140014.

Kim, D.I., Lim, S.K., Park, M.J., Han, H.J., Kim, G.Y., Park, S.H., 2007. The involvement of phosphatidylinositol 3-kinase /Akt signaling in high glucose-induced downregulation of GLUT-1 expression in ARPE cells. *Life Sciences*. **80**, 626-632.

Kischkel, F.C., Hellbardt, S., Behrmann, I., Germer, M., Pawlita, M., Krammer, P.H., Peter, M.E., 1995. Cytotoxicity-dependent APO-1 (Fas/CD95)-associated proteins form a death-inducing signaling complex (DISC) with the receptor. *The EMBO Journal*. **14**, 5579-5588.

-
- Kischkel, F.C., Lawrence, D.A., Tinel, A., LeBlanc, H., Virmani, A., Schow, P., Gazdar, A., Blenis, J., Arnott, D., Ashkenazi, A., 2001. Death receptor recruitment of endogenous caspase-10 and apoptosis initiation in the absence of caspase-8. *The Journal of Biological Chemistry*. **276**, 46639-46646.
- Kitamura, T., Kitamura, Y., Kuroda, S., Hino, Y., Ando, M., Kotani, K., Konishi, H., Matsuzaki, H., Kikkawa, U., Ogawa, W., Kasuga, M., 1999. Insulin-Induced Phosphorylation and Activation of Cyclic Nucleotide Phosphodiesterase 3B by the Serine-Threonine Kinase Akt. *Molecular and Cellular Biology*. **19**, 6286-6296.
- Knowles, M.A., Platt, F.M., Ross, R.L., Hurst, C.D., 2009. Phosphatidylinositol 3-kinase (PI3K) pathway activation in bladder cancer. *Cancer Metastasis Reviews*. **28**, 305-316.
- Kurtoglu, M., Gao, N., Shang, J., Maher, J.C., Lehrman, M.A., Wangpaichitr, M., Savaraj, N., Lane, A.N., Lampidis, T.J., 2007. Under normoxia, 2-deoxy-D-glucose elicits cell death in select tumor types not by inhibition of glycolysis but by interfering with N-linked glycosylation. *Molecular Cancer Therapeutics*. **6**, 3049-3058.
- Kuwana, T., Bouchier-Hayes, L., Chipuk, J.E., Bonzon, C., Sullivan, B.A., Green, D.R., Newmeyer, D.D., 2005. BH3 domains of BH3-only proteins differentially regulate Bax-mediated mitochondrial membrane permeabilization both directly and indirectly. *Molecular Cell*. **17**, 525-535.
- Lee, S.J., Trostel, A., Le, P., Harinarayanan, R., Fitzgerald, P.C., Adhya, S., 2009. Cellular stress created by intermediary metabolite imbalances. *Proceedings of the National Academy of Sciences of the United States of America*. **106**, 19515-19520.
- Lee, Y.J., Galoforo, S.S., Berns, C.M., Tong, W.P., Kim, H.R., Corry, P.M., 1997. Glucose deprivation-induced cytotoxicity in drug resistant human breast carcinoma MCF-7/ADR cells: role of c-myc and bcl-2 in apoptotic cell death. *Journal of Cell Science*. **110 (Pt 5)**, 681-686.
- Leist, M., Single, B., Castoldi, A.F., Kuhle, S., Nicotera, P., 1997. Intracellular adenosine triphosphate (ATP) concentration: a switch in the decision between apoptosis and necrosis. *Journal of Experimental Medicine*. **185**, 1481-1486.
- Letai, A., Bassik, M.C., Walensky, L.D., Sorcinelli, M.D., Weiler, S., Korsmeyer, S.J., 2002. Distinct BH3 domains either sensitize or activate mitochondrial apoptosis, serving as prototype cancer therapeutics. *Cancer Cell*. **2**, 183-192.
- Li, H., Zhu, H., Xu, C.J., Yuan, J., 1998. Cleavage of BID by caspase 8 mediates the mitochondrial damage in the Fas pathway of apoptosis. *Cell*. **94**, 491-501.

-
- Li, J., Jiang, P., Robinson, M., Lawrence, T.S., Sun, Y., 2003a. AMPK-beta1 subunit is a p53-independent stress responsive protein that inhibits tumor cell growth upon forced expression. *Carcinogenesis*. **24**, 827-834.
- Li, J., McQuade, T., Siemer, A.B., Napetschnig, J., Moriwaki, K., Hsiao, Y.S., Damko, E., Moquin, D., Walz, T., McDermott, A., Ka-Ming Chan, F., Wu, H., 2012. The RIP1/RIP3 Necrosome Forms a Functional Amyloid Signaling Complex Required for Programmed Necrosis. *Cell*. **150**, 339-350.
- Li, N., Ragheb, K., Lawler, G., Sturgis, J., Rajwa, B., Melendez, J.A., Robinson, J.P., 2003b. Mitochondrial complex I inhibitor rotenone induces apoptosis through enhancing mitochondrial reactive oxygen species production. *The Journal of Biological Chemistry*. **278**, 8516-8525.
- Lim, C.T., Kola, B., Korbonits, M., 2010. AMPK as a mediator of hormonal signalling. *Journal of Molecular Endocrinology*. **44**, 87-97.
- Lin, J., Li, H., Yang, M., Ren, J., Huang, Z., Han, F., Huang, J., Ma, J., Zhang, D., Zhang, Z., Wu, J., Huang, D., Qiao, M., Jin, G., Wu, Q., Huang, Y., Du, J., Han, J., 2013. A role of RIP3-mediated macrophage necrosis in atherosclerosis development. *Cell Reports*. **3**, 200-210.
- Linkermann, A. & Green, D.R., 2014. Necroptosis. *The New England Journal of Medicine*. **370**, 455-465.
- Liu, H., Jiang, C.C., Lavis, C.J., Croft, A., Dong, L., Tseng, H.Y., Yang, F., Tay, K.H., Hersey, P., Zhang, X.D., 2009. 2-Deoxy-D-glucose enhances TRAIL-induced apoptosis in human melanoma cells through XBP-1-mediated up-regulation of TRAIL-R2. *Molecular Cancer*. **8**, 122-4598-8-122.
- Liu, L.Z., Zhou, X.D., Qian, G., Shi, X., Fang, J., Jiang, B.H., 2007. AKT1 amplification regulates cisplatin resistance in human lung cancer cells through the mammalian target of rapamycin/p70S6K1 pathway. *Cancer Research*. **67**, 6325-6332.
- Liu, Y., Cao, Y., Zhang, W., Bergmeier, S., Qian, Y., Akbar, H., Colvin, R., Ding, J., Tong, L., Wu, S., Hines, J., Chen, X., 2012. A small-molecule inhibitor of glucose transporter 1 downregulates glycolysis, induces cell-cycle arrest, and inhibits cancer cell growth in vitro and in vivo. *Molecular Cancer Therapeutics*. **11**, 1672-1682.
- Llambi, F., Moldoveanu, T., Tait, S.W., Bouchier-Hayes, L., Temirov, J., McCormick, L.L., Dillon, C.P., Green, D.R., 2011. A unified model of mammalian BCL-2 protein family interactions at the mitochondria. *Molecular Cell*. **44**, 517-531.
- Lowman, X.H., McDonnell, M.A., Kosloske, A., Odumade, O.A., Jenness, C., Karim, C.B., Jemmerson, R., Kelekar, A., 2010. The proapoptotic function of Noxa in human leukemia cells is regulated by the kinase Cdk5 and by glucose. *Molecular Cell*. **40**, 823-833.

-
- Lu, J.V., Weist, B.M., van Raam, B.J., Marro, B.S., Nguyen, L.V., Srinivas, P., Bell, B.D., Luhrs, K.A., Lane, T.E., Salvesen, G.S., Walsh, C.M., 2011. Complementary roles of Fas-associated death domain (FADD) and receptor interacting protein kinase-3 (RIPK3) in T-cell homeostasis and antiviral immunity. *Proceedings of the National Academy of Sciences of the United States of America*. **108**, 15312-15317.
- Luo, X., Budihardjo, I., Zou, H., Slaughter, C., Wang, X., 1998. Bid, a Bcl2 Interacting Protein, Mediates Cytochrome c Release from Mitochondria in Response to Activation of Cell Surface Death Receptors. *Cell*. **94**, 481-490.
- MacFarlane, M., 2003. TRAIL-induced signalling and apoptosis. *Toxicology Letters*. **139**, 89-97.
- MacFarlane, M., Ahmad, M., Srinivasula, S.M., Fernandes-Alnemri, T., Cohen, G.M., Alnemri, E.S., 1997. Identification and molecular cloning of two novel receptors for the cytotoxic ligand TRAIL. *The Journal of Biological Chemistry*. **272**, 25417-25420.
- MacFarlane, M., Harper, N., Snowden, R.T., Dyer, M.J., Barnett, G.A., Pringle, J.H., Cohen, G.M., 2002. Mechanisms of resistance to TRAIL-induced apoptosis in primary B cell chronic lymphocytic leukaemia. *Oncogene*. **21**, 6809-6818.
- MacFarlane, M., Robinson, G.L., Cain, K., 2012. Glucose--a sweet way to die: metabolic switching modulates tumor cell death. *Cell Cycle (Georgetown, Tex.)*. **11**, 3919-3925.
- Majewski, N., Nogueira, V., Robey, R.B., Hay, N., 2004a. Akt Inhibits Apoptosis Downstream of BID Cleavage via a Glucose-Dependent Mechanism Involving Mitochondrial Hexokinases. *Molecular and Cellular Biology*. **24**, 730-740.
- Majewski, N., Nogueira, V., Bhaskar, P., Coy, P.E., Skeen, J.E., Gottlob, K., Chandel, N.S., Thompson, C.B., Robey, R.B., Hay, N., 2004b. Hexokinase-Mitochondria Interaction Mediated by Akt Is Required to Inhibit Apoptosis in the Presence or Absence of Bax and Bak. *Molecular Cell*. **16**, 819-830.
- Majno, G. & Joris, I., 1995. Apoptosis, oncosis, and necrosis. An overview of cell death. *The American Journal of Pathology*. **146**, 3-15.
- Marivin, A., Berthelet, J., Plenchette, S., Dubrez, L., 2012. The Inhibitor of Apoptosis (IAPs) in Adaptive Response to Cellular Stress. *Cells*. **1**, 711-737.
- Marroquin, L.D., Hynes, J., Dykens, J.A., Jamieson, J.D., Will, Y., 2007. Circumventing the Crabtree effect: replacing media glucose with galactose increases susceptibility of HepG2 cells to mitochondrial toxicants. *Toxicological Sciences : An Official Journal of the Society of Toxicology*. **97**, 539-547.
- Martelli, A.M., Evangelisti, C., Chiarini, F., Grimaldi, C., Cappellini, A., Ognibene, A., McCubrey, J.A., 2010. The emerging role of the

phosphatidylinositol 3-kinase/Akt/mammalian target of rapamycin signaling network in normal myelopoiesis and leukemogenesis. *Biochimica Et Biophysica Acta*. **1803**, 991-1002.

Martini, M., De Santis, M.C., Braccini, L., Gulluni, F., Hirsch, E., 2014. PI3K/AKT signaling pathway and cancer: an updated review. *Annals of Medicine*. **46**, 372-383.

Martins, L.M., Iaccarino, I., Tenev, T., Gschmeissner, S., Totty, N.F., Lemoine, N.R., Savopoulos, J., Gray, C.W., Creasy, C.L., Dingwall, C., Downward, J., 2002. The serine protease Omi/HtrA2 regulates apoptosis by binding XIAP through a reaper-like motif. *The Journal of Biological Chemistry*. **277**, 439-444.

Maurer, U., Charvet, C., Wagman, A.S., Dejardin, E., Green, D.R., 2006. Glycogen synthase kinase-3 regulates mitochondrial outer membrane permeabilization and apoptosis by destabilization of MCL-1. *Molecular Cell*. **21**, 749-760.

McIlwain, D.R., Berger, T., Mak, T.W., 2013. Caspase functions in cell death and disease. *Cold Spring Harbor Perspectives in Biology*. **5**, a008656.

Medina, R.A. & Owen, G.I., 2002. Glucose transporters: expression, regulation and cancer. *Biological Research*. **35**, 9-26.

Mendivil-Perez, M., Jimenez-Del-Rio, M., Velez-Pardo, C., 2013. Glucose starvation induces apoptosis in a model of acute T leukemia dependent on caspase-3 and apoptosis-inducing factor: a therapeutic strategy. *Nutrition and Cancer*. **65**, 99-109.

Minchinton, A.I. & Tannock, I.F., 2006. Drug penetration in solid tumours. **6**, 583-592.

M'kacher, R., Bennaceur, A., Farace, F., Lauge, A., Plassa, L.F., Wittmer, E., Dossou, J., Violot, D., Deutsch, E., Bourhis, J., Stoppa-Lyonnet, D., Ribrag, V., Carde, P., Parmentier, C., Bernheim, A., Turhan, A.G., 2003. Multiple molecular mechanisms contribute to radiation sensitivity in mantle cell lymphoma. *Oncogene*. **22**, 7905-7912.

Moffat, C. & Harper, M.E., 2010. Metabolic functions of AMPK: aspects of structure and of natural mutations in the regulatory gamma subunits. *IUBMB Life*. **62**, 739-745.

Mohanti, B.K., Rath, G.K., Anantha, N., Kannan, V., Das, B.S., Chandramouli, B.A., Banerjee, A.K., Das, S., Jena, A., Ravichandran, R., Sahi, U.P., Kumar, R., Kapoor, N., Kalia, V.K., Dwarakanath, B.S., Jain, V., 1996. Improving cancer radiotherapy with 2-deoxy-D-glucose: phase I/II clinical trials on human cerebral gliomas. *International Journal of Radiation Oncology, Biology, Physics*. **35**, 103-111.

Munoz-Pinedo, C., Ruiz-Ruiz, C., Ruiz de Almodovar, C., Palacios, C., Lopez-Rivas, A., 2003. Inhibition of glucose metabolism sensitizes tumor cells to death receptor-triggered apoptosis through enhancement of death-inducing signaling complex formation and apical procaspase-8 processing. *Journal of Biological Chemistry*. **278**, 12759-12768.

Nam, S.Y., Amoscato, A.A., Lee, Y.J., 2002. Low glucose-enhanced TRAIL cytotoxicity is mediated through the ceramide-Akt-FLIP pathway. *Oncogene*. **21**, 337-346.

Navarro, A., Clot, G., Royo, C., Jares, P., Hadzidimitriou, A., Agathangelidis, A., Bikos, V., Darzentas, N., Papadaki, T., Salaverria, I., Pinyol, M., Puig, X., Palomero, J., Vegliante, M.C., Amador, V., Martinez-Trillos, A., Stefancikova, L., Wiestner, A., Wilson, W., Pott, C., Calasanz, M.J., Trim, N., Erber, W., Sander, B., Ott, G., Rosenwald, A., Colomer, D., Gine, E., Siebert, R., Lopez-Guillermo, A., Stamatopoulos, K., Bea, S., Campo, E., 2012. Molecular subsets of mantle cell lymphoma defined by the IGHV mutational status and SOX11 expression have distinct biologic and clinical features. *Cancer Research*. **72**, 5307-5316.

Newsholme, E.A., Rolleston, F.S., Taylor, K., 1968. Factors affecting the glucose 6-phosphate inhibition of hexokinase from cerebral cortex tissue of the guinea pig. *Biochemical Journal*. **106**, 193-201.

Nicholls, D.G. & Ferguson, S.J., 2013a. 5 - Respiratory Chains. In Ferguson, D. G. N. J., ed, *Bioenergetics (Fourth Edition)*. Boston: Academic Press. 91-157.

Nicholls, D.G. & Ferguson, S.J., 2013b. 7 - ATP Synthases and Bacterial Flagella Rotary Motors. In Ferguson, D. G. N. J., ed, *Bioenergetics (Fourth Edition)*. Boston: Academic Press. 197-220.

Nicholson, D.W., Ali, A., Thornberry, N.A., Vaillancourt, J.P., Ding, C.K., Gallant, M., Gareau, Y., Griffin, P.R., Labelle, M., Lazebnik, Y.A., 1995. Identification and inhibition of the ICE/CED-3 protease necessary for mammalian apoptosis. *Nature*. **376**, 37-43.

Ning, J., Xi, G., Clemmons, D.R., 2011. Suppression of AMPK activation via S485 phosphorylation by IGF-I during hyperglycemia is mediated by AKT activation in vascular smooth muscle cells. *Endocrinology*. **152**, 3143-3154.

Oudard, S., Poirson, F., Miccoli, L., Bourgeois, Y., Vassault, A., Poisson, M., Magdelenat, H., Dutrillaux, B., Poupon, M.F., 1995. Mitochondria-bound hexokinase as target for therapy of malignant gliomas. *International Journal of Cancer. Journal International Du Cancer*. **62**, 216-222.

Pain, V.M., 1996. Initiation of protein synthesis in eukaryotic cells. *European Journal of Biochemistry / FEBS*. **236**, 747-771.

Park, H.H., 2012. Structural features of caspase-activating complexes. *International Journal of Molecular Sciences*. **13**, 4807-4818.

-
- Parrish, A.B., Freel, C.D., Kornbluth, S., 2013. Cellular mechanisms controlling caspase activation and function. *Cold Spring Harbor Perspectives in Biology*. **5**, 10.1101/cshperspect.a008672.
- Patra, K.C. & Hay, N., 2014. The pentose phosphate pathway and cancer. *Trends in Biochemical Sciences*. **39**, 347-354.
- Pause, A., Belsham, G.J., Gingras, A.C., Donze, O., Lin, T.A., Lawrence, J.C., Jr, Sonenberg, N., 1994. Insulin-dependent stimulation of protein synthesis by phosphorylation of a regulator of 5'-cap function. *Nature*. **371**, 762-767.
- Pelicano, H., Martin, D.S., Xu, R.H., Huang, P., 2006. Glycolysis inhibition for anticancer treatment. *Oncogene*. **25**, 4633-4646.
- Pfeiffer, A., Jaeckel, M., Lewerenz, J., Noack, R., Pouya, A., Schacht, T., Hoffmann, C., Winter, J., Schweiger, S., Schäfer, M.K.E., Methner, A., 2014. Mitochondrial function and energy metabolism in neuronal HT22 cells resistant to oxidative stress. *British Journal of Pharmacology*. **171**, 2147-2158.
- Powley, I.R., Kondrashov, A., Young, L.A., Dobbyn, H.C., Hill, K., Cannell, I.G., Stoneley, M., Kong, Y.W., Cotes, J.A., Smith, G.C., Wek, R., Hayes, C., Gant, T.W., Spriggs, K.A., Bushell, M., Willis, A.E., 2009. Translational reprogramming following UVB irradiation is mediated by DNA-PKcs and allows selective recruitment to the polysomes of mRNAs encoding DNA repair enzymes. *Genes & Development*. **23**, 1207-1220.
- Pradelli, L.A., Beneteau, M., Chauvin, C., Jacquin, M.A., Marchetti, S., Munoz-Pinedo, C., Auberger, P., Pende, M., Ricci, J.E., 2010. Glycolysis inhibition sensitizes tumor cells to death receptors-induced apoptosis by AMP kinase activation leading to Mcl-1 block in translation. *Oncogene*. **29**, 1641-1652.
- Qin, J.Z., Xin, H., Nickoloff, B.J., 2010. 2-deoxyglucose sensitizes melanoma cells to TRAIL-induced apoptosis which is reduced by mannose. *Biochemical and Biophysical Research Communications*. **401**, 293-299.
- Raez, L., Papadopoulos, K., Ricart, A., Chiorean, E.G., DiPaola, R., Stein, M., Rocha Lima, C., Schlesselman, J., Tolba, K., Langmuir, V., Kroll, S., Jung, D., Kurtoglu, M., Rosenblatt, J., Lampidis, T., 2013. A phase I dose-escalation trial of 2-deoxy-d-glucose alone or combined with docetaxel in patients with advanced solid tumors. *Cancer Chemotherapy and Pharmacology*. **71**, 523-530.
- Ramirez-Peinado, S., Alcazar-Limones, F., Lagares-Tena, L., El Mjiyad, N., Caro-Maldonado, A., Tirado, O.M., Munoz-Pinedo, C., 2011. 2-deoxyglucose induces Noxa-dependent apoptosis in alveolar rhabdomyosarcoma. *Cancer Research*. **71**, 6796-6806.
- Rana, P., Nadanaciva, S., Will, Y., 2011. Mitochondrial membrane potential measurement of H9c2 cells grown in high-glucose and galactose-containing media does not provide additional predictivity towards mitochondrial

assessment. *Toxicology in Vitro : An International Journal Published in Association with BIBRA*. **25**, 580-587.

Raught, B., Peiretti, F., Gingras, A.C., Livingstone, M., Shahbazian, D., Mayeur, G.L., Polakiewicz, R.D., Sonenberg, N., Hershey, J.W., 2004. Phosphorylation of eucaryotic translation initiation factor 4B Ser422 is modulated by S6 kinases. *The EMBO Journal*. **23**, 1761-1769.

Renatus, M., Stennicke, H.R., Scott, F.L., Liddington, R.C., Salvesen, G.S., 2001. Dimer formation drives the activation of the cell death protease caspase 9. *Proceedings of the National Academy of Sciences of the United States of America*. **98**, 14250-14255.

Riedl, S.J., Fuentes-Prior, P., Renatus, M., Kairies, N., Krapp, S., Huber, R., Salvesen, G.S., Bode, W., 2001. Structural basis for the activation of human procaspase-7. *Proceedings of the National Academy of Sciences of the United States of America*. **98**, 14790-14795.

Robertson, J.D., Gogvadze, V., Zhivotovsky, B., Orrenius, S., 2000. Distinct pathways for stimulation of cytochrome c release by etoposide. *The Journal of Biological Chemistry*. **275**, 32438-32443.

Robinson, B.H., Petrova-Benedict, R., Buncic, J.R., Wallace, D.C., 1992. Nonviability of cells with oxidative defects in galactose medium: A screening test for affected patient fibroblasts. *Biochemical Medicine and Metabolic Biology*. **48**, 122-126.

Robinson, G.L., Dinsdale, D., Macfarlane, M., Cain, K., 2012. Switching from aerobic glycolysis to oxidative phosphorylation modulates the sensitivity of mantle cell lymphoma cells to TRAIL. *Oncogene*.

Rock, K.L. & Kono, H., 2008. The inflammatory response to cell death. *Annual Review of Pathology*. **3**, 99-126.

Romashkova, J.A. & Makarov, S.S., 1999. NF-kappaB is a target of AKT in anti-apoptotic PDGF signalling. *Nature*. **401**, 86-90.

Ros, S. & Schulze, A., 2013. Balancing glycolytic flux: the role of 6-phosphofructo-2-kinase/fructose 2,6-bisphosphatases in cancer metabolism. *Cancer & Metabolism*. **1**, 8-3002-1-8.

Saitoh, M., Nagai, K., Nakagawa, K., Yamamura, T., Yamamoto, S., Nishizaki, T., 2004. Adenosine induces apoptosis in the human gastric cancer cells via an intrinsic pathway relevant to activation of AMP-activated protein kinase. *Biochemical Pharmacology*. **67**, 2005-2011.

Sakamoto, K., McCarthy, A., Smith, D., Green, K.A., Grahame Hardie, D., Ashworth, A., Alessi, D.R., 2005. Deficiency of LKB1 in skeletal muscle prevents AMPK activation and glucose uptake during contraction. *The EMBO Journal*. **24**, 1810-1820.

-
- Samih, N., Hovsepian, S., Aouani, A., Lombardo, D., Fayet, G., 2000. Glut-1 translocation in FRTL-5 thyroid cells: role of phosphatidylinositol 3-kinase and N-glycosylation. *Endocrinology*. **141**, 4146-4155.
- Sancak, Y., Thoreen, C.C., Peterson, T.R., Lindquist, R.A., Kang, S.A., Spooner, E., Carr, S.A., Sabatini, D.M., 2007. PRAS40 is an insulin-regulated inhibitor of the mTORC1 protein kinase. *Molecular Cell*. **25**, 903-915.
- Santidrian, A.F., Gonzalez-Girones, D.M., Iglesias-Serret, D., Coll-Mulet, L., Cosialls, A.M., de Frias, M., Campas, C., Gonzalez-Barca, E., Alonso, E., Labi, V., Viollet, B., Benito, A., Pons, G., Villunger, A., Gil, J., 2010. AICAR induces apoptosis independently of AMPK and p53 through up-regulation of the BH3-only proteins BIM and NOXA in chronic lymphocytic leukemia cells. *Blood*. **116**, 3023-3032.
- Saraste, A. & Pulkki, K., 2000. Morphologic and biochemical hallmarks of apoptosis. *Cardiovascular Research*. **45**, 528-537.
- Scaffidi, C., Medema, J.P., Krammer, P.H., Peter, M.E., 1997. FLICE is predominantly expressed as two functionally active isoforms, caspase-8/a and caspase-8/b. *The Journal of Biological Chemistry*. **272**, 26953-26958.
- Scarpulla, R.C., 2008. Transcriptional paradigms in mammalian mitochondrial biogenesis and function. *Physiological Reviews*. **88**, 611-638.
- Schultze, S.M., Hemmings, B.A., Niessen, M., Tschopp, O., 2012. PI3K/AKT, MAPK and AMPK signalling: protein kinases in glucose homeostasis. *Expert Reviews in Molecular Medicine*. **14**, e1.
- Scott, J.W., Hawley, S.A., Green, K.A., Anis, M., Stewart, G., Scullion, G.A., Norman, D.G., Hardie, D.G., 2004. CBS domains form energy-sensing modules whose binding of adenosine ligands is disrupted by disease mutations. *Journal of Clinical Investigation*. **113**, 274-284.
- Shamas-Din, A., Kale, J., Leber, B., Andrews, D.W., 2013. Mechanisms of action of Bcl-2 family proteins. *Cold Spring Harbor Perspectives in Biology*. **5**, a008714.
- Shaw, R.J., Kosmatka, M., Bardeesy, N., Hurley, R.L., Witters, L.A., DePinho, R.A., Cantley, L.C., 2004. The tumor suppressor LKB1 kinase directly activates AMP-activated kinase and regulates apoptosis in response to energy stress. *Proceedings of the National Academy of Sciences of the United States of America*. **101**, 3329-3335.
- Shimobayashi, M. & Hall, M.N., 2014. Making new contacts: the mTOR network in metabolism and signalling crosstalk. *Nature Reviews.Molecular Cell Biology*. **15**, 155-162.

-
- Showkat, M., Beigh, M.A., Andrabi, K.I., 2014. mTOR Signaling in Protein Translation Regulation: Implications in Cancer Genesis and Therapeutic Interventions. *Molecular Biology International*. **2014**, 14.
- Singh, D., Banerji, A.K., Dwarakanath, B.S., Tripathi, R.P., Gupta, J.P., Mathew, T.L., Ravindranath, T., Jain, V., 2005. Optimizing cancer radiotherapy with 2-deoxy-d-glucose dose escalation studies in patients with glioblastoma multiforme. *Strahlentherapie Und Onkologie : Organ Der Deutschen Rontgengesellschaft ...[Et Al]*. **181**, 507-514.
- Smith, C.C., Davidson, S.M., Lim, S.Y., Simpkin, J.C., Hothersall, J.S., Yellon, D.M., 2007. Necrostatin: a potentially novel cardioprotective agent? *Cardiovascular Drugs and Therapy / Sponsored by the International Society of Cardiovascular Pharmacotherapy*. **21**, 227-233.
- Solaini, G., Sgarbi, G., Baracca, A., 2011. Oxidative phosphorylation in cancer cells. *Biochimica Et Biophysica Acta (BBA) - Bioenergetics*. **1807**, 534-542.
- Sols, A. & Crane, R.K., 1954. Substrate specificity of brain hexokinase. *The Journal of Biological Chemistry*. **210**, 581-595.
- Sprick, M.R., Rieser, E., Stahl, H., Grosse-Wilde, A., Weigand, M.A., Walczak, H., 2002. Caspase-10 is recruited to and activated at the native TRAIL and CD95 death-inducing signalling complexes in a FADD-dependent manner but can not functionally substitute caspase-8. *The EMBO Journal*. **21**, 4520-4530.
- Stamos, J.L. & Weis, W.I., 2013. The beta-catenin destruction complex. *Cold Spring Harbor Perspectives in Biology*. **5**, a007898.
- Stefanelli, C., Stanic', I., Bonavita, F., Flamigni, F., Pignatti, C., Guarnieri, C., Calderara, C.M., 1998. Inhibition of Glucocorticoid-Induced Apoptosis with 5-Aminoimidazole-4-carboxamide Ribonucleoside, a Cell-Permeable Activator of AMP-Activated Protein Kinase. *Biochemical and Biophysical Research Communications*. **243**, 821-826.
- Stein, M., Lin, H., Jeyamohan, C., Dvorzhinski, D., Gounder, M., Bray, K., Eddy, S., Goodin, S., White, E., DiPaola, R.S., 2010. Targeting tumor metabolism with 2-deoxyglucose in patients with castrate-resistant prostate cancer and advanced malignancies. *The Prostate*. **70**, 1388-1394.
- Stennicke, H.R., Renatus, M., Meldal, M., Salvesen, G.S., 2000. Internally quenched fluorescent peptide substrates disclose the subsite preferences of human caspases 1, 3, 6, 7 and 8. *The Biochemical Journal*. **350 Pt 2**, 563-568.
- Stratton, M.R., Campbell, P.J., Futreal, P.A., 2009. The cancer genome. *Nature*. **458**, 719-724.
- Sun, L., Wang, H., Wang, Z., He, S., Chen, S., Liao, D., Wang, L., Yan, J., Liu, W., Lei, X., Wang, X., 2012. Mixed lineage kinase domain-like protein mediates necrosis signaling downstream of RIP3 kinase. *Cell*. **148**, 213-227.

-
- Tait, S.W.,G. & Green, D.,R., 2010. Mitochondria and cell death: outer membrane permeabilization and beyond.
- Talanian, R.V., Quinlan, C., Trautz, S., Hackett, M.C., Mankovich, J.A., Banach, D., Ghayur, T., Brady, K.D., Wong, W.W., 1997. Substrate specificities of caspase family proteases. *The Journal of Biological Chemistry*. **272**, 9677-9682.
- Tennant, D.A., Duran, R.V., Gottlieb, E., 2010. Targeting metabolic transformation for cancer therapy. *Nature Reviews.Cancer*. **10**, 267-277.
- Tepper, H.L. & Voth, G.A., 2005. Protons May Leak through Pure Lipid Bilayers via a Concerted Mechanism. *Biophysical Journal*. **88**, 3095-3108.
- Thomas, R.L. & Gustafsson, Å, 2013. MCL1 is critical for mitochondrial function and autophagy in the heart. *Autophagy*. **9**, 1902-1903.
- Thornberry, N.A., Rano, T.A., Peterson, E.P., Rasper, D.M., Timkey, T., Garcia-Calvo, M., Houtzager, V.M., Nordstrom, P.A., Roy, S., Vaillancourt, J.P., Chapman, K.T., Nicholson, D.W., 1997. A combinatorial approach defines specificities of members of the caspase family and granzyme B. Functional relationships established for key mediators of apoptosis. *The Journal of Biological Chemistry*. **272**, 17907-17911.
- Topham, C.H. & Taylor, S.S., 2013. Mitosis and apoptosis: how is the balance set? *Current Opinion in Cell Biology*. **25**, 780-785.
- Touzeau, C., Dousset, C., Bodet, L., Gomez-Bougie, P., Bonnaud, S., Moreau, A., Moreau, P., Pellat-Deceunynk, C., Amiot, M., Le Gouill, S., 2011. ABT-737 induces apoptosis in mantle cell lymphoma cells with a Bcl-2high/Mcl-1low profile and synergizes with other antineoplastic agents. *Clinical Cancer Research : An Official Journal of the American Association for Cancer Research*. **17**, 5973-5981.
- Vander Heiden, M.G., 2011. Targeting cancer metabolism: a therapeutic window opens. *Nature Reviews.Drug Discovery*. **10**, 671-684.
- Vander Heiden, M.G., Plas, D.R., Rathmell, J.C., Fox, C.J., Harris, M.H., Thompson, C.B., 2001. Growth factors can influence cell growth and survival through effects on glucose metabolism. *Molecular and Cellular Biology*. **21**, 5899-5912.
- Vivanco, I. & Sawyers, C.L., 2002. The phosphatidylinositol 3-Kinase AKT pathway in human cancer. *Nature Reviews.Cancer*. **2**, 489-501.
- Wagner, A., Marc, A., Engasser, J.M., Einsele, A., 1991. Growth and metabolism of human tumor kidney cells on galactose and glucose. *Cytotechnology*. **7**, 7-13.

-
- Walczak, H. & Haas, T.L., 2008. Biochemical analysis of the native TRAIL death-inducing signaling complex. *Methods in Molecular Biology (Clifton, N.J.)*. **414**, 221-239.
- Wallace, K.B., 2008. Mitochondrial off targets of drug therapy. *Trends in Pharmacological Sciences*. **29**, 361-366.
- Wang, Q., Imamura, R., Motani, K., Kushiya, H., Nagata, S., Suda, T., 2013. Pyroptotic cells externalize eat-me and release find-me signals and are efficiently engulfed by macrophages. *International Immunology*. **25**, 363-372.
- Wang, X., Li, W., Williams, M., Terada, N., Alessi, D.R., Proud, C.G., 2001. Regulation of elongation factor 2 kinase by p90(RSK1) and p70 S6 kinase. *The EMBO Journal*. **20**, 4370-4379.
- Wang, Z., Jiang, H., Chen, S., Du, F., Wang, X., 2012. The Mitochondrial Phosphatase PGAM5 Functions at the Convergence Point of Multiple Necrotic Death Pathways. *Cell*. **148**, 228-243.
- Warburg, O., 1956. On respiratory impairment in cancer cells. *Science*. **124**, 269-270.
- Warburg, O., Wind, F., Negelein, E., 1927. The Metabolism of Tumors in the Body. *The Journal of General Physiology*. **8**, 519-530.
- Warden, S.M., Richardson, C., O'Donnell, J., Jr, Stapleton, D., Kemp, B.E., Witters, L.A., 2001. Post-translational modifications of the beta-1 subunit of AMP-activated protein kinase affect enzyme activity and cellular localization. *The Biochemical Journal*. **354**, 275-283.
- Watson, R.T., Kanzaki, M., Pessin, J.E., 2004. Regulated membrane trafficking of the insulin-responsive glucose transporter 4 in adipocytes. *Endocrine Reviews*. **25**, 177-204.
- Welz, P.S., Wullaert, A., Vlantis, K., Kondylis, V., Fernandez-Majada, V., Ermolaeva, M., Kirsch, P., Sterner-Kock, A., van Loo, G., Pasparakis, M., 2011. FADD prevents RIP3-mediated epithelial cell necrosis and chronic intestinal inflammation. *Nature*. **477**, 330-334.
- Wheaton, W.W., Weinberg, S.E., Hamanaka, R.B., Soberanes, S., Sullivan, L.B., Anso, E., Glasauer, A., Dufour, E., Mutlu, G.M., Budigner, G.R.S., Chandel, N.S., 2014. Metformin inhibits mitochondrial complex I of cancer cells to reduce tumorigenesis. *eLife*. **3**, 10.7554/eLife.02242.
- Wictome, M., Henderson, I., Lee, A.G., East, J.M., 1992. Mechanism of inhibition of the calcium pump of sarcoplasmic reticulum by thapsigargin. *Biochemical Journal*. **283**, 525-529.

-
- Wiederkehr, A., Park, K.S., Dupont, O., Demaurex, N., Pozzan, T., Cline, G.W., Wollheim, C.B., 2009. Matrix alkalization: a novel mitochondrial signal for sustained pancreatic beta-cell activation. *The EMBO Journal*. **28**, 417-428.
- Will, Y. & Dykens, J., 2014. Mitochondrial toxicity assessment in industry--a decade of technology development and insight. *Expert Opinion on Drug Metabolism & Toxicology*. **10**, 1061-1067.
- Willis, S.N., Chen, L., Dewson, G., Wei, A., Naik, E., Fletcher, J.I., Adams, J.M., Huang, D.C., 2005. Proapoptotic Bak is sequestered by Mcl-1 and Bcl-xL, but not Bcl-2, until displaced by BH3-only proteins. *Genes & Development*. **19**, 1294-1305.
- Willis, S.N., Fletcher, J.I., Kaufmann, T., van Delft, M.F., Chen, L., Czabotar, P.E., Ierino, H., Lee, E.F., Fairlie, W.D., Bouillet, P., Strasser, A., Kluck, R.M., Adams, J.M., Huang, D.C., 2007. Apoptosis initiated when BH3 ligands engage multiple Bcl-2 homologs, not Bax or Bak. *Science (New York, N.Y.)*. **315**, 856-859.
- Wilson, K.P., Black, J.A., Thomson, J.A., Kim, E.E., Griffith, J.P., Navia, M.A., Murcko, M.A., Chambers, S.P., Aldape, R.A., Raybuck, S.A., 1994. Structure and mechanism of interleukin-1 beta converting enzyme. *Nature*. **370**, 270-275.
- Wood, T.E., Dalili, S., Simpson, C.D., Hurren, R., Mao, X., Saiz, F.S., Gronda, M., Eberhard, Y., Minden, M.D., Bilan, P.J., Klip, A., Batey, R.A., Schimmer, A.D., 2008. A novel inhibitor of glucose uptake sensitizes cells to FAS-induced cell death. *Molecular Cancer Therapeutics*. **7**, 3546-3555.
- Woods, A., Dickerson, K., Heath, R., Hong, S.P., Momcilovic, M., Johnstone, S.R., Carlson, M., Carling, D., 2005. Ca²⁺/calmodulin-dependent protein kinase kinase-beta acts upstream of AMP-activated protein kinase in mammalian cells. *Cell Metabolism*. **2**, 21-33.
- Woods, A., Johnstone, S.R., Dickerson, K., Leiper, F.C., Fryer, L.G., Neumann, D., Schlattner, U., Wallimann, T., Carlson, M., Carling, D., 2003. LKB1 is the upstream kinase in the AMP-activated protein kinase cascade. *Current Biology : CB*. **13**, 2004-2008.
- Wu, C.H., Ho, Y.S., Tsai, C.Y., Wang, Y.J., Tseng, H., Wei, P.L., Lee, C.H., Liu, R.S., Lin, S.Y., 2009. In vitro and in vivo study of phloretin-induced apoptosis in human liver cancer cells involving inhibition of type II glucose transporter. *International Journal of Cancer. Journal International Du Cancer*. **124**, 2210-2219.
- Wu, J., Huang, Z., Ren, J., Zhang, Z., He, P., Li, Y., Ma, J., Chen, W., Zhang, Y., Zhou, X., Yang, Z., Wu, S., Chen, L., Han, J., 2013. Mkl1 knockout mice demonstrate the indispensable role of Mkl1 in necroptosis. *Cell Research*. **23**, 994-1006.

-
- Wurstle, M.L., Laussmann, M.A., Rehm, M., 2012. The central role of initiator caspase-9 in apoptosis signal transduction and the regulation of its activation and activity on the apoptosome. *Experimental Cell Research*. **318**, 1213-1220.
- Xi, H., Barredo, J.C., Merchan, J.R., Lampidis, T.J., 2013. Endoplasmic reticulum stress induced by 2-deoxyglucose but not glucose starvation activates AMPK through CaMKKbeta leading to autophagy. *Biochemical Pharmacology*. **85**, 1463-1477.
- Xi, H., Kurtoglu, M., Liu, H., Wangpaichitr, M., You, M., Liu, X., Savaraj, N., Lampidis, T.J., 2011. 2-Deoxy-D-glucose activates autophagy via endoplasmic reticulum stress rather than ATP depletion. *Cancer Chemotherapy and Pharmacology*. **67**, 899-910.
- Xiang, X., Saha, A.K., Wen, R., Ruderman, N.B., Luo, Z., 2004. AMP-activated protein kinase activators can inhibit the growth of prostate cancer cells by multiple mechanisms. *Biochemical and Biophysical Research Communications*. **321**, 161-167.
- Yamaguchi, R., Janssen, E., Perkins, G., Ellisman, M., Kitada, S., Reed, J.C., 2011. Efficient Elimination of Cancer Cells by Deoxyglucose-ABT-263/737 Combination Therapy. *PLoS ONE*. **6**, e24102.
doi:10.1371/journal.pone.0024102.
- Yamaguchi, R. & Perkins, G., 2012. Finding a Panacea among combination cancer therapies. *Cancer Research*. **72**, 18-23.
- Yasuda, M., Miyazawa, M., Fujita, M., Kajiwara, H., Iida, T., Hirasawa, T., Muramatsu, T., Murakami, M., Mikami, M., Saitoh, K., Shimizu, M., Takekoshi, S., Osamura, R.Y., 2008. Expression of hypoxia inducible factor-1alpha (HIF-1alpha) and glucose transporter-1 (GLUT-1) in ovarian adenocarcinomas: difference in hypoxic status depending on histological character. *Oncology Reports*. **19**, 111-116.
- Youle, R.J. & Strasser, A., 2008. The BCL-2 protein family: opposing activities that mediate cell death. *Nature Reviews.Molecular Cell Biology*. **9**, 47-59.
- Yu, Seon-Mi & Kim, Song-Ja, Endoplasmic reticulum stress (ER-stress) by 2-deoxy-D-glucose (2DG) reduces cyclooxygenase-2 (COX-2) expression and N-glycosylation and induces a loss of COX-2 activity via a Src kinase-dependent pathway in rabbit articular chondrocytes.
- Yuneva, M., Zamboni, N., Oefner, P., Sachidanandam, R., Lazebnik, Y., 2007. Deficiency in glutamine but not glucose induces MYC-dependent apoptosis in human cells. *The Journal of Cell Biology*. **178**, 93-105.
- Zagorodna, O., Martin, S.M., Rutkowski, D.T., Kuwana, T., Spitz, D.R., Knudson, C.M., 2012. 2-deoxyglucose-induced toxicity is regulated by Bcl-2 family members and is enhanced by antagonizing Bcl-2 in lymphoma cell lines. *Oncogene*. **31**, 2738-2749.

-
- Zamaraeva, M.V., Sabirov, R.Z., Maeno, E., Ando-Akatsuka, Y., Bessonova, S.V., Okada, Y., 2005. Cells die with increased cytosolic ATP during apoptosis: a bioluminescence study with intracellular luciferase. *Cell Death & Differentiation*. **12**, 1390-1397.
- Zhang, D., Li, J., Wang, F., Hu, J., Wang, S., Sun, Y., 2014. 2-Deoxy-D-glucose targeting of glucose metabolism in cancer cells as a potential therapy. *Cancer Letters*. **355**, 176-183.
- Zhao, J., Jitkaew, S., Cai, Z., Choksi, S., Li, Q., Luo, J., Liu, Z.G., 2012. Mixed lineage kinase domain-like is a key receptor interacting protein 3 downstream component of TNF-induced necrosis. *Proceedings of the National Academy of Sciences of the United States of America*. **109**, 5322-5327.
- Zhao, Y., Butler, E.B., Tan, M., 2013. Targeting cellular metabolism to improve cancer therapeutics. **4**, e532.
- Zhao, Y., Coloff, J.L., Ferguson, E.C., Jacobs, S.R., Cui, K., Rathmell, J.C., 2008. Glucose metabolism attenuates p53 and Puma-dependent cell death upon growth factor deprivation. *The Journal of Biological Chemistry*. **283**, 36344-36353.
- Zhong, D., Liu, X., Schafer-Hales, K., Marcus, A.I., Khuri, F.R., Sun, S.Y., Zhou, W., 2008. 2-Deoxyglucose induces Akt phosphorylation via a mechanism independent of LKB1/AMP-activated protein kinase signaling activation or glycolysis inhibition. *Molecular Cancer Therapeutics*. **7**, 809-817.
- Zhong, D., Xiong, L., Liu, T., Liu, X., Liu, X., Chen, J., Sun, S.Y., Khuri, F.R., Zong, Y., Zhou, Q., Zhou, W., 2009. The glycolytic inhibitor 2-deoxyglucose activates multiple prosurvival pathways through IGF1R. *The Journal of Biological Chemistry*. **284**, 23225-23233.
- Zong, H., Ren, J.M., Young, L.H., Pypaert, M., Mu, J., Birnbaum, M.J., Shulman, G.I., 2002. AMP kinase is required for mitochondrial biogenesis in skeletal muscle in response to chronic energy deprivation. *Proceedings of the National Academy of Sciences of the United States of America*. **99**, 15983-15987.